Australian Government
Geoscience Australia

Review of Australian Offshore Natural Hydrocarbon Seepage Studies

Graham Logan, Andrew Jones, Georgina Ryan, Magnus Wettle, Medhavy Thankappan, Emmanuelle Grosjean, Nadege Rollet and John Kennard

Record
2008/17

GeoCat # 65973

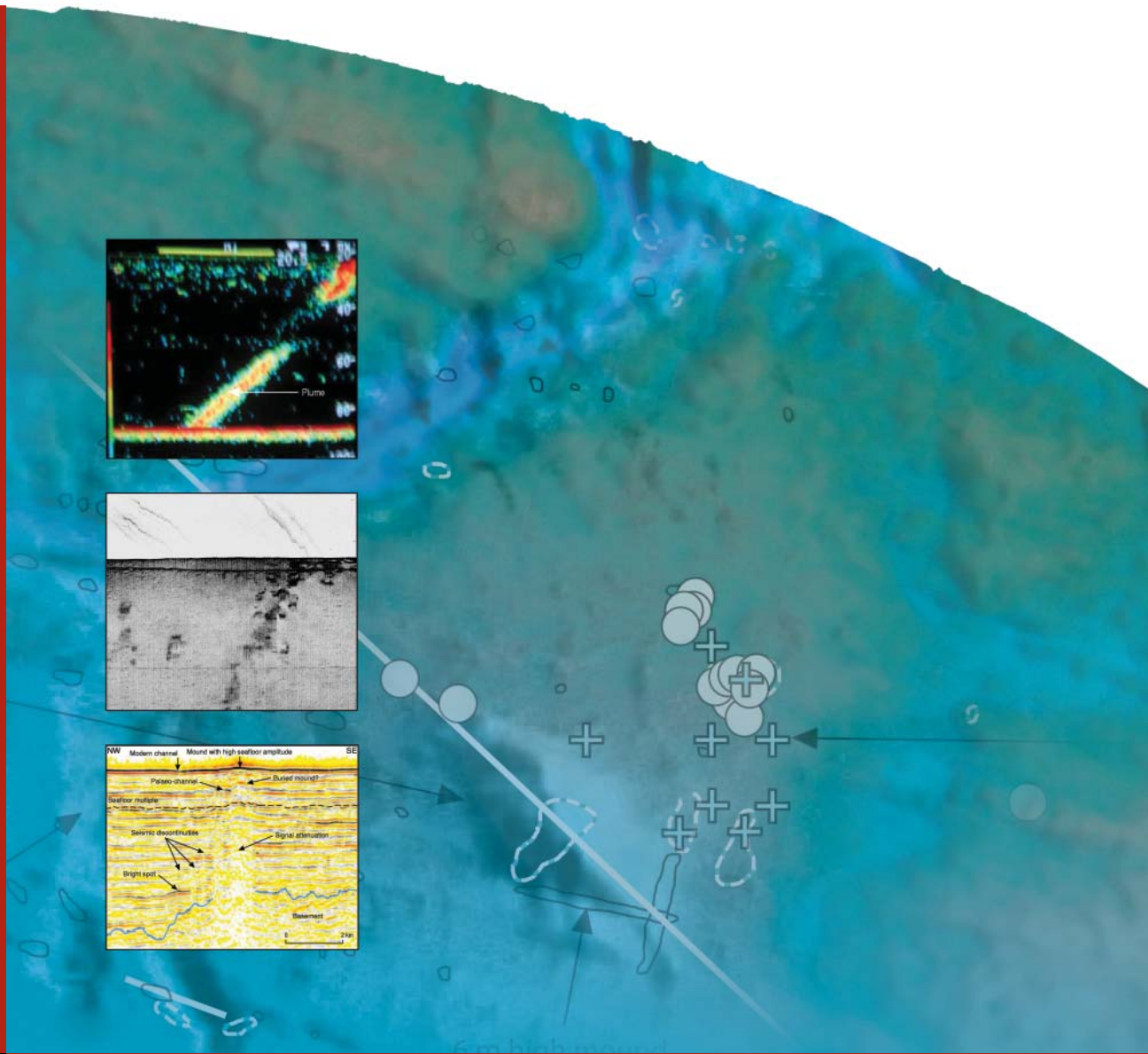

Review of Australian Offshore Natural Hydrocarbon Seepage Studies

GEOSCIENCE AUSTRALIA
RECORD 2008/17

by

G.A. Logan, A.T. Jones, G.J. Ryan, M.Wettle, M. Thankappan, E. Groesjean, N. Rollet and J.M. Kennard.

1. Geoscience Australia

Department of Resources, Energy and Tourism
Minister for Resources and Energy: The Hon. Martin Ferguson, AM MP
Secretary: Dr Peter Boxall, AO

Geoscience Australia
Chief Executive Officer: Dr Neil Williams PSM

ISSN 1448-2177
ISBN 978-1-921498-16-9

GeoCat # 65973

Bibliographic reference: G.A. Logan, A.T. Jones, G.J. Ryan, M.Wettle, M. Thankappan, E. Groesjean, N. Rollet and J.M. Kennard. Review of Australian Offshore Natural Hydrocarbon Seepage Studies. Geoscience Australia Record: 2008/17.

Executive Summary

A wide variety of studies have been carried out around the Australian margin to infer or detect natural hydrocarbon seepage. Hydrocarbon seepage can, in selected geological settings, delineate subsurface petroleum accumulations and provide information on hydrocarbon charge type. However, the relationship between near-surface hydrocarbon seepage and subsurface petroleum generation and entrapment is often complex. Rates and volume of hydrocarbon seepage to the surface produce a variety of near-surface geological and biological responses, which require a range of sampling techniques to detect the seepage effectively. Interpreters must firmly grasp these issues to understand the significance of migrated hydrocarbons within near-surface sediments. Thus, it is important to understand the data types that have been used to infer seepage in Australia and the results of these studies, if natural hydrocarbon seepage is to be assumed in this region. Furthermore, the strengths and weaknesses of different approaches need to be understood and the data often need to be set in a global context to appreciate the significance of results obtained. This report is aimed at providing an overview of natural hydrocarbon seepage studies that have been carried out around Australia and to provide information on techniques and approaches that have proved to be successful during studies carried out by Geoscience Australia between 2004 and 2007.

Initial studies of potential seepage in Australia's offshore jurisdiction were generally based around the application of a particular technique, which included geochemical analysis of stranded bitumens, water column geochemical 'sniffer' sampling, synthetic aperture radar (SAR) and airborne laser fluorsensor. Later studies involved the integration of these remote sensing and geochemical techniques with mutli-channel and shallow seismic.

A re-assessment of many of the earlier studies indicates that seepage interpretations are no longer appropriate and that previous data sets, when set in a global context, often represent normal background hydrocarbon levels. A critical aspect of this re-assessment has been an increased understanding of the technologies employed and the difficulties of working in the Australian environment. Specific examples include:

- Strong tidal currents, high tidal ranges and biological communities on the

North West Shelf produce false positives in SAR images that can be misinterpreted as natural hydrocarbon seepage;

- Interpreted sniffer anomalies are only twice the concentration of regional background concentrations, and high levels of gas wetness are more likely to be related to low gas concentrations and/or leakage of methane during sampling than an oil-prone source;
- It is not possible to differentiate between hydrocarbon-related and biological ALF anomalies on the basis of spectral signature, or to characterise hydrocarbon-related anomalies as being condensate or oil-prone without information regarding the concentration of the solution;
- Gas concentrations for interpreted head-space gas anomalies would be regarded as background in other settings, in Australia (Arafura Sea) and around the world (Gulf of Mexico), and increasing gas wetness in these analyses may be an artefact related to the leakage of methane during sampling.

Down-grading many seepage interpretations in previous studies leads to the conclusion that there are few sites of proven hydrocarbon seepage around Australia. To increase success of detecting natural hydrocarbon seepage around Australia's margin, data need to be interpreted both within the context of the local geological setting, and with an understanding of what is observed globally, to avoid misinterpreting normal background variation. Potential for geophysical and geochemical characterisation of thermogenic seeps is improved in deep-water silici-clastic environments, relative to shallow, carbonate shelves.

The tectonic, environmental and geomorphological setting determines the mode of seepage and influences the potential for successful seepage detection. Active faulting to the sea-floor and rapid subsidence and burial will improve the chances of hydrocarbon expulsion to the shallow subsurface and release at natural hydrocarbon seep sites. The dominantly passive margin setting of Australia's offshore sedimentary basins, and low recent sedimentation rates, are therefore not favourable for high rates of seepage. An exception to this is the Timor Sea, where Late Miocene tectonic reactivation is widespread and a thick section of Late Tertiary carbonate sediments have been deposited. The best example is on the Yampi Shelf where both palaeo- and

currently active seepage have been described.

This investigation provides an increased understanding of seepage detection technologies and techniques, particularly in relation to the Australian environment, and appropriate interpretation of potential seepage indicators in a global context. Consequently, seepage studies can be undertaken with greater confidence in Australia's offshore jurisdiction, in locations and at times that are optimal for effective seepage detection.

Contents

Introduction

1 Aims of Report

This report aims to provide a review of natural hydrocarbon seepage studies that have been carried out in Australia and to provide information on techniques and approaches that have proved to be successful during studies carried out by Geoscience Australia between 2004 and 2007. The first part of the report will review previous studies and provide the reader with a reference to data and reports related to natural hydrocarbon seepage. Later sections will provide information on:

- remote sensing techniques, their uses and quality control approaches that are applied within Geoscience Australia;
- geophysical methods used to identify seepage; and
- sea bed sampling methods and geochemical approaches for sample analysis, within the offshore Australian environment.

2 Natural Hydrocarbon Seepage

Seepage was the stimulus for exploration drilling by the pioneers of the petroleum industry as long ago as the 1860s in Pennsylvania and Azerbaijan (Williams and Lawrence, 2002). Seepage gave the first indication of the presence of petroleum in most of the world's petroleum producing regions, with at least half the reserves proved by 1952 discovered by drilling on or near seeps (Link, 1952; Judd and Hovland, 2007). Surface geochemistry methods have been used extensively for more than 70 years (Horvitz, 1985), primarily for regional source rock evaluation i.e. to confirm the presence of a mature source rock (Abrams, 2005). In selected geological settings hydrocarbon seepage can also delineate subsurface petroleum accumulations and provide information on hydrocarbon charge type (gas versus oil) or oil quality (sulfur and fluid gravity). Surface geochemistry practitioners demonstrate how effective the surface geochemical tools can be in handouts and publications (e.g. Schumacher and LeSchack, 2002), yet many petroleum explorationists have experienced 'failures'. According to Abrams (2005), this perceived unreliability reflects a lack of understanding of the petroleum seepage system and poor interpretations of surface geochemical data.

Petroleum, including dry gas derived during coal formation, wet gas, crude oil, and microbial gas, is generally mobile, and less dense than the waters that normally occupy the pore spaces of sedimentary rocks (Judd and Hovland, 2007). Once expelled from source rocks or sediments, these fluids migrate upwards or laterally towards the surface due to buoyancy associated with lithostatic pressures (Figure 1). Natural seepage introduces between 0.2 and 2.0 x 10^6 (best estimate 0.6 x 10^6) tonnes of crude oil per year into the marine environment (Kvenvolden and Cooper, 2003). This is about 47% of all the crude oil currently entering the marine environment, with anthopogenic activities responsible for the rest (Judd and Hovland, 2007). Hornafius et al. (1999) estimated that the air pollution emission rates from the present-day natural hydrocarbon seeps in Santa Barbara Channel, offshore California, are twice the rate from all the on-road vehicle traffic in Santa Barbara County.

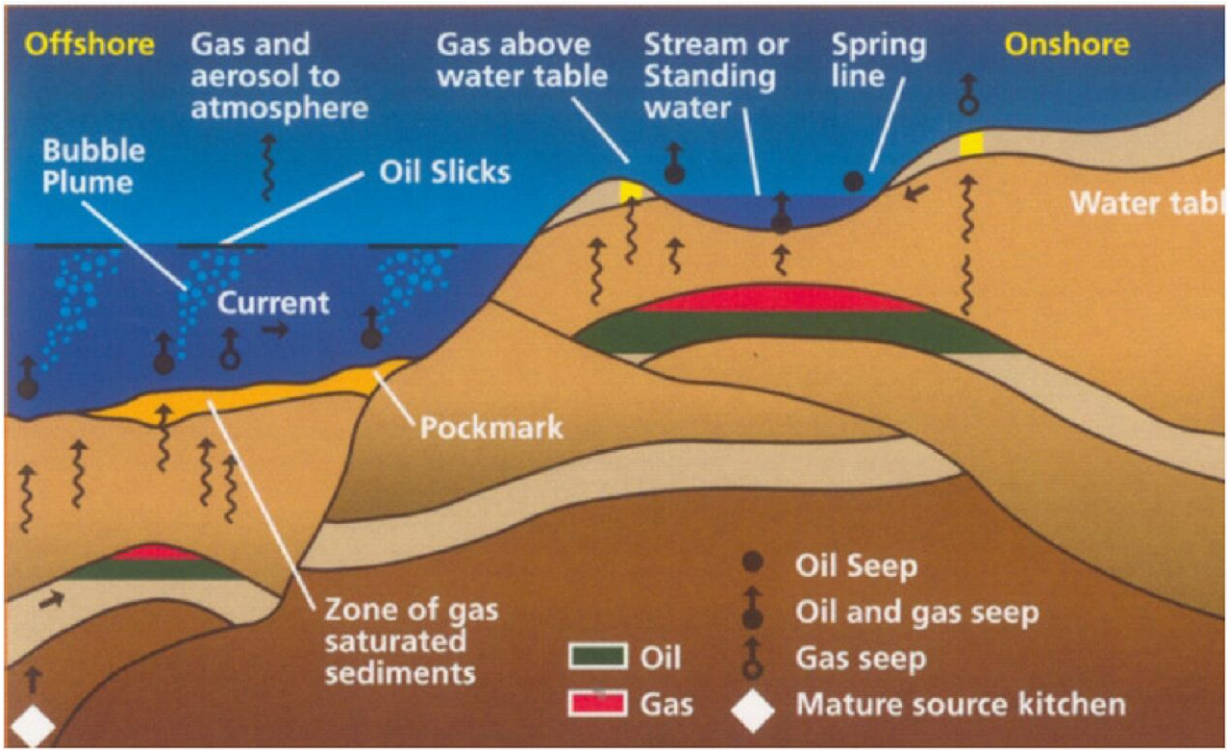

Figure 1. Schematic representation of a natural hydrocarbon seepage system (NPA et al., 2003).

The relationship between near-surface hydrocarbon seepage and subsurface petroleum generation and entrapment is often complex (Abrams, 2005). The near-surface expression of hydrocarbon migration varies greatly due to changes in leakage rates and concentration, major direction of bulk flow, and near-surface processes which alter or block seepage. Rates and volume of hydrocarbon seepage to the surface control the near-surface geological and biological responses (Roberts et al., 1990), and, thus, the type of sampling required to detect hydrocarbon leakage effectively. Interpreters must firmly grasp these issues to understand the significance of migrated hydrocarbons within near-surface sediments (Abrams, 2005).

In summary, it is important to understand the data types that have been used to infer seepage in Australia's offshore jurisdiction. Furthermore, the strengths and weaknesses of different approaches need to be understood and the data often need to be set in a global context to appreciate the significance of results obtained.

3 Previous Studies of Seepage in Australia

A wide variety of studies involving the interpretation and assessment of natural hydrocarbon seepage have been published based on work carried out around offshore Australia (Figure 2; Table 1). In the following section these studies will be discussed and, in some cases, the results will be re-interpreted based on our current understanding. Key implications and findings for specific study types will also be provided to allow readers to more carefully judge the findings of older studies where the limitations of technologies may not have been appreciated at the time.

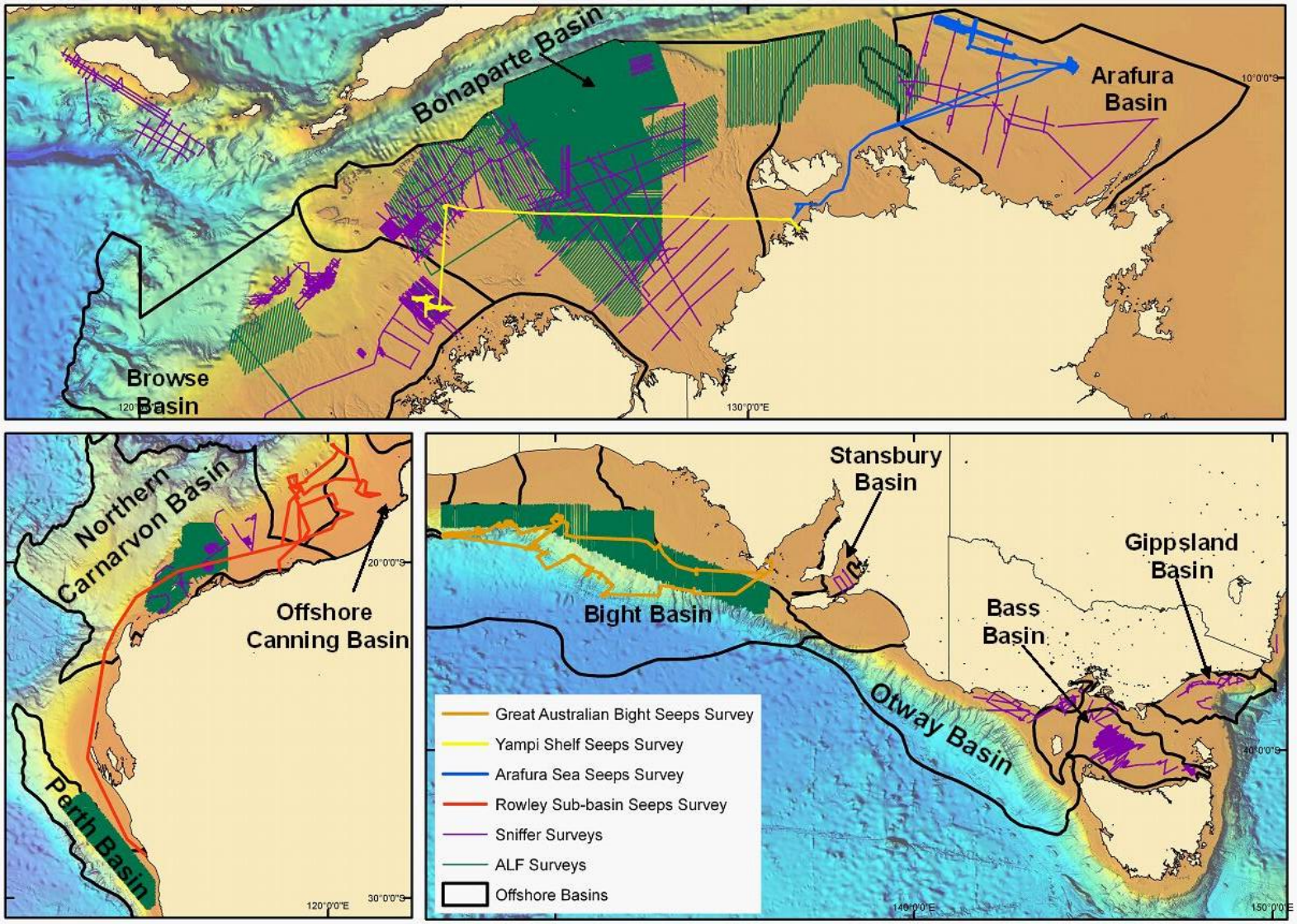

Figure 2. Spatial distribution of natural hydrocarbon seepage studies in Australia's offshore jurisdiction (SAR coverage not shown).

Table 1. Seepage studies undertaken around Australia, characterised by study type, methods and location.

Location	Study Type	Methods	References
Western Australian Coast to Tasmania	Stranded coastal bitumen	Geochemistry	McKirdy et al., 1986 & 1994; Currie et al., 1992; Summons et al., 1993; Alexander et al., 1994; Dowling et al., 1995; Padley 1996; Edwards et al., 1998
Otway Basin (EPP-18)	Sniffer	Geochemistry	Sprigg, 1986
Gippsland Basin	Sniffer	Geochemistry	Burns & Emmet, 1984
Gippsland, Bass, Otway Basins and Stansbury and Torquay Sub-basins	Sniffer	Geochemistry	O'Brien et al., 1992a; O'Brien & Heggie, 1990
Bonaparte Basin	Sniffer	Geochemistry	Bishop et al., 1992
Dampier Sub-basin	Sniffer	Geochemistry	O'Brien et al., 1992b
Vulcan Sub-basin	Sniffer	Geochemistry	O'Brien et al., 1992c
Australia Wide Seeps databases	Remote Sensing	SAR	www.npagroup.com; www.infoterra.co.uk
Timor Sea	Remote Sensing	SAR	Jones et al., 2006
Great Australian Bight	Remote Sensing	ALF Mark II	Cowley, 2001a
North Perth Basin	Remote Sensing	SAR	Diggens et al., 2006a
Otway Basin	Remote Sensing	SAR	Diggens et al., 2006b
Perth Basin	Remote Sensing	ALF Mark II	Cowley, 2001b
Barrow and Dampier Sub-basins	Remote Sensing	ALF Mark II	Cowley, 2001c
Browse Basin	Remote Sensing	ALF Mark II	Cowley, 2001d
Arafura Sea	Remote Sensing	ALF Mark II	Martin & Cawley, 1991; Cowley, 2001e
Vulcan Sub-basin, Nancar Trough, western Bonaparte Basin	Remote Sensing	ALF Mark II	Cowley, 2001f
Bonaparte Basin	Remote Sensing	ALF Mark II	Cowley, 2001g
Vulcan Sub-basin, western Bonaparte Basin	Remote Sensing	ALF Mark II	Cowley, 2001f
Petrel Sub-basin, Bonaparte Basin	Remote Sensing	ALF Mark II	Cowley, 2001g
Northern Bonaparte Basin	Remote Sensing	ALF Mark III	Cowley, 2001h
Laminaria High (AC/P16)	Remote Sensing	ALF Mark III	Cowley, 2000a; O'Brien et al., 2004
Nancar Trough	Remote Sensing	ALF Mark III	Cowley, 2000b; Bishop and O'Brien, 1998
Yampi Shelf	Remote Sensing	ALF Mark III	Cowley, 2000c, 2000f
Vulcan Sub-basin	Remote Sensing	ALF Mark III	Cowley, 2000d , 2000e; O'Brien et al., 1998a
Northern Carnarvon Basin	Remote Sensing	ALF Mark III	O'Brien et al., 2003a
Vulcan Sub-basin	Seismic	Core analysis and HRDZ interpretation	O'Brien & Woods, 1995
North West Shelf and Gippsland Basin	Seismic	HRDZ interpretation	Bishop & O'Brien, 1998; Cowley and O'Brien, 2000
Vulcan Sub-basin, Nancar Trough	Integrated	ALF, structural interpretation	Cooper et al., 1998
Timor Sea (S267)	Integrated	SAR, sniffer, seismic, bathymetry	O'Brien et al., 2000, 2001, 2002, 2004, 2005; Jones et al., 2005a & 2005b; Rollet et al., 2006
Cartier Trough	Integrated	Bathymetry, water column and sediment geochemistry	Burns et al., 2001, 2003
Great Australian Bight (SS01/2007)	Integrated	SAR, ALF, seismic	Struckmeyer et al., 2002; Totterdell et al., in press, in prep
Arafura Sea (S282)	Integrated	SAR, seismic, sidescan, geochemistry	Logan et al., 2006; Grosjean et al., 2007; Rollet et al., 2007
Off shore Canning Basin (SS06/2006)	Integrated	SAR, seismic, sidescan, geochemistry	Jones et al., 2007
West Tasmanian margin	Sea-bed sampling	Geochemistry	Hinz et al., 1986
Voluta Trough and eastern Otway Basin	Sea-bed sampling	Geochemistry	Heggie et al., 1988
Otway and Gippsland Basins	Sea-bed sampling	Geochemistry	Heggie et al., 1988; O'Brien & Heggie, 1989
Outer Browse Basin	Integrated	SAR, airborne hyperspectral, seismic, geochemistry	BHP Billiton, Unpublished data (2003), submitted to Geoscience Australia under PSLA Act.

3.1 Stranded bitumens

Various types of petroleum products have been washed onto beaches around Australia's coasts. Records of these strandings date back to the 1800s (Brough-Smyth, 1869; Tate, 1883; Brown, 1898) and elsewhere in the world these sometimes represent evidence of active oil seepage in the surrounding region. Geochemical studies of these naturally occurring bitumens have shown that there are two distinct groups.

The first and most important group by volume and extent of occurrence are the 'waxy bitumens'. These occur as soft waxy, paraffinic, small to medium sized (5-120 mm diameter) rounded lumps and are found from Elcho Island in the Northern Territory, round the southwestern Australian coast along to western Victoria and Tasmania (Dowling et al., 1995; Edwards et al., 1998) (Figure 3). They are geochemically distinct, with high concentrations of biomarkers associated with tropical angiosperms, and closely resemble botryococcane-rich non-marine oils from Central Sumatra (McKirdy et al., 1986, 1994; Currie et al., 1992; Summons et al., 1993; Alexander et al., 1994; Dowling et al., 1995; Padley, 1996). Bitumens collected from the Northern Territory tend to be highly weathered compared to those from temperate latitudes which can contain n-alkanes ranging between C_{16} to C_{35} (Dowling et al., 1995). Long distance oceanic transport is supported by the record of dammar resins washed ashore on the southern Australian coast, as far east as Wonthaggi in Victoria (Murray et al., 1994). The 'waxy bitumens' are interpreted to be derived from natural oil seeps in Indonesia and are transported to southern waters by the Leeuwin current (Currie et al., 1992).

The second group of strandings consists of asphaltic bitumens or 'asphaltites' (Volkman et al., 1992; Edwards et al., 1998). This group typically strands as large (up to 7 kg), flattened, ovoid lumps with deep shrinkage cracks on the upper surfaces (Edwards et al., 1998). Samples have been recorded in Western Australia from as far north as northern Perth (Currie et al., 1998), and along the Southern Australian coastline from the Eyre Peninsula, Kangaroo Island to Cape Otway and around Western Tasmania, Flinders Island and King Island (Sprigg and Wooley, 1963; Sprigg, 1986; Edwards et al., 1998) (Figure 3). However, they have not been recorded in the Northern Territory despite extensive field surveys (Burckhardt and

Bradshaw, 1991; Summons et al., 1993). Early records indicate that 'asphaltite' has been washed ashore in a viscus condition (Wade, 1915) and, in 1965, Reg Sprigg observed 5-cent-sized pieces arriving copiously at Cape Northumberland, South Australia. These were noted to release small gas bubbles when examined under a hand lens (Sprigg, 1986). Lumps, blocks and sheets of often very fresh and sticky oil have been recorded along southern strand lines on open beaches and rocky headlands in South Australia (Sprigg and Wooley, 1963). The asphaltite strandings between the Eyre and Yorke Peninsulas were also noted to arrive in the summer seasons under the influence of strong southerlies (Sprigg, 1964). They are usually found at the high tide mark on medium to high-energy, sandy beaches with gentle to moderate slopes (McKirdy et al., 1994).

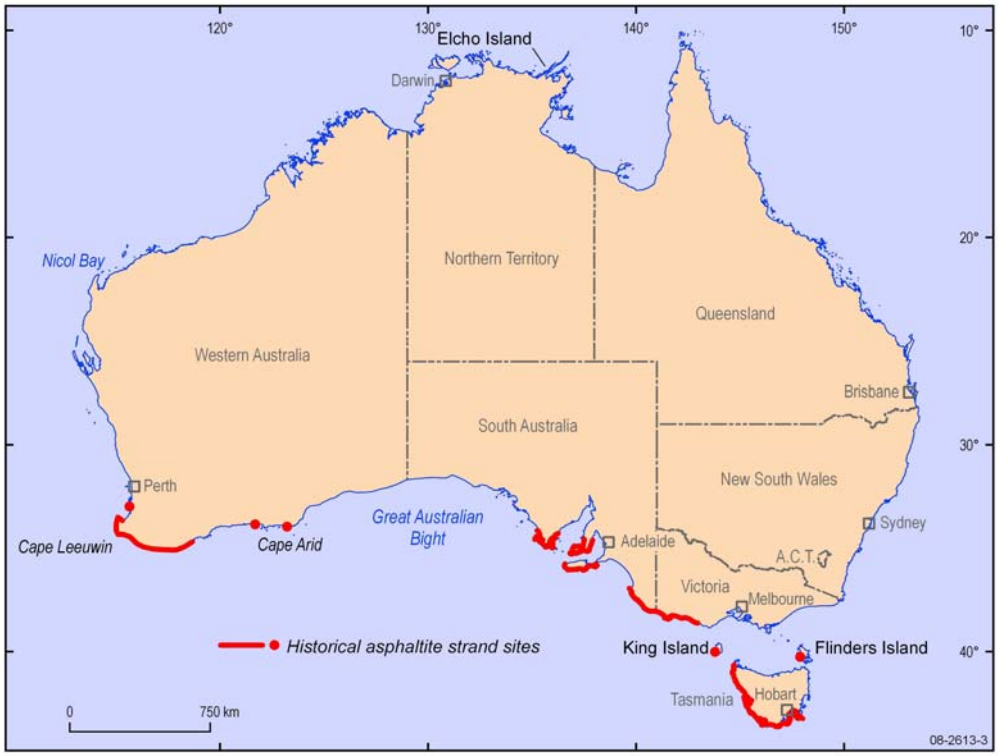

Figure 3. Map of bitumen strandings.

Geochemical analysis of ten bitumen samples collected between 1880 and 1915 from Western Australia to Tasmania indicate they are chemically distinct from the waxy bitumens and not derived from land-pant derived oils of the Bass, Otway or Gippsland Basins (Volkman et al., 1992). This study is significant because the samples were derived from material collected before the widespread importation of oil to Australia

and before any commercial oil discoveries in the region. The asphaltites are marked by a high sulphur content (3-6%) and high proportions of asphaltenes (57-84%) (Volkman et al., 1992; McKirdy et al., 1994; Edwards et al., 1998). Generally the asphaltites are not strongly biodegraded and have n-alkane profiles ranging between C_{10} to C_{40} (max C_{15}-C_{20}), a broad Unresolved Complex Mixture (UCM), with pristane to phytane ratios of around 1 (Figure 4). Biomarker data indicate that the asphaltites are derived from an early mature, siliciclastic marine source rock of late Jurassic to Cretaceous age (Volkman et al., 1992; McKirdy et al., 1994; Edwards et al., 1998).

Thus, the asphaltites provide evidence of an active Late Jurassic to Cretaceous age marine petroleum system somewhere along the southern margin of Australia. Despite the long history of strandings, and suggestions of relatively fresh seepage (Sprigg, 1986), no direct evidence for the location of this seepage has yet been found. However, a recent sampling survey in the Great Australian Bight recovered Late Cretaceous marine organic rich rocks which have a strong geochemical correlation to these asphaltites, thus strengthening the argument that the Ceduna Sub-basin of the Bight Basin may be the source for this distinctive group of asphaltites (Totterdell et al., in press).

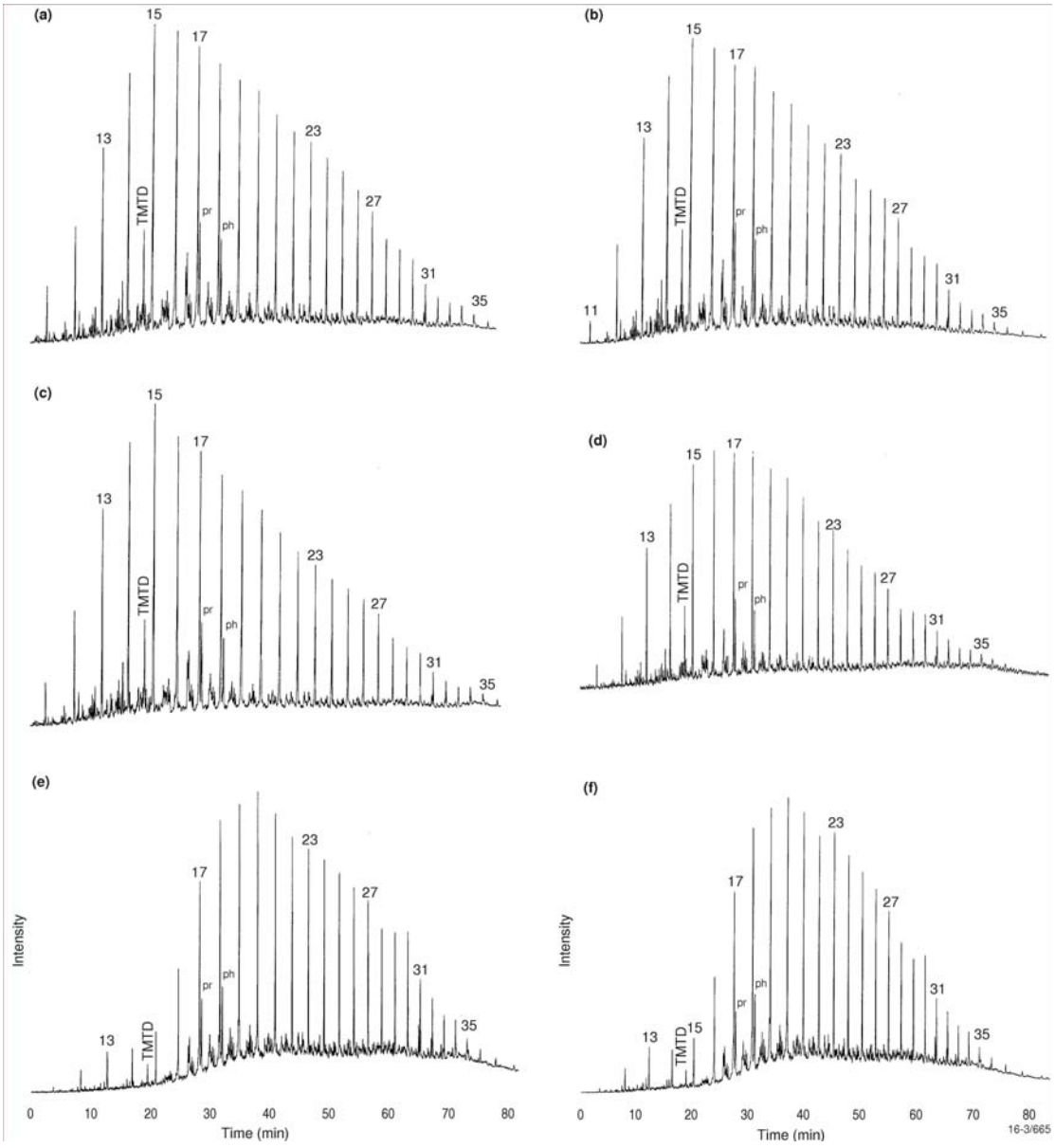

Figure 4. GC traces of stranded asphaltites (Edwards et al., 1998).

3.2 Sniffer studies

Prior to 1988, a marine geochemical 'sniffer' had been used on commercial surveys by InterOcean Systems Inc. in Australia. The sniffer consisted of a submerged 'fish' towed close to the seafloor (Figure 5). Water was continuously pumped from the 'fish' onto the survey vessel, where the water was de-gassed and the resulting gases analysed by gas chromatography. Details of this technique have been published (Sigalove and Pearlman,1975; Sackett, 1977) and results from the North Sea were reviewed by Scheiner et al. (1985).

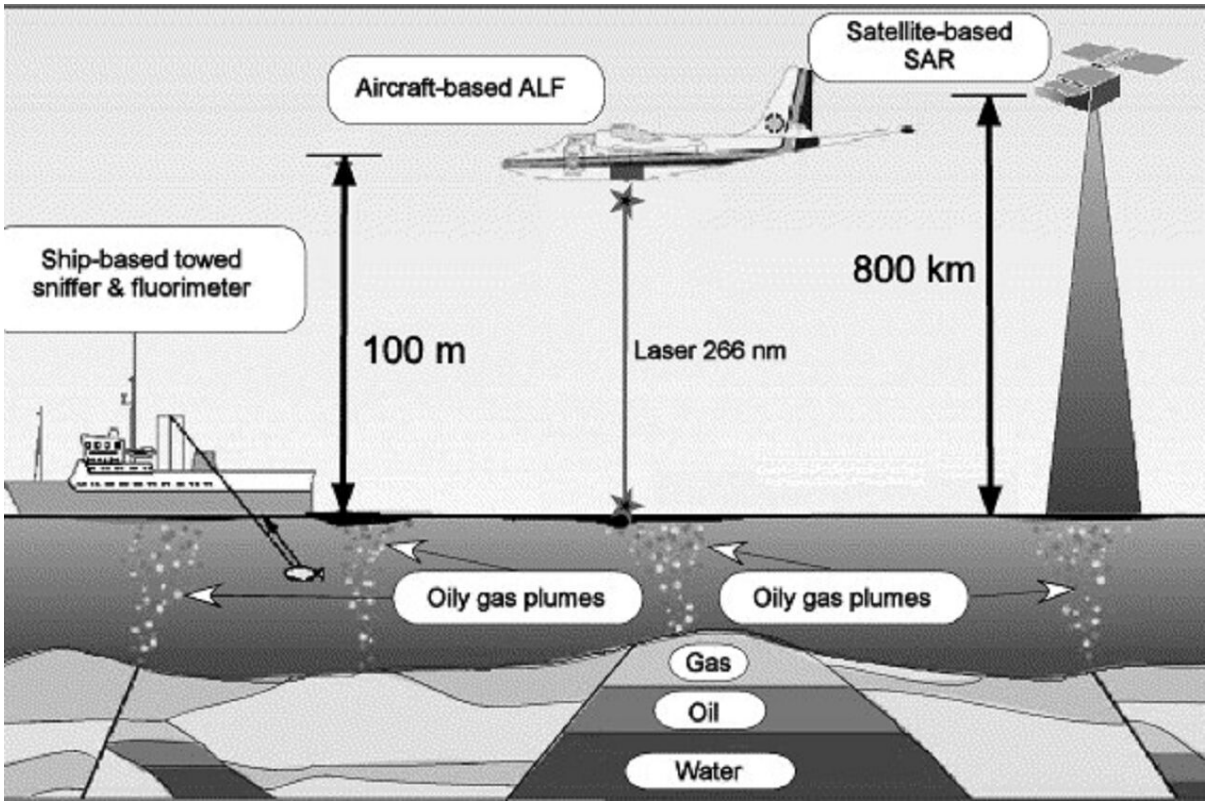

Figure 5. Tools that have been used for detecting and characterising hydrocarbon seeps around Australia, including ship-based water column geochemical 'sniffer' data, aircraft-based Airborne Laser Fluorosensor (ALF) and satellite-based Synthetic Aperture Radar (SAR) (O'Brien et al., 2005).

In 1981, two interpreted seeps were located in the Otway Basin in EPP-18 on a 1634 km survey conducted for Shoreline Exploration Company and Ultramar Australia. One very large gas escape, which coincided with gas bubbles on the sonar

record, was identified 16 km south of Port MacDondell, close to the Nautilus Fault (Sprigg, 1986).

In 1983, two surveys were carried out by Esso Australia in the Gippsland Basin (Figure 2) over several known oil and gas accumulations. On the first survey (May 1983), two significant anomalies were discovered near the Kingfisher Field, close to the Salmon-1 and Swordfish-1 wells. These anomalies could not be detected on the second follow-up survey (November 1983) but this survey did detect several other anomalies associated with the Marlin and Kingfisher Fields. The anthropogenic inputs from petroleum activities provided a complication in this region and Esso Australia concluded that most of the anomalies were related to hydrocarbon production and discharge in the area (Burns and Emmet, 1984). A sniffer survey was also conducted for Getty Oil Development Company Ltd in the Duntroon Basin during 1983 by InterOcean Systems Inc.

In 1989 the Bureau of Mineral Resources (now Geoscience Australia) began a program using a marine based geochemical sniffer under a joint agreement with Transglobal Environmental Geosciences of Leucadia California (Heggie et al., 1990). The aim of the work carried out over the following 6 years was to assess the technology and apply it to regional and prospect surveys, often in conjunction with seismic surveys.

As part of the BMR Continental Margins Program, a 30-day geochemical research program was conducted in the Gippsland, Bass, Otway and Stansbury Basins (Figure 2), to calibrate the sniffer technology and assess the usefulness of the application in assessing basin prospectivity (O'Brien et al., 1992a). Four strong anomalies were identified in the Gippsland Basin. Two of these anomalies were found north of the Barracouta and east of the Seahorse Fields but had low C_1/C_2 ratios (<20) and were enriched in propane. Produced formation waters (PFW) were known to be discharged at 20 m depth, which was close to the tow depth of the 'fish' (25 m), and this, coupled with the distinct molecular composition suggested that these two anomalies had a PFW source. The other two anomalies had a composition more typical of a natural hydrocarbon source and were interpreted to represent seepage of thermogenic hydrocarbons from seeps between the Tuna and Sunfish fields and just north of the Rosedale Fault, close to Wahoo-1. Additionally, four weak anomalies were also

detected, but a vertical profile of gases taken through the water column showed variation of methane concentration with water depth. A surface layer, extending to 50 m depth, was found to be relatively enriched in methane and slightly enriched in ethane and propane. The apparent weak anomalies detected during the survey may therefore relate to variation in tow fish depth, as three of the anomalies were noted to correspond to decreases in depth of the fish (O'Brien et al., 1992a). The anomalies located between Seahorse and Barracouta and between Sunfish and Tuna provided sufficient quantities of gas for isotopic analysis. Methane from sniffer-derived gas near Seahorse had $\delta^{13}C$ compositions ranging between -44.3 to -45.1 ‰, and the seep between Sunfish and Tuna had methane $\delta^{13}C$ compositions ranging between -37.1 to -37.8 ‰. These values indicate that the gas has a thermogenic origin and is not derived from microbial production of shallow biogenic gas.

Data collected in the Bass Basin provided no indications of thermogenic hydrocarbons and variations of ethane and propane were interpreted to be biologically related and correlated with changes in water depth of the tow fish. No thermogenic hydrocarbons were observed over the Stansbury Basin (O'Brien et al., 1992a). A weak propane and butane anomaly was observed in the Otway Basin but this was not accompanied by increases in methane or ethane (O'Brien et al., 1992a).

In the Torquay Sub-basin of the Otway Basin, ethane and propane were observed to significantly increase but this was largely independent of methane concentrations. The anomaly was also observed to increase progressively towards Port Philip Bay. These changes were suggested to be related to anthropogenic hydrocarbons derived from Port Philip Bay under tidal influence (O'Brien and Heggie, 1990). A more subtle anomaly, located at 38º 40.328'S 144º 07.333'E was identified in association with pockmarks and acoustic blanking in seismic data (O'Brien and Heggie, 1990; O'Brien et al., 1992a), but concentrations were too low to determine if the gas had a thermogenic or biogenic origin.

Between 1990 and 1991 the Bureau of Mineral Resources conducted three surveys over the Bonaparte Basin (BMR Surveys 99 and 100; Bishop et al., 1992; O'Brien et al., 1992c) and the Dampier Sub-basin of the Carnarvon Basin (BMR Survey 97; O'Brien et al., 1992b) (Figure 2). Gas levels were observed to increase very sharply

by two orders of magnitude above background in the vicinity of the Petrel 1 well head (water depth ~100 m) which blew out in 1969, whereas only a two-fold increase was observed over a more extensive area in association with the Tern accumulation (Bishop et al., 1992). Seven hydrocarbon anomalies, thought to have a thermogenic origin, were detected along 44 lines and 2730 km of sniffer data (O'Brien et al., 1992c). Lines were run over a series of commercial hydrocarbon discoveries and accumulations to allow 'ground-truthing', and then tested against undrilled prospects. Two distinct groups of anomalies were recorded. The first group occurred around the Skua oil-gas field and to the north-east in the Swan graben. Methane increased by two-fold above background, but ethane was enriched by an order of magnitude. The second group was located along an interpreted NW-trending transfer fault and its intersection with the Vulcan Sub-Basin/Londonderry High boundary zone. Gas wetness did not increase with methane concentration in this group (O'Brien et al., 1992c). Vertical profiles taken through the water column showed an increase in methane between 95 m and the seafloor. This indicates that caution needs to be used when interpreting subtle anomalies (O'Brien et al., 1992c), because relatively small changes in methane concentration may be related to changes in tow-fish depth.

Twenty-five lines of sniffer data were acquired in co-operation with Woodside in the Dampier Sub-basin in permit WA-28-P between the Angel gas field and Madeleine 1 (Figure 2). No significant hydrocarbon anomalies were detected, even though many lines were collected over the Wanaea, Cossack and Angel accumulations (O'Brien et al., 1992b).

In 1996, AGSO Marine Survey 176 collected 3535 km of sniffer data in 150 survey lines across the Yampi Shelf and Sahul Platform (Wilson, 2000). The principal areas of interpreted seepage were inboard of the Cornea trend on the Yampi Shelf, where an area of active gas seepage with gas concentrations two orders of magnitude above background was detected. This dataset is well documented for the Yampi Shelf in O'Brien et al. (2000, 2002, 2005). However, many of the interpreted anomalies are within a few parts per million (ppm) of background and are probably not related to seepage.

Summary of Key Points and Implications

The success of the sniffer methodology was dependent on the instrument being towed through a field of active gas seeps. Such seeps are not common, and even in locations of long-lived seepage, the gas release can be episodic or strongly influenced by tidal cycles (Rollet et al., 2006). Furthermore, much of the data collected during sniffer surveys contains interpreted gas anomalies that are only twice the concentration of regional background concentrations, for example 3.5 to 5.5 ppm over the Skua Field (O'Brien et al., 1992c).

There is also a tendency in the reports to over-interpret gas compositions, in particular the wetness of extracted gases, where gas wetness values of up to 16% were noted in the Petrel Sub-Basin (Bishop et al., 1992). This increasing gas wetness was often interpreted as a sign of an oil-prone source. However, a re-examination of the data and procedures suggests that apparent high levels of gas wetness are more likely to be related to low gas concentrations and/or leakage of methane during sampling. The data have also been shown to be influenced by variation in tow depth, where gases varied in concentration with depth, and also anthropogenic effects related to release of produced formation waters and petroleum hydrocarbons. Therefore, caution needs to be applied when reviewing sniffer data, and interpretations should not be taken at face value.

Despite these problems, several seeps were identified using these data. An anomaly two orders of magnitude above background identified close to the Cornea oil and gas field (Figure 6; Figure 7) (O'Brien et al., 2000) is clearly derived from natural seepage and this was confirmed by geochemical analysis of the gas extracted from the water (O'Brien et al., 2000) and later field studies (Jones et al., 2005a; Rollet et al., 2006). These data are very important because they also have implications for interpreted gas anomalies at lower gas concentrations. Figure 8 shows an image presented in O'Brien et al. (2000) that was used to illustrate a gas anomaly with seismic context. The scale used to present the gas data in Figure 7 and Figure 8 are different and this leads to a rise in gas concentrations in Figure 8 potentially gaining greater significance than it merits. When both datasets are plotted on the same scale (Figure 9) it becomes apparent that the gas anomaly in Figure 7 is far greater than that in Figure 8. The anomaly shown in Figure 7 is definitely a seep but the data presented

in Figure 8 must be disregarded (Figure 9). Significantly, gas levels in the vicinity of the blown out well head of Petrel 1 were also two orders of magnitude greater than background. This indicates that active gas seepage into the water column should have a detectable and significant effect when measured using the gas sniffer. It also suggests that low level gas concentration variations, previously interpreted as seepage, may not be related to seepage unless other supporting evidence can be provided. For example, low level anomalies found in association with pockmark fields and acoustic blanking in the Torquay Sub-basin are probably related to shallow gas (O'Brien and Heggie, 1990; O'Brien et al., 1992a). However, it is not clear from the data whether this gas was biogenic or thermogenic. The sniffer program was discontinued by the Australian Geological Survey Organisation in 1997.

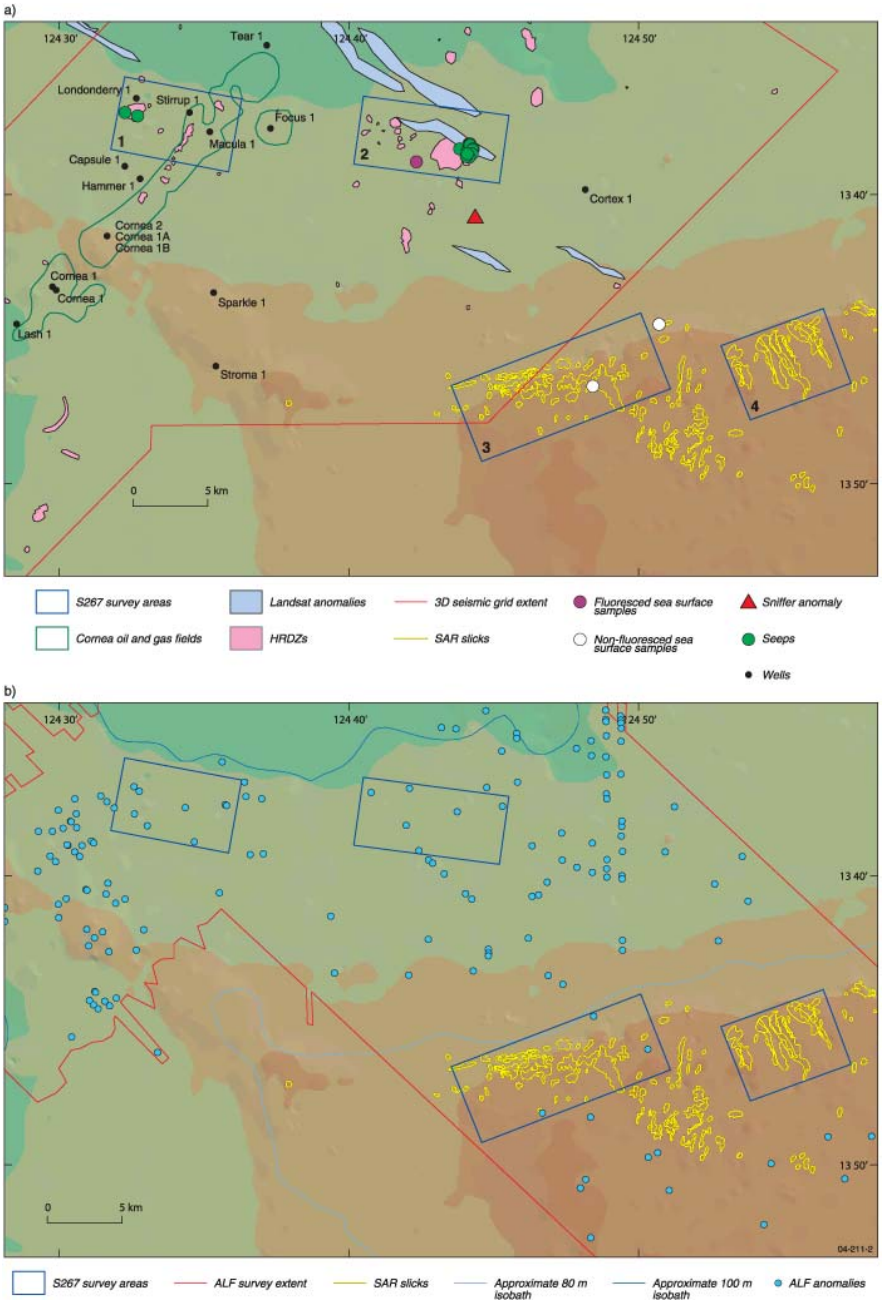

Figure 6a. SAR (NPA et al., 1999) and LANDSAT (IAM, 2000) datasets and interpreted HRDZs (Shell, 2000; see section 3.5 for description of HRDZs) utilised in planning GA survey 267. Location of the Cornea oil and gas field (Ingram et al., 2000), active seeps imaged and observed during GA survey 267, the 100 times background sniffer anomaly (O'Brien et al., 2000, 2005) and surface seawater samples from GA survey 207 (Edwards and Crawford, 1999) are also shown. Note that the SAR slicks are the only potential indicators of hydrocarbon seepage over the Yampi Shelf headland. 6b. ALF anomalies across the Yampi Shelf. Note that the density of anomalies is significantly greater to the north of the headland than in the vicinity of the slick cluster interpreted from SAR data (O'Brien et al., 2000, 2005).

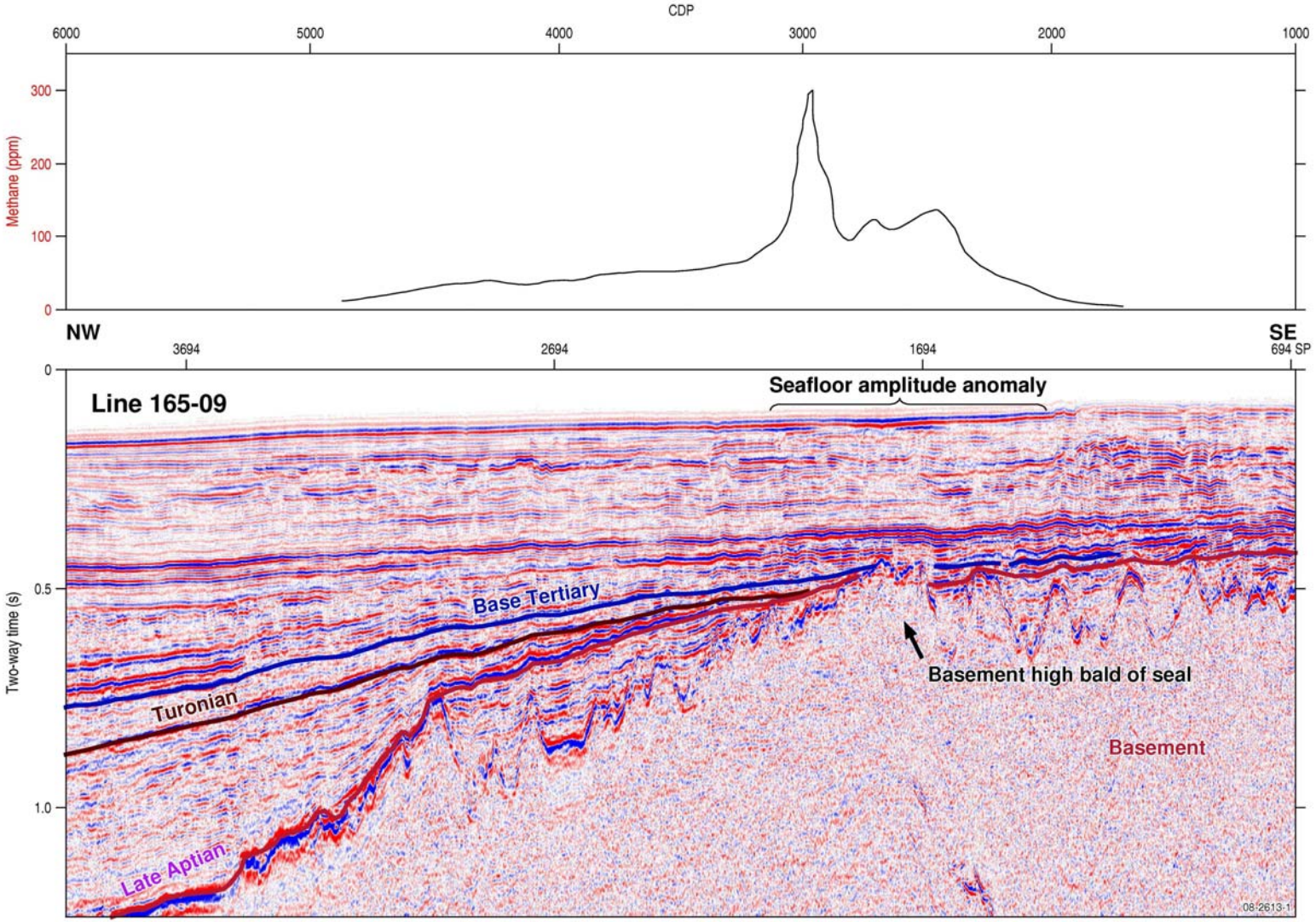

Figure 7. Water column geochemical sniffer profile overlain on regional seismic line YST 165-09 from the Yampi Shelf, showing a methane anomaly two orders of magnitude above background (O'Brien et al., 2000, 2005).

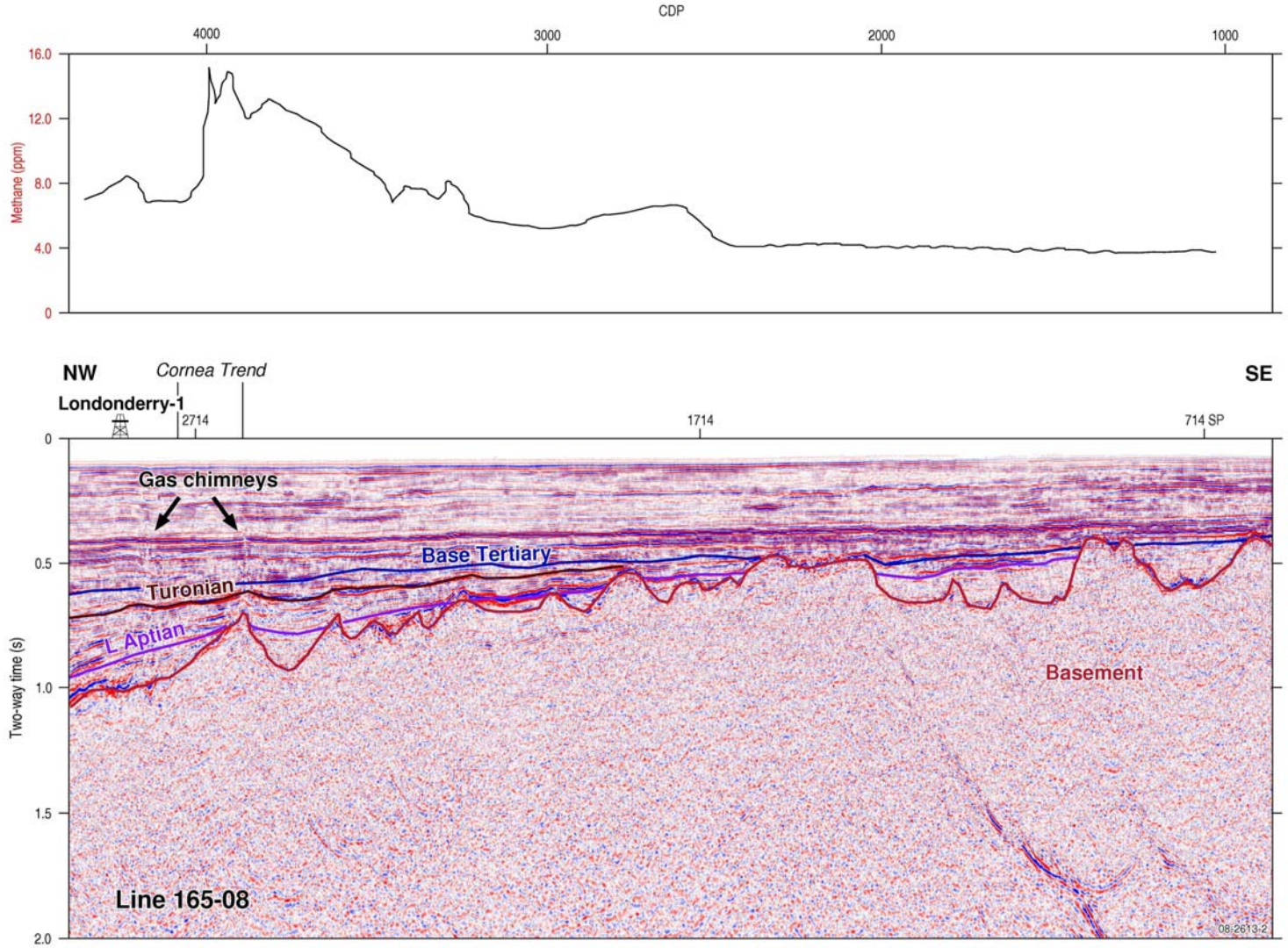

Figure 8. Water column geochemical sniffer profile overlain on regional seismic line YST 165-08 from the Yampi Shelf. O'Brien et al. (2000, 2005) interpreted the methane peaks over the Cornea Trend as being the result of natural seepage associated with the underlying gas chimneys.

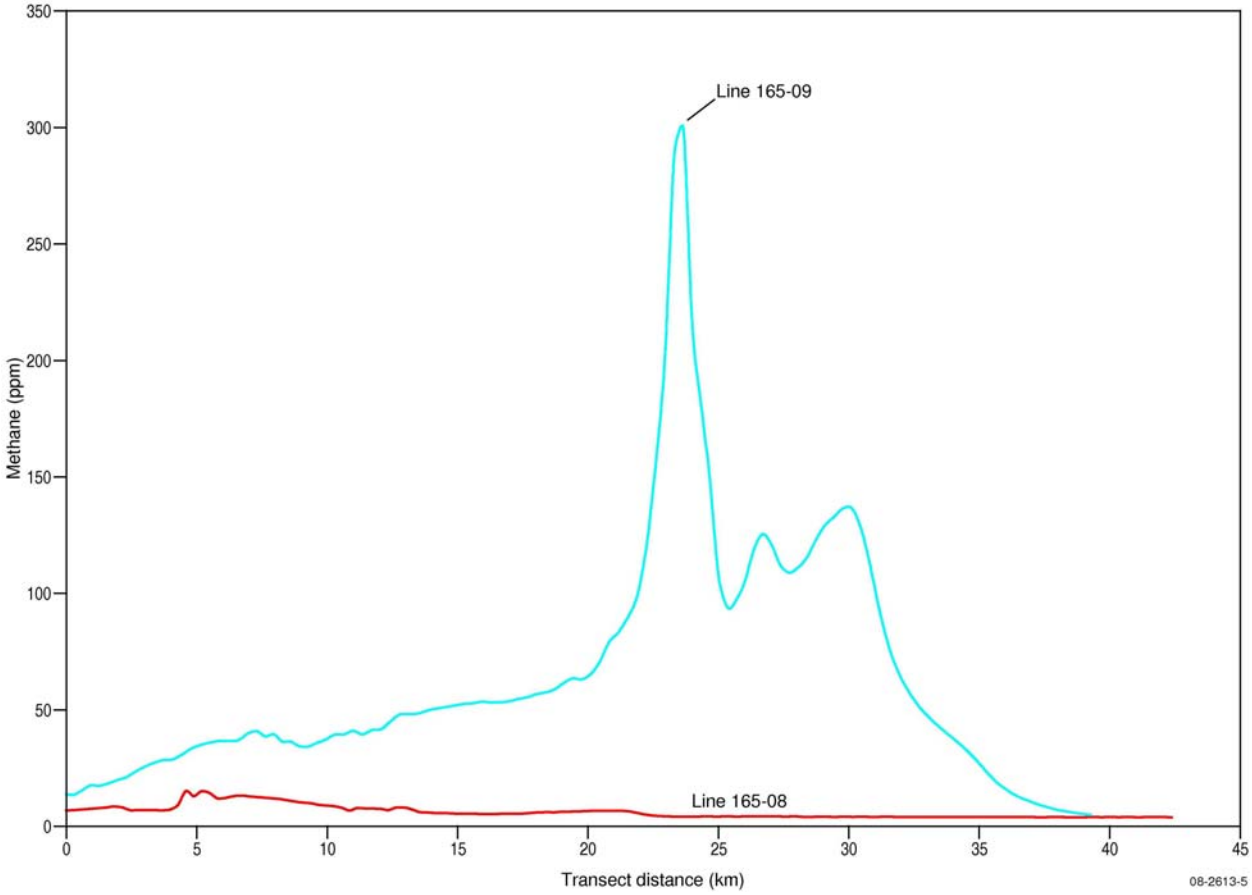

Figure 9. Methane profiles from the preceding figures plotted at the same scale. The magnitude of the genuine seep from line 165-09 suggests that line 165-08 records variations in background methane levels.

3.3 Satellite-based remote sensing studies in Australia

Satellite-based remote sensing technologies have been utilised in numerous studies to determine the distribution and frequency of hydrocarbon slicks within basin systems around Australia. The remote sensing tool that has been most commonly used for detecting natural hydrocarbon seepage slicks in Australia's offshore environments is Synthetic Aperture Radar (SAR). SAR has become a highly successful tool for delineating where natural hydrocarbon seepage forms oil slicks on the sea surface (eg. Offshore Angola, Caspian Sea; Williams and Lawrence, 2002). Advantages of SAR include the relatively low cost of acquisition in relation to data coverage, and the ability of the instrument to penetrate cloud cover. SAR is a side-looking radar mounted on a moving satellite platform (Johannessen et al., 1994). SAR sensors send

out a microwave signal, typically with a wavelength of several centimetres, and build an image from the radiation reflected back to the satellite. Incident radar waves are emitted at an oblique angle to the ocean surface (e.g. 23° for ERS-1 SAR); therefore backscatter relies on a roughened sea surface. SAR slicks are areas that have anomalously low backscatter values in the context of the surrounding data i.e. areas in which the capillary waves on the ocean surface have been dampened. Dampening of capillary waves may occur through a variety of processes, which include films of oil, the sea surface microlayer (natural film) or biological material (eg. algae), or through physical processes such as current flow or wind shadowing (Espedal et al., 1996; NPA et al., 2003).

Detection of slicks depends critically on wind speed/shear; therefore it is important to have information on wind and sea state conditions coincident with image acquisition. Optimum wind speeds for oil slick detection are between 3 and 6 m/s according to Harahsheh *et al.* (2004). Wind speeds less than 3 m/s produce little difference in backscatter between the relatively calm ocean surface, oil damped slicks and natural film slicks (Brekke and Solberg, 2005). The upper threshold for SAR based oil slick detection is between 10 and 14 m/s, as higher wind speeds result in the disintegration of slicks (Ivanov, 2000). Details of different remote sensor applications and their limitations are discussed in Section 4.

Global SAR coverage of Australia's offshore jurisdiction, including interpretations of natural hydrocarbon seepage and pollution slicks, is available in two independent datasets from Infoterra Ltd and NPA Ltd. Details of their commercial, non-exclusive products are available from:

Infoterra – www.infoterra.co.uk and by contacting info@infoterra-global.com

NPA - www.npagroup.com and by contacting info@npagroup.com

Assessments of natural hydrocarbon seepage that have included interpreted SAR slicks have been documented for the Timor Sea (O'Brien et al., 2000, 2001, 2002, 2003b, 2004, 2005; Jones et al., 2005b, 2006; Rollet et al., 2006), the central North West Shelf (NWS) (O'Brien et al., 1998b, 2003a,b, 2004; Jones et al., 2007), the Great Australian Bight (Struckmeyer et al., 2002), and the Arafura Sea (Rollet et al.,

2007).

Early studies of natural hydrocarbon seepage in the Timor Sea revealed SAR signatures interpreted to indicate widespread and intense palaeo- and present day natural hydrocarbon seepage (O'Brien et al., 2000, 2001, 2002, 2003b). A subsequent marine survey identified hydrocarbon seepage on the Yampi Shelf, but active seepage was not observed in association with the SAR slicks (Figure 6a) (Jones et al., 2005a; Rollet et al., 2006). Mapping of bathymetric channels, in 50 to 80 m water depth, directly beneath the Yampi Shelf SAR slicks using multibeam swath bathymetry indicated that tidal current flows most likely contributed to slick formation. In contrast, coral spawning appears to have contributed to the formation of annular to crescent-shaped SAR slicks associated with submerged reefs and shoals over the nearby Browse-Bonaparte transition zone (Jones et al., 2005b, 2006). Details of the Timor Sea SAR reassessment is presented in Section 4.4.

Landsat is an alternate satellite-based remote sensing technology that has been used to characterize seepage in the Timor Sea (Jones et al., 2005b; Rollet et al., 2006). Landsat Thematic Mapper (TM) is a multispectral scanning radiometer that was carried on board Landsats 4 and 5. TM image data consist of seven spectral bands with a spatial resolution of 30 m for most bands (1-5 and 7). Sea surface features identified in Landsat scenes covering the Yampi Shelf (Figure 6), which were interpreted to represent potential hydrocarbon slicks, were clustered in the vicinity of active seepage sites (IAM, 2000).

A number of SAR slicks on the southern edge of the Bedout Sub-basin (Figure 10), suggested to be related to hydrocarbon seepage at the edge of the regional seal by O'Brien et al. (2003), were investigated during the course of marine survey SS06/2006 to determine whether they may be related to bathymetric features (Jones et al., 2007), as had been demonstrated on the Yampi Shelf. The Bedout Sub-basin slicks were found to be located above a shallow bathymetric high (0 to 50 m water depth) and, given that no evidence of hydrocarbon seepage was detected, it is assumed that they are related to the bathymetry. However, there was not a 'one-to-one' correlation between the shapes of the slicks and the underlying bathymetric features, as there was on the Yampi Shelf (Jones et al., 2005b, 2006).

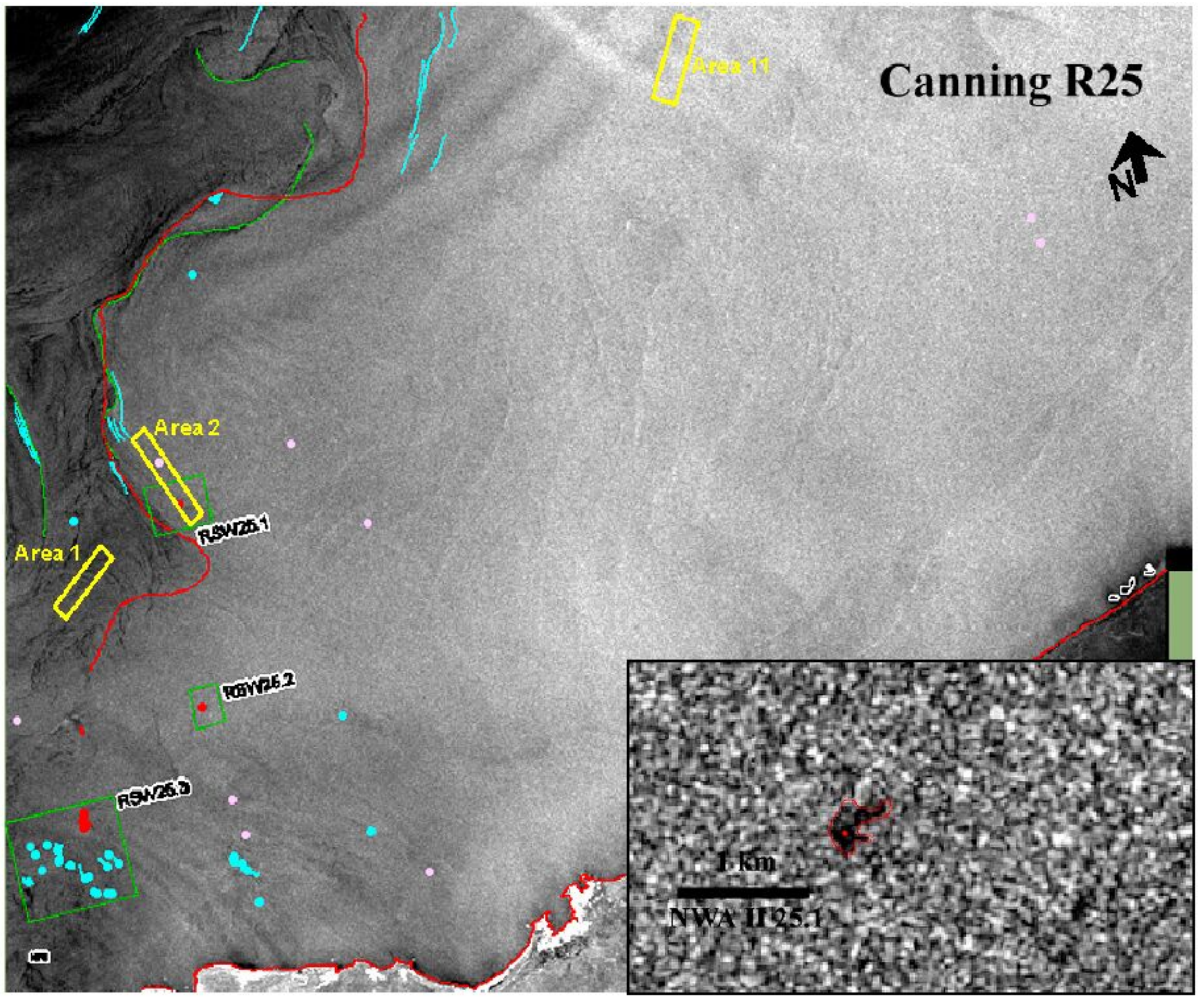

Figure 10. NPA SAR scene showing interpreted slicks over the southern edge of the Bedout Sub-basin (red points – 2nd rank slicks; pink points – 3rd rank slicks; blue points – natural film slicks). Yellow boxes are survey areas from SS06/2006. The red line marks a weather front and the blue lines are interpreted internal waves. Green boxes mark extracts presented in O'Brien et al. (1998b). Inset shows extract RSW25.1, displaying a 2nd rank SAR slick.

A site of interpreted SAR slicks from the shallow water (<250 m) Arafura Sea (Figure 11) was studied for active seepage using sidescan sonar and 12 kHz echosounder during Survey S282 (Rollet et al., 2007). No evidence of active seepage flares in the water column was identified in the area, but the juxtaposition of a deep sediment depocentre, various vertical fluid migration pathways (partly along faults), seabed pockmarks and the sea surface SAR slicks suggest that there may be an active petroleum system that is seeping.

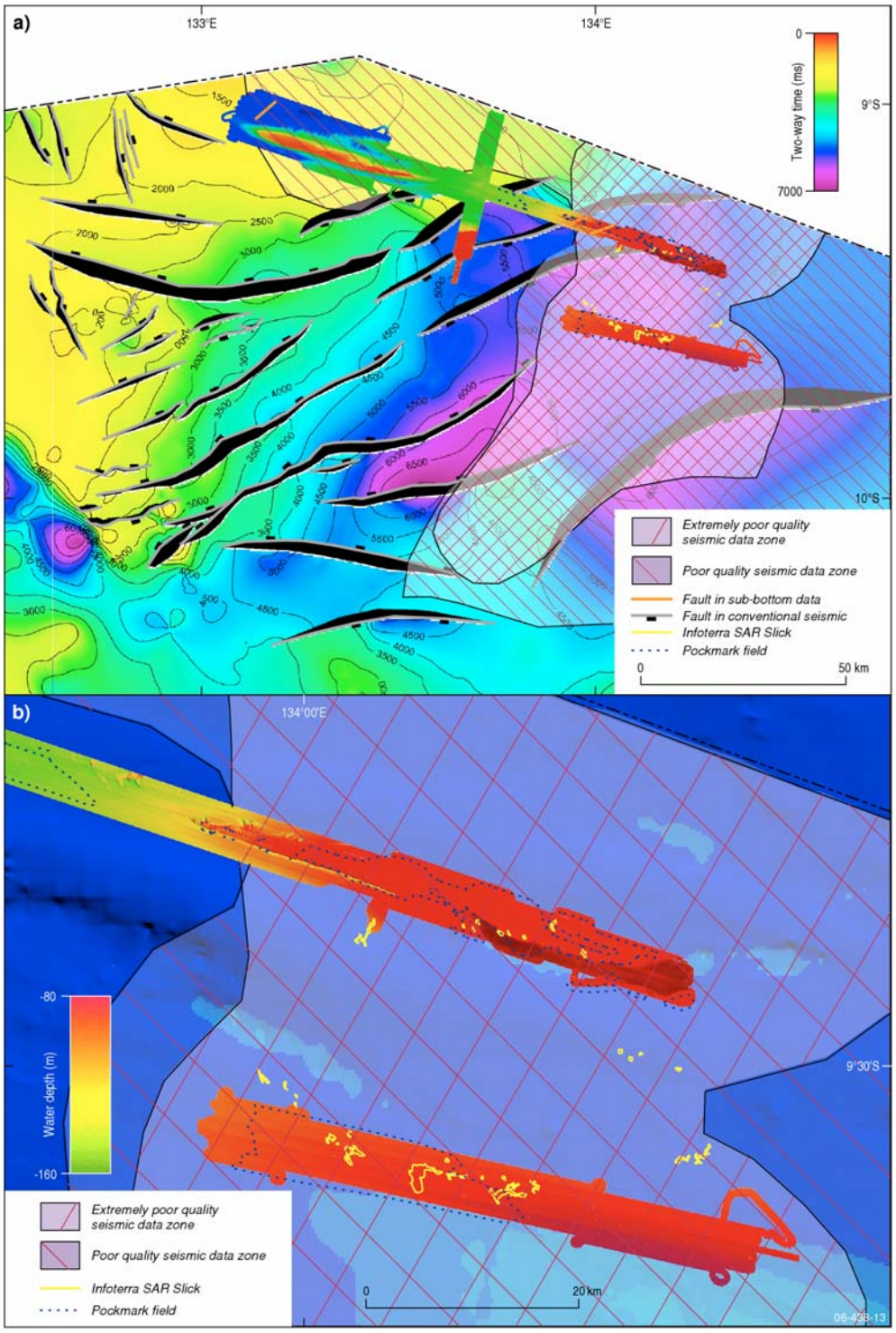

Figure 11. (a) Structure map (in twt) of the Base Wessel Group (Proterozoic) showing major SW-NE Proterozoic faults (Totterdell, 2006) and interpreted SAR anomalies (Infoterra) and pockmark fields. (b) Multibeam bathymetry image for Areas C and D showing pockmark fields interpreted from sidescan sonar data and interpreted SAR anomalies (Infoterra). The PQDZ correlates with a deeper part of the structure map. The SAR and pockmarks appear to correlate with the edge of the interpreted regional seal across one of the depocentres (from Rollet et al., 2007).

Locations of interpreted SAR slicks from the Great Australian Bight (Struckmeyer et al., 2002) were investigated during marine survey SS01/2007 (Mitchell, 2007), but detailed results of the survey were not available at the time of writing.

3.4 Airborne Laser Fluorosensor (ALF) studies

The Airborne Laser Fluorosensor (ALF) was first described by Clarke et al. (1988) and in subsequent publications by Martin and Cawley (1991) and Williams (1996). ALF was developed by British Petroleum's (BP) Research Centre during the 1970s and 1980s as a means of identifying hydrocarbon seepage in frontier basins around the world. The ALF technology was subsequently sold to World Geoscience Corporation Ltd (now Fugro Airborne Surveys) in 1990, as part of BP's technology outsourcing program (O'Brien et al., 2003a, 2004).

The ALF system comprises a solid state laser pulsed at high frequency (50 Hz) from an aircraft flying at 80 or 100 m above sea level. At sites of natural hydrocarbon seepage the laser induces fluorescence in any polyaromatic hydrocarbons derived from crude oil that have leaked to the sea surface. The photo-excited emission and back-scatter from the sea surface is captured by a telescope and separated into its constituent spectral wavelengths by a spectrograph, with the dispersed light fed onto an array of detectors that define a series of wavelength bands. Early versions of the system used an emission wavelength of 308 nm; this was later reduced to 266 nm to give a wider spectral window in the Mark III system (Martin and Cawley, 1991; Williams, 1996).

Reported advantages (Martin and Cawley, 1991; Williams, 1996; O'Brien et al., 2003a, 2004) of using ALF to detect natural hydrocarbon seepage include:

- Very high sample rate – with a sample 'shot' being acquired every 1.5 m on the surface (approximately 20 cm^2) of the sea. This is two orders of magnitude greater than SAR. Consequently, ALF can detect very small slicks which SAR would fail to detect.
- ALF is sensitive to very thin films – as thin as 0.01 microns, which is ten times thinner than visible to the naked eye.

A fluorescence anomaly (fluor) can be detected by an increase in the area of the

fluorescence response region of the ALF spectrum. For a variety of reasons, the magnitude of each ALF spectrum can vary significantly from shot to shot. The fluorescence area value is usually normalized using the Raman area to produce a more consistent measure of fluorescence intensity. This ratio is called the fluorescence on Raman area ratio, usually denoted as F/R, which provides an estimate of the fluorescence intensity. Because of the changing F/R trends, a constant F/R cutoff level cannot be used to detect fluors. An average of the F/R ratio is used as an estimate of the background F/R level at any point. Only spectra having an F/R value significantly above the background level are selected as possible fluors. A scaling factor (usually selected between values of 1.05 and 1.5 for each line depending on the amount of scatter in the F/R plot) moves the averaged curve above the F/R values of most of the spectra. Confident fluors are then manually picked from the possible fluors (Cowley, 2001a-h).

The following discussion presents a summary of some of the significant ALF surveys that have been undertaken around Australia, particularly those with which Geoscience Australia were involved. The major findings and subsequent interpretations from these studies are described, and some of the short-comings are discussed.

A series of ALF (Mark II) surveys were acquired around Australia in 1989 by BP, with the data reprocessed by Signalworks Pty Ltd under contract to Geoscience Australia (O'Brien et al., 2001) (Figure 2). The surveyed areas were located in the Great Australian Bight (Cowley, 2001a), Perth Basin (Cowley, 2001b), Carnarvon Basin (Cowley, 2001c), Browse Basin (Cowley, 2001d), Bonaparte Basin (Cowley, 2001f-h) and Arafura Sea (Cowley, 2001e). The survey areas varied from 850 km by 100 km for the Bight survey to 150 km by 80 km for the Browse Basin survey. Line spacing varied from 5 km in the majority of surveys to 1.9 km in the northern Bonaparte Basin. The surveys were designed to detect natural oil seepage in an effort to improve knowledge about petroleum prospectivity.

Cowley (2001a-h) reported no significant findings related to natural hydrocarbon seepage from the Mark II ALF surveys acquired around Australia in 1989. Variations in the spatial density of fluors, such as in the Bight (Cowley, 2001a) and Bonaparte Basin surveys (Cowley, 2001g,h), were attributed to variations in sea state or water properties. However, the fluors in the Bight were presented as possible evidence of

seepage in Struckmeyer et al. (2002). High intensity fluors in the vicinity of islands and reefs in the Perth (Cowley, 2001b), Carnarvon (Cowley, 2001c) and Browse Basin surveys (Cowley, 2001d) were attributed to 'exposed island material fluorescing'. A patch of very strong fluors over the Jabiru Field in the western Bonaparte Basin was interpreted to be anthropogenic slicks related to the field development rather than natural oil seepage (Cowley, 2001f). In general, the Mark II ALF system acquired relatively noisy data comparative to the subsequent Mark III ALF system, and in most cases the line spacing was insufficiently close to detect most fluor clusters (Cowley, 2001a-h).

A series of ALF (Mark III) surveys were acquired over the northern North West Shelf in 1996 by World Geoscience Corporation (now Fugro Airborne Surveys) for Geoscience Australia (formerly AGSO) (Figure 2). These data were also reprocessed by Signalworks Pty Ltd, under contract to Geoscience Australia (O'Brien et al., 2001). The surveyed areas were located in permit AC/P8 over the Laminaria High (Cowley, 2000a), permit AC/P16 over the Nancar Trough (Cowley, 2000b), the Yampi Shelf (Cowley, 2000c), and the Haydn (Cowley, 2000d) and Skua (Cowley, 2000e) areas in the Vulcan Sub-basin. The survey areas were generally much smaller than the previous Mark II surveys, and the line spacing was similarly reduced (down to 300 m in the Vulcan Sub-basin; Cowley, 2000e). The data from the ALF Mark III surveys were relatively noise free with no serious navigation problems (Cowley, 2000a-e). Fluors interpreted as showing confident oil fluorescence spectra were identified in all the of the North West Shelf ALF Mark III surveys undertaken in 1996.

In the AC/P8 survey, relatively high densities of fluors ranging up to medium size (maximum fluorescence intensity (F/R) in the AC/P8 survey was 1.05-1.20) were interpreted to indicate a working source and migration system, although fluor clusters were notably absent from the Corallina Field and only a few fluors were located over the Laminaria Field (Cowley, 2000a; O'Brien et al., 2004) (Figure 12). O'Brien et al. (2004) stated that fluor distribution in the vicinity of the fields appears as a halo; fluors are present around the circumference of the fields but there are no fluors directly over the field. O'Brien et al. (2004) interpreted this to represent no leakage over the fields due to high fault seal integrity, with prolific seepage away from the

fields in areas of poor fault seal.

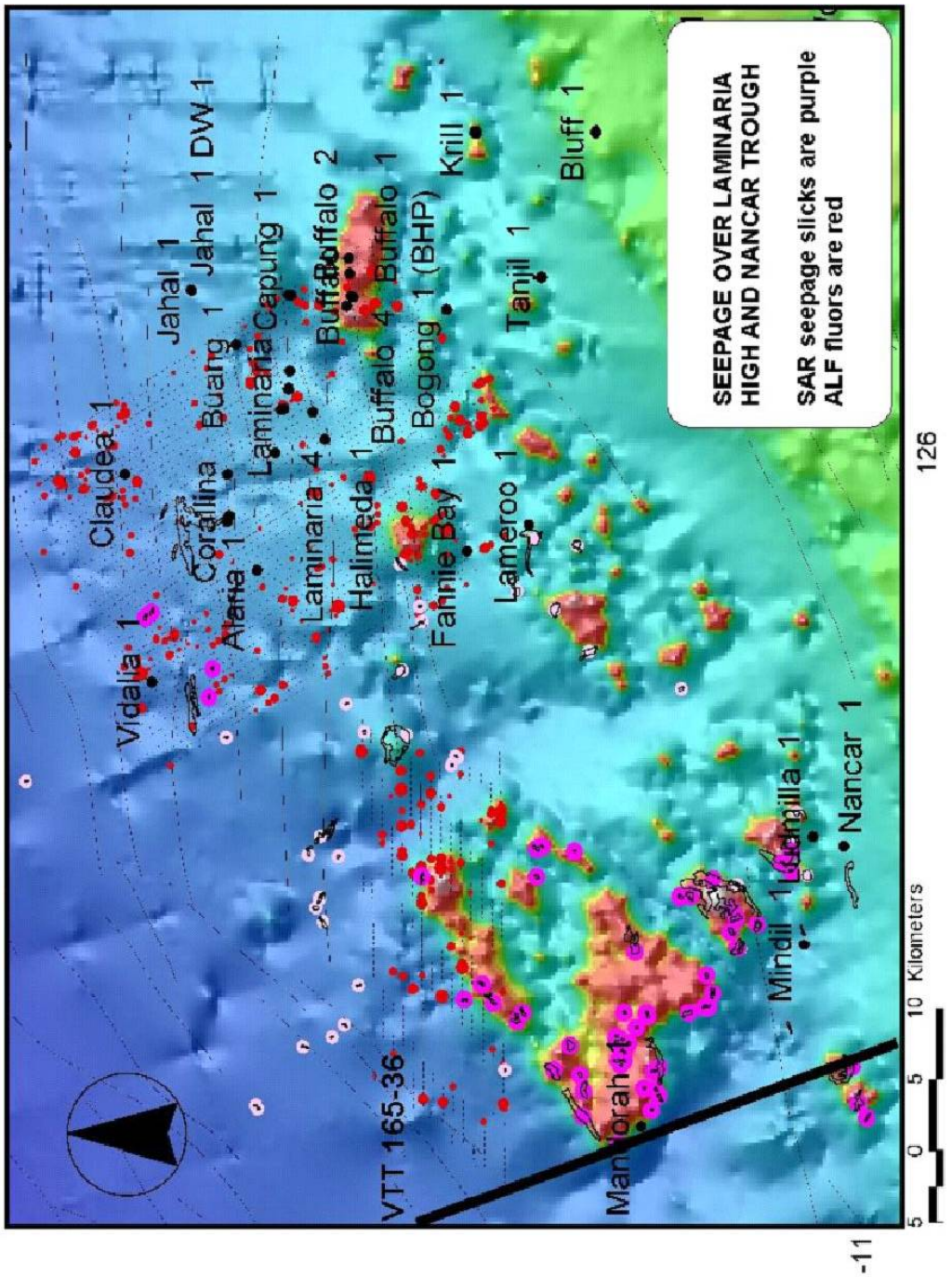

Figure 12. Location map in Nancar Trough-Laminaria High area (O'Brien et al., 2004). Positions of Second Rank (large purple dots) and Third Rank (smaller, lighter mauve dots) are indicated, as are locations of ALF survey lines. ALF anomalies or fluors are shown as red dots, with larger dots representing stronger anomalies. Background is bathymetry.

Cowley (2000b) described 111 fluors, mostly in two clusters from the eastern half of the AC/P16 survey, as showing confident oil fluorescence spectra. Cowley (2000b) further stated that the fluors are of small to medium intensity, with none having F/R area ratios larger than 0.75. In contrast, Bishop and O'Brien (1998) described the intensity of the fluors as variable, but that many were of high intensity. Bishop and O'Brien (1998) attributed the fluors to condensate on the sea surface, except for five fluors in the northwest that were attributed to algae (the reasons for these interpretations were not presented). Correlation of the ALF anomalies from this area with other indicators of natural hydrocarbon seepage are discussed in Section 3.5.

Of the 183 fluors picked during the interpretation of the Skua survey, 70 were high intensity fluors (Cowley, 2000e). Three main clusters of high intensity fluors were identified: near the Eclipse 1 well, southwest of East Swan 1 and over the Skua Field (Figure 13). The latter may be related to natural leakage of hydrocarbons from the Skua Field. Cowley (2000e) concluded that direct correlation between fluor clusters and accumulations is tenuous, although the discovery of oil in Swift North 1 in the area covered by the southernmost of the three main clusters (DPIFM, 2007) improves the correlation. Cowley (2000e) suggested that the remaining fluor clusters to the northeast and southwest of East Swan 1 may indicate improved prospectivity in those regions, but the presence of fluors to the northwest is inconsistent with the lack of hydrocarbons in Eclipse 1. O'Brien et al. (1998a) suggested that the ALF fluors in the northeast of the area reflect present day migration into, and up out of, the breached East Swan and Eclipse structures. This interpretation was likely based on the data prior to reprocessing by Signalworks Pty Ltd in 2000.

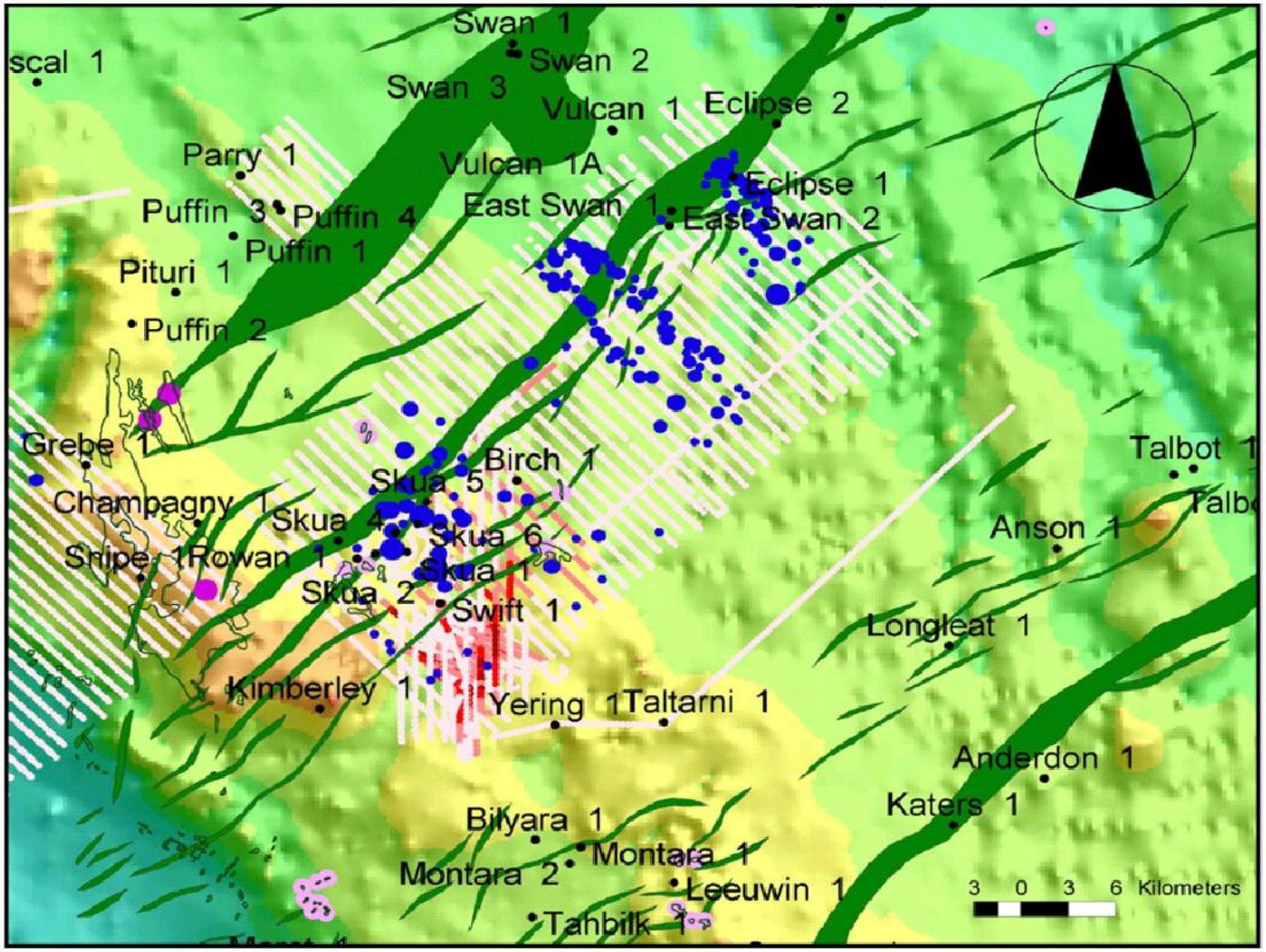

Figure 13. SAR, ALF and sniffer results from the southern Vulcan Sub-basin (O'Brien et al., 2004). SAR slicks are purple (Second Rank) and light mauve (Third Rank); ALF anomalies are blue, with larger dots representing larger anomalies; sniffer results represent ethane in bottom waters, with pink being background concentrations, and red over 100 times background. Sniffer, SAR and ALF anomalies are all focused around the Skua-Swift area. Also shown are Callovian fault trends (green).

In contrast to the adjacent Skua area, only 21 fluors were interpreted as showing confident oil fluorescence spectra from the Haydn survey. With the exception of one fluor (F/R area ratio 1.17), none of the fluors have an F/R ratio exceeding 0.6. Cowley (2000d) stated that no significant fluorescence clusters were observed. In contrast, and presumably also on the basis of the data prior to reprocessing, O'Brien et al. (1998a) described four well-defined zones of seepage from the ALF data, with one particularly prominent zone associated with the Haydn prospect. However, the most intense fluor from the area documented by Cowley (2000d) is not included in one of these four zones documented by O'Brien et al. (1998a).

In the 1996 Yampi survey, 57 fluors with confident oil fluorescence spectra were found mostly in the eastern half of the survey area (Cowley, 2000c). These were mostly low intensity fluors distributed in broad clusters. A second Yampi ALF survey was undertaken 1998 (Cowley, 2000f), re-covering and expanding on the area covered in the earlier survey. Together, these surveys encompassed the area in which natural hydrocarbon seepage was subsequently directly observed on the Yampi Shelf (Rollet et al., 2006) (Figure 6b). From the second survey, 37 fluors were selected as confident fluorescence spectra in an initial interpretation, and 132 fluorescence spectra were picked in a second more detailed interpretation (through changing the channel on which the ratio was calculated). The high confidence fluors are focussed along the oil-prone Cornea trend (O'Brien et al., 2005), in the vicinity of the western seep site identified by Rollet et al. (2006). A high amplitude fluor and a cluster of lower amplitude fluors are located in the northern part of the survey. The remaining survey area contains a scattering of low amplitude fluors showing no obvious patterns. Fluors were not identified in the vicinity of the primary (eastern) seep site identified in Rollet et al. (2006) (Figure 6b).

A Mark III ALF survey was acquired in the western Roebuck and northern Carnarvon Basins by World Geoscience Corporation (now Fugro Airborne Surveys) for BHP Petroleum and a number of its joint venturers in 1998 (O'Brien et al., 2003a) (Figure 14). A total of 1016 fluors were detected, primarily in the southeastern part of the study area. O'Brien et al. (2003a) interpreted the majority of the fluors to have a spectral signature that is consistent with a condensate origin. They also suggested that fluors classified by their spectral signature as being heavier or more oil-prone, are

even more strongly clustered in the southeast (Figure 14).

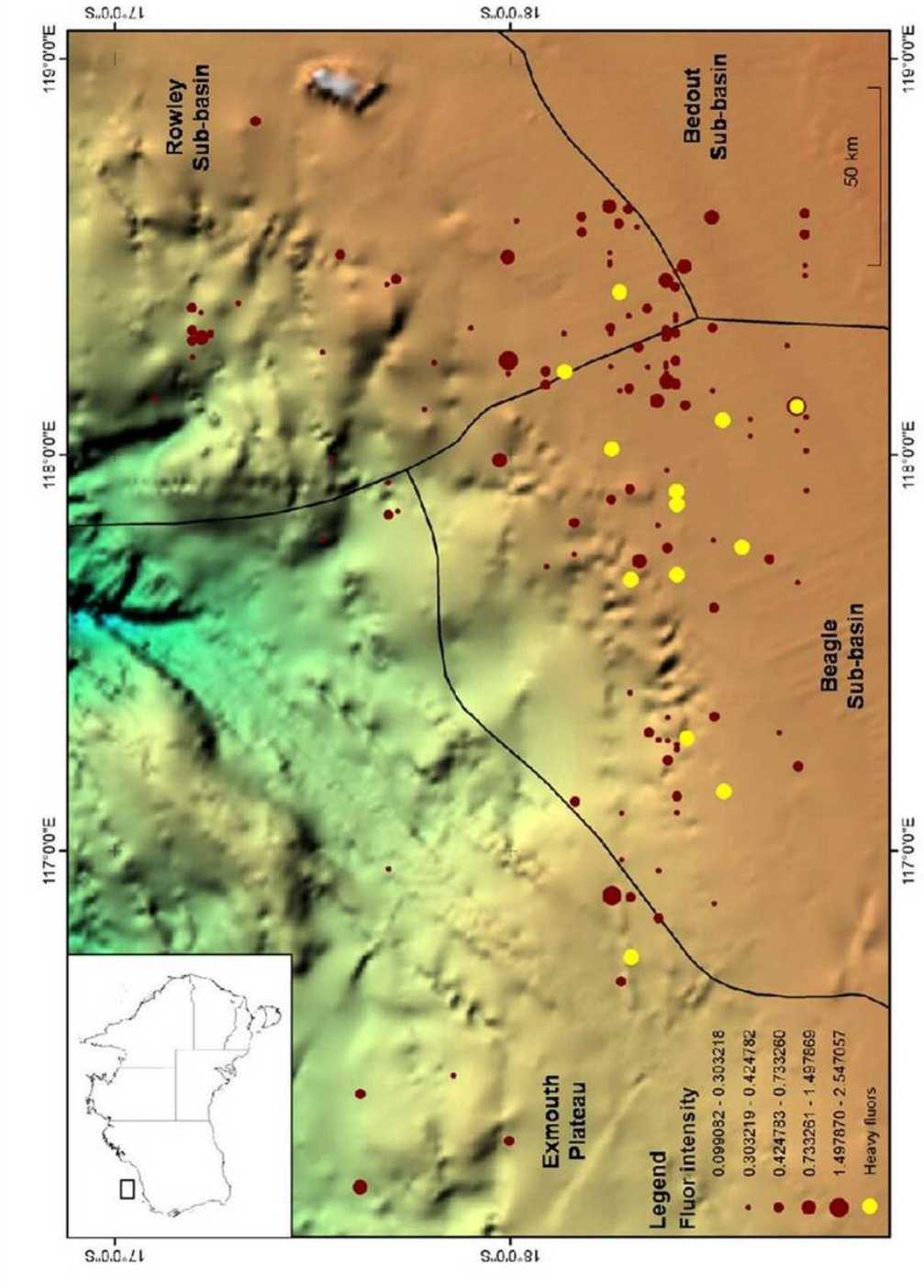

Figure 14. ALF anomalies over the Roebuck and northern Carnarvon Basins shown as brown dots, with larger dots being stronger anomalies. Location of ALF fluors interpreted by O'Brien et al. (2003a) as being oil-prone are shown in yellow.

Summary of key points

ALF has had a chequered history in the exploration industry, mainly due to lingering doubts about its ability to discriminate between seep oils, pollution and algae, and the difficulty in synthesising the results with other geochemical and geological information (Murray et al., 1998). These doubts are well founded; some of the basic assumptions regarding ALF are not fully explored in the literature, and many of the findings in the preceding discussion are over-interpretations of the data. For example:

- The emitted laser pulse is not reflected from the sea-surface, but penetrates the water column (Segelstein, 1981). At a wavelength of 266 nm (the emitted signal for the Mark III ALF), the laser penetrates approximately 3 m (SAR, with a wavelength of several cm, penetrates approximately 0.2 mm). Therefore, the intensity of an ALF fluor does not directly correspond to the size or thickness of an oil slick on the surface. The ALF fluorescence intensity of neat oil (a slick on the surface) is about the same as for a 5 ppm molecular solution in water, and 50 times less than for a 1000 ppm molecular solution. Thus, the signal does not respond in a linear way to concentration.

- It is not possible to differentiate between hydrocarbon-related and biological fluorphores on the basis of spectral signature (Coble et al., 1998; Blough and Del Vecchio, 2002). For an excitation wavelength of approximately 266 nm (the emitted signal for the Mark III ALF) the peak emission wavelength for a molecular dispersion of light oil (330-360 nm) is in the range of that for tryptophan (340 nm – tryptophan-like molecules are a fluorescing component of particulate organic matter that is preferentially distributed in the upper part of the water column in some ocean systems; Determann et al., 1996), and the peak emission wavelength for a surface layer of light oil (450-460 nm) is similar to that for UV-humic matter (400-460nm). Therefore, any or all of the fluors identified with ALF may represent biological material.

- The intensity, position and the spectral shape of fluorescence peaks dramatically vary with concentration (Radlinski, 2004a) (Figure 15). Experiments performed on hexane solutions of a mixture of typical Australian North West Shelf oils showed that fluorescence spectra are similar up to

concentrations of about 1000 ppm, but that above this value there is a very pronounced shift of the fluorescence peak towards the longer wavelengths. Therefore it is not possible to characterise a hydrocarbon-related fluor as being a condensate or oil-prone (as in O'Brien et al., 2003a) without information regarding the concentration of the solution.

- The nature of the processing involves arbitrary cut-offs and scaling factors that are not consistent between surveys and vary between survey lines.

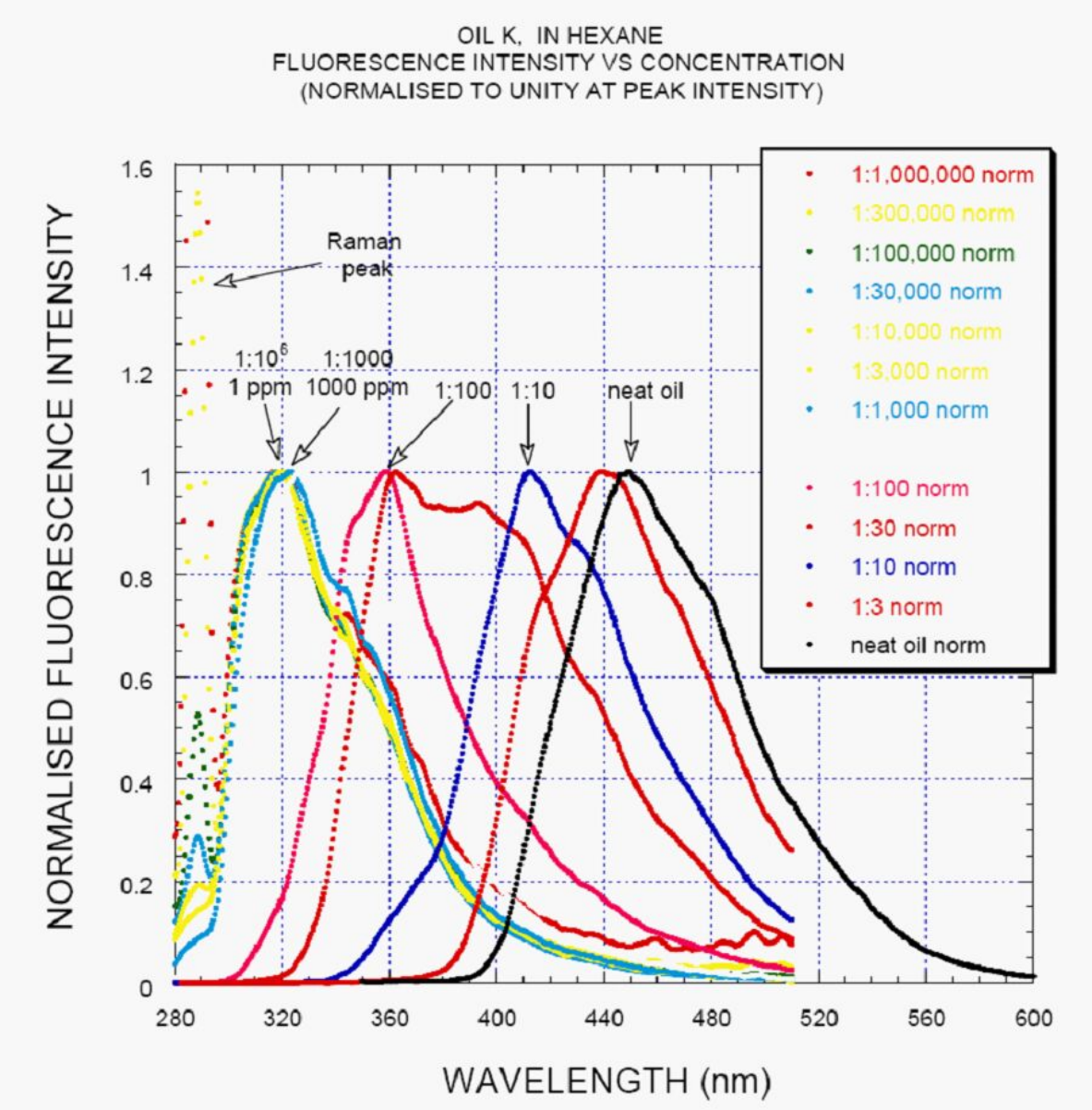

Figure 15. Fluorescence spectra for solutions of oil in hexane normalised to unity at the maximum of fluorescence signal (Radlinski, 2004a).

The use of ALF in offshore hydrocarbon exploration has been almost entirely discontinued as the technique is perceived as being unreliable in terms of accurately discriminating anomaly sources. This study presents a number of basic physical principles regarding lasers and their interactions with fluids which have not been given due consideration in previous ALF studies, and have therefore contributed to this perception of unreliability. A number of these principles cannot be overcome remotely, and require a physical sample of the water to determine the nature and concentration of the solution. Therefore, ALF surveying has the potential to be an effective exploration technique only when it is undertaken with concurrent water sampling to provide a baseline for interpretation of the ALF data.

3.5 Integrated geological and remote sensing studies

Signatures of natural hydrocarbon seepage can be imaged in conventional seismic data due to a variety of acoustic responses including, for example, low velocity zones associated with interstitial gas (gas chimneys, 'pull-downs') or high velocity zones ('pull-ups') associated with carbonate cementation within zones of leakage. These Hydrocarbon Related Diagenetic Zones (HRDZs) are generated when oil and/or gas leaking through a section is oxidised by bacteria and the resulting products precipitate carbonate (O'Brien and Woods, 1995). A distinctive feature of these carbonates is the isotopic composition of carbon which is highly depleted in ^{13}C relative to normal marine and most diagenetic forms of carbonate. These zones provide important evidence that seepage has been active at some stage, but do not provide evidence for modern seepage without other lines of evidence from recent sediments or active gas flares. The intense cementation within an HRDZ produces anomalously high seismic velocities, causing stacking problems and leading to seismic 'pull-up'. The cementation may also result in wipe-out zones where high amplitude reduces signal penetration. Based upon seismic evidence and isotopic analysis of cuttings, O'Brien and Woods (1995) have shown that five wells within the Vulcan Sub-Basin (Keeling 1, Skua 3, Jabiru 2, East Swan 2 and Avocet 2) have intersected HRDZs. This work lead to the interpretation of leaking hydrocarbons in seismic data over several major fields across the North West Shelf and Gippsland Basin (Cowley and O'Brien, 2000).

A link between carbonate shoals and natural hydrocarbon seepage in Australian waters of the Timor Sea has been inferred from 2D and 3D seismic, high-resolution

bathymetry and ALF data (Bishop and O'Brien, 1998). Hovland et al. (1994) documented the presence of Late Tertiary to Recent seabed mounds (carbonate knolls or bioherms) along the Vulcan Sub-basin margin and intra-basinal highs. These mounds are generally associated with deep-seated faults that could act as conduits for hydrocarbon migration (Hovland et al., 1994). Shallow gas was interpreted in seismic data and correlated with seafloor mounds and craters believed to be structures associated with gas escape. However, areas of interpreted shallow gas (eg. northwest of Karmt Shoal; figure 14 in Bishop and O'Brien, 1998) did not have a strong spatial relationship with areas of relatively dense ALF fluors (eg. northeast of Karmt Shoal; figure 14 in Bishop and O'Brien, 1998,). Bishop and O'Brien (1998) concluded that this was the result of hydrocarbons being trapped in the subsurface (seismic indicators and low fluors) versus hydrocarbons leaking to the sea surface (no seismic indicators and many fluors).

Further work, involving the integration of SAR data with bathymetry, water column sniffer and seismic data, concluded that the majority of reefs and carbonate build-ups in the Timor Sea were associated with active and palaeo-hydrocarbon seeps (O'Brien et al., 2002). This conclusion was heavily based on the relationship of SAR slicks to bathymetric highs in this region. The potential relationship between seepage and shoal/reef formation lead to the Australian Institute of Marine Science carrying out chemical and oceanographic studies in the Timor Sea around Karmt Shoals and the Cartier Trough (Burns et al., 2003). No convincing evidence for seeps from water column salinity, temperature, optical backscatter or oxygen profiles were found, (Burns et al., 2003) but sediment traps within the region demonstrated a flux of hydrocarbons in the water column (Burns et al., 2001). A point of note is that the 'Second Rank' oil slicks displayed over Karmt Shoals in O'Brien et al. (2004) were originally reported as remnant pollution slicks and were not thought to be seepage related in the original data report (NPA et al., 1999; O'Brien et al., 2001). However, the reported flux of hydrocarbons appears to be unrelated to any known petroleum system in the region (Burns et al., 2001). A core taken from the edge of Jabiru Shoals provided evidence of hydrocarbons in the top 6 cm of seafloor sediment, but no hydrocarbons were found deeper in the core (Burns et al., 2003). This finding is in keeping with the observation of a regional flux of hydrocarbons in the water column, but that no active seepage was observed associated with the shoals or reefs.

O'Brien et al. (2000) presented convincing evidence that active seepage was occurring across the Yampi Shelf through combining water column sniffer, regional seismic, high resolution bathymetry and SAR data. A major gas seep with methane concentrations up to 300 ppm was detected with the sniffer system and a direct correlation was reported between enhanced sea floor cementation and water column gas anomalies (Figure 7). The molecular composition of the gas and the isotopic composition of methane were also reported to be remarkably similar to the gas reservoired within Cornea 1. These data provided evidence for active seepage in association with interpreted HRDZs in seismic profiles and clearly demonstrated that this area is currently actively seeping. An important observation was that the SAR slicks were not located over the areas of active gas seepage, but occurred ~10-15 km inboard along a bathymetric high, interpreted to be the regional edge of seal (O'Brien et al., 2000).

O'Brien et al. (2004 & 2005) further analysed the relationships between different data sets used to interpret seepage over the Yampi Shelf, to develop a seepage model for the Browse and Bonaparte Basins (Figure 16). Sniffer data were used to show gas seepage and SAR data were used to infer oil seepage over bathymetric highs and in association with the edge of the regional seal. It was also noted that the SAR slicks tended to fall into several discrete groupings (O'Brien et al., 2004):

- At the edge of the regional seal in the northern Browse Basin, located inboard of the Cornea oil field (Yampi Shelf).
- At the boundary between the Bonaparte and Browse basins
- Around carbonate banks (Yampi Shelf and Karmt Shoals)

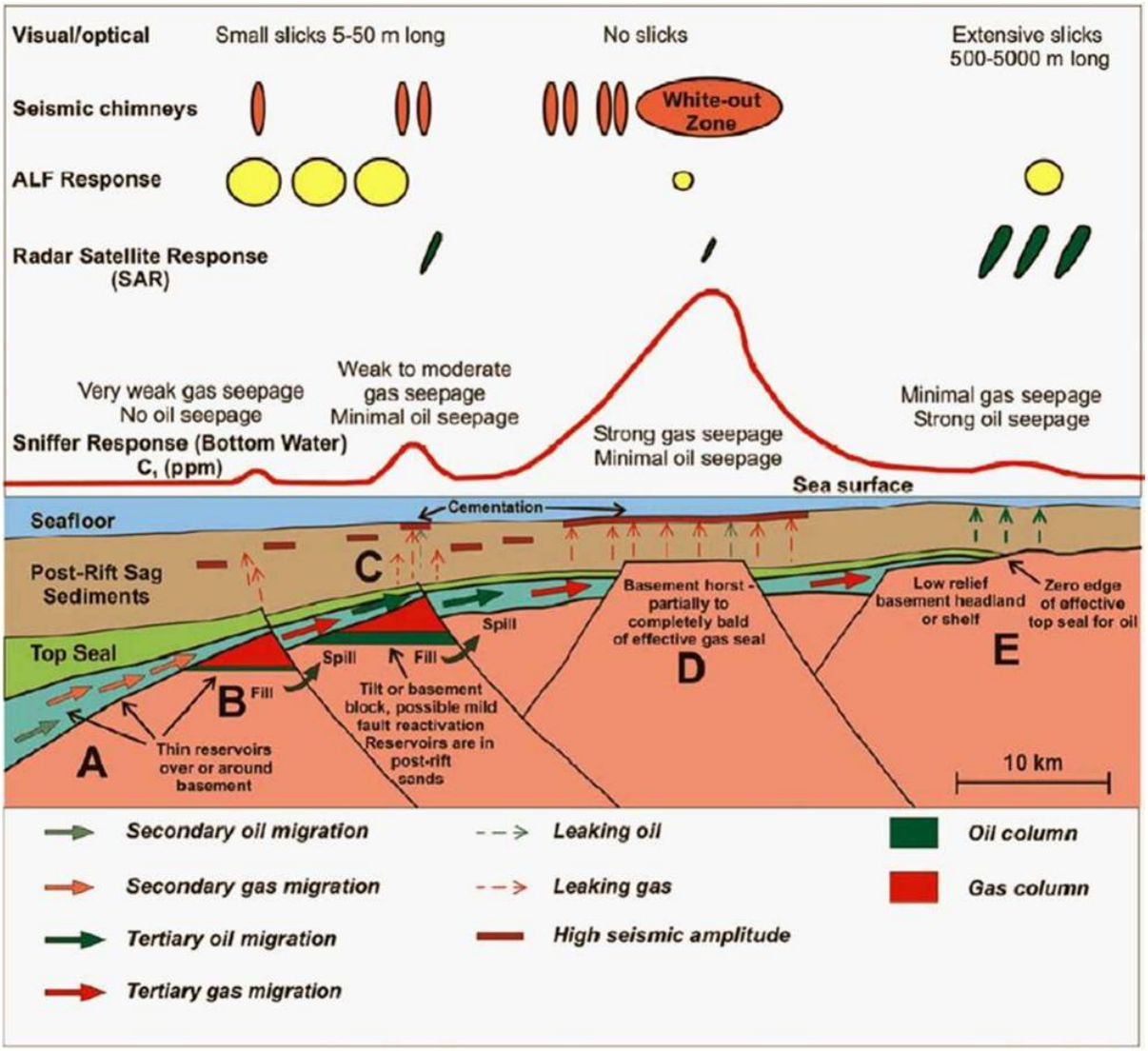

Figure 16. Schematic model of hydrocarbon migration, leakage and seepage across the Yampi Shelf, with attendant responses of assorted remote sensing responses. Size of arrows is proportional to amount of migrating or leaking hydrocarbons. Accumulations are developed over or around basement highs; vertical exaggeration is extreme (O'Brien et al., 2005).

These reports of seepage from the Yampi Shelf provided the most compelling evidence for seepage in Australia. Therefore Geoscience Australia revisited this area (Survey S267 in 2004) to test methods for seepage detection (Jones et al., 2005a). The aim of this survey was to test several geophysical techniques (single-beam echosounder, sidescan and multibeam echosounder) to see if seepage could be detected and examine how sampling could be undertaken (Figure 17). The survey successfully showed that gas flares could be visualised in the water column using

echosounder and sidescan sonar, and that active seepage has a strong tidal dependence (Rollet et al., 2006) (Figure 18). Gas release is strongest during low tide and, as the tide rises, the pressure change appears to 'shut off' or significantly decrease gas release. There was also a strong spatial relationship between seeps and the mapped edges of HRDZs in 3D seismic data (Figure 6a). This suggests that, as cementation generates the HRDZ, gas will flow around the outside of the cemented zone. Greater details of the detection methods and how to employ them will be covered in later sections of this report.

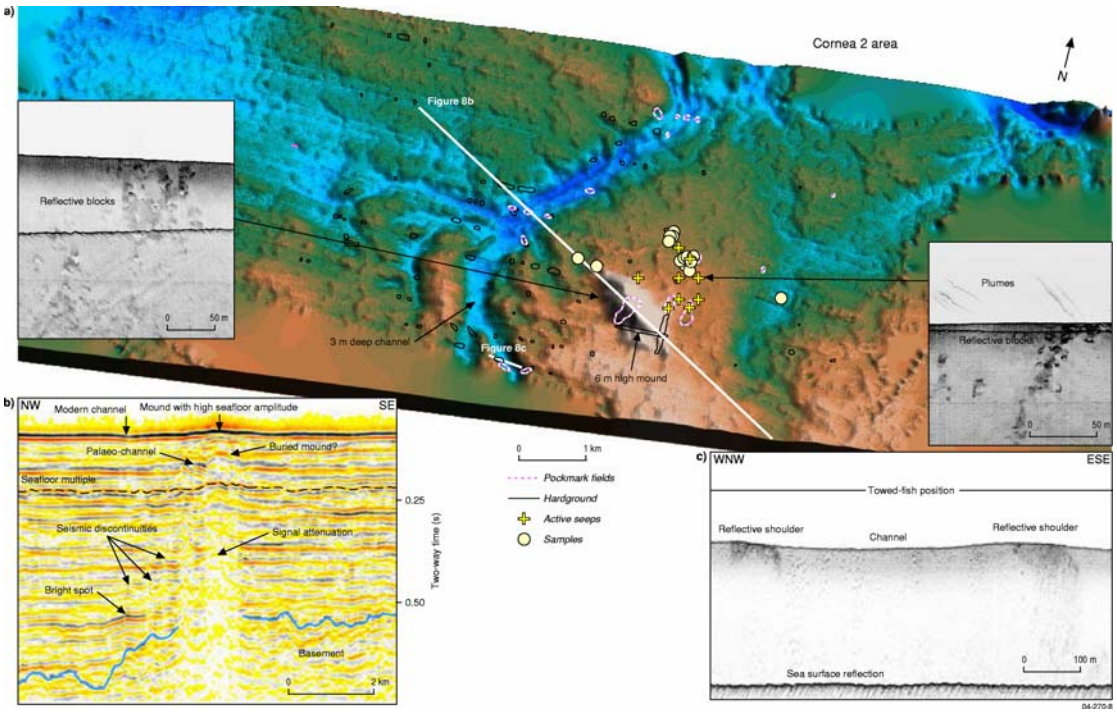

Figure 17. (a) Shaded multibeam bathymetry over Cornea Area 2 (see Figure 6a for location) revealing a six-metre high mound surrounded by a three-metre deep channel and other features. (b) 3D seismic section showing the sub-surface features coinciding with the six-metre high mound on the seabed. (c) Sidescan sonar data across the three metre deep channel (from Rollet et al., 2006).

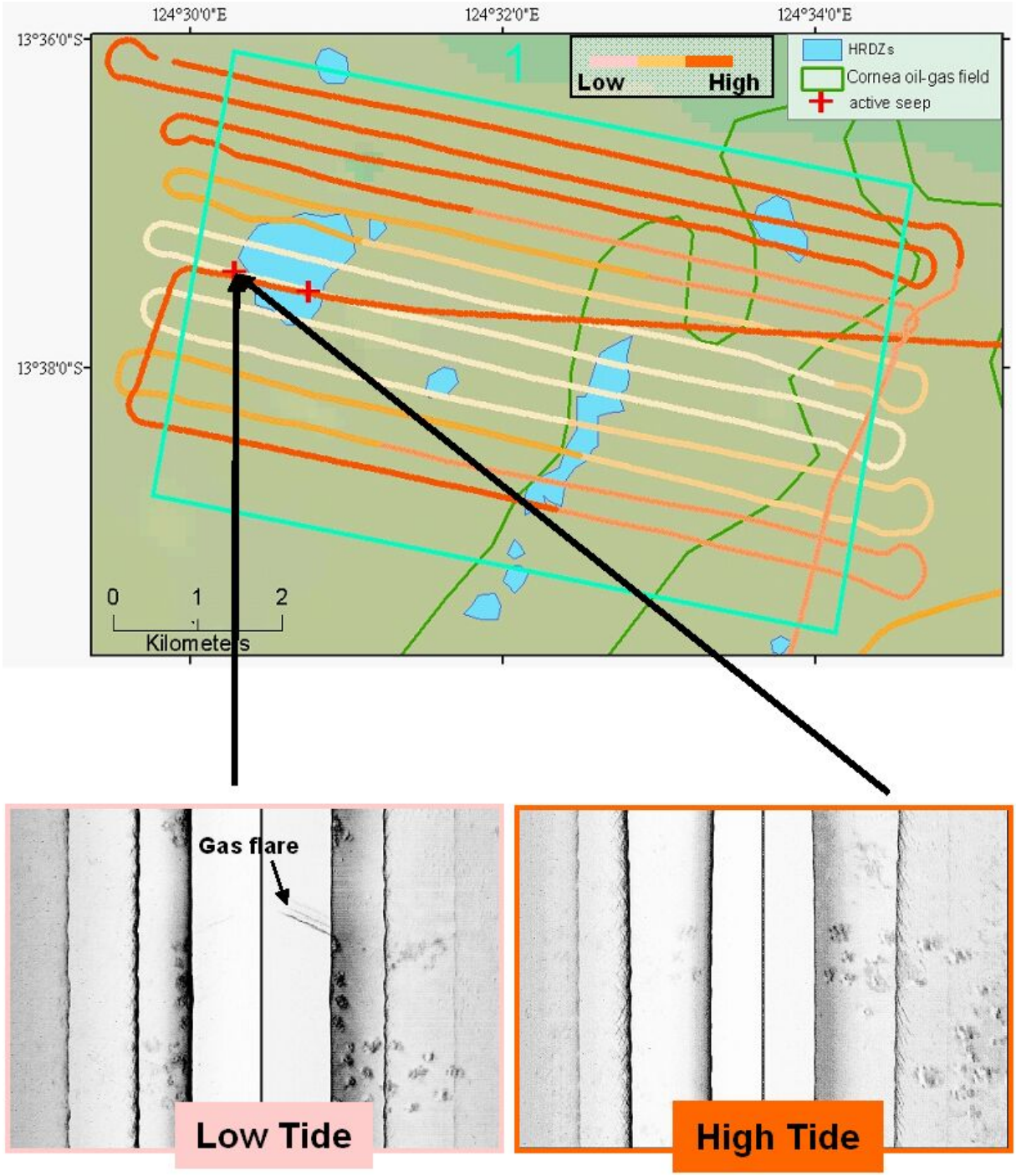

Figure 18. Sidescan sonar data showing gas flares in the water column at different phases of the tidal cycle in the Cornea area. Gas flares form during low tide but are absent during high tide due to the increased hydrostatic pressure (from Rollet et al., 2006).

A very important finding from this 2004 S267 survey was that detailed bathymetry collected using multibeam, in areas where SAR slicks were extremely common, showed that the slicks correlated with seabed channels that were not mapped on the hydrographic charts (Jones et al., 2005b). This was significant because the

interpretation of prolific 'edge of seal' or 'basin-margin' seepage in this region using SAR (Figure 6) was now called into question. On the other hand, the relationship between gas seepage, strong sniffer signals (two orders of magnitude above background) and HRDZs was confirmed. Therefore, the evidence for oil leakage at the edge of seal appears to be an artefact of bathymetry and current flow leading to a decrease in ocean surface roughness. This is a phenomenon that is typically observed in SAR data from areas where the water depth is much less than the Timor Sea. The reasons for its occurrence here are the high tidal currents (1 to 2 m/s) and extreme tidal ranges (up to 5 m) in the region. The correlation between SAR slicks and carbonate shoals and reefs is also significant. The extensive slick formation observed over these features is only observed on two consecutive SAR scenes collected during one satellite pass. Detailed analysis of the timing of data collection and the shape of the slicks indicates that these two SAR scenes were collected during a coral spawn event (Jones et al., 2005b & 2006). This greatly weakens the reef/seep relationship previously proposed and also further downgrades the evidence for oil leakage across the region. When both the bathymetric effects and coral spawn event are taken into account, only 3% of the originally interpreted hydrocarbon slicks are likely to be natural oil seepage (Jones et al., 2005b). More detailed coverage of these issues will be provided in Section 3.4.

The new data and observations (Jones et al., 2005a,b & 2006; Rollet et al., 2006) support the previous findings of gas seepage in the Browse Basin and the relationships between gas leakage and the development of HRDZs. However, the SAR evidence for oil seepage and its relationship to edge of seal or reefs and shoals are not supported and these correlations appear to be artefacts of tidal currents, bathymetry and coral spawning. These artefacts are particularly common in this region, where reefs and shoals are abundant and tidal currents and ranges are extreme. Methods of quality control for SAR data collected on the North West Shelf of Australia are provided in Section 4.4.

A marine survey in the Arafura Sea also used an integrated approach (Logan et al., 2006; Grosjean et al., 2007; Rollet et al., 2007). The locations of the study areas for the survey were initially selected on pre-existing 2D conventional seismic data and the presence of interpreted hydrocarbon slicks from SAR studies. The marine survey

collected multi-beam bathymetric data, along with side-scan and sub-bottom profiles, and sea-bed coring was carried out based on pre-survey data analysis and on-board data collection. Results provided direct evidence for shallow gas, although the gas sampled in cores was interpreted as biogenic (Logan et a., 2006; Grosjean et al., 2007). An interesting aspect of this study was the correlation of SAR slicks in association with the interpreted edge of regional seal across one of the depo-centres (Figure 11) (Logan et a., 2006; Rollet et al., 2007).

An integrated approach has also been taken for the study of natural hydrocarbon seepage in the Great Australian Bight (Struckmeyer et al., 2002). Regionally, there is evidence of stranded coastal bitumens (see Sections 3.1 and 6.7.2) and oil and gas shows in several wells in the Duntroon, Ceduna and Eyre Sub-basins. SAR slicks interpreted to be low to medium confidence natural oil slicks are generally located around the edges of the main depocentre of the Ceduna Sub-basin. However, direct correlation between individual slicks and seismic data was not possible due to the 20 km line spacing of the seismic grid. The slicks are up to 1,200 m long and between 30 and 150 m wide and occur in water depths from 5000 m to less than 200 m. Issues related to bathymetric effects observed on the Yampi Shelf (Jones et al., 2005b & 2006) are not thought to be present in this data set because of the water depths and limited effects of tidal currents. ALF Mark II data were also collected in the region but interpretation of the data only yielded two weak fluors (Mackintosh and Williams, 1990). This may be related to limitations with the acquisition system or the lack of significant seepage (Mackintosh and Williams, 1990; Struckmeyer et al., 2002). Reprocessing of the ALF data (Cowley, 2001a) generated '941 confident fluors', with an average density of 0.52 fluors per 1000 thousand spectra. However, there appears to be little correlation between the SAR slicks and ALF fluors. This lack of correlation, coupled with the limited data quality of the Mark II ALF system and the possibility that ALF may not differentiate biological from hydrocarbon signals (Coble et al., 1998; Blough and Del Vecchio, 2002) suggests that the ALF data should be treated with caution. During the course of SS01/2007 sea-floor sampling was undertaken in the area of the Bight covered by the ALF anomalies (Mitchell, 2007), partly in an attempt to validate the natural hydrocarbon seepage interpretation for these features, but the results of the survey were not available at the time of writing.

3.6 Seafloor geochemical studies of shallow gases

An important line of evidence for the presence of natural hydrocarbon seepage and shallow gas is the analysis of interstitial gases in shallow sediment cores. Initial studies that combined the analysis of sea-floor sediments and geological assessments of potential seepage sites focused on south-eastern Australia (Hinz et al., 1986; Heggie et al., 1988; O'Brien and Heggie, 1989). In 1985, the *R/V Sonne* carried out a combined seismic and sampling survey across the west Tasmanian margin. Thirty-seven samples were taken from nineteen cores for gas analysis using an acid treatment within a vacuum (Hinz et al., 1986). The gas concentrations (C_1 to C_5 yields ranging between 1363 and 30 parts per billion - ppb) consisted predominantly of methane. Sites with the highest concentrations were found on the upper continental slope off west Tasmania. Significantly, gas wetness percentages ($\Sigma(C_2\text{-}C_4)/ \Sigma(C_1\text{-}C_4)$ x100) frequently had values around 40 to 45%. These results were used to suggest that a thermogenic source of hydrocarbons was present. A reassessment of the data for this report now suggests that the abnormally high gas wetness values and relatively low gas concentration values probably relate to a combination of analytical method and low initial interstitial gas concentrations. The analytical method used has been shown to lead to enhanced gas wetness values and to generate artefacts that are often interpreted as thermogenic, but relate to the way the analysis is performed (Abrams et al., 2004, 2007). The conclusion that 'wet gas of thermogenic origin is abundant in surface sediments' (Hinz et al., 1986) can no longer be supported.

In 1987, the *R/V Rig Seismic* performed a geochemical sampling program seeking evidence of thermogenic hydrocarbons in the Voluta Trough and eastern Otway Basin (Heggie et al., 1988). Thirty three gravity cores were collected, from water depths between ~500 m and ~5000 m, along four seismic profiles (BMR Lines 48-42, 48-43, 48/7, 40-22/33). Each core was analysed for C_1-C_5 hydrocarbons using a head space gas method to collect the gas from wet sediment. This method has been shown to provide robust results but data can be prone to misinterpretation at low gas concentrations (Abrams et al., 2004 & 2007). Nine locations were interpreted to have gases anomalously above background. These sites were located above major faults. Despite a variation of up to 300 times in concentration, comparing 'background' samples and those considered 'anomalous', all samples contained relatively low levels

of C_1-C_4 gases. The highest value of C_1-C_4 was 488 µl/L, which converts to 488 ppm. Gas concentrations of this level would be regarded as background in the Gulf of Mexico (Abrams, 2005) and in sediments from the Arafura Sea (Logan et al., 2006; Grosjean et al., 2007). Therefore, none of the data presented in Heggie et al. (1988) now appear to support the presence of seepage based on the geochemical data reported.

In 1988, the *R/V Rig Seismic* carried out a geochemical sampling program in the Otway and Gippsland basins (O'Brien and Heggie, 1989). Sampling was focussed mostly in the Otway Basin, specifically the Mussel Platform, Crayfish Platform and Voluta Trough. Fifty two vibracores were collected from water depths between 44 m and 1944 m and sampled using the head space gas analysis method used by Heggie et al. (1988). Twenty gravity cores and ten vibracores were collected and sampled for head space gas in the Gippsland Basin. When these data are re-examined, several issues become apparent. Many of the samples are taken from very shallow substrate depths (<2 m) and there also appears to be a correlation between low gas concentrations and higher values for gas wetness. When these data are replotted to show gas wetness against gas (C_1-C_4) concentration, the relationship becomes clear (Figure 19). The trend of increasing gas wetness with decreasing gas concentrations is an artefact related to the leakage of methane from samples during sampling (Abrams, 2005; Abrams et al., 2004 & 2007). All samples collected from this survey also exhibit low gas concentrations and should not be interpreted as evidence of natural hydrocarbon seepage. For comparison, the highest value in this study is equivalent to 305 ppm, whereas a study of data from the Gulf of Mexico reported 'anomalous' gas concentrations between 10,000 and 1,000,000 ppm, using a very similar technique (Abrams, 2005). The highest gas values recorded in near surface sediments from the Arafura Basin were 70,000 ppm (Logan et al., 2006; Grosjean et al., 2007) and from the Central NWS only up to 20 ppm (Jones et al., 2007).

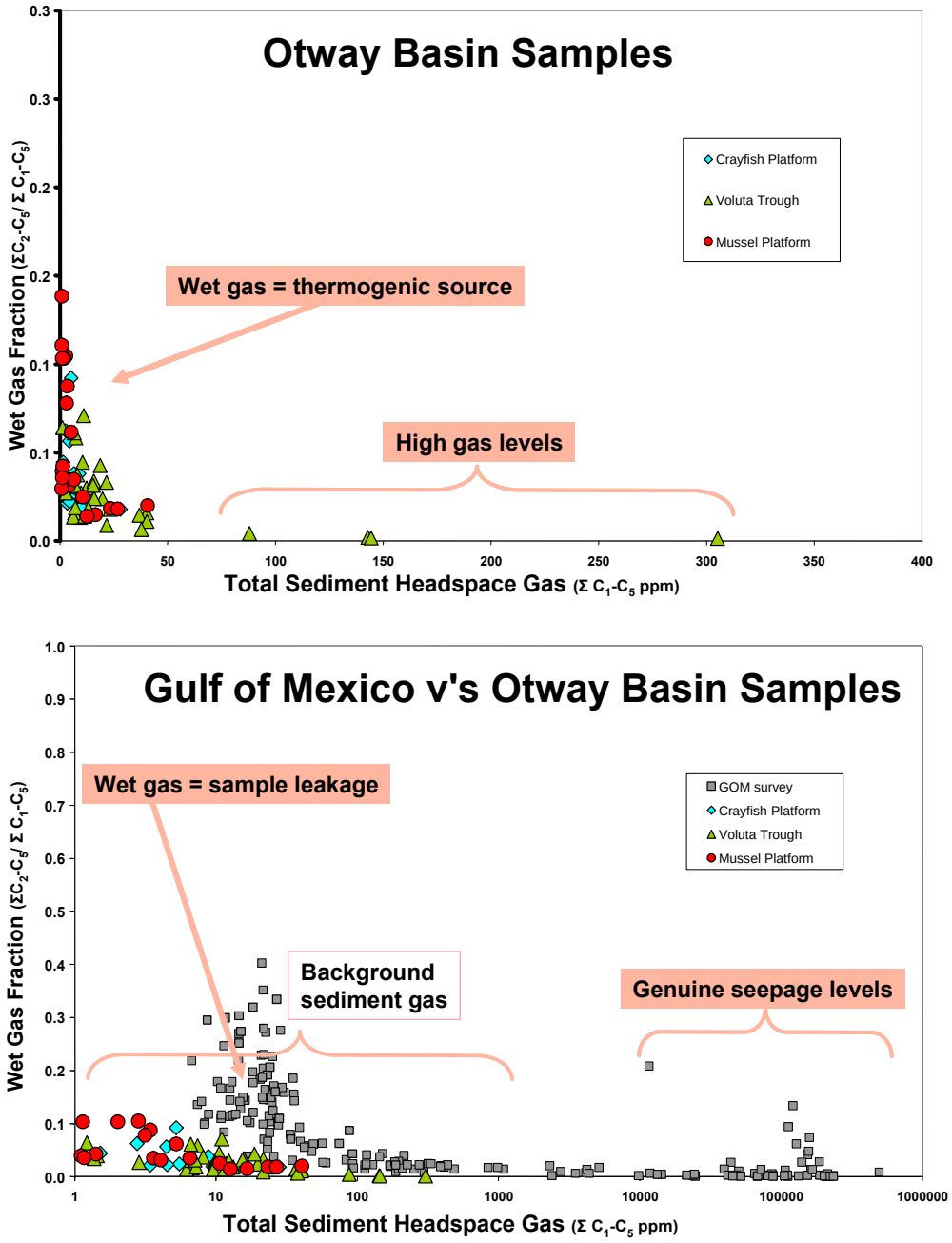

Figure 19. a) Head space gas concentrations plotted against gas wetness ratio for data published by O'Brien & Heggie (1988) for the Otway Basin. Interpretations shown are based on the original publication, with high gas concentrations interpreted between 50 and 350 ppm total head space gas concentrations. This contrasts with the same data plotted in (b) where data from a proven seepage site in the Gulf of Mexico is used. Note the change to a log scale in the second plot. Genuine seepage levels are between 10,000 and 1,000,000 ppm total head space gas concentrations and the trend to increased wetness observed at lower concentrations of total head space gas is an artefact of leakage of volatile methane during sampling and storage.

Between 2004 and 2007, Geoscience Australia conducted several marine surveys that included geochemical sampling as part of their core aims. The first survey was carried out over proven gas seeps in the Timor Sea over and around the Cornea oil and gas field (Jones et al., 2005 a,b; Rollet et al., 2006). Sea floor sampling during this survey was limited due the nature of the shelf sediments. Many of the areas where gas seeps were observed, were characterised by a substrate of indurated carbonate cement, and coring, to allow head space gas sampling, was not possible. Nonetheless, geochemical samples were obtained and results are reported in a later section of this report.

Gravity cores were obtained for head space gas analysis during a survey in the Arafura Sea (water depths ~70-240 m) (Logan et al., 2006; Grosjean et al., 2007). Up until this survey, a notable factor in all head space data collected from around Australia had been the low gas concentrations reported from all studies. However, data from the Arafura survey showed that some sample areas did have very high levels of methane and/or carbon dioxide. In both cases, the gas data are interpreted to represent biogenic gases generated from the decay of organic matter and not directly related to natural hydrocarbon seepage (Logan et al., 2006; Grosjean et al., 2007). These data are important, as they support laboratory and field assessments of the head space gas method, which indicate that it does provide a robust and reliable method for the sampling and analysis of gases in marine sediment pore space (Abrams et al., 2004 & 2007). Samples collected during the offshore Canning marine survey (water depths 50-667 m) (Jones et al., 2007) yielded uniformly low methane levels (generally between 1 to 5 ppm, maximum 20 ppm), but high carbon dioxide concentrations at specific sample sites (generally between 1,000 to 4,000 ppm, maximum 232,000 ppm), with elevated values occurring between depths of 3 and 5 m in the cores. Samples collected in 2007 from the Great Australian Bight (water depth ~500-4500 m), also exhibit uniformly low methane concentrations (generally 1 to 4 ppm, maximum 9.5 ppm) and do not show strongly enhanced carbon dioxide (between 55 to 2,500 ppm) (Abrams et al., 2007).

3.7 BHP Billiton Petroleum outer Browse Basin seepage studies

Between December 2000 and May 2002, BHP Billiton carried out a series of data acquisition programs for an integrated seepage assessment over 5 deep water (1000-

3000 m) permit areas (WA-301-P, WA-302-P, WA-303-P, WA-304-P, WA-305-P) west of Scott Reef in the outer Browse Basin. To date, this program represents the largest study of its kind carried out in Australian waters. The initial part of the study involved the collection of 17,000 km of 2D seismic data and the acquisition and interpretation of 12 SAR scenes from RadarSat. Based on the initial results from these datasets, 25,000 line km of airborne hyperspectral data were collected by BallAIMS using the CASI sensor. These data provided swath widths of 500 m and 1 m pixel resolution and were analysed for evidence of natural films, algal blooms and oil slicks. Interpreted locations and areas of potential hydrocarbon seepage were then selected for a multibeam bathymetric survey with a grid resolution of 35-60 m, depending on water depth, covering an area of 9,500 km^2. The final part of the program involved the collection of 400 sea bed piston cores for geochemical analysis (head space gas and hydrocarbon biomarker analysis) and 33 temperature probes by TDI-Brooks. Core sites were based on the following criteria:

- Location of slick anomalies (SAR and airborne hyperspectral data).
- Presence of sea floor relief and fault scarps.
- Interpreted fault conduits from source.
- Areas of thin seal.
- Presence of amplitude anomalies in seismic data.

The results of the study have not been formally published but data collected as part of this seepage assessment have been deposited at Geoscience Australia under the PSLA Act. The interpretive reports related to the SAR, hyperspectral survey and biomarker analysis are currently confidential, but the data related to the coring program and associated head space gas data are now open file and these data are analysed below.

The head space gas data collected from the 400 cores are notable for the low levels of gas present in all the cores. Total head space gas concentrations do not rise above 40 ppm, which indicates that none of the cores intersected any zones containing shallow gas (Figure 20). Data also show that increasing wet gas concentrations are associated with lower levels of total gases (Figure 20). This trend is related to the loss of volatile methane from samples during sampling and storage. The enhancement in gas wetness is more marked when samples initially start with low total gas concentrations. When this dataset is compared to one collected from a known seepage location in the Gulf of Mexico (Abrams et al., 2007), it becomes apparent that none of the cores provides support for seepage and that the data represent background levels of methane and wet

gases normally present within sediments. These gas levels are also similar to those reported from cores taken across the Central NWS (Jones et al., 2008). Our interpretation of the open file data is that, despite the extensive program undertaken by BHP Billiton, the results of the coring program did not help support any evidence of hydrocarbon seepage.

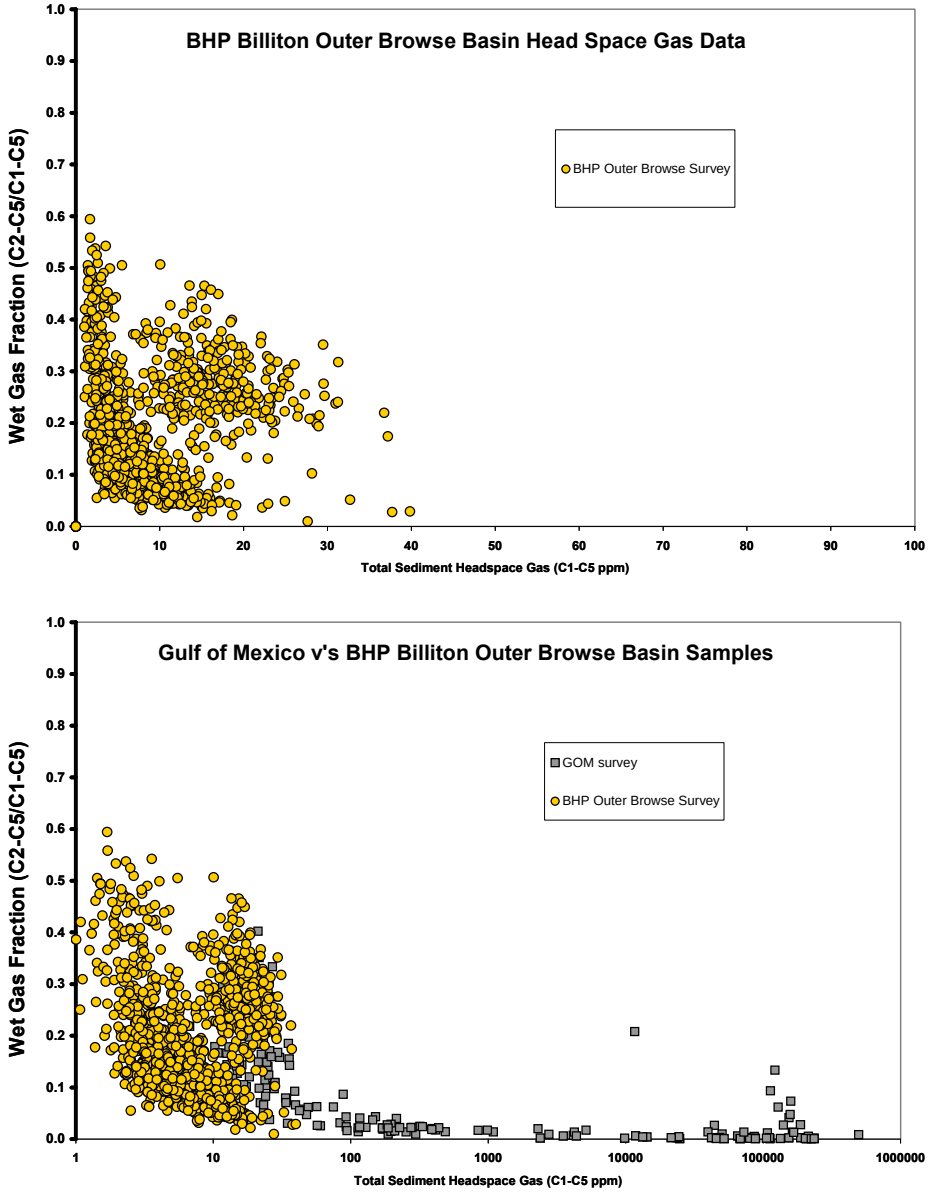

Figure 20. a) Head space gas concentrations plotted against gas wetness ratio for data from 400 piston cores collected for BHP Billiton during the Outer Browse Seepage Survey. No values were observed over 40 ppm total head space gas concentration. This contrasts with the same data plotted in (b) where data from a proven seepage site in the Gulf of Mexico is used (Abrams et al., 2007). Note the change to a log scale in the second plot. Genuine seepage levels are between 10,000 and 1,000,000 ppm total head space gas concentrations and the trend to increased wetness observed at lower concentrations of total head space gas is an artefact of leakage of volatile methane during sampling and storage.

Summary of Key Points and Implications: The head space gas method used in almost all surveys is a reliable and proven technique, but data need to be interpreted with an understanding of sediment gas variation in the marine environment and also with knowledge of method artefacts that can lead to mis-interpretation of gas wetness data in low concentration samples. Excluding the samples that contained biogenic methane in the Arafura Sea, all Australian studies that have attempted to use sediment gases to infer thermogenic hydrocarbons have not provided reliable evidence to successfully support such interpretations. Early studies have suffered from data mis-interpretation and have related apparent enhanced wet gases as evidence for thermogenic gas seepage. However, this feature of the data is due to a method artefact related to methane leakage during sampling and low interstitial gas concentrations. These studies did not set their survey data in a wider context and also did not compare gas concentrations to studies with proven gas seepage. This lead to values which were high within an individual survey data set, being considered as anomalous. However, in these cases, the values are not anomalous when compared to other global studies. They lie within the background range of values, and are within the variation expected in normal marine sediments.

Another feature which has limited the potential for this method to help in the assessment of Australian seepage systems has been the depth of substrate sampling. It is vital to collect interstitial gas samples from sediment taken below the surface mixed zone and within anaerobic sediments. In many of the surveys, often due to limitations of available sampling equipment, samples were collected from relatively shallow cores, often within the top 2 m of sediment. In some surveys, for example the Arafura survey and Great Australian Bight SS01/2007, geophysical indicators of shallow gas were identified beneath the core sites but the sample cores did not penetrate the potential gas horizon (see Section 5.3.1).

Methods and Techniques

4 Remote Sensing Methods for Seepage Detection

4.1 Review of sensors and their applications

4.1.1 Earth Observation

Earth Observation (EO), or space-based remote sensing of the Earth, is the study of the properties and interactions of land, oceans, environment and climate using satellite data. Earth observation is vital to ensure our ability to understand physical and ecological systems, to anticipate and respond to global trends, and manage our environment in a sustainable way.

EO satellites are usually in low earth orbit (200 to 2000 km) or geostationary (36,000 km). Almost all the satellites discussed in this report are in low earth orbit. Satellites which orbit over the poles when their orbits are inclined at about 90° to the Equator are called polar orbiting satellites. They provide images in much greater detail, but also orbit the Earth much more quickly. Typically, orbits will last for about 90 minutes and information must be recorded by ground stations in the few minutes as the satellite flies by. A satellite's 'revisit' refers to the period of time after which the satellite can collect an image at the same place on Earth from the same spot above the earth, whereas its 're-look' capability corresponds to its ability to collect another image of the same place irrespective of its position.

EO satellites are generally categorised as "operational" or "science" missions, but this distinction is artificial. Science can be undertaken on commercially available satellite imagery, and satellites conceived for science can be used for operational purposes. A more important distinction exists between missions that can deliver data regularly and rapidly, according to established operating procedures, and those that operate on an ad hoc basis and are not equipped for acquiring large volumes of data or rapid satellite tasking. The list of operational EO satellites is continuously growing – over the next few years, there will be a huge increase in satellite based EO capabilities. Tables 1 and 2 list the potential EO data sets available from various sources now and in the near future. The list of EO satellites is not exhaustive; only the most relevant sources from a seeps perspective are included. Some of the datasets listed in Table 1 are also

acquired directly at the Australian Centre for Remote Sensing (ACRES) ground station facilities.

4.1.2 Passive sensing

Passive remote sensing is the collection of reflected or emitted energy from the Earth by space-borne sensors. The most common form of passive sensing uses reflective visible light (optical sensing), but other forms include ultraviolet and near and far infrared (thermal) sensing. There are very few satellites which are capable of detection in the ultraviolet wavelength region; these satellites cover very wide swaths and have very coarse ground resolution in the order of tens of kilometres (eg. TOMS and SBU). The optical wavelength range covers the range from 400 to 2500 nm (visible, near-infrared and middle infrared region). There are a number of satellite-borne sensors that operate in this wavelength region. They range from coarse resolution of ~1km to very high resolution of ~1m resolution. The most commonly used optical satellites are Terra/ Aqua MODIS, ASTER, Landsat-5 and 7, SPOT 2, 4 and 5, IKONOS and QuickBird. Remote sensing in the thermal infrared wavelengths relies on differences in thermal characteristics between the background and feature of interest. Space-borne multispectral sensors such as the ASTER and MODIS have capability to detect in the thermal region.

While traditional optical sensors record “visible” light, usually in three colour bands, and near infrared energy, “hyperspectral” sensors record reflected energy in hundreds of narrowly separated colour bands. They allow the recognition of precise resource signatures useful for geology, resource identification, pollution monitoring and control, agriculture, forestry, coastal zone monitoring and land use applications. A section on hyperspectral sensing as it applies to seepage studies at Geoscience Australia appears later in this report.

4.1.3 Active sensing

The most commonly known active sensors are radar sensors or Synthetic Aperture Radar (SAR) when mounted on a space-borne platform. SAR actively transmits microwaves to the Earth and receives their reflection, called “backscatter”. As the transmitted waves react differently to different substances and roughness of the Earth’s surface, this approach is particularly useful for surface mapping. Radar remote sensing is possible in many frequencies with variable bandwidths. To date, radar

sensors have flown in S-band (Almaz), L-band (SEASAT, JERS-1 and ALOS), X-band (Shuttle Radar Topographic Mission and TerraSAR-X) and C-band (RADARSAT-1, ERS-1 and -2, ENVISAT's ASAR and RADARSAT-2).

Space-borne SAR was inaugurated with the SEASAT mission in 1978. The European Space Agency launched ERS-1 in 1991 to demonstrate C-band SAR in the research community. Canada launched RADARSAT-1 in 1995, the world's first operational, commercial SAR program, offering 7 m resolution images available in near real-time. RADARSAT-2, launched in 2007, offers 3 m resolution. C-band radar data are of particular importance to flooding, agriculture and coastal applications including natural hydrocarbon seepage studies. These data clearly distinguish land from water.

Data from passive and active sensing are available in archived format (historical images to monitor change) and "real-time" or "near real-time" (images acquired, processed and delivered within hours of the satellite pass).

4.1.4 Limitations of EO data

In the context of seepage detection, a number of factors limit the application of data from optical sensing. The key factors that impact on detection capability are spatial resolution, lack of coverage, satellite revisit time, cloud cover and processing and interpretation of the data. The identification of false positives on optical data remains a challenge, biogenic material like natural film slicks, partially or fully submerged vegetation and algal blooms can be mistaken for oil slicks. Sun glint on optical images is also a challenge when using optical data. In contrast to optical sensing thermal sensing can be done during night and day, but thermal sensing also suffers from misinterpretation of false positives like vegetation, and oceanic frontal and upwelling systems that could generate signatures similar to oil on water.

SAR imaging can be done during day or night and through cloud cover, this is particularly beneficial for applications like offshore oil seep detection. However, the interpretation of SAR images can be challenging due to the presence of false positives. A number of studies within GA have demonstrated the need for using SAR with a good understanding of various mechanisms that could lead to potential misinterpretation of SAR features as oil slicks. While this review of EO applications to seepage studies in GA covers a range of sensor types, there is a major focus on the

use of SAR due to its applicability to large area screening.

4.1.5 Availability of EO data for seepage studies

A range of EO datasets are available for seepage studies at GA. These data sets are either directly acquired at ACRES facilities or acquired from commercial providers (see Table 1). Data from sensors on airborne platforms are also available for seep studies; notable among these are HyMap and CASI hyperspectral data. In addition to the operational missions that provide satellite data, there is potential for accessing data through Announcement of Opportunities from satellite operators mostly for research applications. In addition to the ongoing data acquisition, GA holds a considerable archive of SAR data, acquired from 1991 to present. The archive includes ERS-1, ERS-2, RADARSAT-1, JERS and ALOS PALSAR data.

4.1.6 Weather windows for acquisition of remote sensing data over Australian study sites

Weather influences the capacity of a remote sensing system to discriminate a slick feature from the ocean background. Therefore, it is essential to have information about weather at the time of data acquisition. The sea state, sea surface roughness or wave height is directly related to wind speed and direction, and tide conditions to a lesser extent, at the time of data acquisition and also in the few days leading up to the data acquisition.

To illustrate the importance of targeting suitable weather windows for remote sensing data acquisition, the average daytime wind speeds in the Arafura Sea based on 20 years or more of climate data (10 years for Nhulunbuy) from the Bureau of Meteorology have been plotted in Figure 21and Figure 22. The figures suggest that SAR acquisitions between November and March are most likely to satisfy wind speed criteria for any new data acquisition for discriminating slicks in the ArafuraSea. Similar analyses of climate data for any study areas in the offshore petroleum provinces can enable the identification of the most appropriate windows to increase the chance of weather compliant SAR acquisitions for future acquisition programs.

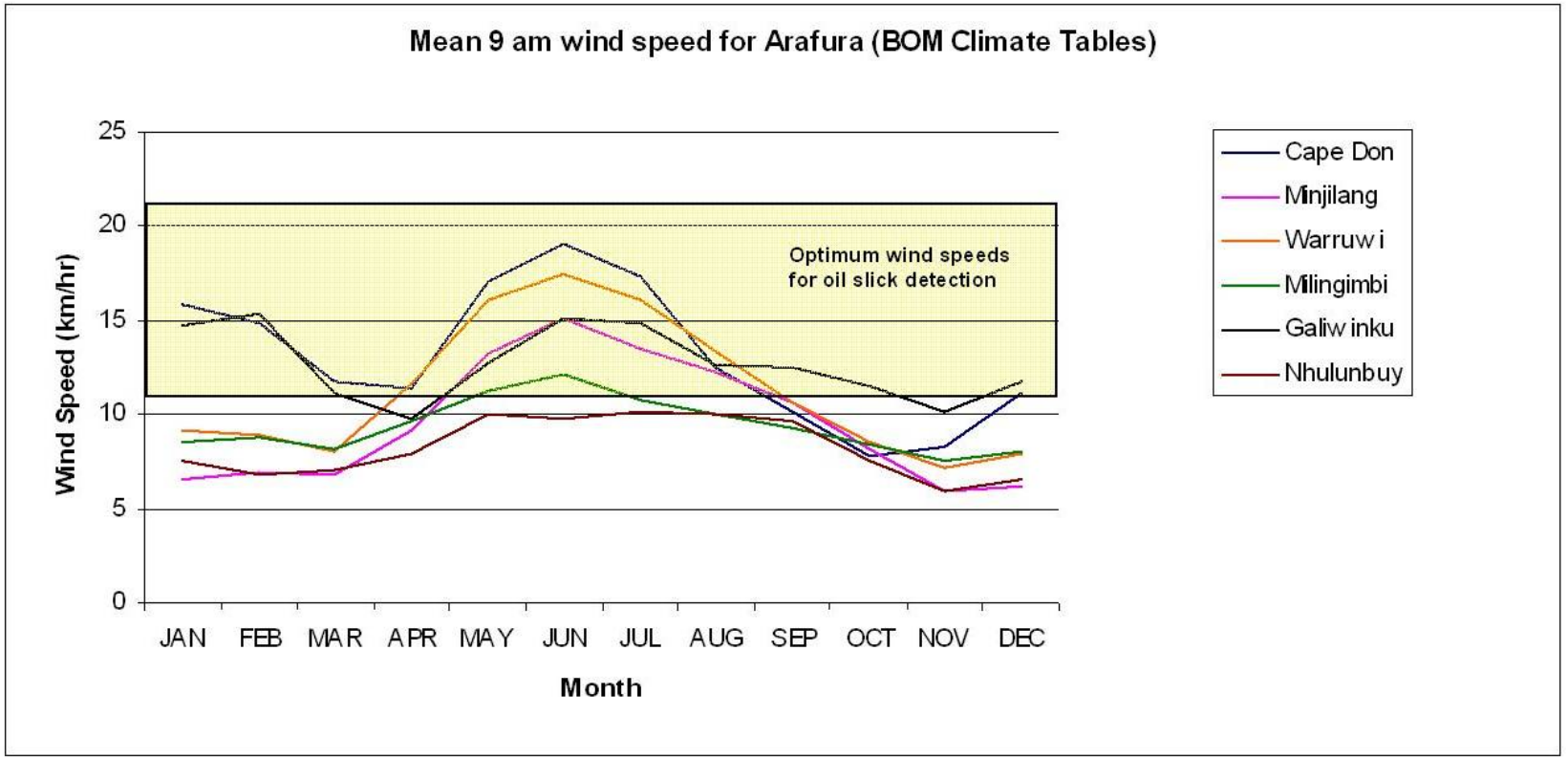

Figure 21. Average 9 am wind speeds for six coastal locations in the Arafura.

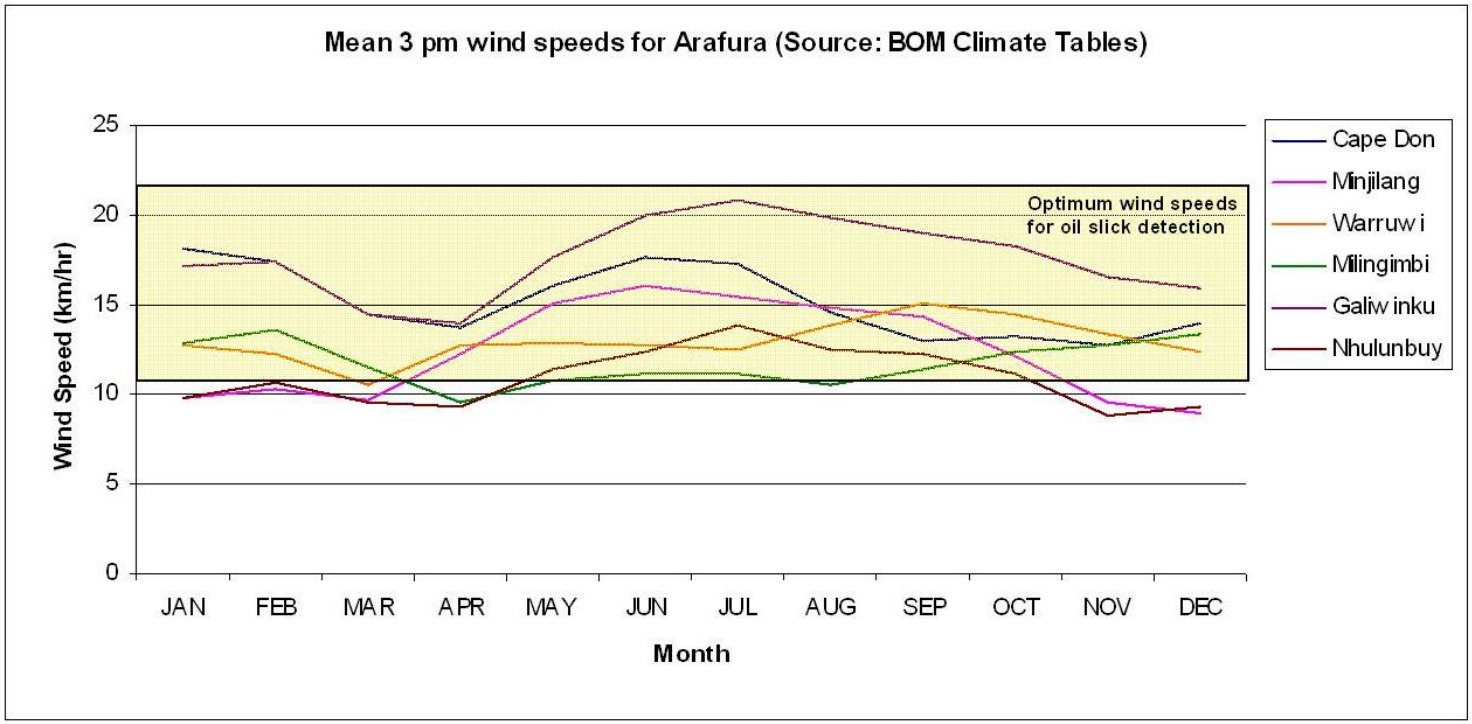

Figure 22. Average 3 pm wind speeds for six coastal locations in the Arafura.

It is quite possible that despite the choice of the appropriate weather windows, remote sensing data acquired over certain areas may not be weather compliant. To determine the weather-compliance of data that have already been acquired, a number of supporting or ancillary data sets are used. A description of the range of ancillary data used in determining weather-compliance follows.

4.1.7 Ancillary data used to determine weather compliance of SAR data

4.1.7.1 Wind speed and direction

Scatterometers transmit microwave pulses down to the Earth's surface and measure the power that is scattered back to the instrument. This 'backscattered' power is related to surface roughness. For water surfaces, the surface roughness is highly correlated with the near-surface wind speed and direction. Hence, wind speed and direction at a height of 10 metres over the ocean surface is retrieved from measurements of the scatterometer's backscattered power.

The scatterometer QuikSCAT[1] provides daily data on global winds. Binary and ASCII data on winds are available from QuikSCAT for 0.25 x 0.25 degree grid cells. Maps of the speed and direction of Ocean Surface Winds derived from QuikSCAT are also available in different formats from a number of sources. QuikSCAT wind data have an RMS error of 2 m/s for speed and 20 degrees for direction. Wind data is also available from the scatterometer on board the ERS-2[2] satellite. Wind data from ENVISAT is available as graphical maps, but the coverage is limited. Local ERS-2 Scatterometer and Altimeter data coincident with ERS-2 SAR are available for some areas, Rain is known to affect scatterometer derived measurements, resulting in cross track vectors with errors and/or wind speeds that are unrealistically high. Scatterometer data processing uses microwave radiometer measurements acquired simultaneously for rain flagging and sea ice detection. In the case of QuikSCAT, microwave radiometers like SSM/I on board the US Defense Meteorological Satellite Program (DMSP) series of satellites[3] are used to determine if rain or ice is present at

[1] The microwave scatterometer SeaWinds was launched on the QuikBird satellite in June 1999. The name QuikSCAT is used to distinguish it from the nearly identical SeaWinds scatterometer on Midori-II (ADEOS-II), launched in December, 2002. The SeaWinds instrument is third in a series of NASA scatterometers that operate in the Ku-band (frequency around 14 GHz).

[2] The scatterometer on the ERS-2 spacecraft operates in the C-band (frequency around 5 GHz).

[3] The DMSP series includes the satellites F13, F14 and F15 which have SSM/I instruments on board.

the location of the QuikSCAT observation. When QuikSCAT data is not available over a given SAR footprint, SSM/I wind data can be used. This means wind direction information would be unavailable for the given ERS footprint.

The Fleet Numerical Meteorology and Oceanography Center (FNMOC) of the US Navy provides maps of wind speed and direction derived by combining data from ERS-2 and QuikSCAT scatterometers and data from the DMSP-SSMI instruments for resolving directional ambiguity caused by rain and sea-ice. The FNMOC charts are useful but archived data is available only for the previous three days.

A graphical plot of QuikSCAT-derived wind speeds for each 0.25 x 0.25 degree grid cell in an ERS SAR footprint (approximately 100 x 100 km) is shown in Figure 23 to illustrate the use of QuikSCAT data for determining weather-compliance.

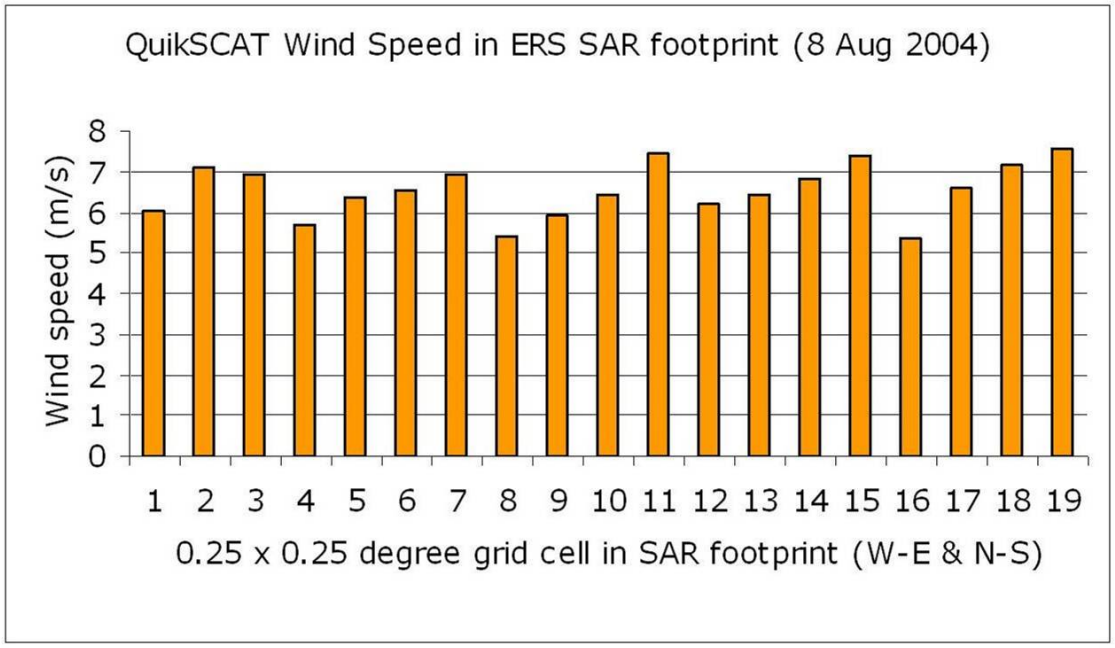

Figure 23. QuikSCAT derived wind speeds in SAR footprint.

Additional information on wind speed and direction is also available through weather reports made by ships in the vicinity of the ERS SAR footprint. Ships report weather under a WMO voluntary reporting regime. The reports include parameters such as, wind speed, wind direction, air temperature, water temperature and barometer readings for geographical coordinates that occur along a ship's route at regular intervals during the day.

However, not all ships provide weather reports and the detail or frequency of reports made by ships differ considerably. When available, the ship-based weather reports can be used to verify QuikSCAT-derived wind data and also provide redundancy when lack of QuikSCAT coverage for an area necessitates the use of interpolated or temporally averaged data.

A comparison of ship reported wind speed around the QuikSCAT data acquisition time revealed similar orders of magnitude for speed and direction between the two sources for most observations (Figure 24. Comparison of ship and QuikSCAT (2 m/s error bars) based wind speeds. (Figure 24). A randomly selected sample of 18 observations from five ships over three days was used for the comparison. The difference in data acquisition times between the two observation platforms ranges from 1 to 10 hours.

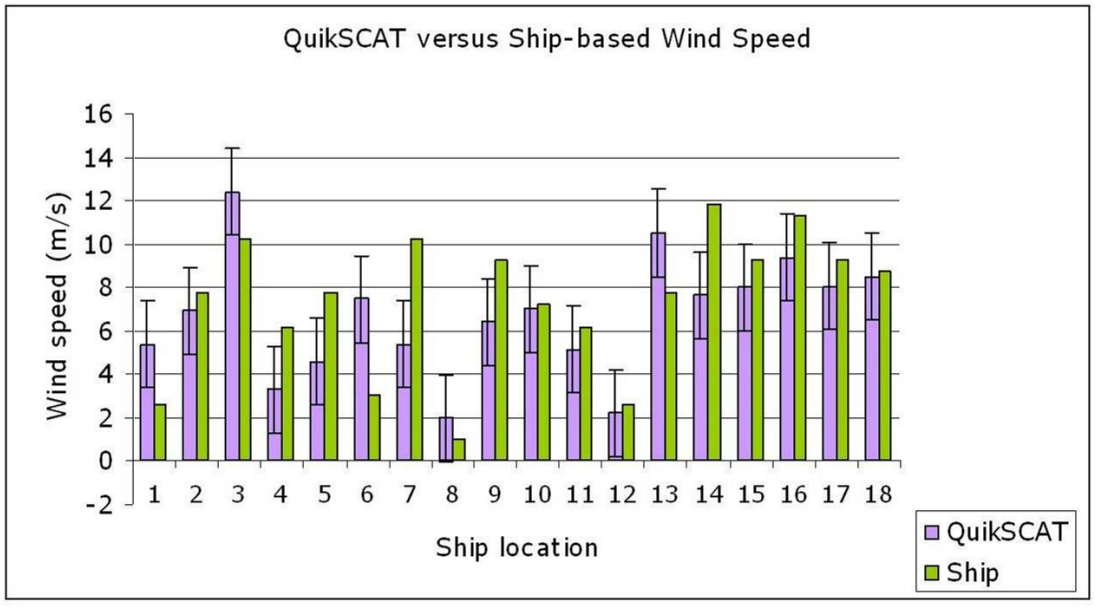

Figure 24. Comparison of ship and QuikSCAT (2 m/s error bars) based wind speeds.

4.1.7.2 Significant wave height

WAVEWATCH III (WW3), a sea-state prediction system, is used operationally at FNMOC. The global implementation of WW3 is forced by surface winds provided by the Navy Operational Global Atmospheric Prediction System (NOGAPS). Global WW3 runs twice per day, producing wave forecasts out to 144 hours from 0000 UTC and 1200 UTC. Regional WW3 implementations obtain lateral boundary conditions from Global WW3 and are forced by the surface winds provided by the Coupled Ocean/Atmosphere Mesoscale Prediction System (COAMPS). The model usually produces wave forecasts out to 48 hours from 0000 UTC and 1200 UTC on a grid which has 27 km spacing.

The FNMOC website provides graphical charts describing various sea-state parameters including significant wave height and direction. A typical FNMOC regional wave height and direction chart is shown in Figure 25. Similar data are also available from ENVISAT-based altimetry, but temporal coverage is limited. ERS-2 altimeter data that is coincident with the SAR image acquisition is more reliable than the modelled wave height information. ERS-2 altimeter data is now available for areas within the acquisition circle of the Hobart ground station.

4.1.7.3 Tide cycles

Tide cycle predictions for various locations are available from a number of sources. A web-based tide predictor system - XTide at http://www.mobilegeographics.com:81/ provides tide information for over 7000 tide stations around the world. The algorithm that XTide uses to predict tides is used by the National Ocean Service in the US. Deviations of 1 minute from official predictions are typical for US locations and deviations of 20 minutes are typical for non-US locations or locations not using current harmonics data.

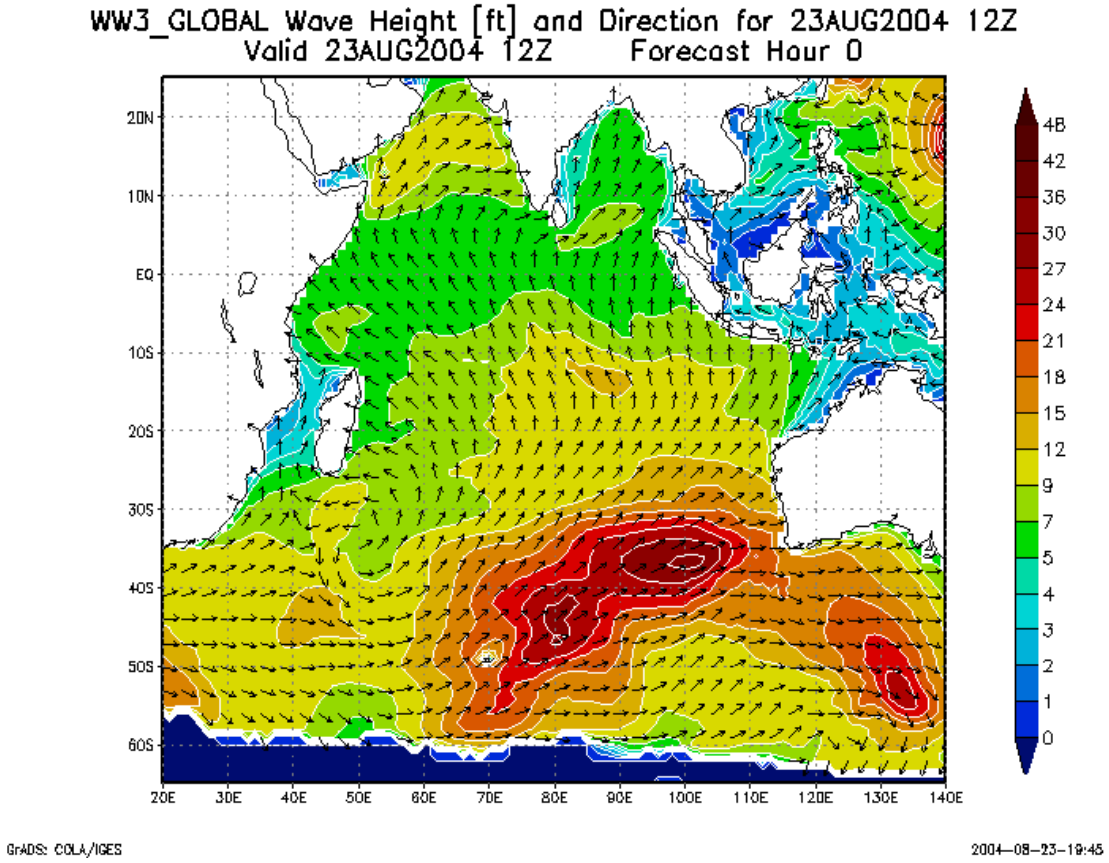

Figure 25. Regional WAVEWATCH 3 chart showing wave height & direction.

XTide also provides information about shipping in the vicinity of the tide station including access to weather details (wind speed & direction) reported by the ships. Retrospective tide cycle information is also available. Examples of tide cycle information in tabular and graphic forms for Cape Croker are shown in Table 2 and Figure 26 respectively.

Table 2. Tide cycle information for Cape Croker.

Cape Croker, Australia 11.0000° S, 132.5667° E		
2004-10-08	5:42 PM CST	0.95 meters Low Tide
2004-10-08	6:35 PM CST	Sunset
2004-10-09	1:07 AM CST	1.60 meters High Tide
2004-10-09	4:20 AM CST	1.52 meters Low Tide
2004-10-09	6:18 AM CST	Sunrise
2004-10-09	11:47 AM CST	1.75 meters High Tide
2004-10-09	6:35 PM CST	Sunset
2004-10-09	7:08 PM CST	0.98 meters Low Tide
2004-10-10	1:50 AM CST	1.66 meters High Tide
2004-10-10	6:18 AM CST	Sunrise
2004-10-10	7:33 AM CST	1.42 meters Low Tide
2004-10-10	1:06 PM CST	1.78 meters High Tide
2004-10-10	6:35 PM CST	Sunset
2004-10-10	8:10 PM CST	0.97 meters Low Tide
2004-10-11	2:23 AM CST	1.75 meters High Tide
2004-10-11	6:17 AM CST	Sunrise
2004-10-11	8:32 AM CST	1.25 meters Low Tide
2004-10-11	2:07 PM CST	1.85 meters High Tide
2004-10-11	6:35 PM CST	Sunset
2004-10-11	8:55 PM CST	0.95 meters Low Tide
2004-10-12	2:53 AM CST	1.85 meters High Tide
2004-10-12	6:17 AM CST	Sunrise
2004-10-12	9:14 AM CST	1.06 meters Low Tide
2004-10-12	2:59 PM CST	1.94 meters High Tide

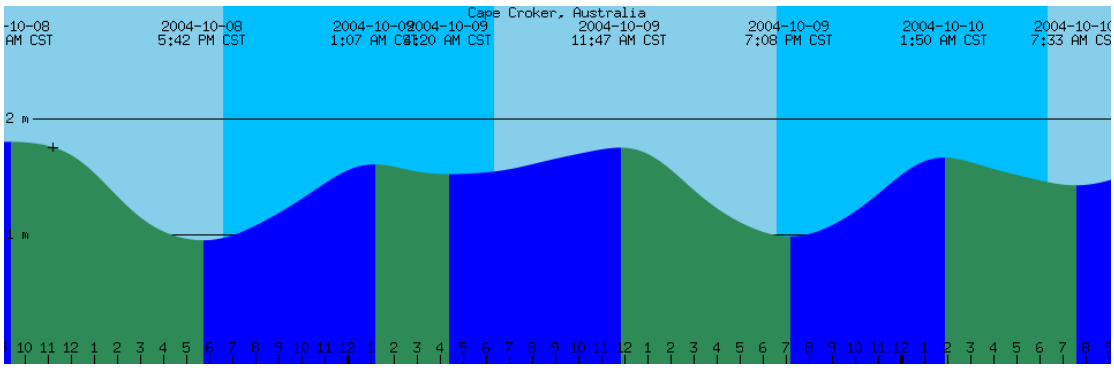

Figure 26. Graphic tide-cycle chart for Cape Croker.

4.1.7.4 Optical datasets

Data from optical sensors can support SAR interpretation under cloud-free conditions and when observation is coincident with SAR data. For example, data from MODIS or MERIS can help isolate slicks with a biological origin by virtue of their sensitivity to the presence of chlorophyll. The MODIS instruments onboard both NASA's Terra and Aqua satellites have the necessary wavebands to detect phytoplankton fluorescence from chlorophyll-a, which can be used to help identify whether phytoplankton is present in slicks.

The key limitations for the extensive use of commonly available optical data in offshore seepage studies are:

- Low revisit frequency and low spectral and temporal resolution;
- Cloud cover;
- Accurate identification of false positives;
- High cost;

Optical data sets provide complementary information to support SAR interpretation and can be used to target detailed studies over the seep areas identified on SAR. The section on hyperspectral applications exemplifies this idea.

4.2 Effect of sensor resolution on slick detection – various sensors

Spectral and spatial resolution are two important considerations when evaluating the potential of remote sensing data for oil slick detection are. With regards to spectral resolution, the use of hyperspectral data for natural oil slick detection is reviewed in section 4.5 (for the visible and near-infrared wavelength range).

The literature reports on the use of optical sensors with a range of spatial resolution for oil slick detection. However, these case studies typically involve the detection oil spills, typically of large extent and known timing and location (Malthus and Karpouzli, 2007). Examples of these case studies range from the use of the airborne 2.5 m spatial resolution CASI sensor to detect an intentionally created localised oil spill (Lennon et al, 2005) to the use of 250 m spatial resolution MODIS sensor to detect a large oil spill in Lake Maracaibo, Venezuela (Hu et al, 2003). There are no studies reported in the literature that provide information on the effect of spatial

resolution on the detection of seepage-derived oil slicks. Such naturally occurring oil slicks are typically of a smaller spatial extent than significant oil spills, and are expected to require relatively high spatial resolution data to be detectable using optical remote sensors. Furthermore, they exhibit spatial patterns that, if discernable - given sufficiently high spatial resolution remote sensing data - may aid in the correct diagnosing of the presence of hydrocarbon oil. In the following section, we discuss initial, qualitative findings regarding the effect of spatial resolution on natural, seepage-derived oil slick detection.

We compared imagery from four different sensors over the same study site off Coal Point in the Santa Barbara Channel, USA. This location features some of the world's most prolific seeps, manifesting as extensive oil slicks on the water surface (Figure 27). The four sensors used were Quickbird (approximate spatial resolution 2.4 m), HYMAP (approximate spatial resolution 4 m), ASTER (approximate spatial resolution 10 m), and Landsat ETM (approximate spatial resolution 30 m). The coverage of each sensor over a similar area, for differing dates, off Coal Point is shown in Figure 28. Note that the location and extent of the oil slicks vary in each image due to differing wind and current conditions.

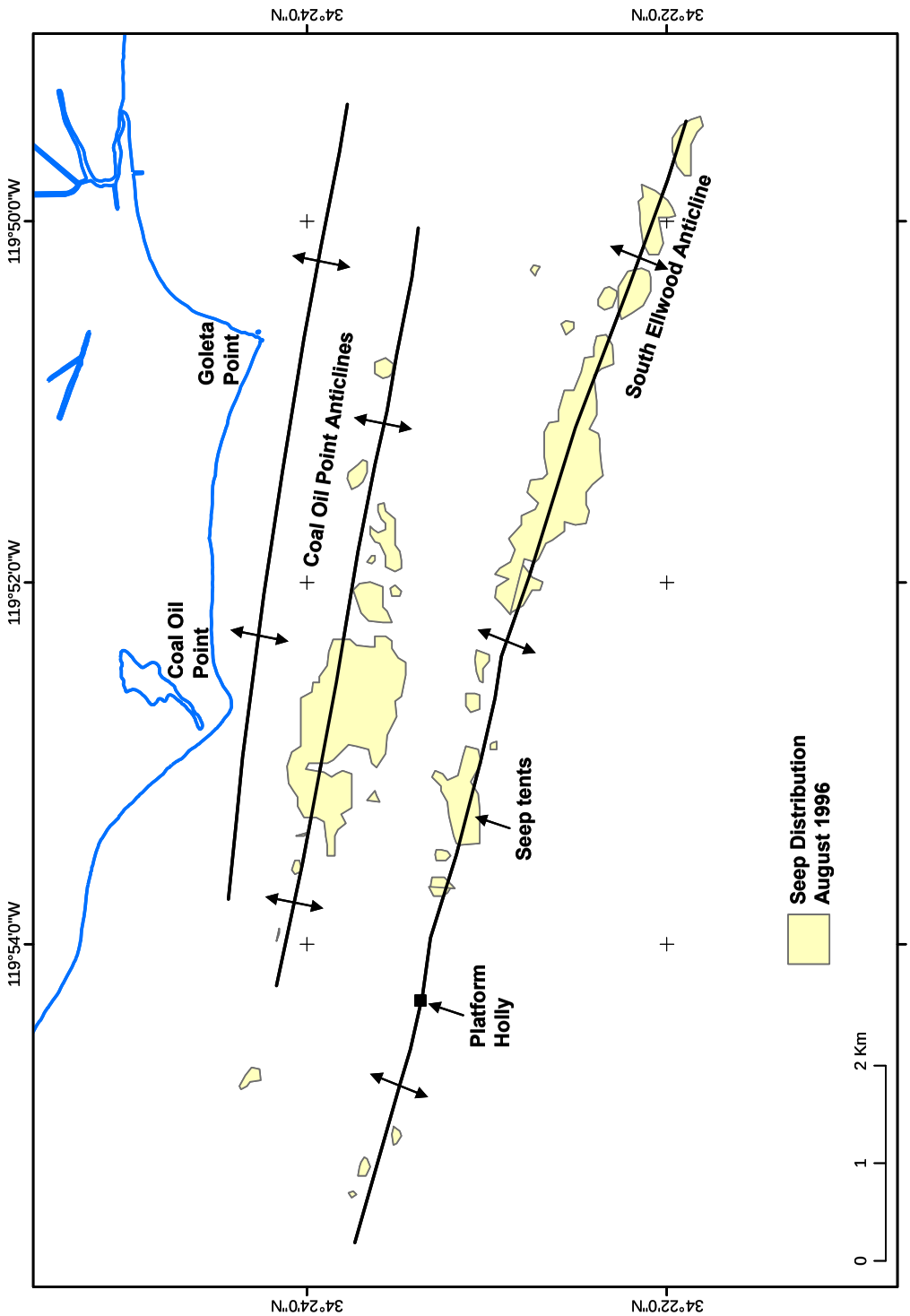

Figure 27. Location of some of the more important sources of seeps off of Coal Point in the Santa Barbara Channel (modified from Boles et al., 2001).

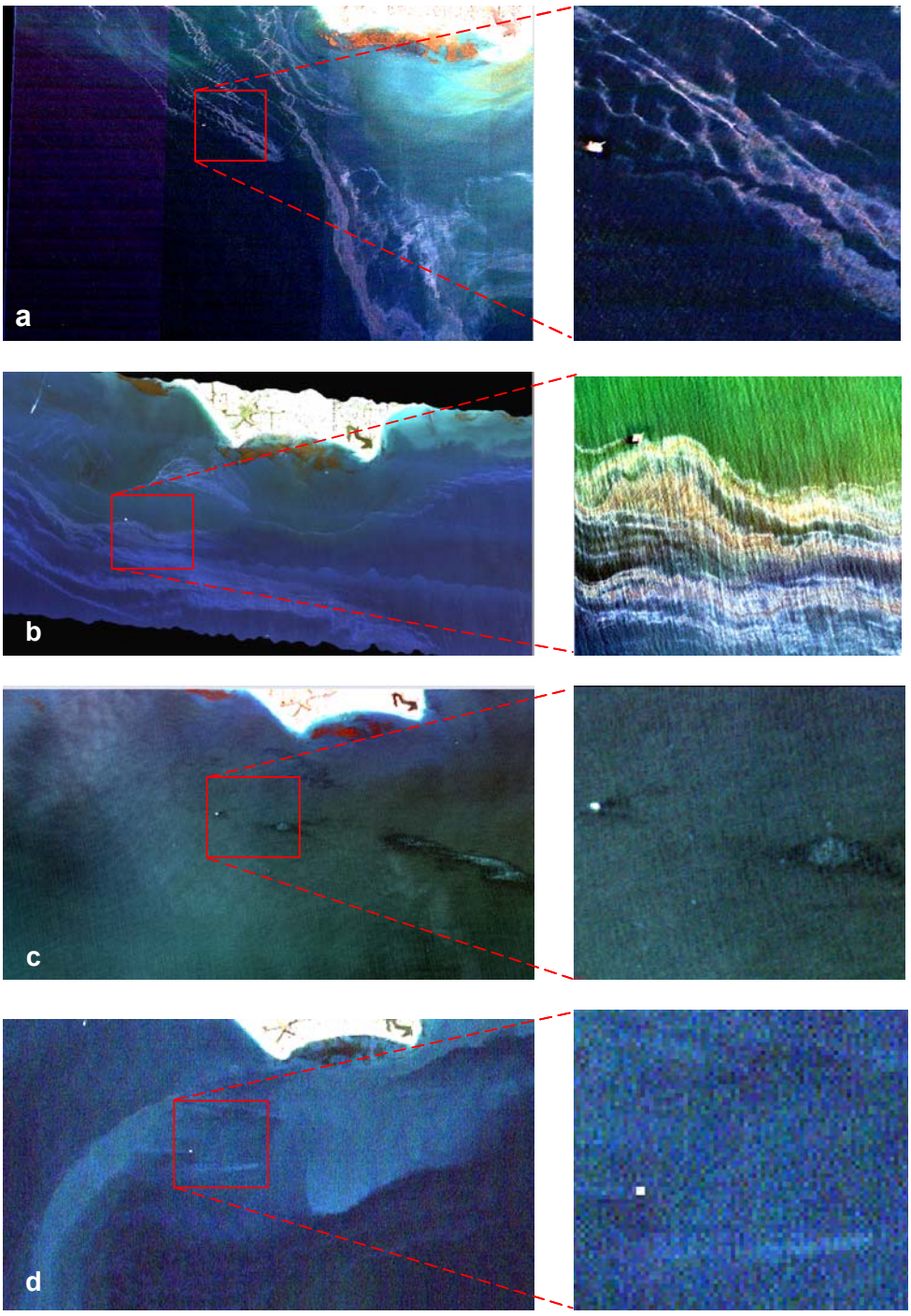

Figure 28. Pseudo-true colour imagery, covering a similar area off Coal Point, from the a) Quickbird b) HYMAP c) ASTER and d) Landsat sensors.

The spatial heterogeneity and patterns of the oil slicks are discernable in both the 2.4 m (Quickbird) and the 4 m (HYMAP) data (Figure 28a and Figure 28b respectively). In the 30 m spatial resolution data (Landsat), areas of relatively brighter contrast are seen in the water, which are most likely representative of the broadscale distribution of the oil slick areas in the scene. However, the typical spatial patterns of the slicks, as seen in the 2.4 m data, are not discernable (Figure 28d).

Oil layers on water will exhibit a range of contrasts and colours, depending on thickness and viewing/illumination geometry. As a general rule, relatively thicker oil will appear reddish brown through to black, whereas relatively thinner oil layers will appear as a light blue or silvery sheen. These variations in colour are visible in both the 2.4 m and 4 m data (Figure 28a and Figure 28b), whereas the 30 m pixels are averaging the spectral response and only show an overall change in contrast over what is (presumed to be) oil-covered and oil-free water (Figure 28d).

We conclude that 30 m spatial resolution is not sufficient to identify these natural oil slicks based on spatial patterns, although given sufficiently widespread slicks, the overall distribution of oil covered waters can be inferred.

The ASTER scene (Figure 28c) is markedly different from the other three scenes. Firstly, the ASTER multispectral sensor does not have a channel in the blue region of the visible spectrum, giving the pseudo-true colour image a different colouring. More importantly, the widespread slicks visible in the other images (particularly Figure 28a and Figure 28b) are not seen in the ASTER image. Instead, the ASTER scene shows anomalous features corresponding well with the location of the seep sources (Figure 27). These features appear as relatively bright elongated objects surrounded by a dark border in the lower right hand half of the scene.

According to theoretical work in the literature (Otremba, 2000; 2001; Otremba and Krol, 2002), the following general rules for the appearance of oil on water apply

- Oil on water may have negative (darker), positive (brighter) or zero (no) contrast with oil-free water.
- Relatively thin oil layers often appear brighter than oil-free waters (depending on illumination and viewing geometry).

- Sufficiently thick oil layers appear darker than oil-free waters, due to wavelength-dependent absorption of light by the oil.
- Emulsions of oil in water (relatively high concentrations of oil mixed into water column) may appear brighter than oil-free waters due to backscattering by the emulsion (depending on illumination and viewing geometry).

Thus, the oil surface layer thickness at which the contrast with clear waters changes (e.g. from positive to negative by progressing through the first two conditions (above) is both wavelength- and oil type-dependent.

We suggest that the ASTER scene is showing the areas of highest oil-in-water concentrations (directly above the seeps) as highly reflective emulsions. These are surrounded by relatively thicker layers of oil, which are revealed as absorbing (dark) features. Beyond these high density areas, the thinner layers of oil visible in the other three scenes (as relatively brighter than surrounding waters) are not visible. This is most likely due to the illumination conditions of this scene.

By comparison, the Landsat scene appears to show more widespread areas of relatively brighter waters that may correspond to thinner oil layers. The sun elevation of the ASTER and Landsat scenes was 29 and 57 degrees respectively. The more pronounced oblique illumination conditions in the Landsat scene could account for the apparent presence of thinner oil layers, which are not visible in the ASTER scene. Additionally it should be noted that the blue wavelength region is more sensitive to oil-relevant information and this wavelength region is not sampled by the ASTER sensor.

The MERIS sensor features approximately seven channels in the visible spectrum, and has global coverage with high re-visit frequencies (2-3 days). It could therefore be a suitable tool for global, broadscale oil slick detection. As a first qualitative inspection, we re-sampled the 2.4 m Quickbird data to full resolution 300 m pixel equivalent MERIS data. Not surprisingly, this synthetic image shows no apparent oil-diagnostic spatial patterns (Figure 29). As an example, the relatively brighter shallow water areas in the northern part of the image - which in the Quickbird image clearly do not have the same spatial pattern as the oil slicks - are not spatially distinct from

the oil slicks areas in the MERIS simulation. As with the Landsat image, no oil-diagnostic colour variations are visible, and the spatial patterns typically associated with natural oil slicks of Santa Barbara are not apparent. At the same time, the heightened contrast from oil-covered waters is discernable. It may therefore be that MERIS can provide complementary information on the potential presence of oil. An example would be for imagery where viewing and illumination conditions of oil slicks create a positive contrast, and where the target is sufficiently offshore so as to avoid false positives from e.g. shallow waters and sediment plumes.

In conclusion, of the five sensors discussed here, only the 2.4 m and 4 m resolution of the Quickbird and HYMAP sensors, respectively, were sufficient for observing the spatial patterns typical of the oil slicks of Santa Barbara waters. As we consider these natural seep systems to be best-case scenarios, we submit that sensors with a spatial resolution equal to or coarser than the Landsat sensor (30 m) are not applicable for oil layer diagnosing applications that rely to some extent on spatial patterns. We believe the ASTER data featured viewing and illumination conditions that were prohibitive to viewing the thinner slicks and direct comparison with the other images was therefore not possible. The absence of these thinner slicks may also be in part due to the absence of a blue channel in the ASTER sensor.

The above qualitative analyses discussed above focused on spatial resolution and its limitations in positively identifying natural oil slicks based on their spatial patterns. It is our experience that spectral resolution (with the potential of spectral un-mixing techniques), as well as signal-to-noise characteristics, may significantly skew the spatial resolution rules-of-thumb for a given application.

Figure 29. The a) Quickbird scene of oil slicks in the Santa Barbara channel b) re-sampled to MERIS full resolution 300 m pixels. The unique spatial patterns attributable to the oil slicks, apparent in the Quickbird scene, are not evident in the MERIS simulation, where the shallow waters in the upper right-hand area of the scene look similar to the oil slicks in the lower half.

4.3 Analysis of SAR for identification and characterisation of slicks

The Geoscience Australia methodology framework for SAR-based slick detection and seep identification (Jones et al, 2005b, 2006; Thankappan et al, 2006, 2007) is summarised in the flowchart in Figure 30. Various elements outlined in the methodology flowchart are described in greater detail in the following sections.

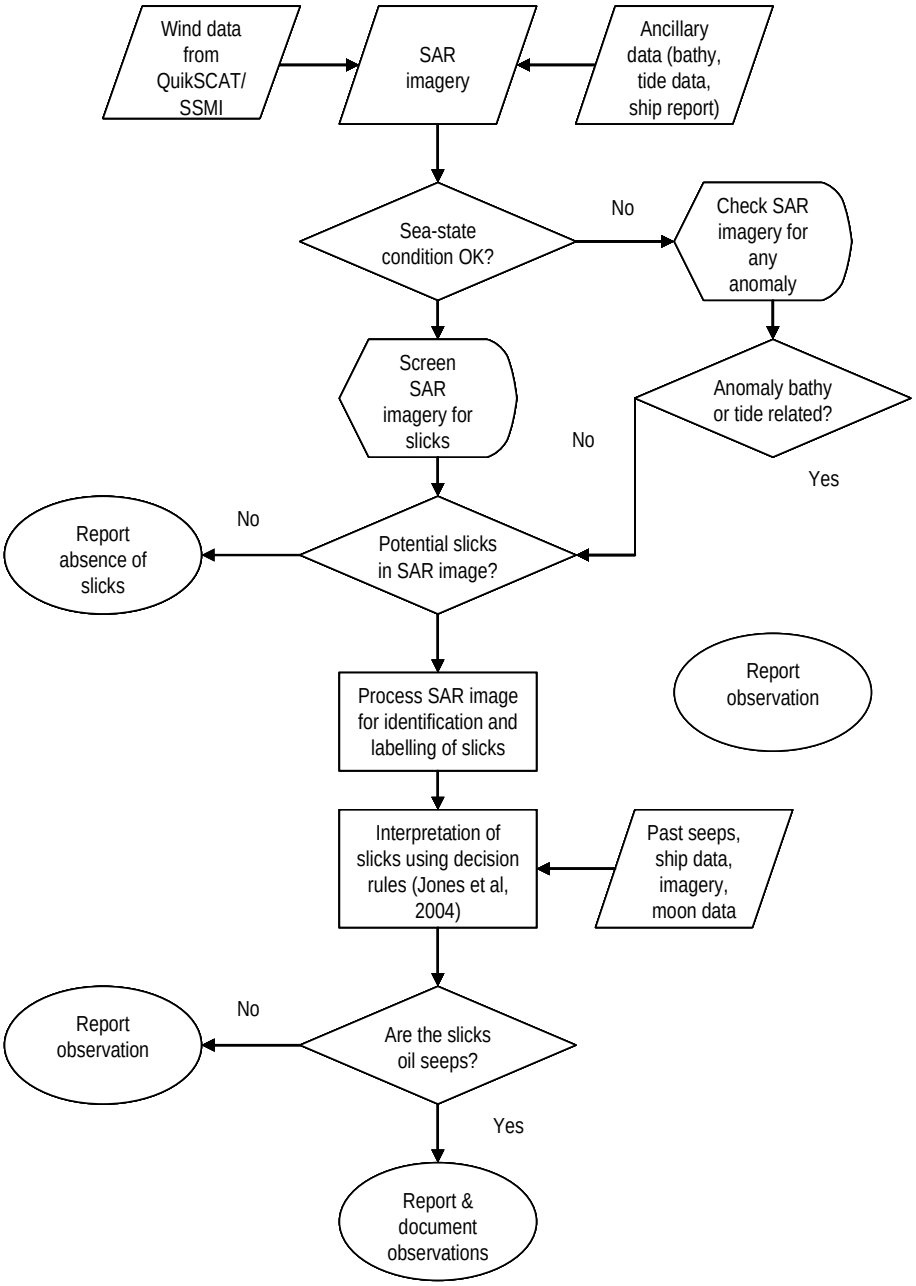

Figure 30. Methodology for screening SAR imagery for hydrocarbon seep identification.

Screening SAR imagery for the presence of slicks consists of three main steps, SAR image calibration, visual inspection of image and analysis in a GIS. Regardless of weather screening for SAR imagery, it needs to be visually inspected for anomalies. The reason for this exercise is that the ancillary data source being used for weather screening may not be coincident with the acquisition of SAR imagery, may have errors, may be of a coarser resolution or poor quality or, have incomplete coverage for a given SAR footprint.

4.3.1 SAR image calibration

Calibration of SAR data involves converting digital values in the images to estimates of the radar cross section or sigma 0 (σ_0). This is essential when SAR data is used for precise measurements.

Calibrating the SAR imagery to σ_0 values helps to normalise apparent brightness variations associated with uncalibrated ocean SAR data. Calibrating the image data to backscatter values also helps to characterise slicks in terms of the backscatter reduction. An example of raw and calibrated ERS SAR imagery is shown in Figure 31, where brightness variations associated with local incidence angle variations are normalised in the calibrated image.

4.3.2 Visual inspection of calibrated SAR image

The calibrated image is displayed on an image processing system for visual assessment and identification of low backscatter features. When a low backscatter feature is identified, the feature's location, shape, backscatter suppression and edge characteristics are recorded. Demarcation of the low backscatter feature(s) outline(s) is also carried out on the image for further analysis.

4.3.3 Analysis in a GIS environment

To ensure that a comprehensive analysis is carried out using supporting datasets, the calibrated SAR image is loaded into a GIS environment. Ancillary data including bathymetry, wind speed & direction, wave height and direction and location of ships present in the vicinity (to identify potential pollution related slicks) are also loaded into the GIS. Often, not all datasets are easily ported into a GIS and analysis has to be made outside the GIS environment, for example, where supporting datasets are not geocoded but available as charts.

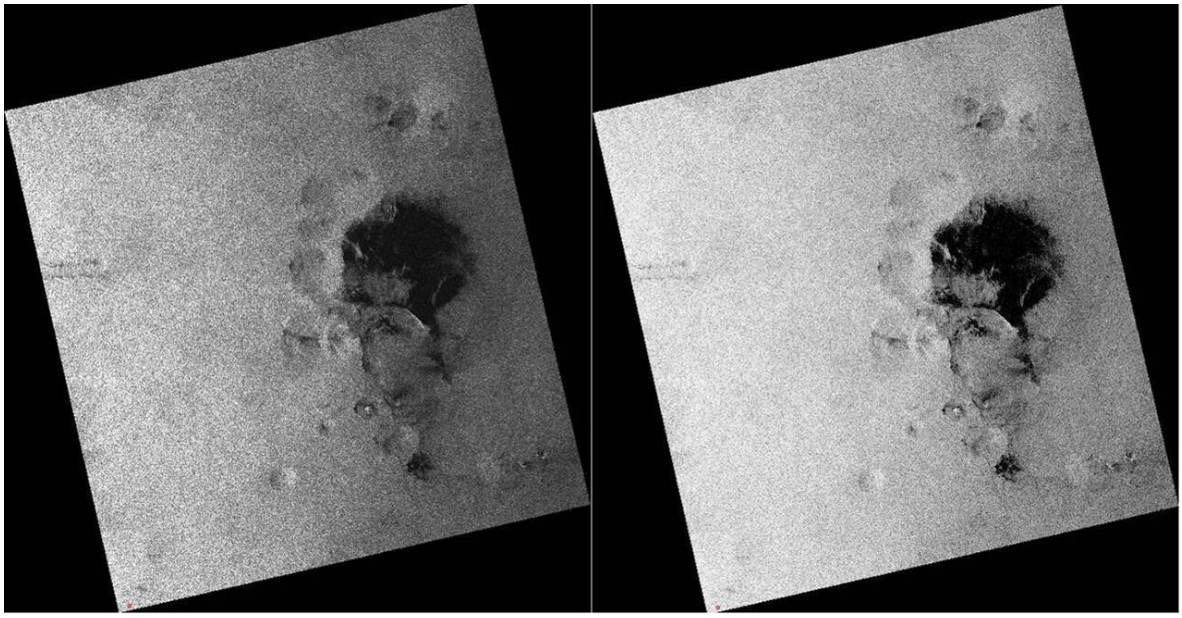

Figure 31. Raw (left) versus calibrated (right) SAR image

4.3.4 Interpretation summary

Based on analysis within the GIS and other supporting information (Jones et al, 2006), slick interpretation results for each SAR scene can be summarised as shown in the Table 3.

Table 3. Typical summary of scene-wise analysis & interpretation (Jones et al, 2006).

Scene Name : ARAF01 **Orbit: 48589 Frame: Mode: Ascending** **Acquisition date/time: 05-Aug-2004 UTC 13:47:37 (CST 23:17:37)** **Scene centre coordinates: S10:33:53 E134:34:56**					
Wind speed & direction (where available)	**Significant Wave height**	**Tide cycle data for Cape Croker**	**Ships in the vicinity**	**Low backscatter features**	**Notes**
8 - 10 m/s SSMI - F14 E At UTC 10:06 3-day average SSMI – F14 2.5 – 5.0 m/s	3 – 6 ft At UTC 12:00	2004-08-05 7:21 PM CST 2.14 metres High Tide 2004-08-06 1:34 AM CST 0.78 metres Low Tide	Gulf Cloud S12°42' E140°36' reported wind speed of 20 knots from 210 at UTC 15:00 (10.28 m/s from SW)	None identified	High wind speed around SAR acquisition time. Wind speeds leading up to the SAR acquisition have been favourable.
Result No low backscatter features identified on the SAR image. Wind speed around the time of SAR acquisition was at the upper end of the threshold for slick detection.					

4.4 Quality controls applied to slick interpretations at Geoscience Australia

The following sections discuss details on how SAR-based interpretations have been reassessed to provide greater confidence for oil slick interpretations. Initially, the quality control assessment of interpreted SAR slicks in the southern Timor Sea used in Jones et al. (2005b) will be illustrated. The seepage slicks that were re-analysed were a subset of the slick suite that has been detected, characterised and interpreted in the broader Timor Sea region (O'Brien et al., 2001, 2002, 2003b). Dense clusters of seepage slicks were identified over the Yampi Shelf headland and over the Browse Bonaparte Transition Zone, with scattered slicks throughout the majority of the area (Figure 32). The data were acquired on the RADARSAT platform. Fourteen Wide 1 Beam Mode scenes cover the area, giving up to five-fold coverage of some regions, including the Yampi Shelf headland (Table 4). This assessment was not a reinterpretation of the primary SAR data. Rather, it was based on a re-evaluation of the size and shape of the previously identified seepage slicks (NPA et al., 1999) in the context of ancillary environmental and bathymetric data. The primary data were analysed by NPA Ltd. and Treico Ltd. (NPA et al., 1999), who differentiated discrete slicks from meteorological effects (eg. wind fronts, rain cells) and internal waves. The sea surface slicks were originally interpreted as natural film, pollution slicks and seepage slicks, with varying levels (ranks) of confidence (NPA et al., 1999). The primary differentiation between seepage slicks and natural film or pollution slicks was based upon the experience and expertise of NPA Ltd. and TREIC^{o} Ltd., and was assumed to be valid. Therefore only those slicks characterised as Rank 2 (the highest confidence rank without verification from sea surface samples) and Rank 3 seepage slicks were considered for further re-analysis. For these slicks alternative formative processes were investigated. It should be noted that the reappraisal was facilitated to a large extent by the descriptive supplementary data and metadata provided in the original SAR interpretation report.

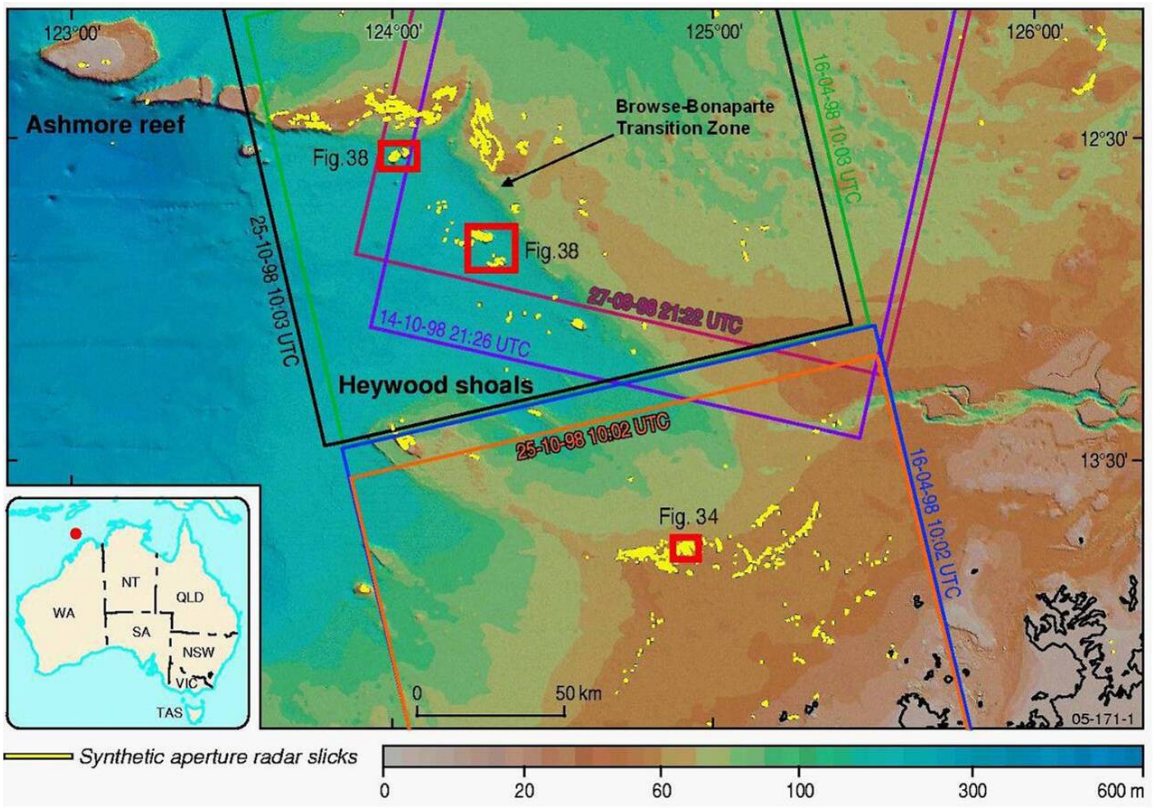

Figure 32. Area of the Timor Sea in which SAR data were assessed for quality control showing bathymetry, distribution of SAR slicks throughout the region (NPA et al., 1999) and outlines of scenes from Table 4.

Table 4. Time of synthetic aperture radar scene capture, supplemented with environmental data (NPA et al., 1999) and tide times calculated with XTide tidal prediction software. Times in Western Australian standard time.

SCENE	DATE	TIME	TIDE	TURN OF TIDE	WIND	SWELL	TOTAL NO. SLICKS
Yampi Shelf							
RSW1-32	16–4–98	18:02	Ebb	Low tide in 1 hour	1-2 knots – 090°	1m	106
RSW1-54	15–10–98	5:26	Flood	High tide in 2 hours	2-3 knots – 190°	1m	2
RSW1-55	25–10–98	18:02	Ebb	Low tide in 30-45 minutes	2 knots – 260°	<1m	210
RSW1-58	11–9–98	5:18	Ebb	Low tide in 2 hours	2 knots – 080°	1m	3
RSW1-125	13–4–98	5:22	Low tide	Precisely at low tide	2-3 knots – 260°	1m	1
Browse-Bonaparte Transition Zone							
RSW1-53	25–10–98	18:03	Ebb	Low tide in <1 hour	2 knots – 170°	<1m	26
RSW1-56	15–10–98	5:26	Flood	High tide in 1-2 hours	1-2 knots – 225°	1m	76
RSW1-65	28–9–98	5:22	Ebb	Low tide in 3 hours	2 knots – 180°	1m	3
RSW1-129	16–4–98	18:03	Ebb	Low tide in 1 hour	2 knots – 070°	<1m	71

The following sections outline the details of the re-assessment of SAR data, and is based on to a large extent on the findings of Jones et al., (2005b and 2006). The methods used can be applied to other existing datasets and provide the basis for part of a quality control assessment that is now applied within Geoscience Australia.

4.4.1 SAR slicks related to bathymetry – Yampi Shelf

The SAR slicks identified on the Yampi Shelf represent the greatest density of slicks in the Timor Sea (O'Brien et al., 2001). They occur in water depths of about 55 to 75 m on the northeastern Yampi Shelf (Figure 32). They form part of a dense cluster of slicks on the northern margin of a bathymetric headland that extends westward to Heywood Shoals. The two RADARSAT scenes that show multiple slicks were acquired between neap and spring tides, when the tidal range was approximately 4 m i.e. when significant volumes of water were moving across the headland during each tide. The slicks display a relatively high slick/ocean radar backscatter contrast, and while the majority have highly irregular shapes, numerous examples have an elongate or complex lobate morphology, and are up to 4.8 km long and 1.25 km wide (Figure 33). A number of these slicks repeat almost precisely in terms of morphology and

position in two of the five interpreted SAR scenes across the Yampi Shelf. This repetition was the primary basis for the seepage interpretation previously presented for these slicks (NPA et al., 1999).

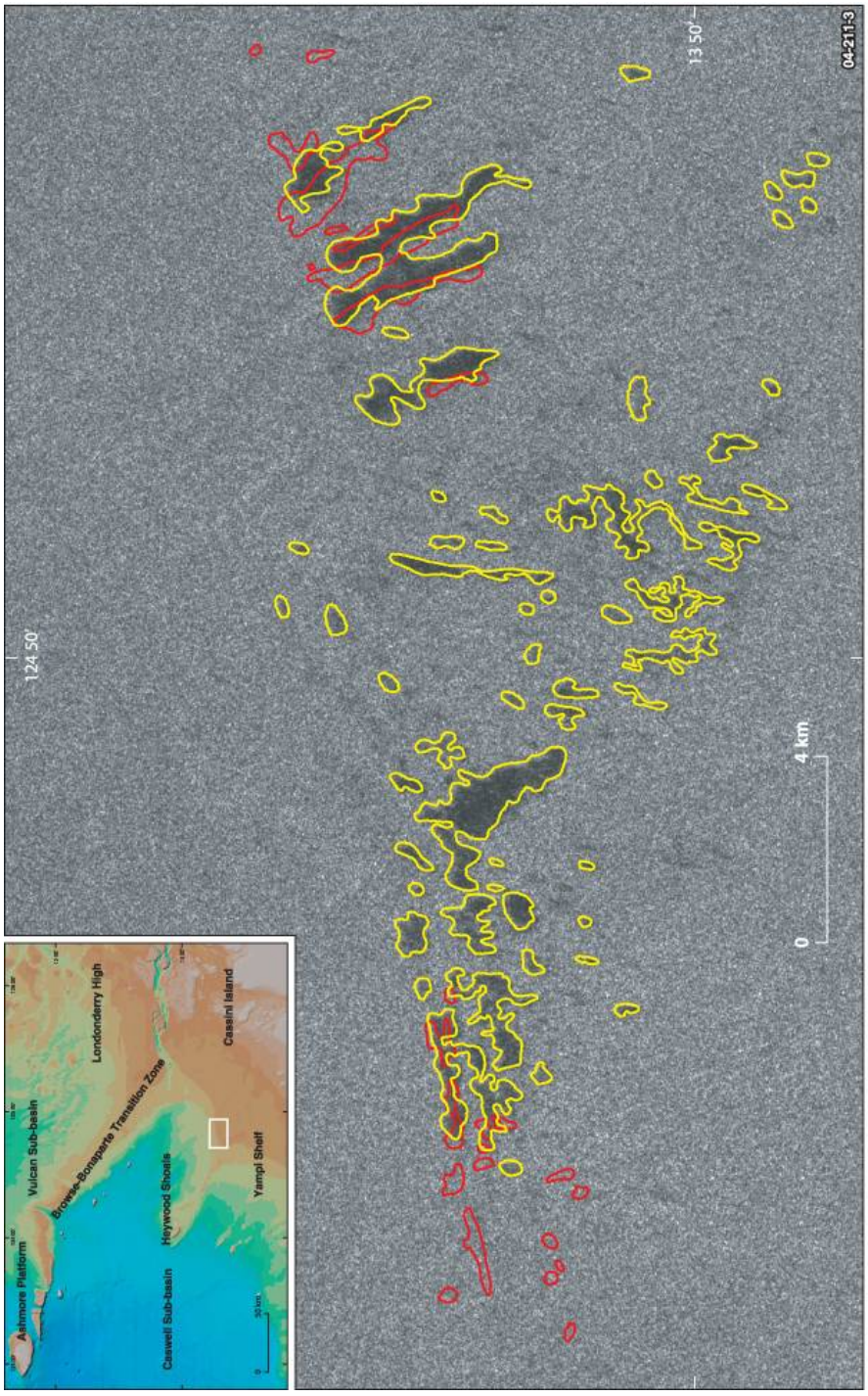

Figure 33. Slicks in part of a synthetic aperture radar scene (RSW1-55;) that covers the greatest density of interpreted slicks over the Yampi Shelf Headland (NPA et al., 1999). The red outlines are from an alternate scene (RSW1-32; Table 4), with the two scenes being captured six months apart. Note the repetition of some of the significant slicks, particularly in the eastern part of the area (from Jones et al., 2005b, 2006).

Swath data from S267 revealed numerous subtle bathymetric features (100 m across and 10-20 m deep in 50 to 80 m water depth), which were not identified on hydrographic charts of the region. They have been interpreted as tidal channels and they display a distinct spatial correlation with the major SAR slicks in this part of the Timor Sea (Figure 34). The size, number, orientation and spacing of the channels matches that of the large SAR slicks that repeat in two of the five scenes interpreted (Jones et al., 2005). The precision of the spatial relationship between the SAR slicks and the mapped channels strongly suggests a bathymetric control on the formation of the SAR slicks, which is a phenomenon that has been well documented in the literature (eg. Kasischke et al., 1983; Harris et al., 1986).

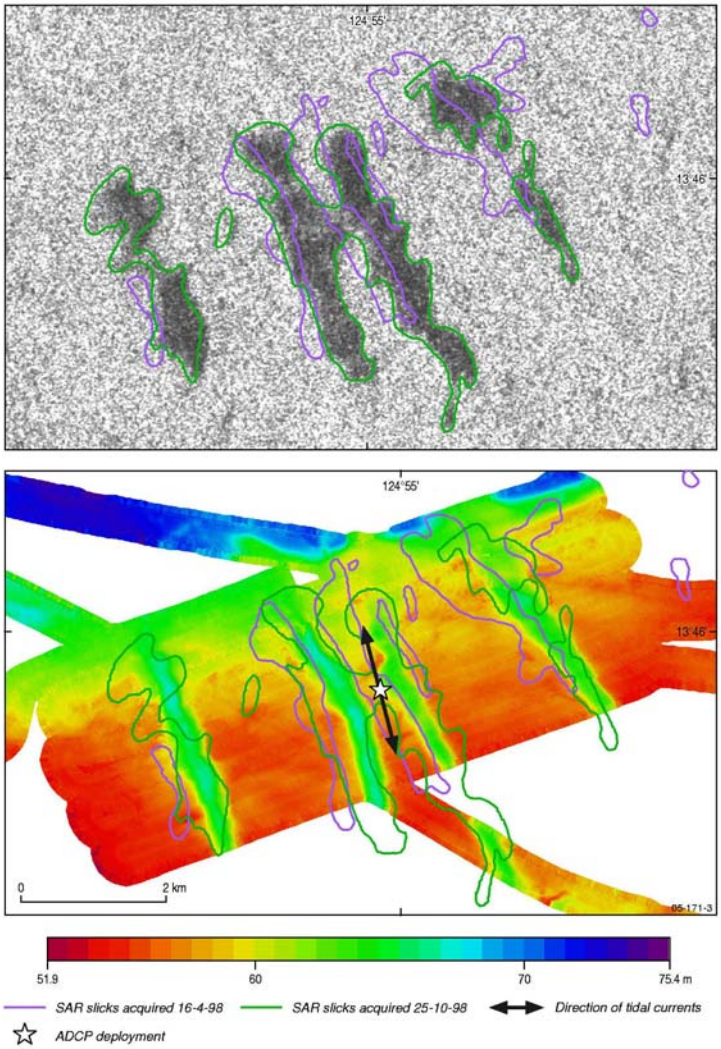

Figure 34. a) SAR slicks from 10:02 UTC 25-10-98 and outlines of slicks from 10:03 UTC 16-4-98, showing overlapping nature of slicks. b) Multibeam swath bathymetry of the area showing palaeo-tidal channels underlying the SAR slicks (from Jones et al., 2005b, 2006).

The Acoustic Doppler Current Profiler (ADCP) data acquired during S267 indicates that the direction of the tidal flow is aligned with the orientation of the channels and the SAR slicks (Figure 34), and that flow direction is essentially consistent throughout the water column during peak tidal flows. Figure 35 shows the averaged directionless velocities from S267 ADCP deployments at different points in the tidal cycle. Figure 35 also shows the same data normalised to the lowest value within each profile, to highlight the velocity differences within the water column at each point in the cycle. The greatest differences (ie. accelerated surface flows) are seen in the upper section of the water column just before the turn of the tide (Figure 35). The ADCP data also provide insight into the frequency of repetition (ie. in two of the five SAR scenes), as they indicate that the greatest potential for formation of sea surface features associated with tidal flow over the channels on the Yampi Shelf is during the last hour of the tidal cycle. Therefore, the ADCP data provide good supporting evidence for slick formation due to capillary wave dampening associated with accelerated surface current flow above bathymetric features immediately before low tides, which is consistent with the timing of acquisition for the SAR scenes with the highest number of slicks (Table 4).

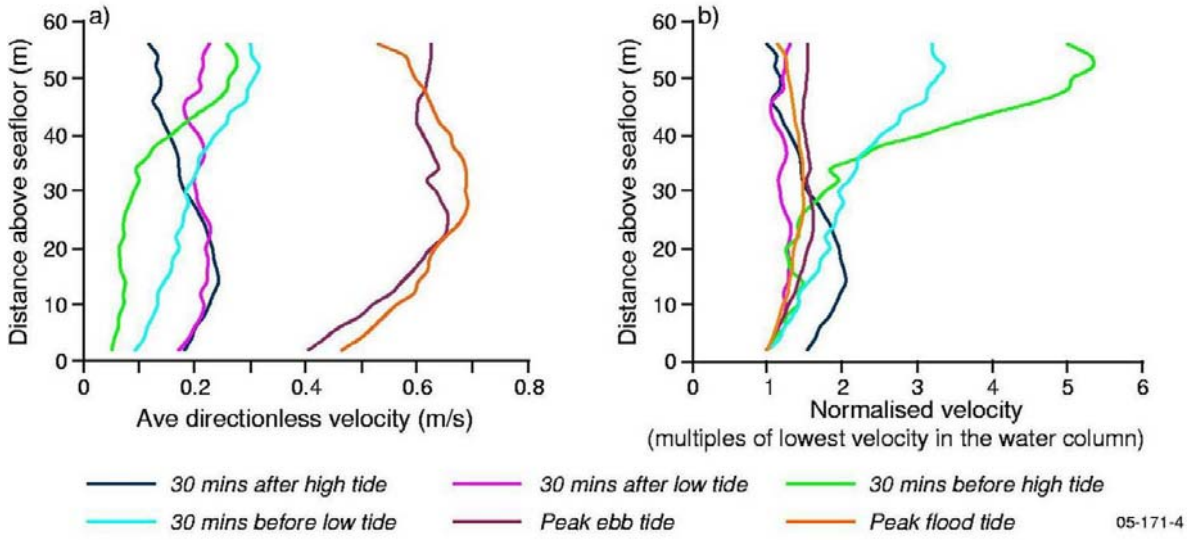

Figure 35. a) Averaged directionless velocities from both deployments at different points in the tidal cycle. b) Velocities normalised to the lowest value to highlight the velocity differences within the water column at each point in the cycle (from Jones et al., 2005b, 2006).

The cluster of large slicks over the Yampi Shelf headland most likely formed through the enhancement of natural film on a sea surface smoothed by bathymetric/current interactions. Such configuration of natural film slicks by surface currents has been recognised in previous SAR studies (eg. Johannessen et al., 1993; Espedal et al., 1996).

The correlation between seafloor bathymetry and features in remote sensing data was also demonstrated on the central NWS (Figure 36; Thankappan et al. 2007) and in the wider Timor Sea (Figure 37; Thankappan & Smith, 2006). Mesoscale and local SAR ocean features (Figure 36) were observed in multiple SAR scenes over the central NWS during a study of seepage in this region (Jones et al., 2007). A number of the scenes were acquired coincident with a marine survey. Oceanographic and bathymetric data acquired during this survey indicate that the SAR features correlated well with observed ocean current flow directions, and with the local bathymetry (Figure 36; Thankappan et al. 2007). In the Timor Sea, a series of bathymetric features on the relatively shallow shelf were observed on near-coincident SAR and optical images (Figure 37; Thankappan & Smith, 2006). This finding was significant in that it demonstrated the potential for deriving information about sea bottom topography from sun glint in optical images to complement similar information from near-coincident SAR images.

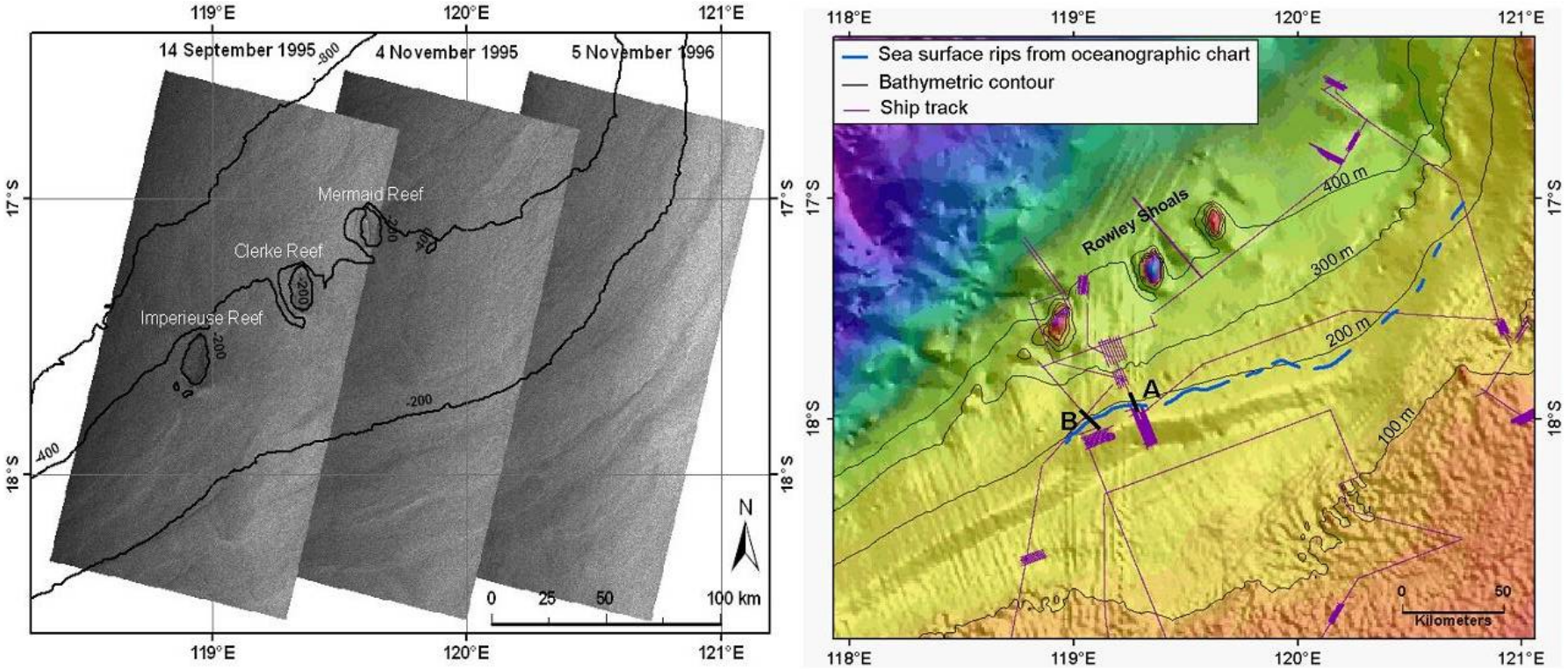

Figure 36. Mesoscale ocean features over the central NWS detected with SAR (from Thankappan & Smith, 2006).

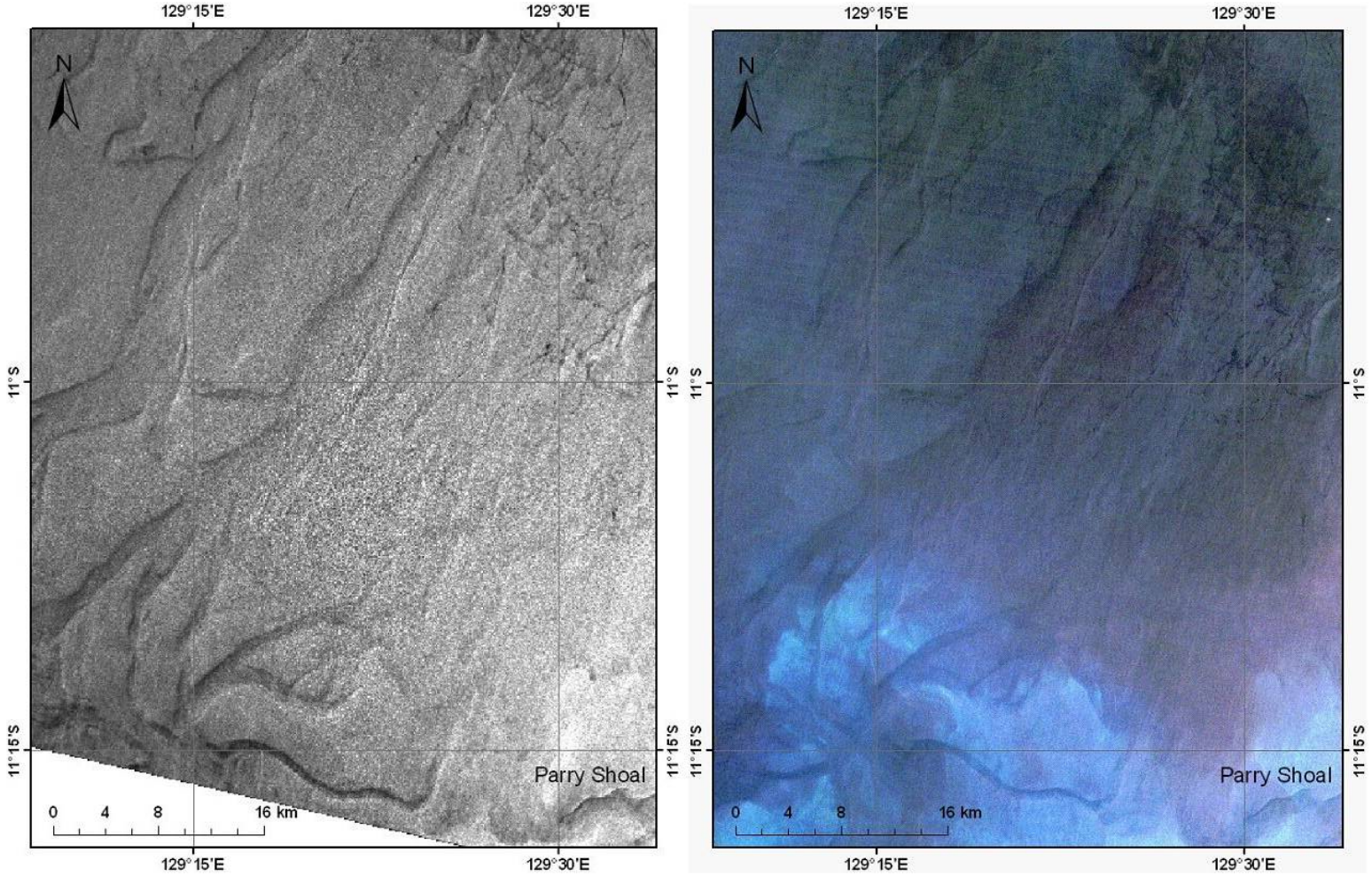

Figure 37. Near-coincident SAR and optical images from the Timor Sea with slicks related to bathymetry (from Thankappan & Smith, 2006).

4.4.2 SAR slicks related to biology - Browse-Bonaparte Transition Zone

The SAR slicks that overlie the Browse-Bonaparte Transition Zone are in an area with water depths of about 20 to 200 m (Figure 32), typically over and around a series of carbonate shoals The majority of slicks imaged in SAR scenes acquired on 15 October 1998 (76 slicks) and 25 October 1998 (26 slicks) are natural film slicks (NPA et al., 1999; Table 4), and as such were not considered for further analysis. In contrast, slicks imaged in the scene acquired on 16 April 1998 (71 slicks) display a complex backscatter pattern, have highly irregular to annular and crescent-like shapes (Figure 38), and sizes that vary from 260 m long and 160 m wide, up to approximately 25 km long and 8 km wide. These slicks, previously interpreted as natural hydrocarbon seepage slicks (NPA et al., 1999; O'Brien et al., 2001, 2002, 2003b), were reassessed on the basis of their shape, their relationship to the underlying bathymetry and time of scene acquisition.

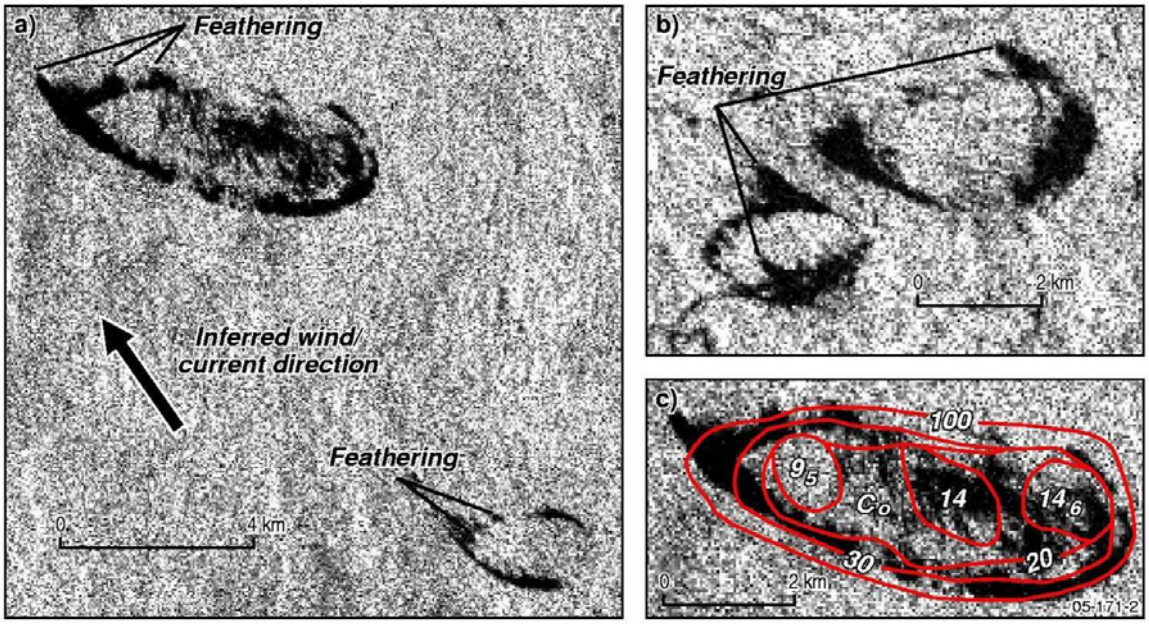

Figure 38. SAR slicks from 10:03 UTC 16-4-98 over (2a) Vulcan and Goeree Shoals, and (2b) Barracouta Shoal which display consistent feathering in a northwesterly direction. (2c) Demarcation of the slick over Vulcan Shoal by the isobath contours taken from the hydrographic chart of the region. Depth is shown in metres (from Jones et al., 2006).

The annular shape of some of the SAR slicks previously interpreted as probable (Rank 2) seepage slicks in this region (NPA et al., 1999) are atypical of seepage slicks characterised with this level of confidence, which tend to have an 'emission-point' with a linear, dog-legged or corkscrew habit related to wind and tidal directions, and a nested habit resulting from multi-emission points (NPA et al., 2003; Figure 39). The size of some slicks also makes an oil seep interpretation unlikely. The largest of the slicks in the Browse–Bonaparte Transition Zone (approximately 25 km long and 8 km wide) is centred around a point approximately 18 km southeast of the Prion-1 well. Seepage slicks of this scale are usually associated with only the most intensely seeping oil provinces, which are most commonly in active thrust belts and in overpressured diapir-rich basins (Macgregor, 1993) (see Section 7).

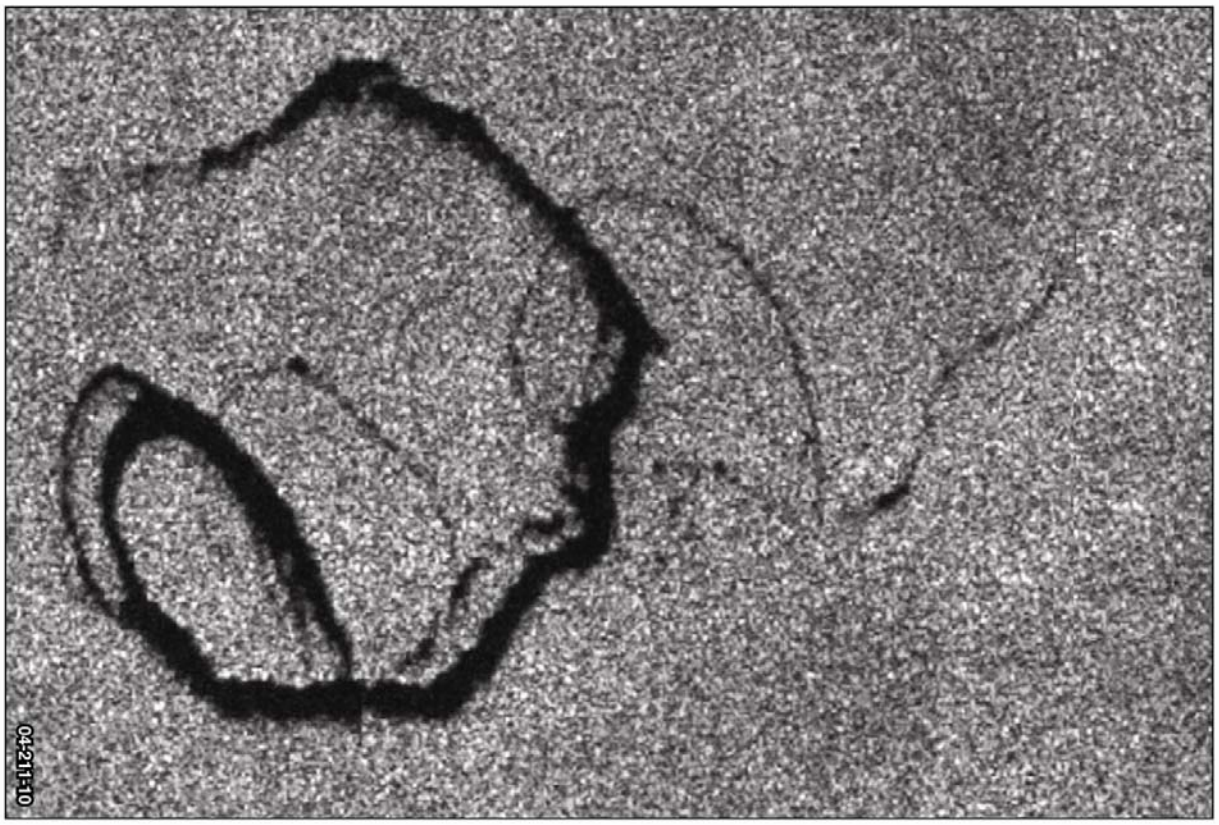

Figure 39. Image of a 'classic' corkscrew natural seepage slick from the South Caspian basin (supplied by A. Williams, NPA Pty. Ltd.). The slick is 2.5 km across.

The distinct annular shape of some slicks over the Browse-Bonaparte Transition Zone matches the morphology of underlying shoals almost precisely, typically occurring above the margins of the shoal (Figure 38). Consistent 'feathering' is evident along the north-northwest boundaries of the slicks. This feathering indicates that the slicks represent relatively thick, wind-driven films on the sea surface, rather than current flow effects over the shoals as may be expected, given the precise morphological match with the underlying shoals and the abundance of features related to current flow on the Yampi Shelf.

These shoals are partly comprised of live corals (Skewes et al., 1999), and coral spawn slicks have the potential to dampen surface capillary waves such that SAR slicks may result. Mass spawning of coral reefs on the North West Shelf usually occurs after a full moon in March or April and/or in October/November (Simpson, 1991; Simpson et al., 1993). More specifically, it usually occurs approximately one week after a full moon, on neap, nocturnal, ebb tides (Simpson, 1991). Spawning typically takes place over two to three consecutive nights, with a small percentage of the coral populations spawning on one or two nights either side of the main spawning nights, and commences between 4 and 10 days after the full moon (Simpson, 1991; Simpson et al., 1993).

The Ashmore Reef area experienced a full moon at 6:24 on 12 April 1998. Sunset at Ashmore Reef on 16 April 1998 was at 17:42, and the scene which contains 71 slicks was acquired 21 minutes later (Table 4). Therefore, it was acquired on the fifth night after a full moon in April. The tide was ebbing at the time the scene was acquired. Given these factors, it is likely that corals were spawning at that time in this region (C. Simpson, WA Department of Conservation And Land Management, written communication, 8–01–04 and 3–12–04; A. Heywood, Australian Institute Marine Science, written communication, 13–01–04). The relatively short period of time between sunset (17:42) and scene acquisition (18:03) provides insight into the coincidence between the slick and the morphology of the shoal margins. In this scenario, 21 minutes would likely have been sufficient time for the spawn to rise to the surface, but insufficient time for reworking of the spawn slick into a more irregular shape by winds and currents.

The preferential development of the slicks at the margins of the shoals possibly

indicates that spawning corals are more prolific on the shoal edge, whereas the central portions are dominated by sediment debris. This is the case at Ashmore Reef, where the density of live corals is higher on the hard substrate of the fringing reef edge (9.9-11.3%) relative to the inner reef flat and sandy zones (0.1-3.8%; Skewes et al., 1999).

A number of the interpreted coral spawn slicks occur over areas with water depths between 60 and 70 m, which is somewhat deeper than typically associated with corals. In the absence of substrate characterisation data suggesting that corals do not exist at these localities, a coral spawn interpretation is still favoured as this is within the photic zone, and hermatypic corals on the Great Barrier Reef have been reported to depths of 80 m (Veron, 2000).

4.4.3 Improving confidence for natural hydrocarbon seepage slick interpretation

The critical re-evaluation of SAR interpretations for the Timor Sea highlights the need to interpret SAR data in conjunction with local bathymetric, oceanographic, meteorological and biological data, and not just geological data, to accurately verify natural hydrocarbon seepage. Slicks confidently identified as having a current flow/bathymetric component to their formation are either above or adjacent to a mapped bathymetric feature, and are imaged in a scene that was acquired close to the turn of the ebb tide. Slicks confidently identified as having a coral spawn component to their formation are interpreted in scenes acquired during a potential coral spawn season, tide and time (as established by Simpson, 1991, and Simpson et al., 1993) and mirror the shapes of underlying shoals. The slicks that could not be readily assigned to the above categories were classified as being of an indeterminate origin. These slicks tend to be small and highly irregular in shape. They may represent coral spawn slicks from unidentified reefs or shoals, current flow effects associated with unidentified bathymetric features, or fragmented seepage slicks. Alternatively they may represent a biological feature, such as an algal bloom (the Timor Sea hosts many blooms of cyanobacteria of the genus *Trichodesmium*; Hallegraeff and Jeffrey, 1984; Negri et al., 2004). Based on the variety of potential slick forming mechanisms in this part of the Timor Sea, independent evidence from alternate remote sensing datasets or field data would be required before making even tentative interpretations regarding the processes of formation for these slicks.

Critically evaluating remote sensing interpretations from external providers through identifying links between features and oceanographic and biological processes in the marine system allows greater confidence in the slicks that are interpreted as being related to natural hydrocarbon seepage. Slicks that have the characteristics of classic seepage slicks (ie. elongate, a length to width ratio of at least 5, with a potential emission point or line of emission points and oriented within approximately 20° of the direction of the prevailing wind at the time of scene acquisition) for which an alternate process of formation is not evident, are classified as likely seepage slicks.

An example of a high confidence interpreted seepage slick can be seen to the east of Heywood Shoals (Figure 40). This slick, identified on a SAR scene acquired on 16 April 1998 (NPA et al., 1999), is elongate and has what is interpreted to be a likely emission point at its eastern terminus. At the time of acquisition the prevailing wind was from the east, therefore it is oriented as would be expected for a wind-driven oil slick with a single emission point at the sea bed. The slick is positioned in the vicinity of a slightly raised area of the seafloor, which may represent a cemented hardground. Such carbonate hardgrounds were found in association with the active hydrocarbon (gas only) seepage discovered to the southeast (Rollet et al., 2006). Whereas all of the slicks over and around the shoals were previously interpreted to be natural seepage slicks, the numerous slicks in the immediate vicinity of the shoals have several potential alternative origins. Therefore the interpreted seepage slick to the east of the shoals can be viewed with high confidence, and is potentially a target for further study.

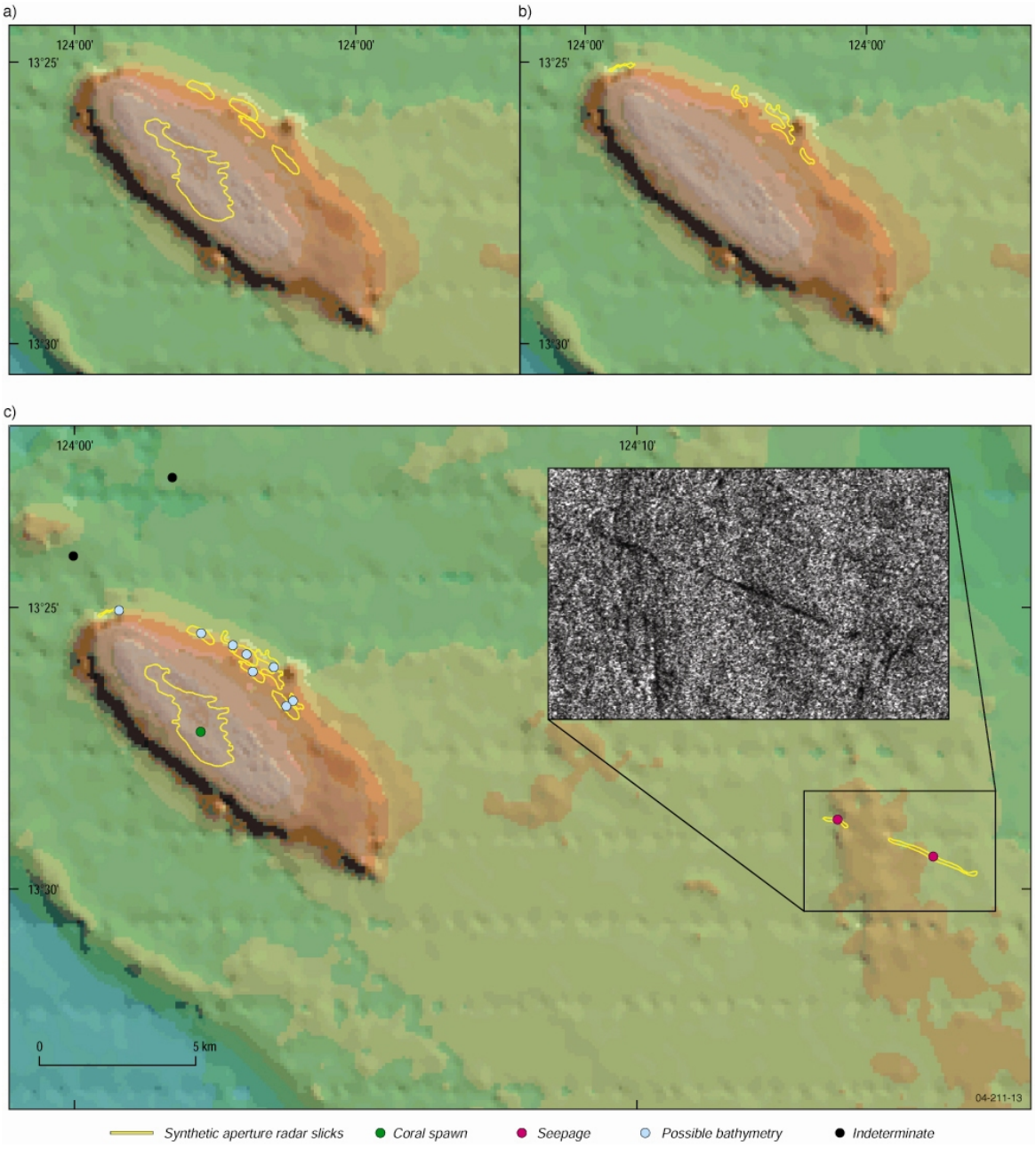

Figure 40. a) Outlines of SAR slicks visualised in a scene acquired on 16–4–98. b) Outlines of SAR slicks visualised in a scene acquired on 25–10–98. Note the absence of the large slick directly over the shoals and the repetition of the small slicks around the northeastern edge of the shoals relative to 13a. c) Re-categorised SAR slicks over Heywood Shoals visualised in multiple scenes. Note the high confidence seepage slick to the east of Heywood Shoals, also shown in the inset (from Jones et al., 2005b).

SAR slicks may also be interpreted as being high confidence seepage slicks on the basis of positive correlations with seepage indicators in alternate datasets, such as those that have been identified in the Arafura Sea (Rollet et al., 2007; Figure 11). A cluster of SAR slicks interpreted as possible natural hydrocarbon seepage slicks was initially given a low confidence rating as there was no repetition in multiple scenes (Infoterra, 2005). Subsequent marine surveying of this area revealed the SAR slicks to strongly correlate with a field of pockmarks. The slick locations also correlate with a zone of poor quality seismic data, and a large depocentre with an interpreted middle Cambrian source rock mapped using conventional seismic data (Totterdell, 2006; Struckmeyer, 2006; Figure 11). Some SAR anomalies in this group overlie a major fault and others appear to correlate with thinner parts of the basin fill. The SAR anomalies also exhibit a correlation with a critical thinning of the interpreted regional seal (Bathurst Island Group, Late Cretaceous; Struckmeyer, 2006). As a result of these positive correlations, the SAR slicks are interpreted as higher confidence natural hydrocarbon seepage features. Acoustic flares were not observed in sidescan sonar and 12 kHz echosounder data, but seepage can be intermittent and the absence of active gas flares during the survey does not rule out hydrocarbon release at these locations at other times.

During the planning phase of SS06/2006, across the central NWS, a quality control assessment of interpreted SAR slicks from the region was undertaken following the process outlined above. The assessment focused on the densest cluster of SAR slicks in the basin (Figure 10). These slicks had previosly been interpreted to represent liquid hydrocarbon seepage at the edge of the regional seal (O'Brien et al., 1998b). O'Brien et al. (1998b) analysed four SAR scenes that cover the Lambert Shelf area, and slicks were identified in three scenes. The metadata for the four scenes over the area is given in Table 5, including date and time of scene acquisition, wind speed and direction (as provided by O'Brien et al., 1998b), and the approximate state of the tide at the time of scene acquisition estimated through web-based tidal modelling software (http://tbone.biol.sc.edu/tide/).

Table 5. Metadata for SAR scenes over the Lambert Shelf analysed as part of this study.

SOURCE	SCENE	DATE	TIME (UTC)	WIND SPEED	WIND DIR	TIDE
NPA	RSW1_25	2/06/1998	21:36	2	135	Neap Ebb - 1 hour after high tide
NPA	RSW1_28	13/07/1998	21:41	1-LV	220	Spring Ebb - 1.5 hours from low tide
NPA	RSW1_44	13/08/1998	21:36	1-2	180	Midway through Spring Ebb
NPA	RSW1_48	30/08/1998	21:41	2	145	Neap Ebb - 2 hours after high tide

Table 5 shows that all of the seepage slicks identified by NPA over the Lambert Shelf lie in 60 m of water or less. Given that tidal flows over submarine channels in 60 m of water on the Yampi Shelf produced SAR slicks, all of the slicks over the Lambert Shelf must be treated with caution, against the possibility that they represent a bathymetric/current flow effect. For example, all of the seepage slicks identified in one scene are in less than 10 m of water. One interpreted natural film slick from this scene lies directly over Bedout Island, at a point approximately 1 m above sea level according to a regional bathymetric grid. A number of slicks that are situated in relatively deeper water and that were identified in a scene that was acquired at relatively higher tide, were selected for surveying during SS06/2006.

The site that was selected for surveying included interpreted slicks in 53 and 60 m of water. Figure 10 shows a weather front quite close to these slicks. NPA state that there are strong currents along the wind front interacting with internal waves (O'Brien et al., 1998b). However, these slicks appear to be situated in the relatively undisturbed area of uniform reflectance to the east of the front. Both slicks have a blobby shape (350 x 250 m) atypical of oil slicks (Figure 10 inset), but they are well isolated in the context of the scene (i.e. they are away from weather fronts and areas of wind calm or natural film slicking) and they have no obvious alternative explanation.

No direct evidence of hydrocarbon seepage was detected within the survey area, and the survey data could not determine a definitive cause of the interpreted SAR slicks. It is postulated that they are related to the bathymetry, but there was not a 'one-to-one' correlation between the shapes of the slicks and the underlying bathymetric features as there was on the Yampi Shelf (Jones et al., 2005b, 2006).

Other remote sensing datasets that have been used to investigate hydrocarbon seepage (eg. LANDSAT, hyperspectral) should also be critically examined in the context of the local oceanography, geology and biology. This will only be possible if sufficient supplementary data and metadata are available. The detailed descriptive nature of the original SAR slick interpretation report for the Timor Sea and central NWS (O'Brien et al., 1998b; NPA et al., 1999) allowed a critical reassessment of the processes that led to slick formation.

4.5 Hyperspectral detection of natural oil seepage

Although potential is often cited for the application of hyperspectral remote sensing data in detecting and diagnosing hydrocarbon slicks, there are to date no conclusive reports of hyperspectral identification of natural seepage. Several examples exist of using both multispectral and hyperspectral data to delineate oil slicks, but in all cases the presence and location of the slick were known (Malthus and Karpouzli, 2007). If optical remote sensing is to be used either as a stand alone or complementary tool (e.g. in combination with SAR) for natural seepage slick identification, some form of oil-diagnostic capability is required. From a spectral point of view, hyperspectral data offer the best case scenario for diagnosing oil slicks. This section contains an overview of hyperspectral oil work done to date, followed by our initial findings from pilot studies underway at Geoscience Australia.

4.5.1 Background on hyperspectral detection of oil

Salem and Kafatos (2004) demonstrated that AVIRIS data can be used in conjunction with a partial un-mixing technique to delineate a known oil spill. However, their approach was empirical and data set-specific; it does not offer diagnostic potential.

Horig et al. (2001) undertook a spectral signature-based approach by comparing (hyperspectral) in situ measurements with Hymap imagery of oil-contaminated sands. They showed that the spectral overtones of C-H vibrational nodes, seen as absorption bands centered at 1.7 μm and 2.3 μm, are detectable in HYMAP imagery data. Their terrestrial-based work suggested that these two absorption features are well suited as diagnostic hyperspectral features for oil identification. However, theoretical modelling work by Radlinski (2004b) suggested that an oil slick layer would need to have a thickness greater than 170 μm and 530 μm for HYMAP-based detection of the

absorption features at 1.7 µm and 2.3 µm, respectively. Such thicknesses are considered greater than those of naturally occurring oil slicks. Field measurements of the prolific and dense natural seepage slicks in the Santa Barbara channel revealed slicks no thicker than 150 µm, and typically significantly less (Svejkovsky and Muskat, 2006). The findings in our pilot study using HYMAP data of the Santa Barbara slicks, reported in the following section, confirm the above predictions and measurements.

Lennon et al. (2005) reported on modelling-, in situ- and image-based hyperspectral work on a controlled release of oil on offshore waters. According to their theoretical model, an increase in oil layer thickness causes a 'spectral rotation' response in reflectance data. Specifically, when an oil reflectance spectrum is normalised to its albedo (i.e. the brightness of the spectrum is removed) the blue end of the reflectance spectrum will exhibit lower values and the red-to-NIR end of the spectrum will exhibit higher reflectance values with a progressively thicker oil layer. The hinge point for this rotation of the spectra occurs at around 600 nm. The authors showed that measurements using the hyperspectral CASI sensor over oil of varying thickness appear to confirm these theoretical predictions. They proceeded to calibrate this observed effect to active fluorescence laser data of the same oil slick in order to produce quantitative maps of oil distribution

The consensus in the literature is that there are no discrete, oil-diagnostic spectral features in the visible region of the spectrum (Malthus and Karpouzli, 2007). However, it is possible that the spectral rotation effect observed by Lennon et al. (2005) may serve as a complementary indicator of the presence of oil on water. Indeed, we observed this spectral rotation phenomenon, and its apparent correlation with oil thickness, in the HYMAP data of the Santa Barbara slicks (as reported in the next section).

4.5.2 Hyperspectral detection of oil seepage in the Santa Barbara channel

We have acquired a range of remote sensing data types of the prolific oil slicks in the Santa Barbara channel. This includes four flight lines from the hyperspectral HYMAP sensor, flown in July 2003 and covering areas of natural seepage surface expressions (Figure 41). The HYMAP data were atmospherically corrected by the data vendor,

using the Atcor4 software.

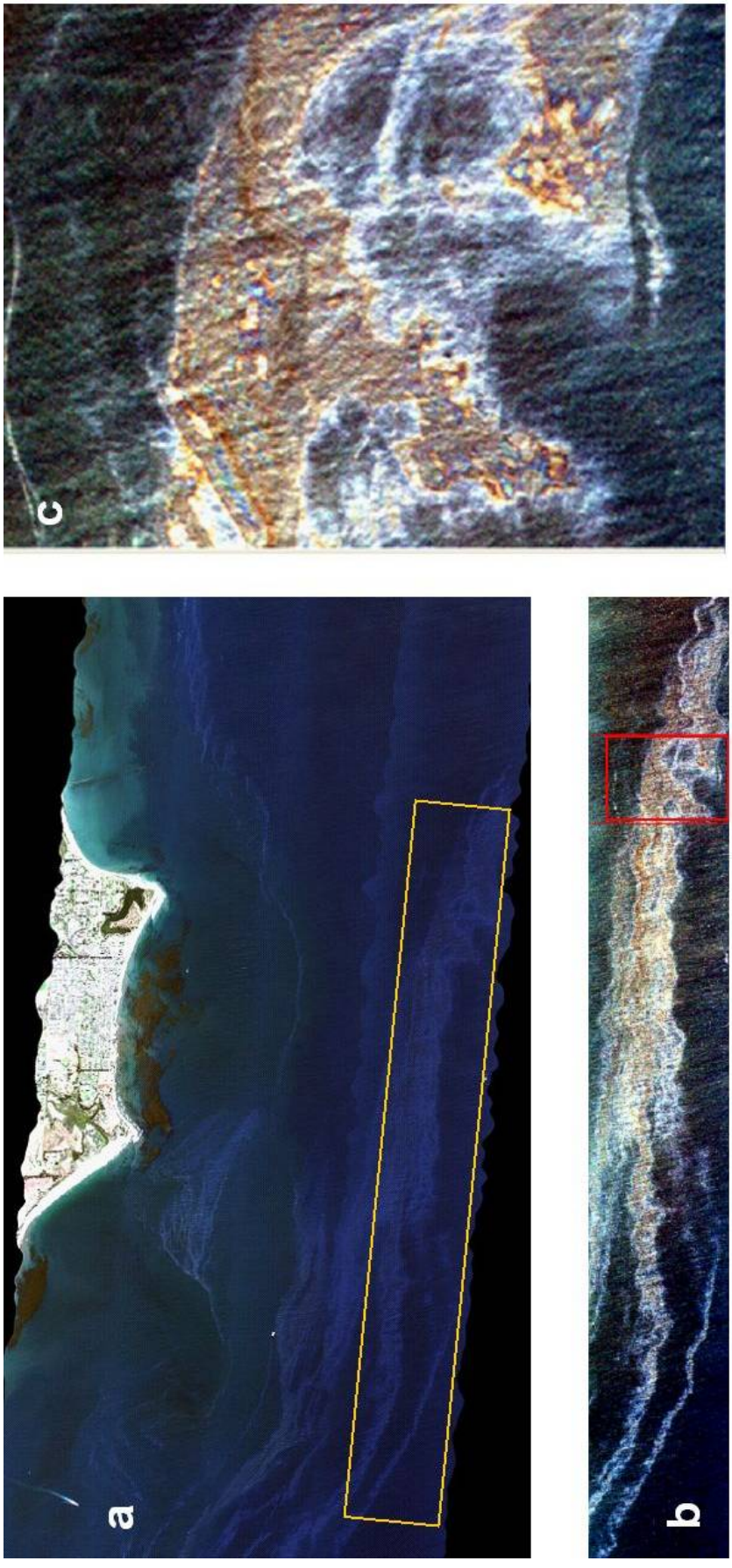

Figure 41. HYMAP imagery of naturally occurring oil slicks in the Santa Barbara channel: a) true colour composite of the four HYMAP flight lines acquired on July 2003, where the yellow rectangle denotes the area shown in b) one of the HYMAP flight lines in pseudo-true colour with a stretch applied, where the red rectangle denotes the area shown magnified in c).

The colour variations of the oil covered waters shown in Figure 41c conform with both predicted and reported observations in the literature. Relatively thin layers of oil often produce a blue-ish or silvery sheen, and progressively thicker layers appear red-through to brown. The latter is caused by the wavelength-dependant absorption of oil: with increasing thickness, absorption occurs first in the blue wavelength region (giving a red appearance). At a given thickness, oil absorbs sufficiently for its true colour to be visible. In the case of heavy crudes, they can be completely absorbing at sufficient thickness, resulting in a black appearance. In addition, the wavelength region at which a given thickness of oil absorbs is also oil type dependant.

Figure 42a shows reflectance spectra collected from the HYMAP data corresponding to three water types: clear water, water covered by thin, blue sheen oil cover, and water covered by thicker oil. For the visible wavelength region (approximately 0.45 - 0.7 μm), the spectral behaviour of the three water types corresponds to findings in the literature: progressing towards the blue end of the spectrum, clear water is typically 1) brighter than water covered by relatively thicker oil and 2) darker than water covered by a relatively thin layer of oil (Lennon et al., 2005; Svejkovsky and Muskat, 2006; Byfield and Boxall, 1998; Otremba and Piskozub, 2001; Samberg, 2005).

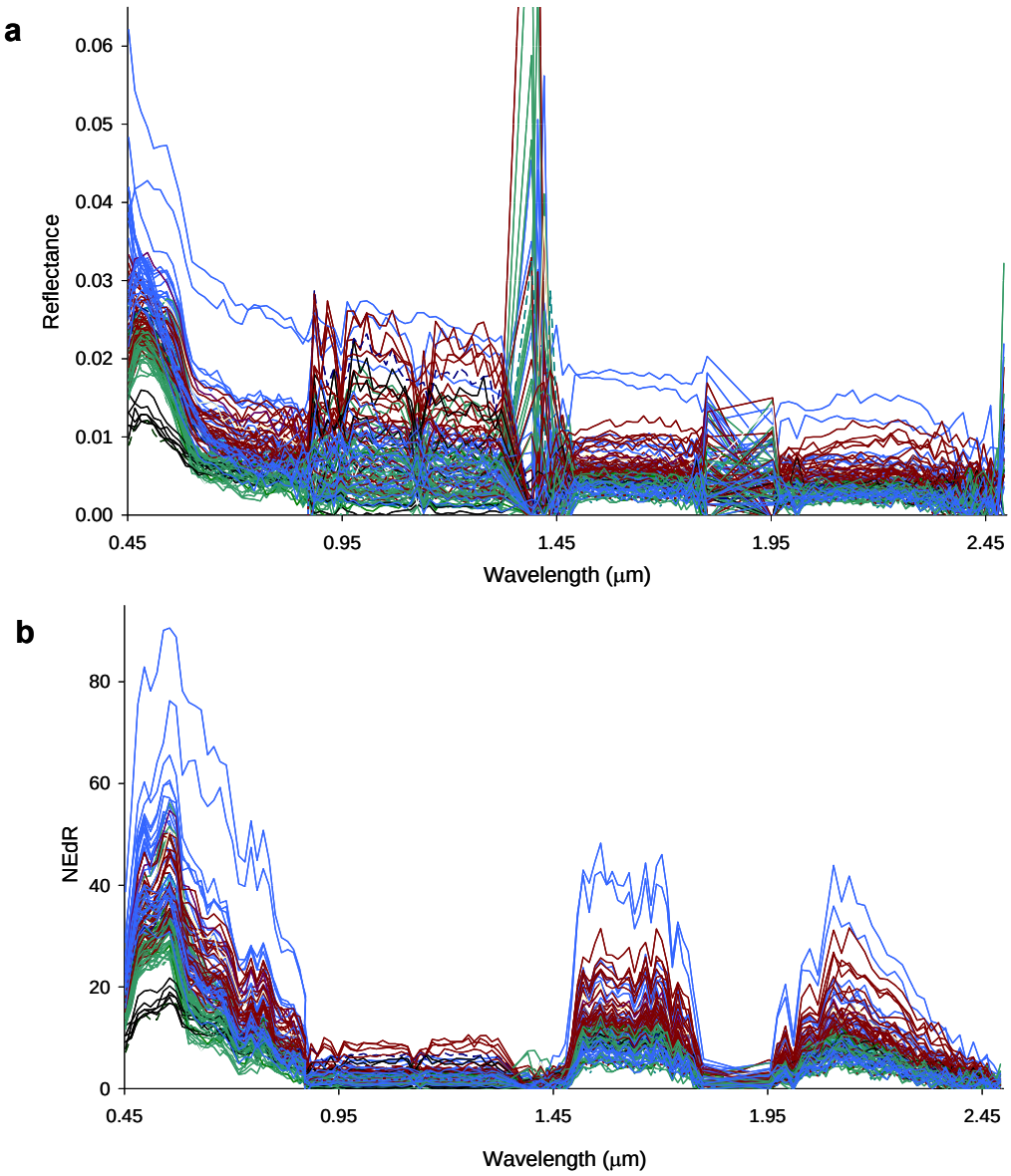

Figure 42. a) HYMAP reflectance spectra of three types of waters: clear water (green lines), water covered by thin, sheen type oil cover (blue lines), and water covered by thicker oil (brown lines). The anomalous spectral behaviour centred at approximately 1.4 μm and 1.8 μm are sensor artefacts and should be disregarded. Normalising these spectra to their corresponding noise equivalent spectra gives the noise equivalent delta reflectance (NEdR) spectra shown in b). For the NEdR spectra, note the low number of levels of information throughout the 0.8-1.5 μm region, and the highest number of levels of information in the visible (0.45-0.75 μm) region.

An important consideration in evaluating a remote sensing data type is the level of noise present in the data. For aquatic remote sensing data, this includes sensor noise, atmospheric noise, as well as noise on the sea surface caused by, for example, sun glint and sea swell. Following a method initially proposed by Dekker and Peters (1993) we assessed system-wide environmental noise equivalent values in the HYMAP images. The noise equivalents were estimated from reflectance data in an as homogeneous area as possible for each flight line (Brando and Dekker 2003, Wettle et al., 2004), in units of noise equivalent delta reflectance (NEdR).

By normalising the HYMAP reflectance data to the NEdR values, the discernable levels of information in the image data were revealed. The result of normalising the spectra in Figure 42a to the corresponding NEdR spectra is shown in Figure 42b, which in turn shows the resolution of information present in the three spectral classes. The most notable feature in Figure 42b is the low number (less than 10) of levels of information in the near infrared region covering approximately 0.8 – 1.5 µm. This suggests that (for HYMAP data of Santa Barbara waters) this wavelength interval is not suitable for detecting oil slicks. This agrees well with the theoretical work by Radlinski (2004b) quoted above. For the wavelength interval of 1.5 - 2.3 µm, the HYMAP sensor showed a moderate ability (less than 20 levels of information) to detect and differentiate between the three spectral classes (Figure 42).

Importantly, Figure 42 suggests that the visible spectral range contains the largest number of levels of information for discerning and potentially classifying oil slicks (based on the HYMAP configuration used in this data acquisition). This is encouraging for future seep detection investigations using readily available data from high spatial resolution, space-borne sensors that operate in the visible range (e.g. Quickbird).

We tested several algorithms for removing spectral albedo (brightness) from the reflectance spectra of the three water classes shown in Figure 43a, and observed the spectral rotation effect discussed by Lennon et al. (2005). Figure 43b shows one example of this albedo removal, wherein a transition from clear water through to water covered with progressively thicker oil is represented by increased absorption in the blue region (0.45-0.5 µm), and increased reflectance in the red/near-infrared (0.65-0.75 µm).

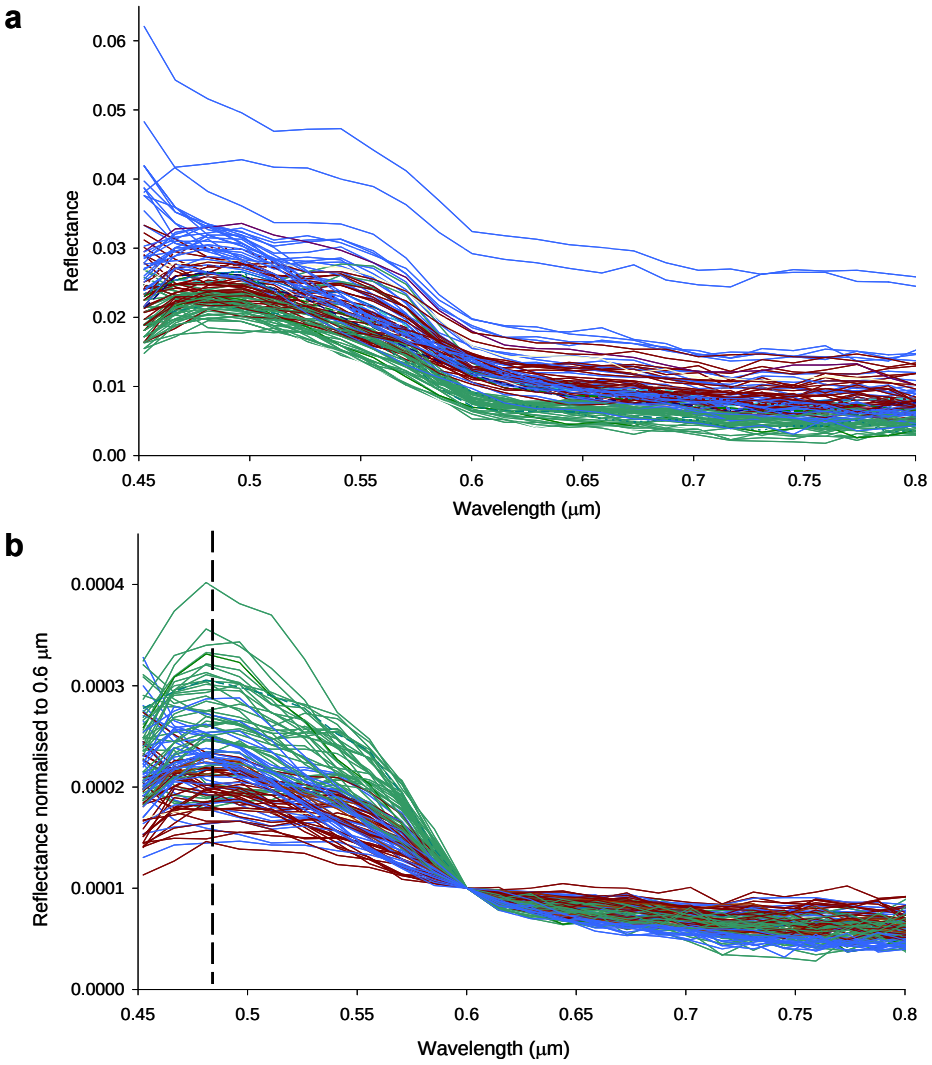

Figure 43. For the visible portion of the spectrum the a) the HYMAP reflectance spectra of the three types of waters, as shown in Figure 42, b) the same spectra normalised by their respective albedo. Note the transition from clear water through to water covered with progressively thicker oil as represented by increased absorption in the blue region (0.45 – 0.5 μm), and increased reflectance in the red/near-infrared (0.65 – 0.75 μm). The dashed line indicates a wavelength region where normalised reflectance values appear to correlate with oil layer thickness.

At approximately the 0.48 μm wavelength (denoted by the dashed line in Figure 43b), the albedo-normalised, or rotated, reflectance correlates with a progression from oil-free, through thin oil layers, to thicker oil layers. This is in contrast to the original spectra, where there is no progression in blue reflectance values (at approximately 0.48 μm in the original spectra, the reflectance values for the oil-free waters are between the values for thick and thin oil layers). Consequently, an image produced using this band would provide a map of the distribution of relative oil layers thickness. For illustrative purposes, Figure 44 provides an example of this for the Santa Barbara slicks.

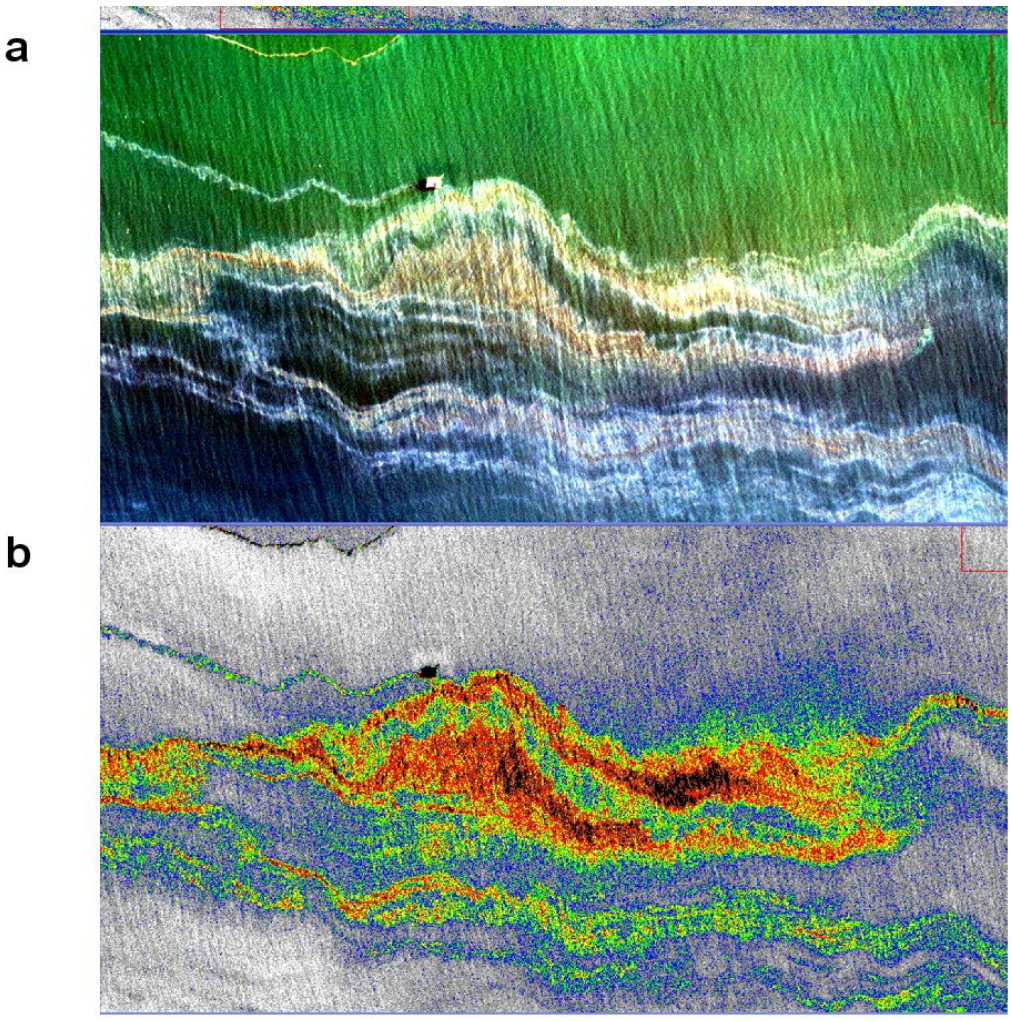

Figure 44. An example of using the albedo-corrected Santa Barbara HYMAP data near 0.48 μm to produce maps of the distribution of relative oil layer thickness. a) Original HYMAP image subset with a colour-enhancing stretch and b) a colour-coded image of the albedo-corrected 0.48 μm band showing relative oil thickness distributions. The thickness distributions have not been validated and this image is for illustrative purposes only.

The HYMAP data of oil-covered water in the Santa Barbara channel appear to confirm the consensus in the literature that oil has no diagnostic absorption features in the visible range. However, it may be that the spectral rotation effect (now observed in two different studies, using two different sensors and different oil/water types) can be used as one of a set of indicators to diagnose the presence of a thin layer of oil on water. We are further investigating this potential for data from both multispectral and hyperspectral, space-borne sensors that operate in the visible range (e.g. Quickbird and Hyperion).

4.5.3 Hyperspectral detection of production water oil on the Yampi Shelf

HYMAP data were acquired to coincide with the release of production waters (PW) from a production tanker located off the North West Shelf of Australia. A subset of the data is shown in Figure 45, where the oil slick resulting from the PW release is visible as an inverted 'U' shape emanating from the tanker in the lower right hand corner of the image. The image is heavily glinted.

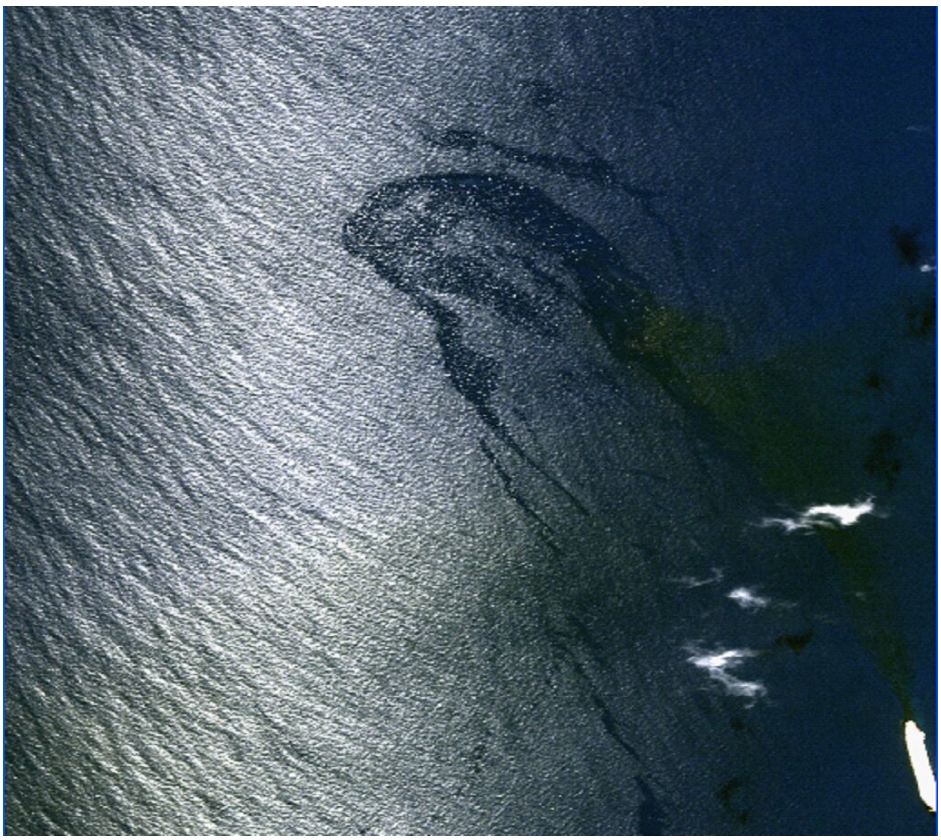

Figure 45. HYMAP image of glinted North West Shelf waters containing a release of production waters (darker, inverted "U" shape) from a production tanker (bright white shape in lower right-hand corner).

We applied a de-glinting algorithm based on a concept by Hochberg (2003) and Hedley et al. (2005), and implemented in IDL at the CSIRO Environmental Remote Sensing laboratories (Wettle et al., 2006). The result of this procedure is illustrated in Figure 46 where, for a transect across the image, values before and after de-glinting are compared. The three colours in Figure 46a refer to sensor wavelength channels corresponding to the blue, green and red regions. The blue, green, and red lines that show higher and noisier values in the left half of the graph correspond to digital numbers (DNs) across the transect prior to de-glinting. The relatively smooth and flat blue, green and red lines correspond to digital numbers across the transect after de-glinting. The location of the transect is shown by the horizontal line in Figure 46b. The eastern-most portion of the image appears to contain no glint. This is in alignment with the de-glinting results, as the values for the sampled transect in this area are essentially the same as for all de-glinted pixels across the entire transect. Importantly, wherever an oil slick occurs across the transect, the DN values of pre-glinted pixels drop to the same values as de-glinted pixels. As the DN values for oil covered waters are not different from those of non-glinted waters, it appears that there is no clear absorption effect due to the oil present. Instead, the presence of a thin layer of oil on the water surface appears to simply be inhibiting sun glint. For this data set, the angle of observation, in combination with the angle of illumination, is causing specular reflection off the capillary waves, referred to here as sun glint. Where a thin layer of oil is present, these capillary waves are dampened, and little to no sun glint occurs as seen from the sensor. The presence of an oil layer is thereby inferred from the change in sea surface roughness, similar to the basis for SAR-based oil slick detection.

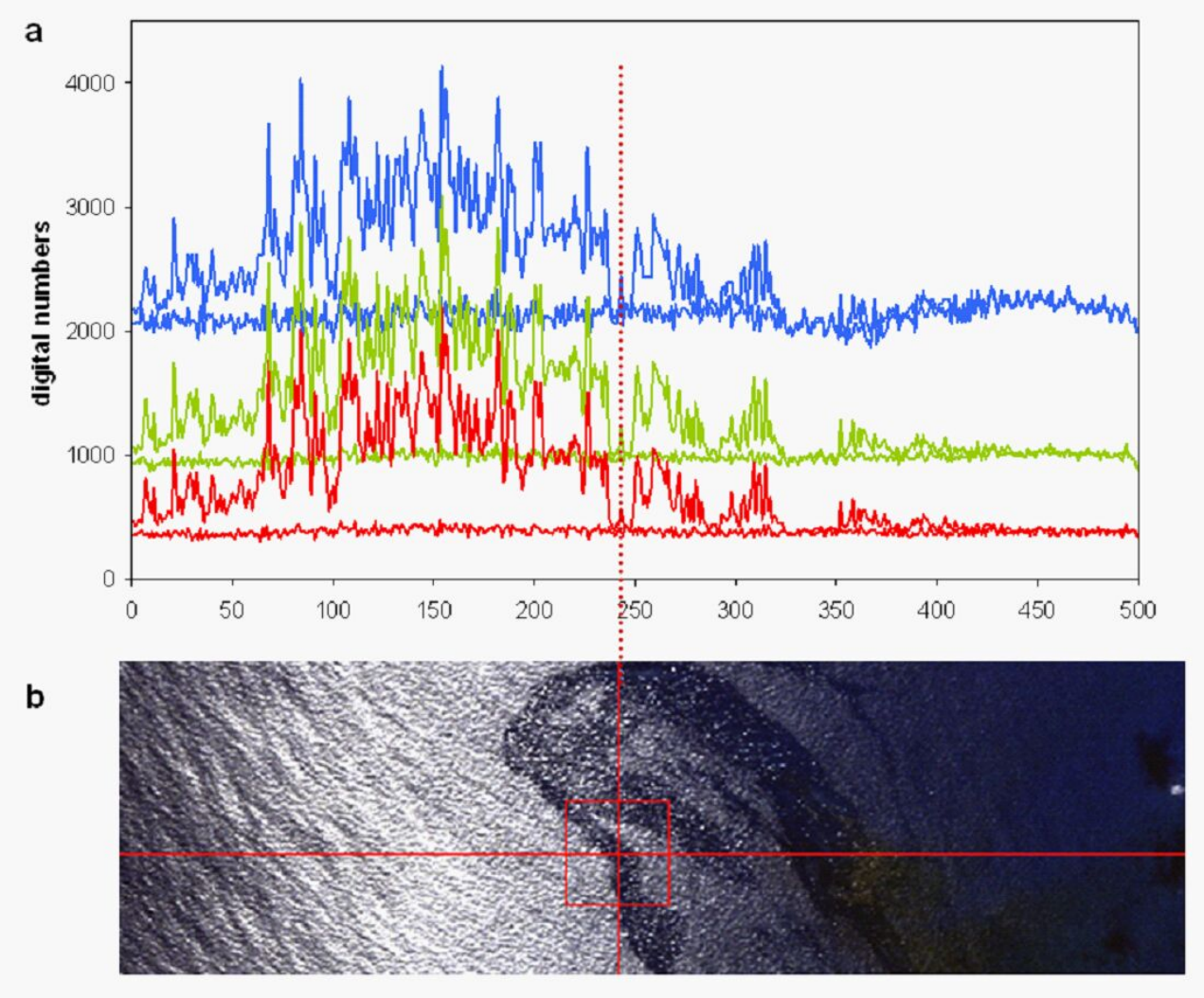

Figure 46. a) Digital number values along a transect of the HYMAP image before and after de-glinting. The three colours in (a) refer to sensor wavelength channels corresponding to the blue, green and red regions. The blue, green, and red lines that show higher and noisier values in the left half of the graph correspond to digital numbers (DNs) across the transect prior to de-glinting. The relatively smooth and flat blue, green and red lines correspond to digital numbers across the transect after de-glinting. b) The location of the sampled transect in the image as shown by the horizontal line. The vertical line denotes a common location in (a) and (b).

The hyperspectral work on the Santa Barbara seeps reported above showed that the highest level of oil-relevant information is to be found in the visible wavelength range of the HYMAP sensor, with progressively higher sensitivity to absorption by oil towards the blue end of the spectrum. For the production waters study, the oil layer appears to be too thin for absorption to be detected even in the blue, suggesting that there is no benefit to be gained by using a hyperspectral compared to a multispectral sensor for such thin oil slicks. Assuming no loss of hydrocarbons to the atmosphere, the oil thickness of these production waters was estimated by Radlinski (2004b) to be on average approximately 1 μm.

Although not present in our datasets, a relatively thin (i.e. too thin to absorb significantly) oil slick may also cause glint, resulting in positive contrast to surrounding waters (Chust and Sagarminaga, 2007).

4.5.4 Hyperspectral detection of natural oil seepage – Conclusions

For the visible through near-infrared wavelength region, oil layers on water will – as predicted in the literature – have negative, positive, or zero (no) contrast with oil-free waters. This is dependent on oil thickness as well as viewing and illumination geometry.

According to HYMAP sensor data, the naturally occurring oil slicks in the Santa Barbara channel have the same spectral behaviour in the visible range as reported by the literature, which in turn is mostly based on oil spill studies. This spectral behaviour includes progressively higher absorption towards the blue end of the visible spectrum, and increased absorption with increasing thickness of the oil layer. An exception to this occurs for very thin oil layers, where reflectance is higher than clear, oil-free waters. It may be that this spectral behaviour (readily apparent through albedo removal and spectral rotation) can be utilised as a contributing indicator for naturally occurring oil slicks. It should be noted that these findings are derived from a best case scenario of mapping an area of prolific, voluminous seepage using a high spatial resolution (airborne) sensor. Although not yet proven, we postulate that this spectral behaviour in the visible range is more apparent using hyperspectral data as opposed to multispectral data.

Conversely, the HYMAP imagery of production waters on the Yampi shelf did not

display the absorption properties described above. This was most likely due to this oil slick being too thin for absorption to take place. Although the location and extent of the slick was visible as darker than surrounding waters, we show that this was due to the thin oil layer damping the capillary waves, and thereby reducing the sun glint otherwise prevalent in the scene. Note that these production waters represent a diluted form of oil, and are therefore likely thinner than a typical naturally occurring oil slick. As the oil layers appear to be too thin for absorption to be detected even in the blue, there would be no benefit to be gained by using a hyperspectral over a multispectral sensor for such thin oil slicks (in this case, estimated to be on average 1 μm thick).

The HYMAP sensor displayed very limited ability in the 800-1500 nm region, and a relatively limited ability in the 1500-2300 nm region, to detect and differentiate between clear waters and waters covered in naturally occurring thicknesses of oil. This potential spectral and physical constraint has important implications for assessing the cost-benefit of utilising hyperspectral data in detecting and diagnosing natural oil slicks.

4.6 Multispectral detection of natural oil seepage

The previous section investigated the potential of the airborne hyperspectral sensor HYMAP in detecting and mapping the oil slicks in the Santa Barbara channel. From both a 1) spectral resolution and 2) natural oil slick abundance and density point of view, this represents a best case scenario for passive optical remote sensing of natural oil slicks.

However, as discussed in the previous section, the remote sensors, such as HYMAP, operating in the wavelength region of 0.800 – 1.5 μm appear insensitive to oil layers of naturally occurring thickness. According to the image-based work on passive remote sensing to date, the visible wavelength range has the most potential for detecting and diagnosing naturally occurring oil slicks (note that the thermal and ultraviolet range are not discussed here). Therefore, since both our findings and the literature suggest that there are no specific, oil-diagnostic spectral features in the visible region, it would appear that there is no diagnostic advantage to using hyperspectral instead of multispectral data. (One factor which may influence this potential conclusion is if techniques such as the albedo-removal discussed in the

previous section are reliant on higher spectral resolution in order to be observed).

With the exception of the spaceborne hyperspectral Hyperion sensor, readily available hyperspectral sensors are typically airborne. The deployment of such systems is at considerably higher cost (two orders of magnitude) than the cost of purchasing commercially available data from spaceborne multispectral systems. Our findings in section 4.2 furthermore suggest that high spatial resolution contributes to the ability to diagnose oil slicks based on their spatial patterns, and that the 30 m spatial resolution Hyperion sensor may not be adequate for naturally occurring oil slick detection.

Following the above reasoning, and further taking into account the advantage of global coverage offered by spaceborne sensors, it is important to investigate the potential for detecting natural oil slicks using multispectral, high spatial resolution, spaceborne sensors operating in the visible range.

Note that there appear to be no reports in the literature of investigations of this type. All reported applications of spaceborne, multispectral sensors detecting oil on water are concerned with, typically large and thick, oil spills of known location and date (Malthus and Karpouzli, 2007). Sensors used include Landsat, Spot, AVHRR, MODIS and MERIS (Dean et al., 1990; Tseng and Chiu, 1994; Howari, 2003; Hu et al., 2003; Adamo et al., 2006) . The MERIS and MODIS sensors have so far only been used to detect the absence of sun glint on oil-covered waters (the same effect as observed in the HYMAP data of the oil production waters in section 4.5.3) , and their spectral capabilities for diagnosing oil slicks have therefore not been investigated. Based on preliminary findings reported in section 4.1.2, we suggest that these capabilities will be limited.

4.6.1 Quickbird data of the Santa Barbara slicks

We have acquired two Quickbird scenes of the Santa Barbara slicks, dated 11/10/03 and 29/11/06. Quickbird data offers 2.4 m spatial resolution at four broad spectral bands (multispectral), corresponding to the blue, green, red, and near-infrared wavlength regions. A Quickbird scene covers approximately 22 x 22 km on the ground, and the spaceborne platform has a global re-visit time of approximately 16 days.

The 11/10/03 scene was atmospherically corrected using the Modtran-based c-WOMBAT-c software (Brando and Dekker, 2003). Reflectance spectra of optically deep, oil-free waters in the Santa Barbara HYMAP data (section 4.1.4) were used as reference for the atmospheric correction of the Quickbird data. Although the absolute accuracy of the resulting correction is not verifiable, good match-ups between the two data types were achieved and allowed for comparison of apparent (above surface) reflectance values. The details of these pre-processing procedures are omitted here for reasons of clarity and space. The following analysis and discussion are based on the 11/10/03 Quickbird scene.

Figure 47 shows examples of pseudo-true colour imagery of Santa Barbara slicks from both the HYMAP and Quickbird sensors, where the data was collected from a height of 1.5 km and 450 km respectively. The oil-typical spatial patterns and colour variations are visible in both images.

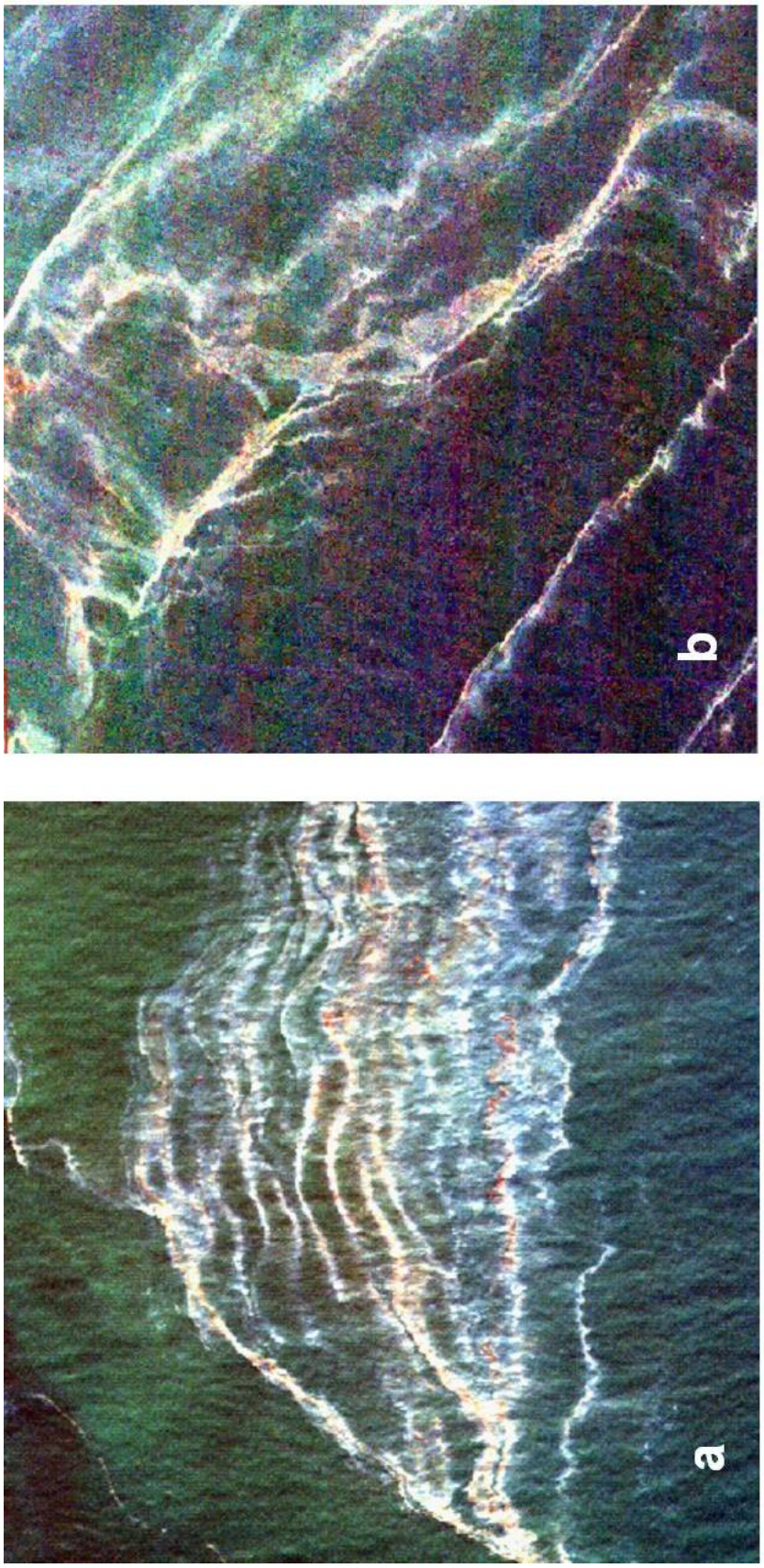

Figure 47. Examples of pseudo-true colour imagery of Santa Barbara slicks from the a) HYMAP and b) Quickbird sensors. The oil-typical spatial patterns and colour variations are visible in both images.

Following on from the hyperspectral work reported on in the previous section, spectra of three types of water were collected: clear water, water covered by what is presumed to be relatively thin layers of oil, and water covered by what is presumed to be relatively thick layers of oil. These spectra are shown in Figure 48a.

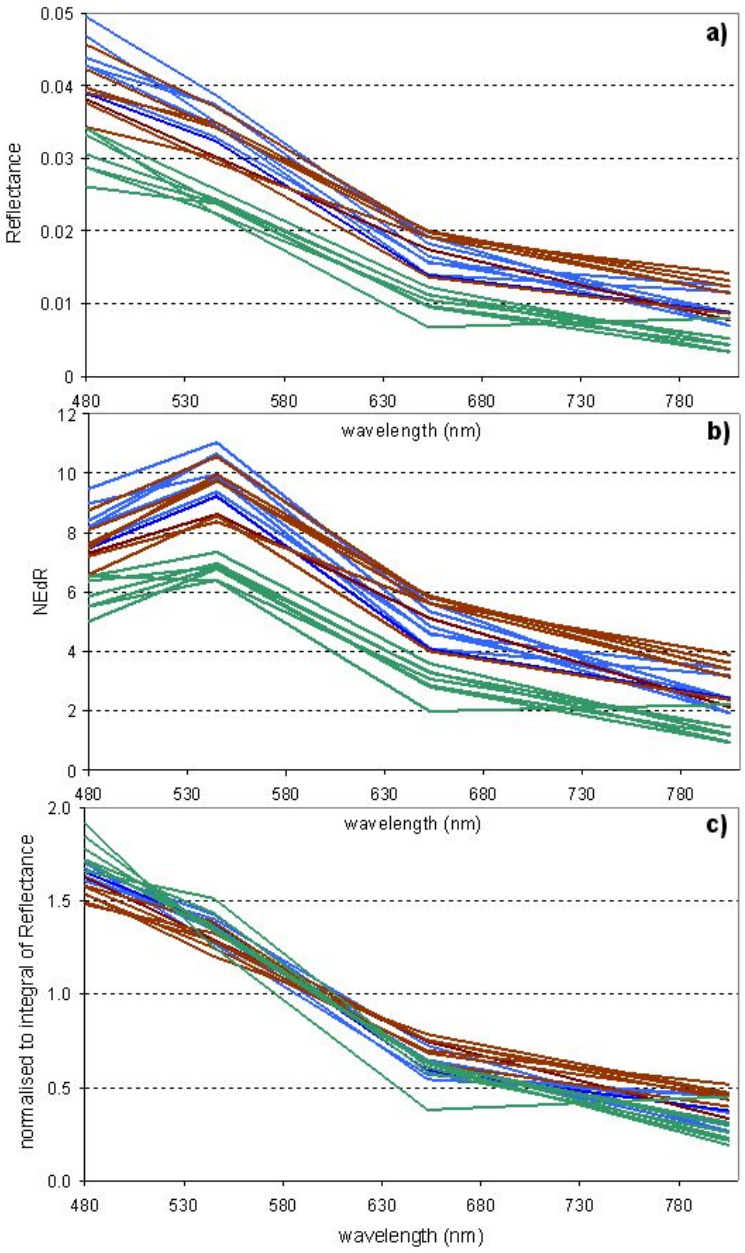

Figure 48. a) Quickbird reflectance spectra of three types of water: oil-free water, water (green lines), water covered by relatively thin layers of oil (blue lines), and water covered by relatively thick layers of oil (brown lines). b) The same spectra normalised to the environmental noise estimated for the Quickbird scene (units of NEdR), and c) the same spectra normalised to their albedo, showing the same rotation effect as discussed in section 4.5.2.

The environmental noise of the Quickbird scene was calculated and used to convert the sample spectra into units of NEdR, thereby revealing the levels of information in the data (see section 4.5 for further details). The result is shown in Figure 48b, and reveals that the Quickbird data (for this particular scene) has significantly less levels of oil slick-relevant information than the HYMAP data. Nonetheless, the oil-free water spectra differ from the oil-covered water spectra by between approximately 1 to 2 noise levels, implying that they can be differentiated. This is confirmed qualitatively in Figure 47b, where oil slicks surrounded by clear water are visible.

We tested several approaches for removing the albedo of the spectra in order to see if the spectral rotation effect reported on in section 4.5.2 could be observed in Quickbird imagery of natural oil slicks. For multispectral data, normalising to the integral of the spectrum - which is a more rigorous approach to removing albedo - gave the most satisfactory results. These are shown in Figure 48c. Analogous to the results achieved for hyperspectral data in section 4.5.2, the albedo removal re-orders the reflectance values in the blue band (at approximately 0.48 μm) so that decreasing values correlate with increasing oil thickness. This is in contrast to the original spectra shown in Figure 48a, where there is no obvious trend in the blue band when progressing from oil-free through progressively thicker oil-covered waters.

We conclude that the spectral rotation effect, reported by Lennon et al. (2005) for CASI and confirmed in this report for HYMAP (both of which are airborne hyperspectral sensors), is observable by the multispectral, high spatial resolution, spaceborne Quickbird sensor. As concluded for the hyperspectral data, the spectral rotation effect may serve as a partially diagnostic characteristic of oil-covered waters. In order for this technique to be usable, the oil layer must be thick enough to absorb light at least in the visible blue range of the spectrum. We re-emphasize that this thickness threshold is oil type dependent, and the detection of this absorption is sensitive to the signal-to-noise characteristics of the remote sensing data.

In summary, natural oil slicks such as those present at Santa Barbara are detectable using the spaceborne multispectral sensor Quickbird. Both the spatial patterns characteristic of the Santa Barbara oil slicks and the spectral behaviour identified in airborne hyperspectral data were observable. The high spatial resolution (2.4 m) of the Quickbird sensor is important for this type of application, as both the recognition

of spatial pattern and the ability to discern thickness-dependent colour variations in the oil covered areas can contribute to the identification of oil slicks. As an example, although it features the same spectral channel configuration as Quickbird, the 30 m spatial resolution Landsat sensor was not able to discern the above features, as discussed in section 4.2.

4.7 Recommendations for remote sensing sensors and future applications

4.7.1 SAR data acquisition timing

From seepage studies carried out at GA, it has become clear that acquisition of ERS and RADARSAT imagery within the appropriate weather windows is crucial to improve the likelihood of detecting slicks on SAR. A proper assessment of quality climate data could help identify appropriate weather windows for a given study site.

4.7.2 Calibrating SAR images

Calibration of raw SAR data to radar cross section values needs to be done with a better understanding of the input parameters. Work done so far is based on conversion modules that are not very transparent. The use of ERS SAR PRI product as input for calibration necessitates geocoding of SAR imagery to enable easy portability into GIS systems. It would be worthwhile for future studies to combine these two steps.

4.7.3 Wind and wave retrieval from SAR

Wind and wave parameter retrieval based on SAR backscattering could provide high resolution wind and wave fields from the single data source, without having to rely on external data sources for wind and wave data and also help overcome problems of measurements not being coincident with SAR acquisition. CMOD-4, CMOD-IFR2 & ENVIWAVE are algorithms that allow extraction of wind/wave fields from ERS SAR and ENVISAT ASAR data. Future studies should consider accessing these.

4.7.4 Models for ocean feature characterisation

The use of SAR backscatter based models for characterising ocean features would greatly reduce ambiguities associated with visual interpretation based purely on analyst knowledge. Future studies should consider accessing these models.

4.7.5 Automation

Local knowledge-based rules could be built into systems that support decision-tree classification (eg. ENVI-IDL or eCognition) to develop semi-automated procedures for slick identification and classification.

5 Geophysical and Acoustic Methods for Seepage Detection

5.1 Acoustic detection of gas within the water column

Gas bubbles, whether free in the water column or in the swim bladders of fish, dramatically affect the acoustic and mechanical properties of the medium: sound attenuation increases, sonic energy becomes scattered and the speed of sound propagation changes (Hampton and Anderson, 1974; D'Arrigo, 1986; Judd and Hovland, 2007). The amount of attenuation and scattering depends primarily on the size of the bubbles relative to the acoustic wavelength. Gas bubbles that have a resonance frequency the same as the source signal, scatter and absorb sound waves very strongly (Clay and Medwin, 1977). At the most basic level, a bubble that is in resonance extracts energy from the acoustic wave, which stimulates pulsation of the bubble at its resonance frequency, re-radiating some of the energy (Greinert and Nützel, 2004). Echo sounding is the most sensitive method to remotely detect gas bubbles in the water column, with tiny gas bubbles that are optically invisible being readily imaged acoustically (Clay and Medwin, 1977; Greinert and Nützel, 2004).

Bubbling (i.e. free-gas releasing) natural hydrocarbon seeps are typically identified as strong backscatter hydroacoustic flares in the water column, which are often 'rooted' to the seafloor (Merewether et al., 1985; Paull et al., 1995; Hornafius et al., 1999; Heeschen et al., 2003; Greinert et al., 2006). Thus, hydroacoustic systems have become a common tool for finding and monitoring bubbling seep sites. Hydroacoustic features of seepage are referred to as 'flares' to clearly differentiate them from geochemical anomalies in the water column and those sites that imply upward migration of water due to thermal heating or massive bubble release (Hornafius et al., 1999; Leifer and Judd, 2002), which are generally called plumes (Greinert et al., 2006).

5.1.1 Natural hydrocarbon seepage flares on the Yampi Shelf

Active seepage in the Cornea area of the Yampi Shelf was imaged using 200 kHz single beam echosounders during S267 (Rollet et al., 2006; Figure 49). Echosounder images of seepage varied considerably, from vertical to inclined flares aligned with tidal currents. The active flares rise to 30-50 m above the sea floor and appear to 'plateau-out' along a sub-horizontal layer, in 40-60 m water depth, possibly following an iso-density surface in the water column (most likely a stable thermocline) or an oceanic methane layer formed when particles lifted by bubbles are abandoned when the bubbles dissolve, which often happens at the thermocline (Leifer and Judd, 2002). This layering in the water column was not visible over all the survey area and may have been accentuated on the echosounder where gas bubbles were trapped along the thermocline.

During SS06/2005 digital echosounder data were recorded across the Yampi Shelf natural hydrocarbon seep sites with a Simrad EK 500 sounder (Brunskill et al., 2005) (Figure 50), which continuously logged data at 12 and 120 kHz frequencies. The seepage flares exhibited a variety of forms, with characteristic types being large masses that are stationary in time and occupy a significant part of the water column (Figure 50a), vertical 'spikes' (Figure 50b), and inclined elongate masses that appear to be related to the direction of tidal current flow at the time of imaging (Figure 50c). Large masses were noted on three occasions at 6:38 UTC on 5 June 2005, 8:28 UTC on 6 June 2005 and 10:10 UTC on 9 June 2005. Figure 50 shows that the masses are stationary while the vessel stopped over the top of them for sampling. It shows that the bubbles are not rising directly to the surface but, in places, they appear to rise to a stratification level and then are distributed laterally, as observed during S267.

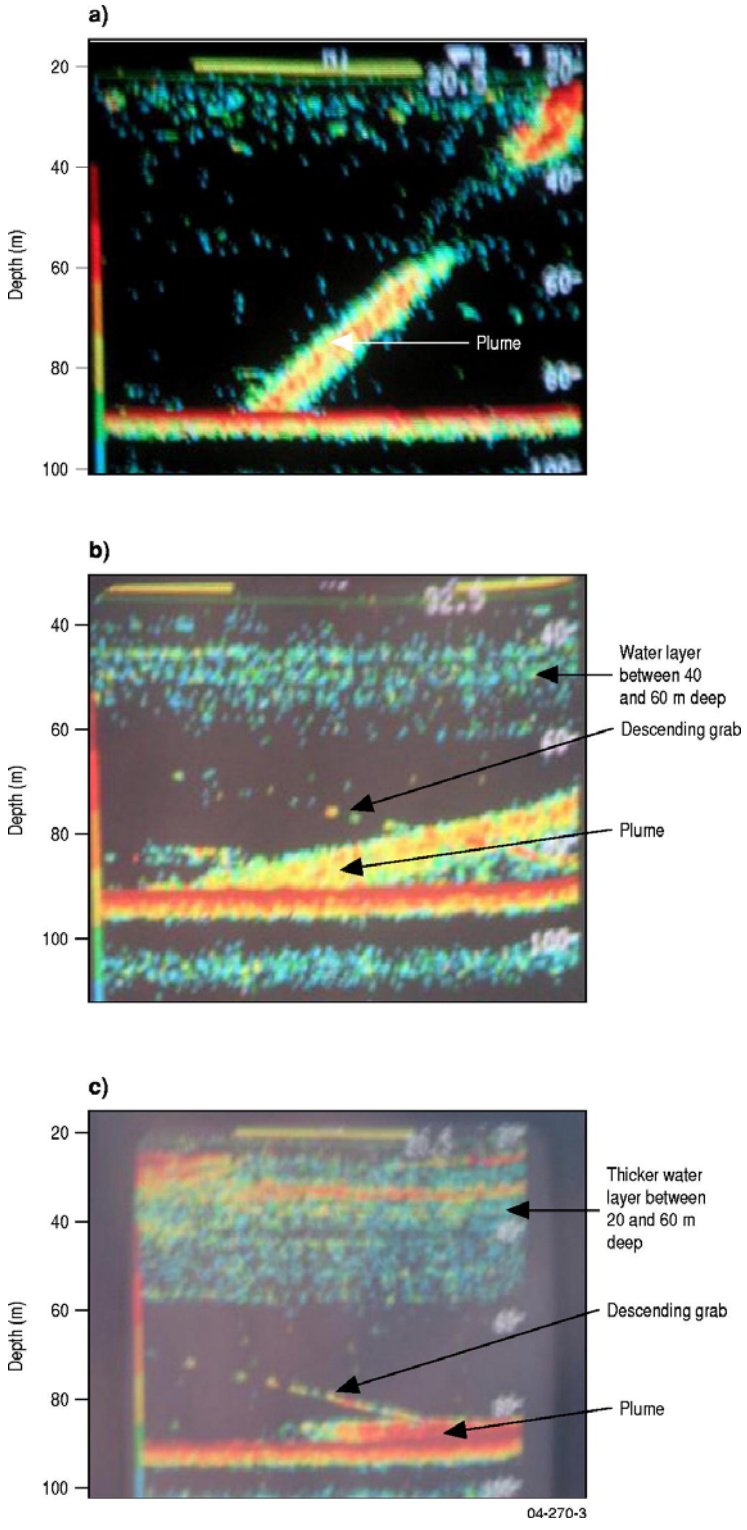

Figure 49. Echosounder screen photos from S267, imaging gas flares in the water column from the Yampi Shelf; a) shows a discontinuous flare, b) illustrates several flares and acoustic layering between 60 m and 40 m depth, and c) images a direct grab sampling of a seep.

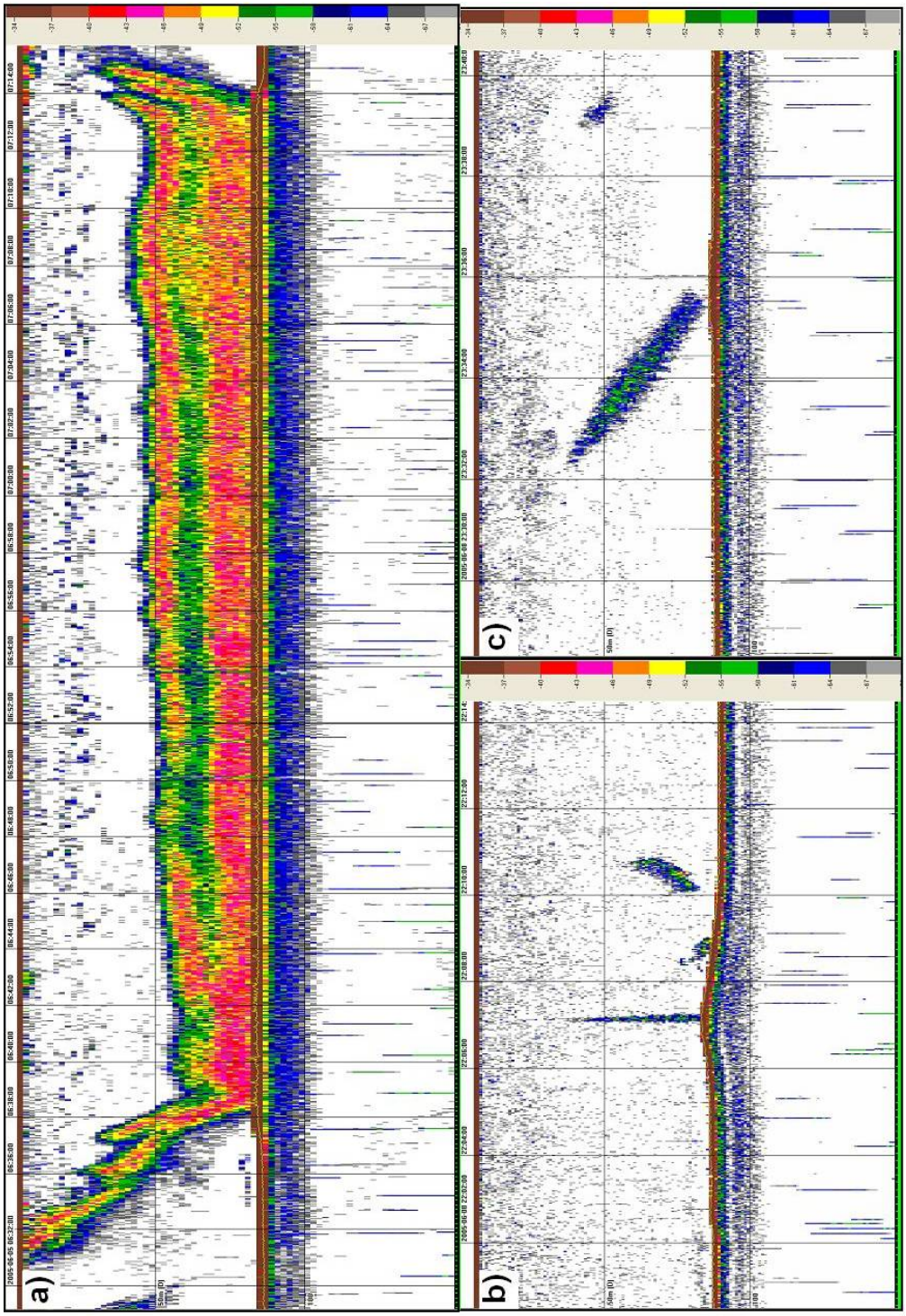

Figure 50. 120 kHz echograms from SS06/2005 showing a variety of gas flare morphologies from the Yampi Shelf: a) shows a large mass, b) illustrates a vertical flare, c) images a flare inclined in the direction of tidal current flow.

The locations of bubble flares were marked on multibeam bathymetry collected during these surveys. The position of active seepage was found to differ between two surveys, which were carried out 14 months apart (Figure 51). This indicates that the points of seepage on the sea-floor had changed over time, while the general zone of seepage above an interpreted HRDZ remained active.

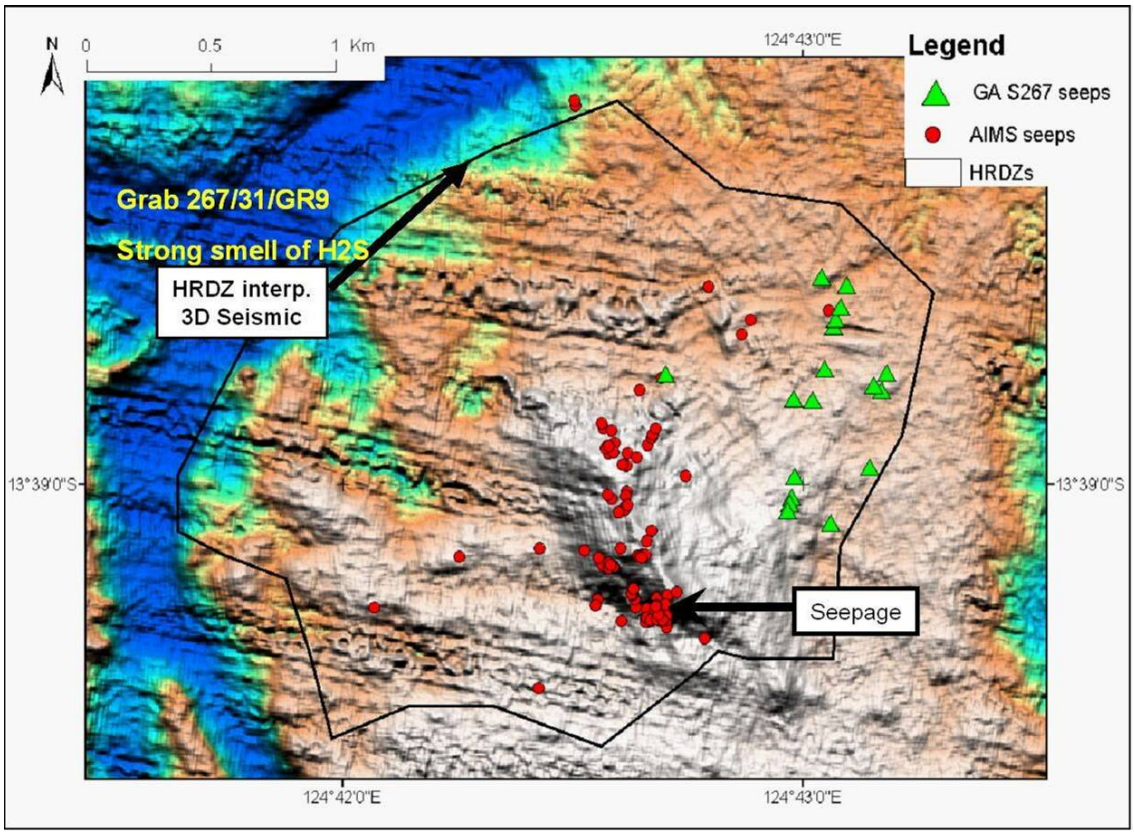

Figure 51. A detailed multibeam bathymetric image showing the location of active seepage sites recorded during S267 and SS06/2005. The sites of active seepage have changed between the different surveys which were carried out 14 months apart.

Sidescan sonar data were also critical for the detection of hydrocarbon seeps on the Yampi Shelf during S267 (Rollet et al., 2006; Figure 52). The sidescan sonar was able to image flares of high back-scatter material streaming from active seeps. In the sidescan sonar data, flares appear as multiple streams of bubbles sloping upward in the direction of the tidal current or as overlapping hyperbolic streams, which appear to arch up through the water column and then dip downwards. Similar hyperbolic responses have been recognised in sonar records of seepage flares in the Gulf of California (Merewether et al., 1985). These arched anomalies may result from: 1)

bubble flares streaming away from the vertical plane traced by the sidescan fish; 2) flares streaming through the horizontal plane traced by the fish; 3) a curved flare that streams vertically from the seabed and then horizontally along an isodensity surface, as observed on our echosounder data, or a combination of all three. The relatively straight responses are the result of flares streaming perpendicular to, parallel to, or towards the vertical plane traced by the sidescan fish, but which do not rise above the depth of the fish's horizontal track.

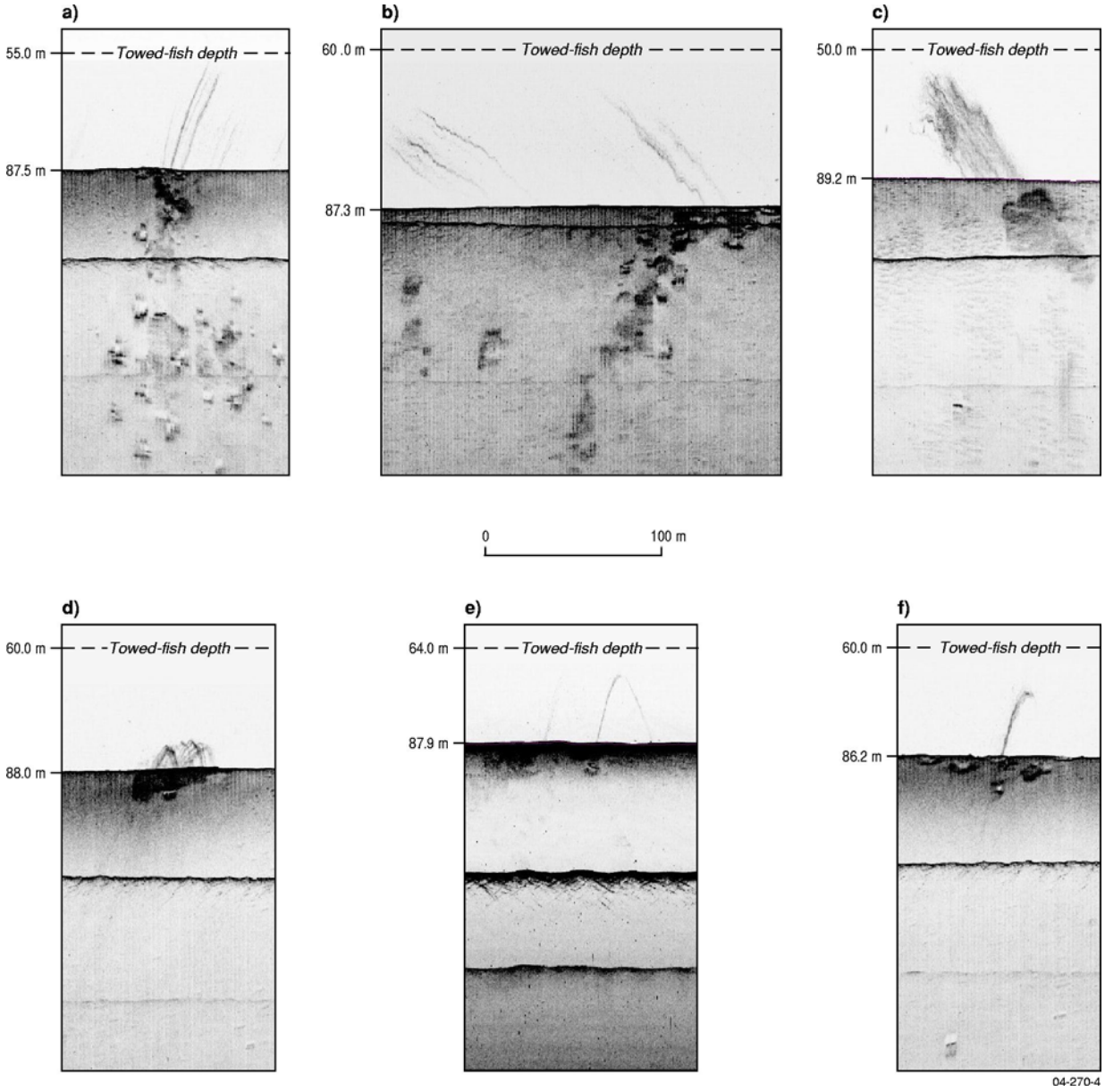

Figure 52. Sidescan sonar data illustrating gas flares into the water column from the Yampi Shelf: a-c) linear flares are sloping upward in the direction of the tidal current, up to a layer between 60 and 40 m depth, which was also observed on the ship's echo sounder: d-e) hyperbolic-shaped flares are reaching up to 20 m above the seafloor.

5.1.2 Differentiating natural hydrocarbon seepage from biota

In echosounder records it can be very difficult to differentiate between gas seeps and biological features. Fish are imaged primarily from their swim bladders (which contain gas) and, together with gas-bubble carrying plankton, they can easily be mistaken for gas seepage flares. Examples of these potentially false positives are seen in numerous near-vertical flare-like features identified in the water column over the Broome Platform on the central North West Shelf during SS06/2006 (Jones et al., 2007; Figure 53). These features have variable backscatter intensity in 12 and 120 kHz echograms. Some features have low intensity and are relatively diffuse, while others have high intensity and are discrete.

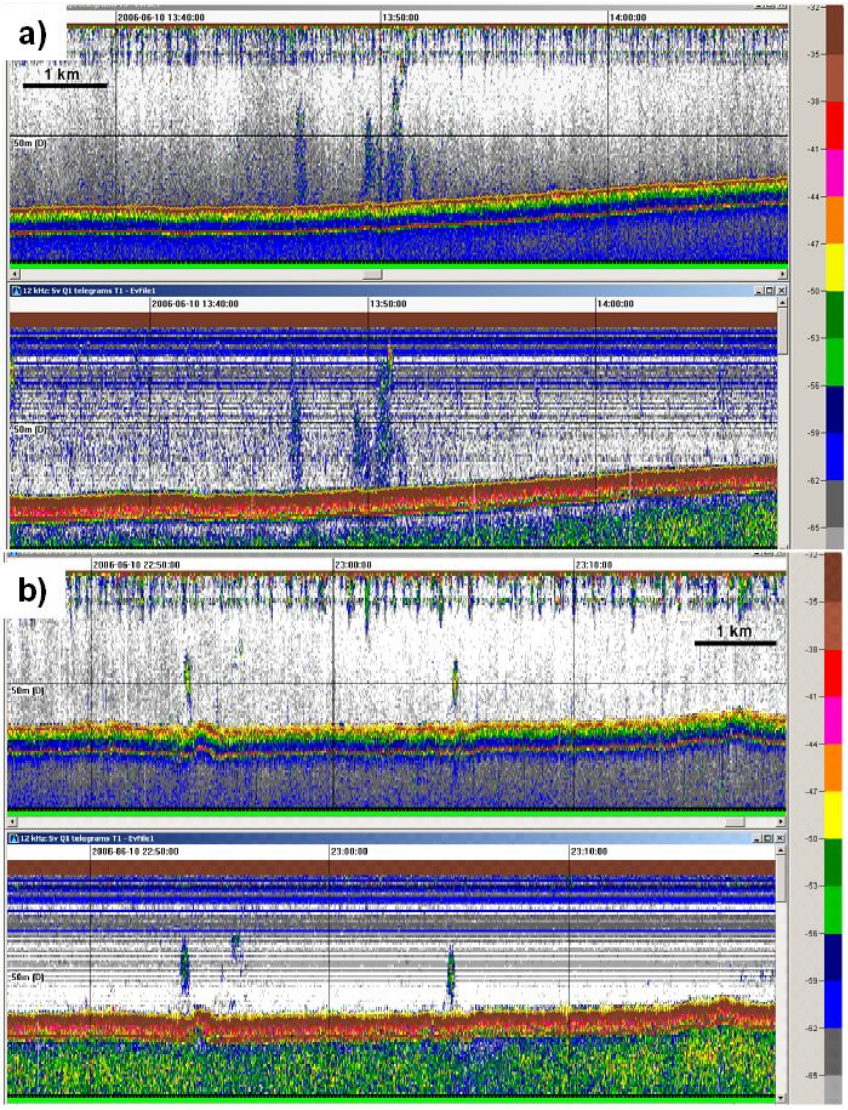

Figure 53. a) Low-intensity, diffuse and b) high-intensity, discrete near-vertical flares in echosounder data from SS06/2006 on the central North West Shelf.

A hydroacoustic 'flare' was detected over a broad seabed mound on the Broome Platform during *RV Franklin* marine survey 05/2000 (Figure 54 and Figure 55). A similar flare was also detected during SS06/2006 at the same location (Jones et al., 2007; Figure 56). This repetition pointed towards a potential seepage origin. However, the sidescan sonar data acquired at this time showed a scattered water-column response (Figure 57), which is not typical of seepage derived gas flares. A 'flare' over the mound was also detected with the 12 and 120 kHz echosounders at the time of an underwater camera tow, but the echograms show the 'flares' to have very complex morphology (Figure 58). Rather than being near-vertical, the features are stratified, with individual components showing evidence of lateral rather than vertical morphology. The underwater camera tow passed directly through the water-column feature recorded by the echosounder data. The camera footage showed that the water above the mound was rich with clouds of tiny pelagic organisms, with no evidence of bubbles in the water. This combined evidence clearly shows that these flare-like features have a biological origin. The apparent vertical form of the 'flare' is an artefact of the survey method. The biological targets were passed at relatively high speeds and data displayed along a 'compressed' time (horizontal) scale, resulting in a feature that initially had the appearance of a gas 'flare'. Thus, recording of potential gas 'flares' is best carried out using slow speed acquisition and is best displayed using a distance horizontal scale to give spatial dimensions, rather than the more typically used time scale which is often misleading.

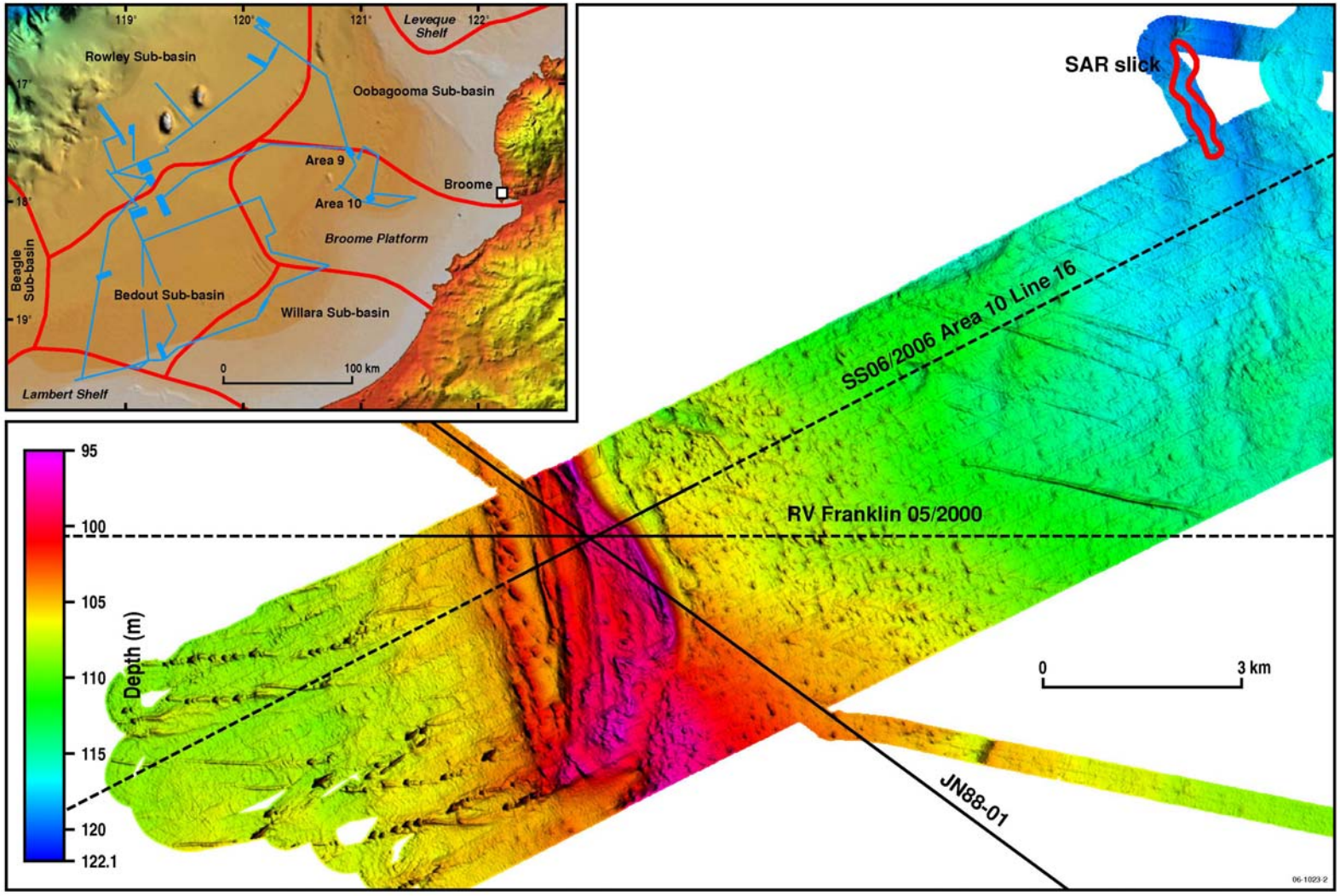

Figure 54. Multibeam swath bathymetry of Area 10 on the Broome Platform that was investigated for repeating water column flares. Regional setting and location of Area 10 shown by the insert.

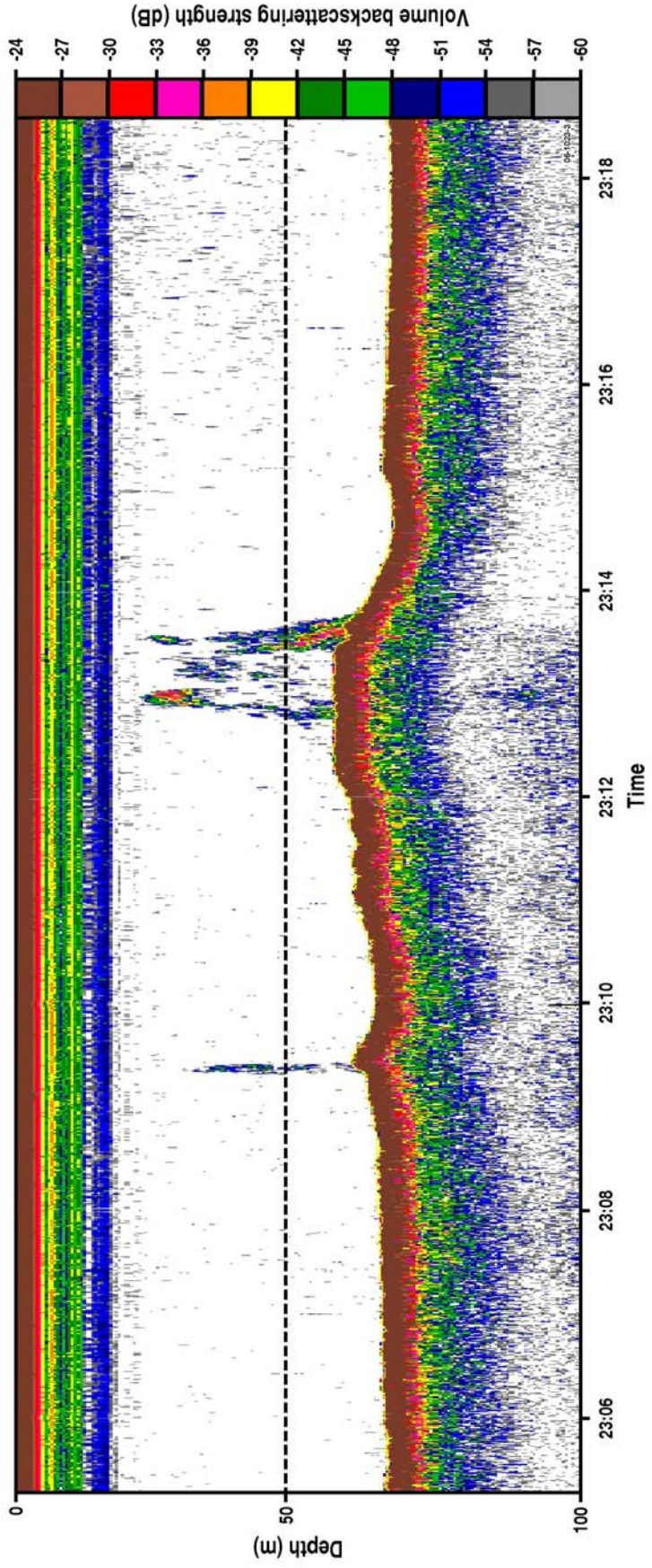

Figure 55. Near-vertical flare imaged by echosounder data from the Broome Platform, acquired during RV Franklin Survey 05/2000.

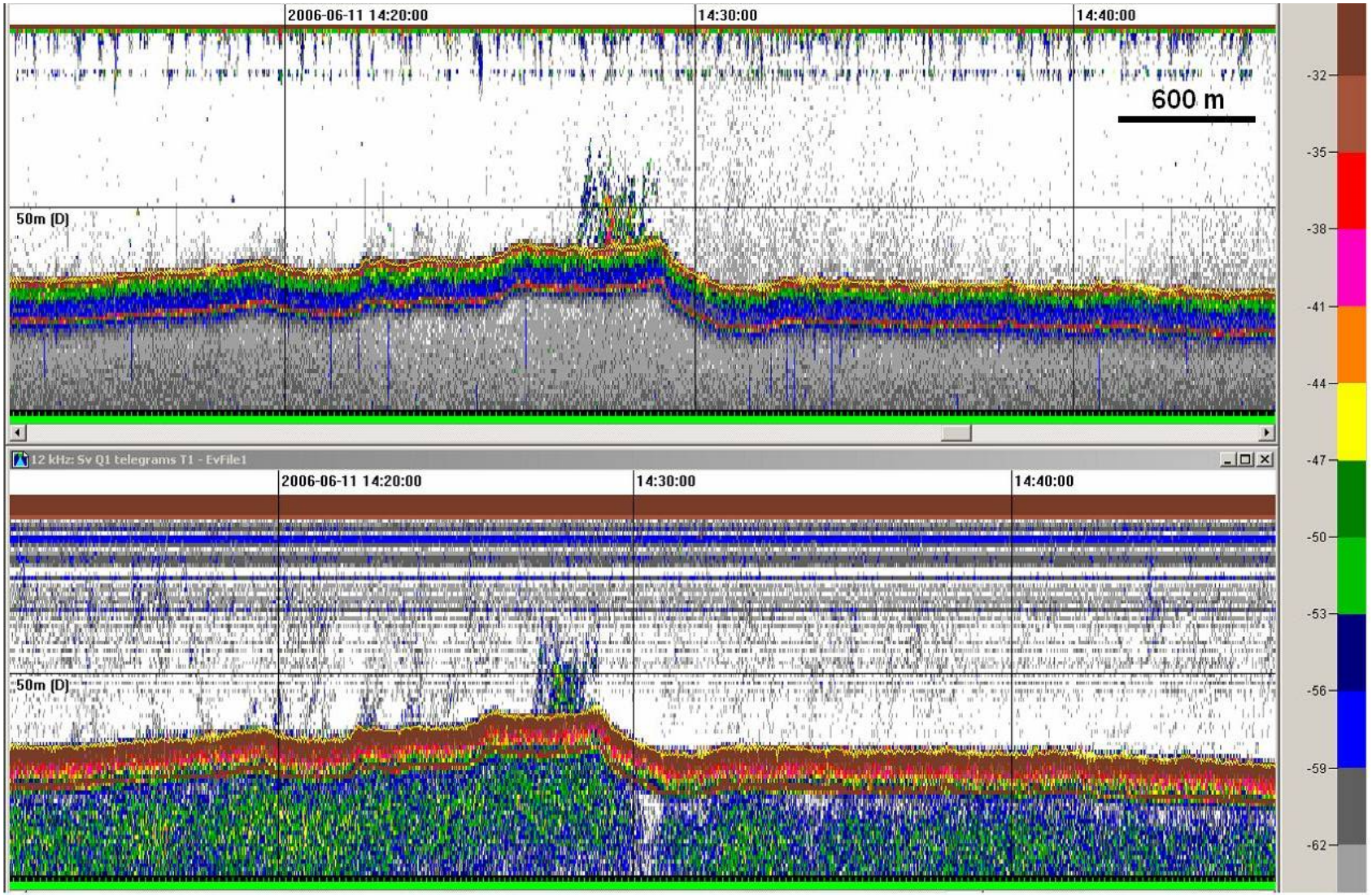

Figure 56. Flare-like feature detected over the positive relief seabed feature on the Broome Platform; feature may be a possible repeat of the flare detected during *RV Franklin* marine survey 05/2000 shown in

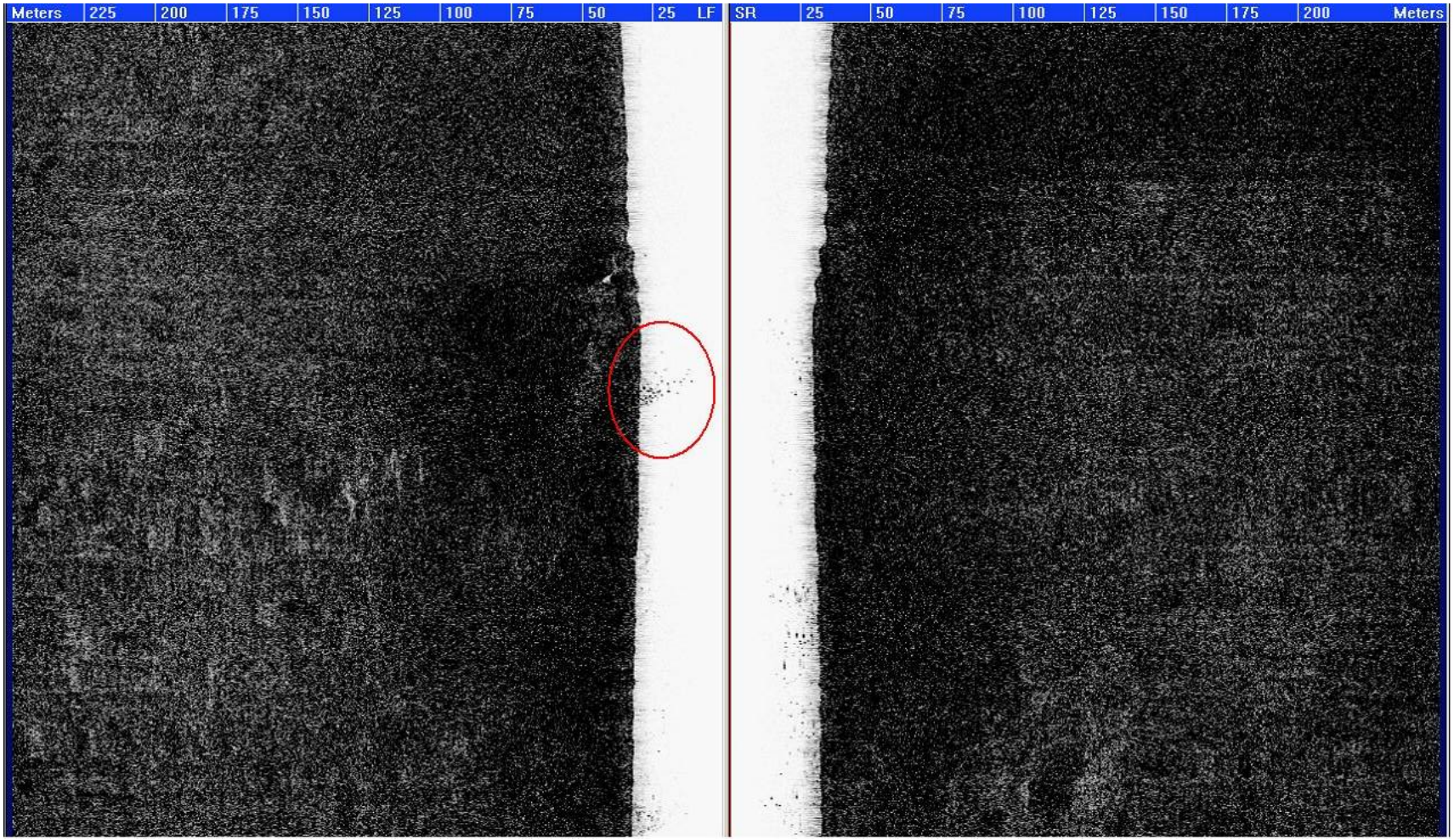

Figure 57. Sidescan sonar data through the 'flare' shown in, imaging a scattered response that is more likely to represent biota rather than seeping free gas bubbles.

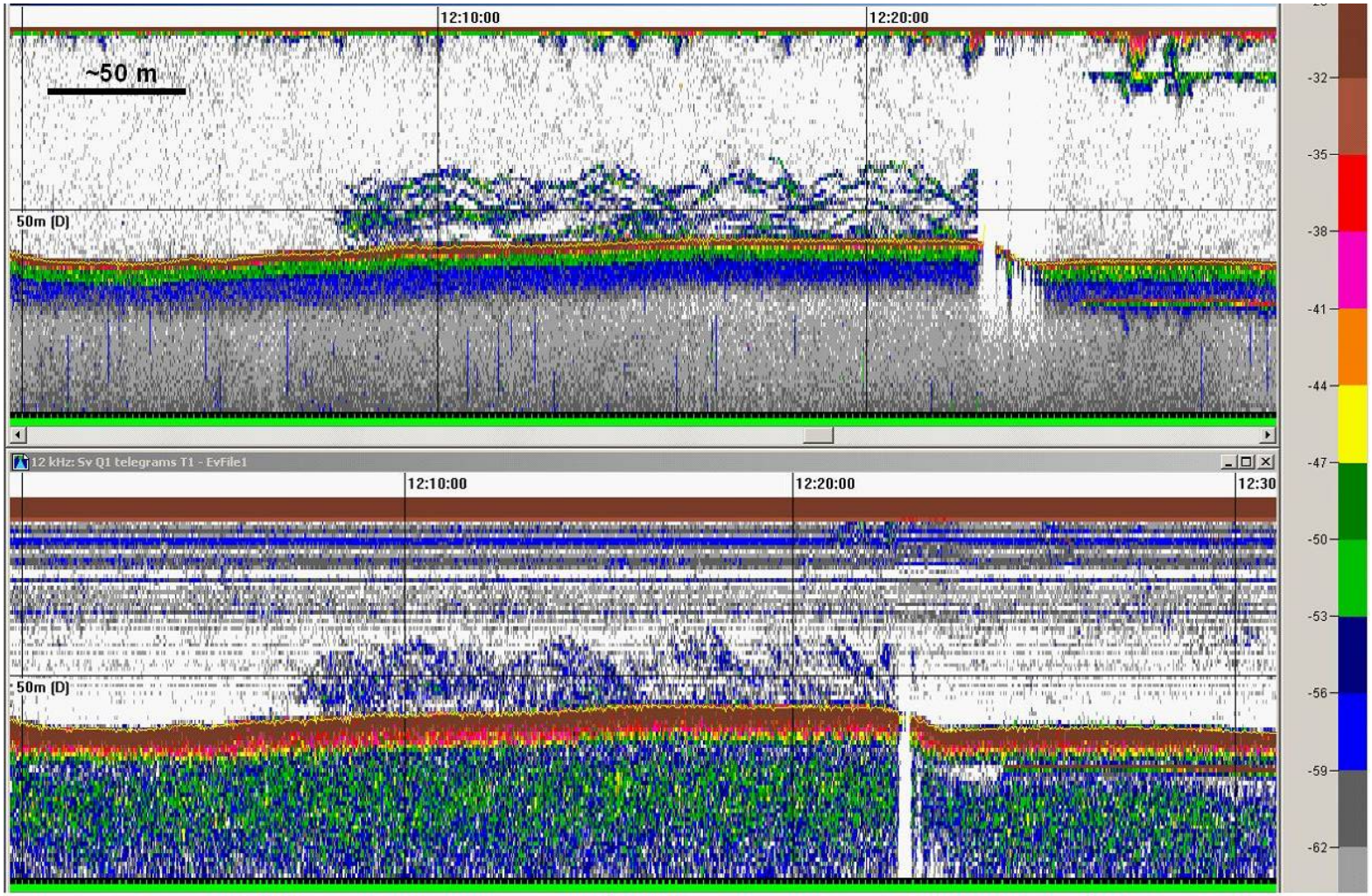

Figure 58. 12 and 120 kHz echograms from the time of camera tow at the Broome Platform site, showing the flares have a complex, horizontally layered, rather than vertical, morphology.

Bubbles rising from hydrocarbon seeps either shrink or expand through the water column, depending on initial bubble size, the rise velocity and the level of methane saturation in the seawater (Leifer and Judd, 2002). This predictable behaviour should lead to systematic variations in echosounder response, which may allow for seepage flares to be differentiated from biological acoustic responses. In theory, it is possible to use the relative response in multiple acoustic frequencies to observe any such systematic variations. A flare from the Yampi Shelf shows a distinct vertical 'spike' at 120 kHz, with a maximum target strength in the lower part of the feature, decreasing upward to a minimum at the top (Figure 59). The 12 kHz response from the same flare shows a vertical feature with a maximum target strength towards the middle, decreasing upwards and downwards. The upward decrease in 120 kHz backscatter for the seepage flare suggests the bubbles in the flare are shrinking and dissolving as they rise through the water column. The upward increase in 12 kHz backscatter is therefore due to either: 1) the bubbles shrinking into the size range for resonance at 12 kHz, or 2) an increase in the relative proportion of big bubbles (as small bubbles dissolve) leading to a higher response in the lower frequency.

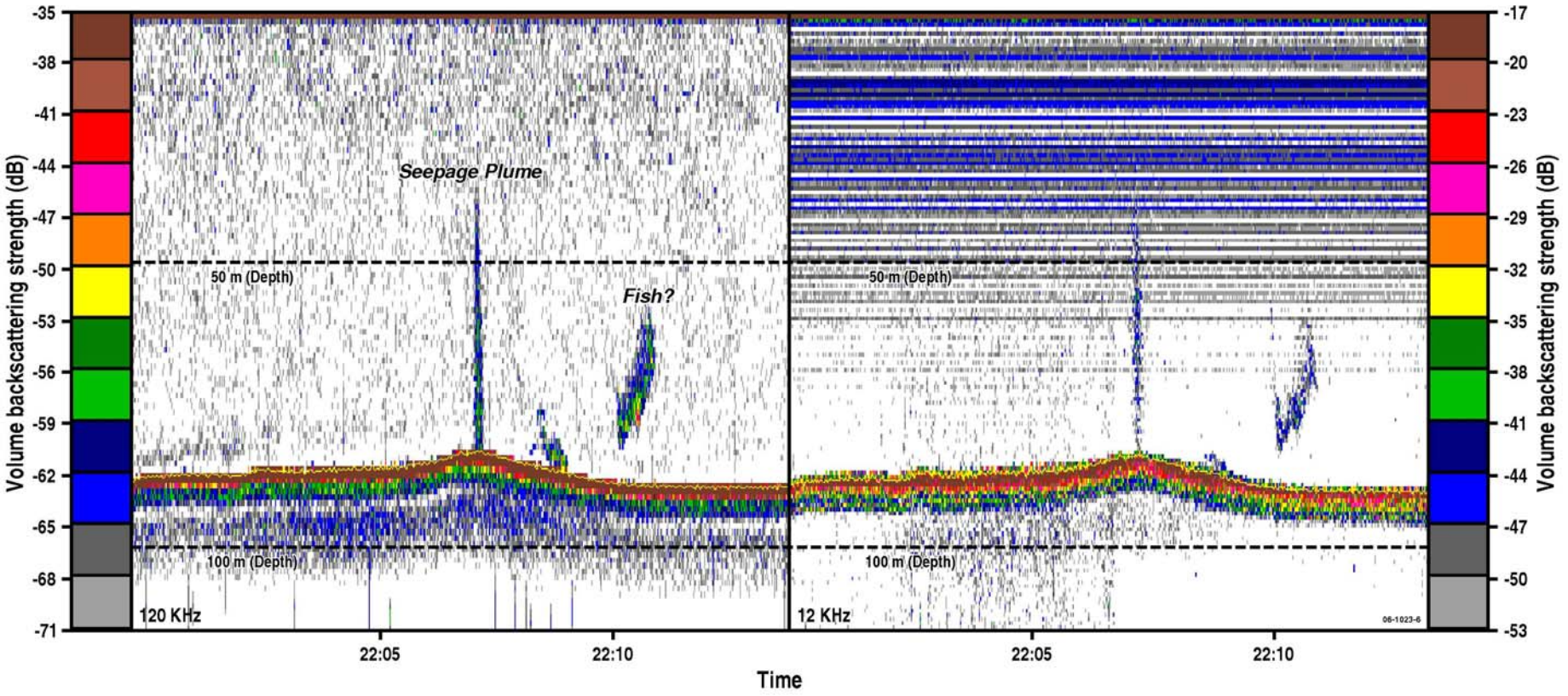

Figure 59. Vertical gas seepage flare from the Yampi Shelf. Note the maximum response in the lower part of the feature at 120 kHz, and in the upper part of the feature at 12 kHz.

5.2 Seabed features associated with seepage/fluid expulsion

The presence of active gas flares in a water column provides direct evidence for gas seepage. However, the release of gas can be intermittent, therefore, seabed features associated with fluid movement can provide indirect evidence of gas release (Judd and Hovland, 2007). They also provide potential sites for sampling for interstitial pore space gas. Features can be observed at various scales with different detection methods. Generally, large scale features (>1000 m across, with relief of >100 m), such as mud volcanoes are easily detected by multibeam sonar (Judd and Hovland, 2007). Medium scale features (100's m across, with relief of 10's m), such as mud or carbonate mounds and large pockmarks (Rollet et al., 2006; Jones et al., 2007), can be detected by multibeam echo sounders. Small scale features (10-20 m across, with relief of 1-2 m), such as pockmarks and vent structures require higher resolution sensors and are more easily identified using sidescan sonar or higher frequency multibeam echo sounders (Rollet et al., 2007). Different scales of features can be super-imposed and thus the higher resolution detection methods can provide far more target detail if sampling is to be carried out.

Pockmarks can vary in size depending on the nature of the seabed sediments, and are generally between a few metres to a few hundred metres across, and from <1 m to 20 m deep (Judd and Hovland, 1992; Judd and Hovland, 2007). Pockmarks were first reported by King and MacLean (1970) to occur in profusion on muddy parts of the Scotian Shelf. A detailed study of pockmarks in the Emerald Basin with sidescan sonar mosaics, led Josenhans et al. (1978) to propose the term "gasturbation" for the process of formation of the pockmarks. The release of gas from upturned sedimentary bedrock beds caused sediment to be suspended (Fader, 1991).

An example of variations in size and density of pockmarks is provided by a recent study of in the Arafura Sea using sidescan sonar (Rollet et al., 2007). Occurring in 80-220 m water depth, pockmarks are generally present where surface sediments, consisting of soft muds, are thick (>15 m) (Figure 60). Most pockmarks are small (5-35 m long, 5-15 m across and <2 m deep). High, medium and low density pockmark fields were identified. High-density pockmark fields are characterised by individual

pockmarks varying between 5-20 m in length, 5-10 m in width and <2 m in depth, with a pockmark density of ~350 per km^2 (Figure 61a). These pockmarks formed in muddy Holocene sediment which has filled palaeo-channels.

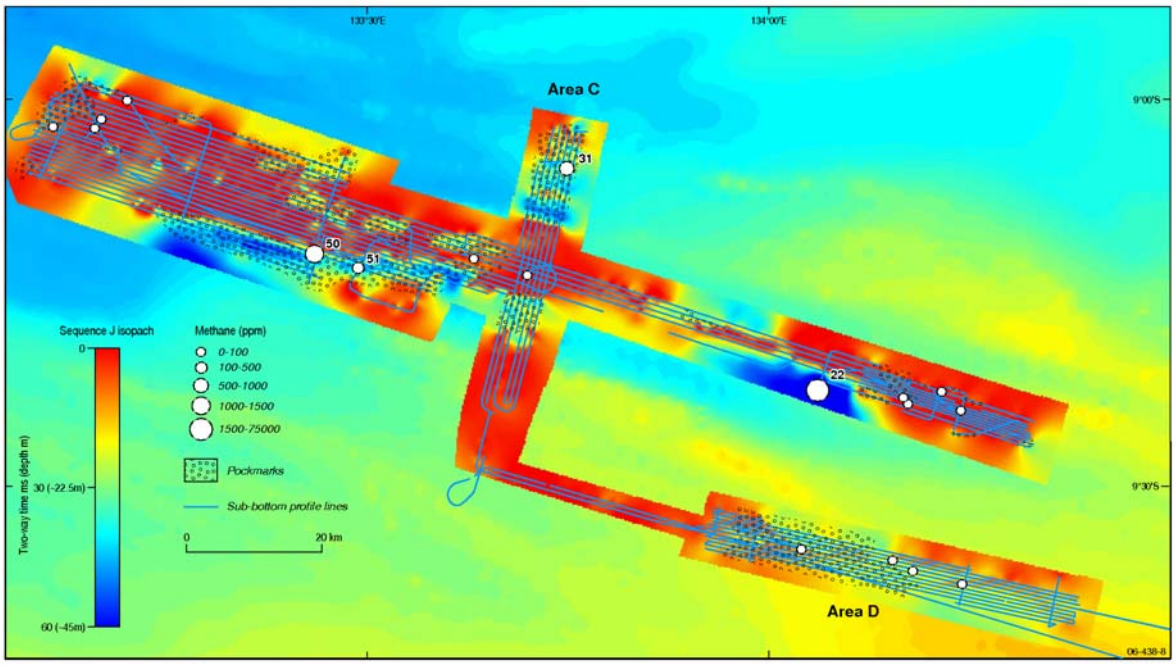

Figure 60. Pockmark fields mapped using sidescan sonar show a strong relationship with the thickness of Holocene mud fill in palaoe-channels in the Arafura Sea

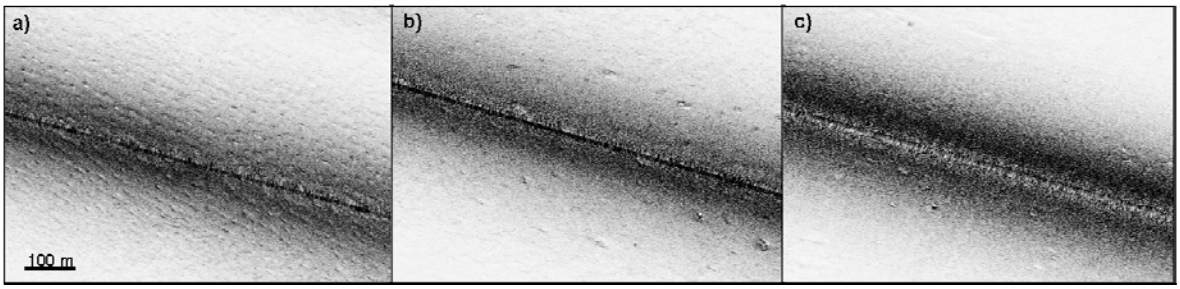

Figure 61. Sidescan sonar images from the Arafura Sea survey SS05/2005 showing pockmarks (Rollet et al., 2006): a) high density pockmark field b) medium density field and c) low density field.

High methane and carbon dioxide gas concentrations are associated with the high-density pockmark fields in the Arafura Sea and this gas appears to be microbially generated, based on carbon isotope data and gas wetness (Logan et al., 2006). The microbial gas most probably generated within organic-rich mud which filled the

Holocene channels.

Medium-density pockmark fields are characterised by individual pockmarks that are between 15-35 m long, 10-15 m across and <2 m deep, with a pockmark density of ~150 per km^2 (Figure 61b). They are also often associated with palaeo-channels, observed in sub-bottom profile data, but the infilling sediments are generally not as muddy as in the areas of high-density pockmarks. Gas levels in sediments from these areas were not significantly higher than the background level (Logan et al., 2006). These low gas levels may be related to the coarse nature of the sediment because coarse sediments generally have relatively high permeablity, and therefore do not trap gas if they are near the sea surface. Alternatively, the cores may not have intersected sediment with high pore gas levels.

Low-density pockmark fields have individual pockmarks that are between 5-25 m long, 5 m across and <2 m deep with a density of ~30 per km^2 (Figure 61c). Seabed samples did not contain gas concentrations above background levels and these sediments were generally composed of coarse, bioclastic, muddy sand. The density of pockmarks correlates with seabed sediment grain size and their occurrence is also correlated with mud filled palaeo-channels where *in situ* gas generation is occurring (Figure 60).

Therefore, where sediments are muddier, as for example in the Holocene mud packages which fill palaeo-channels (Figure 60), pockmarks are smaller and more densely spaced. As the sediment grain size increases, according to core and grab samples, pockmarks become larger and less densely spaced. However, this second correlation is at least partly related to *in situ* generation of microbial gases in the finer sediments.

Various seabed features are associated with gas seeps on the Yampi Shelf, around the Cornea oil and gas field (Figure 6, Figure 17, Figure 62). The most common features are clusters of hard, reflective 'blocks' (each 'block' is roughly 1 m in diameter) which are often arranged in a circular ring, possibly around the vent (Figure 17, Figure 62a-c). They are also associated with observed flares of material in the water column (Figure 17; Figure 52). The nature of these strong reflective blocks is not proven, although dredges taken over seepage areas often retrieved fragments of crusts

of cemented bioclastic material. Other common features are larger, hard, reflective hard-grounds and mounds of varying size and shape that appear as bright irregular patches on the 100 kHz records (Figure 62d). Pockmarks are also present (Figure 62e) and some are associated with gas seeps. The pockmarks are roughly circular and vary from 1-2 m across and up to 1 m deep, to larger features, 10 m across and 2 m deep. Sand waves (<1 m) occur between the reflective blocks, the hard mounds and the pockmarks, indicating sediment transport by waves and currents (Figure 62f). Above the Cornea oil and gas field, clusters of reflective blocks, larger hard-grounds and some pockmarks are clearly visible on the seafloor (Figure 62b). The variety of features, from well defined pockmarks to reflective blocks arranged around the vent areas, seems to be related to the same process of seepage, but with a different degree of erosion. Water current and/or seepage erosion have probably modified the shape and size of the seabed features related to seepage, exposing the carbonate-cemented sediments.

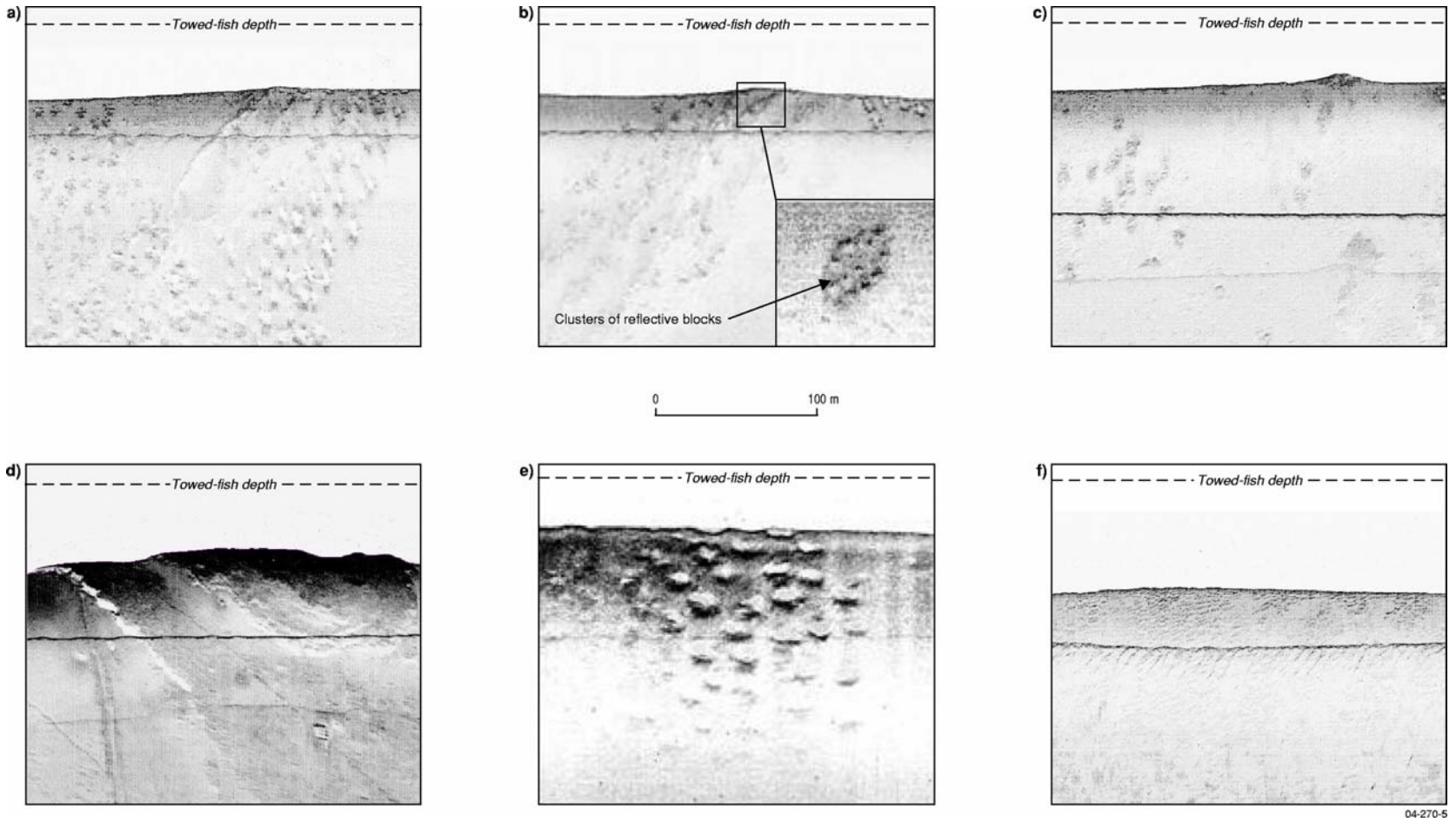

Figure 62. Sidescan sonar images (starboard only) of seabed features related to seepage in Cornea areas 1,2 and 4: (See Figure 6 for location) a-b) Clusters of strong reflective blocks aligned on a linear trend, c) clusters of strong reflective blocks and a cemented mound, d) a reflective hardground, e) a pockmark field, and f) ripples on the seabed suggesting recent seabed current activity.

Pockmarks were also identified in a restricted area of the mid-shelf on the boundary between the Broome Platform and the Oobagooma Sub-basin on the central North West Shelf (Jones et al., 2007; in prep; Figure 63). A camera tow undertaken in the area showed what appeared to be a vertical flare of fluid above the seabed (Figure 64), potentially formed through active venting at the seabed. The resulting pockmarks are roughly circular in shape, approximately 2-15 m in diameter and occur with a semi-regular spacing in sub-circular clusters (Figure 65). Mapping the spatial distribution of pockmarks on the Broome Platform in sidescan data shows that, in every case, pockmarks are found in association with laterally-restricted, high-amplitude sand waves (Type II sand waves, as distinct from laterally continuous, low amplitude Type I sand waves; Figure 63). A number of factors suggests that these sand waves are anomalously high and steep. The average slope of the high amplitude (Type II) sand waves is approximately 10° (max. 16.5°; Figure 66), which is steeper than generally associated with this bedform (Harris et al., 1986; Ashley et al., 1990). The height of most of the sand waves plots above the typically observed limit (relative to length) for flow transverse bedforms based on the observations of Flemming (1988) and the review of Ashley et al. (1990) (Figure 66). Sand waves that have unusual height-slope-length relationships (‘freak’ sand waves) have been suggested to be indicators of fluid seepage at a site in the Southern North Sea (Figure 67; Hovland, 1993; Judd and Hovland, 2007).

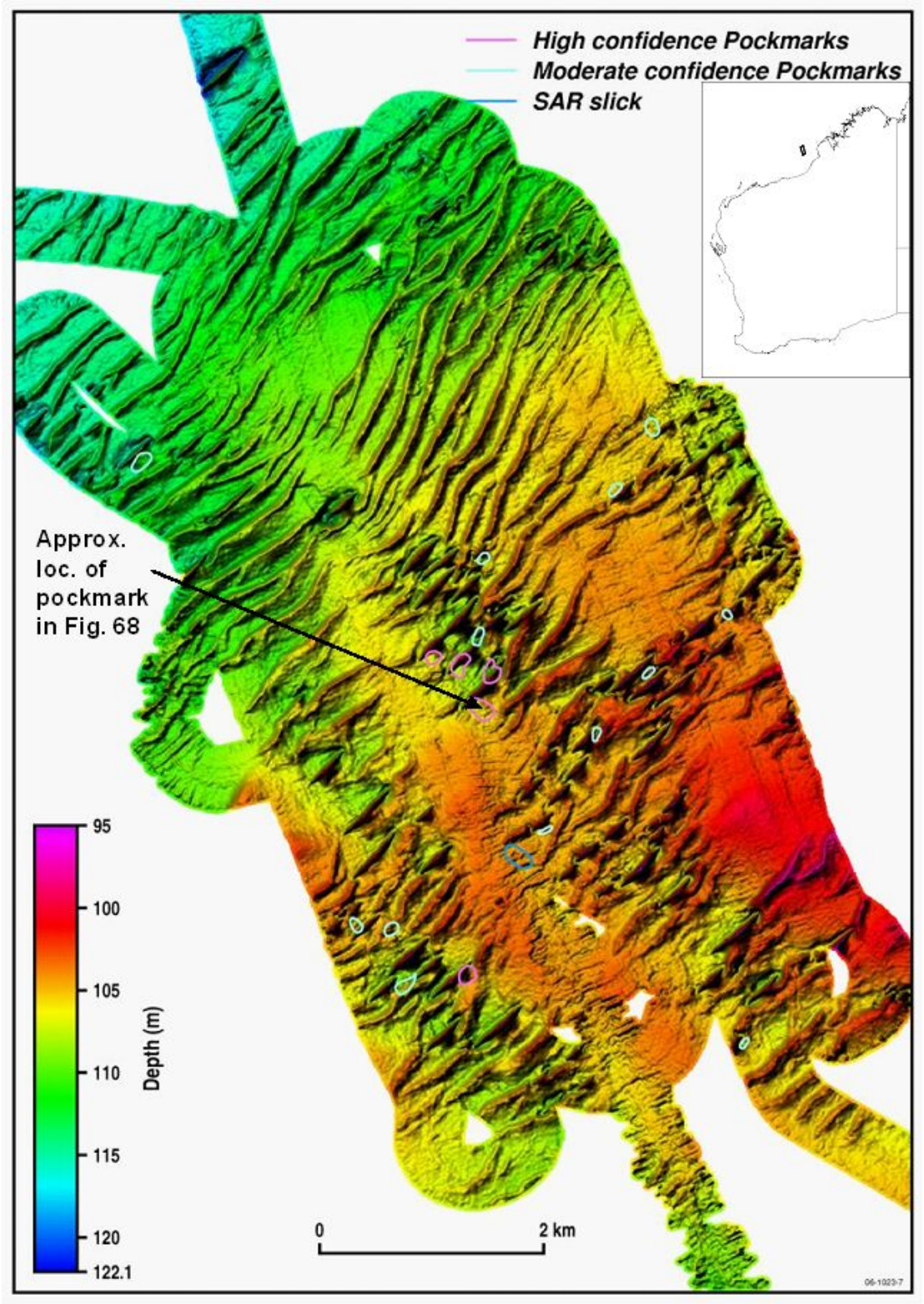

Figure 63. Multibeam swath bathymetry of an area above the Broome Platform /Oobagooma Sub-basin boundary in the Offshore Canning Basin showing sand waves and distribution of pockmarks and SAR slick.

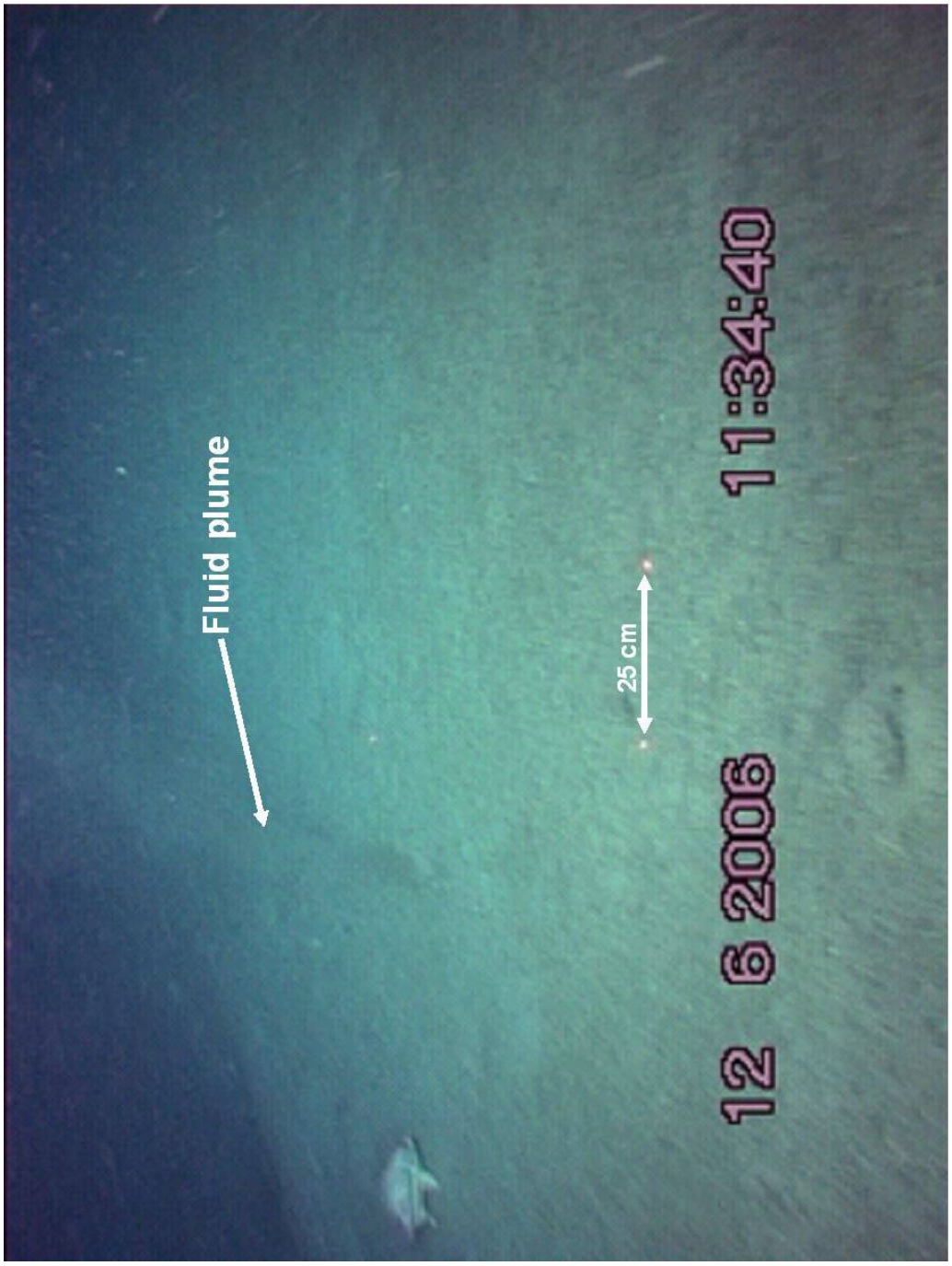

Figure 64. Photograph from the Broome Platform/Oobagooma Sub-basin boundary site taken near the seabed showing what appears to be a fluid flare, potentially formed through active seabed venting. Red laser points are 25 cm apart.

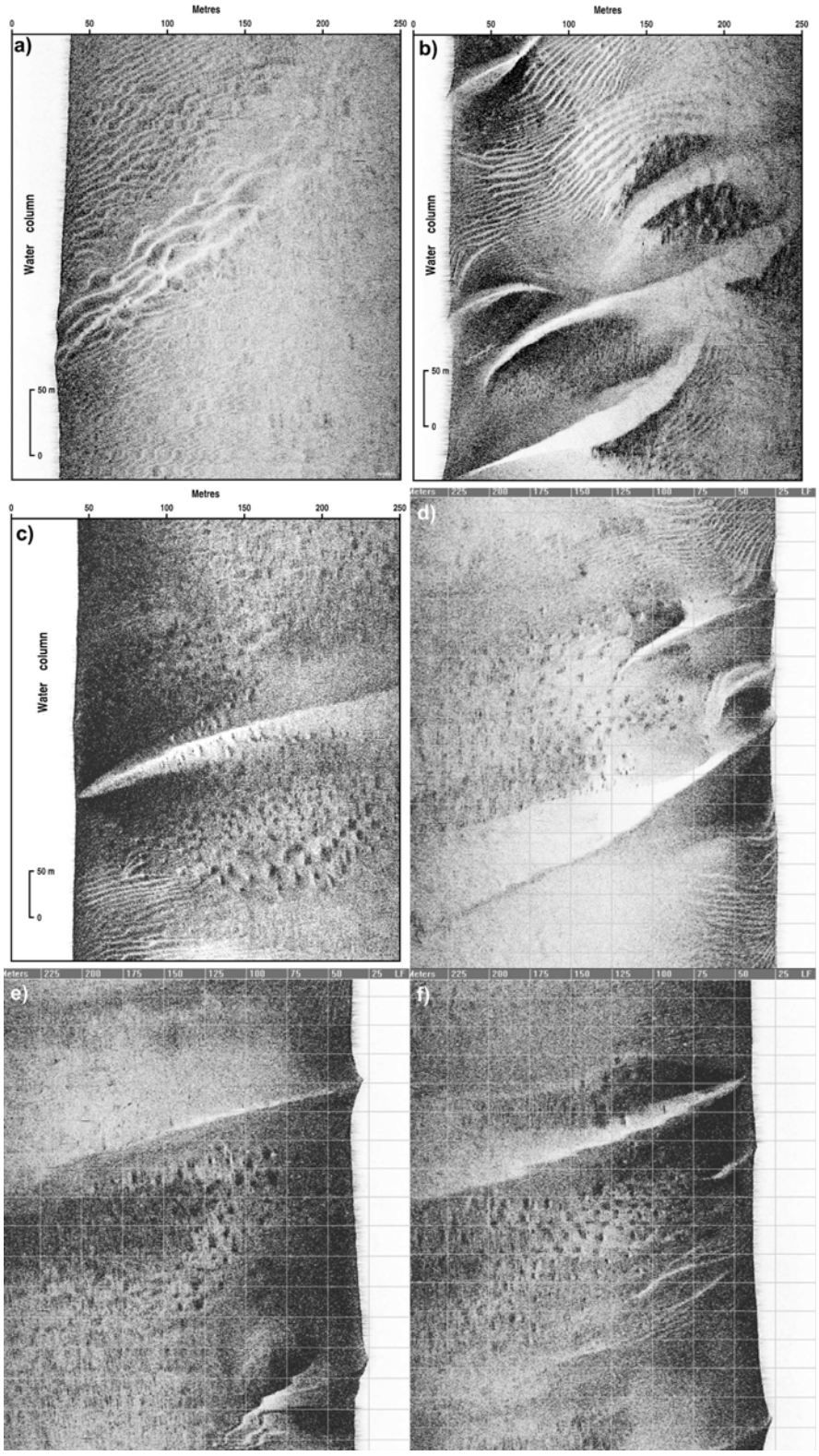

Figure 65. Examples of pockmarks identified in the Broome Platform/Oobagooma Sub-basin boundary area. Pockmarks appear to pierce sand waves in places, suggesting that fluid expulsion is a present-day process.

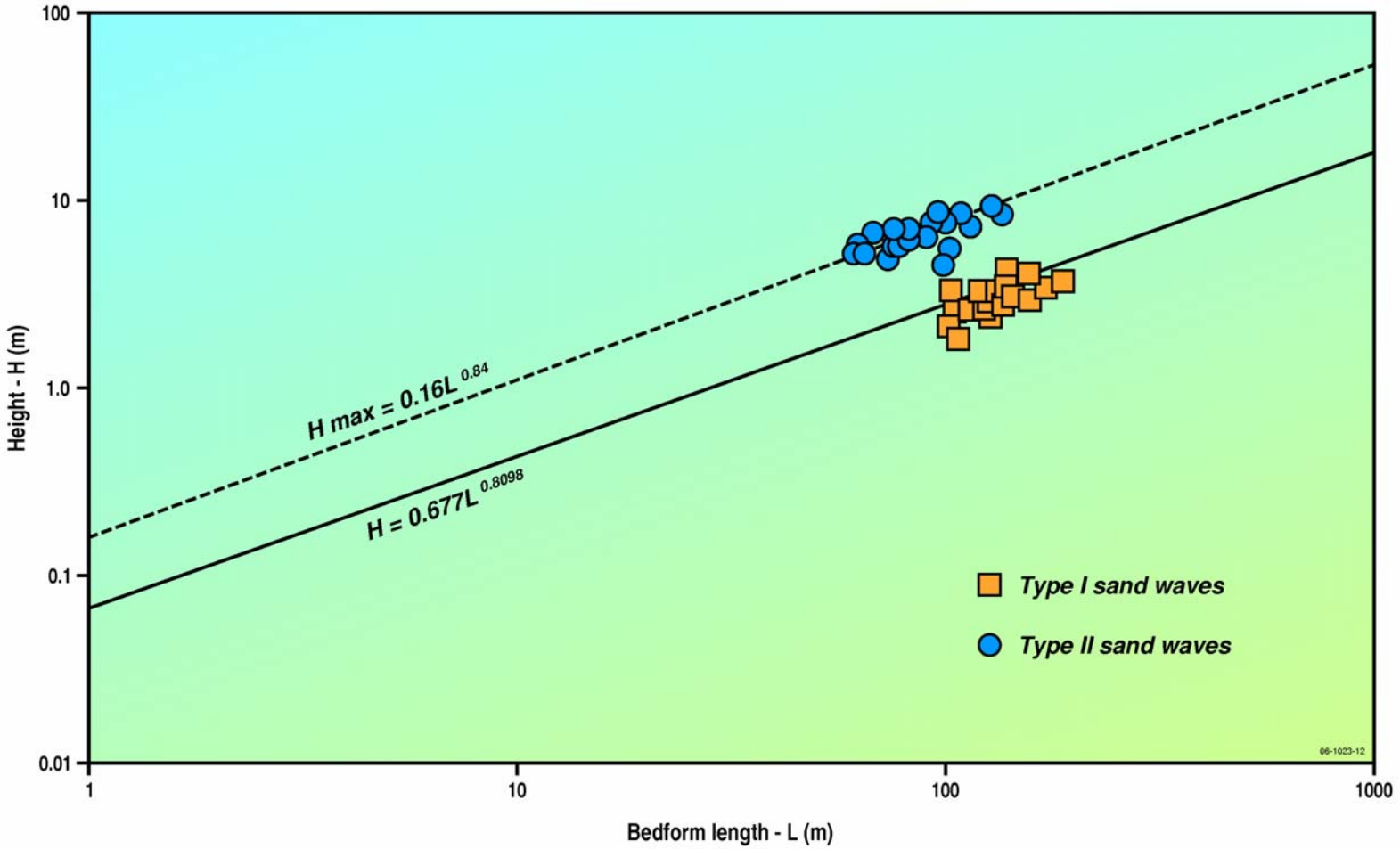

Figure 66. a) Lee vs stoss slopes of sand waves showing that Type II sand waves are distinctly steeper than Type I sand waves; b) global and upper height limit relationships for submarine sand waves from measurements of 1,491 subaqueous marine bedforms (Flemming, 1988). Note that the Type I sand waves plot on and around the global average, whereas many of the Type II sand waves plot above the upper height limit.

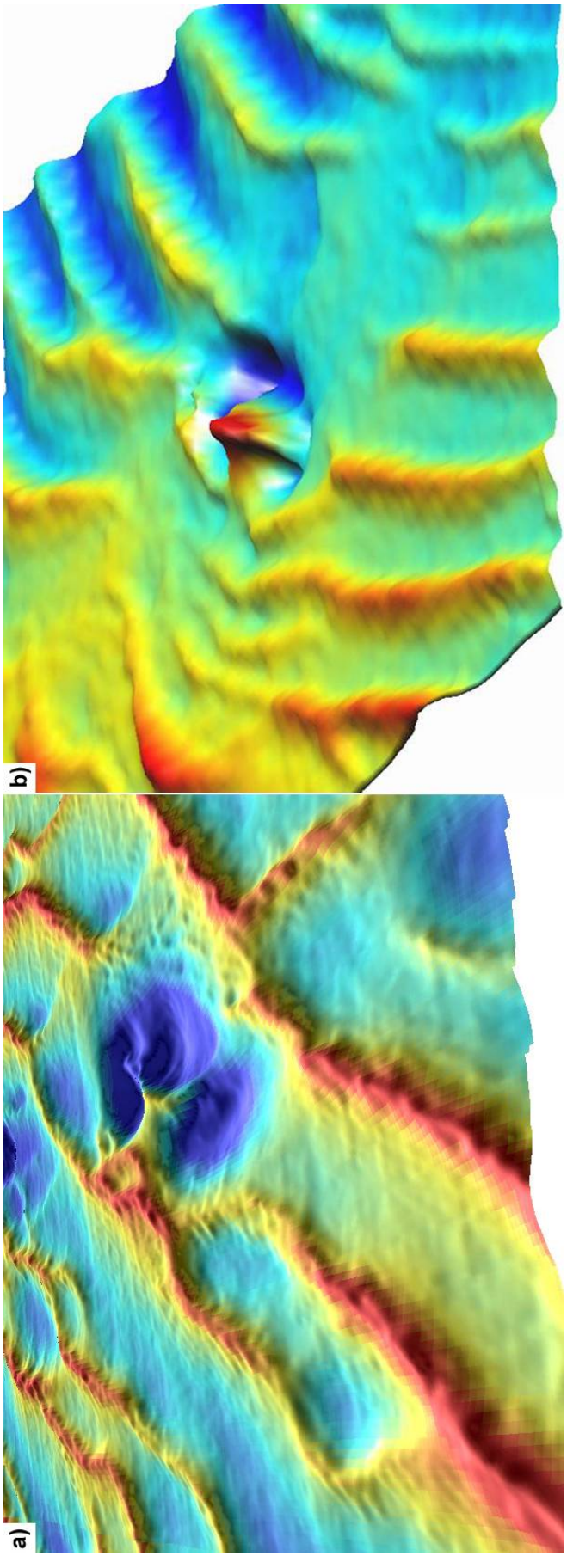

Figure 67. Sand waves with anomalous height-slope-length relationships, likely due to preferential scour in the troughs over areas of seabed fluid flow, in a) the North Sea (Hovland, 1993; Judd and Hovland, 2007; image courtesy of A. Judd) and b) the the Broome Platform/Oobagooma Sub-basin boundary.

Footage from a camera tow that traversed the cluster of pockmarks on the Broome Platform shows that some of the pockmarks are lined with carbonate concretions (Jones et al., 2007; in prep; Figure 68). A number of dredges returned a variety of concretions (Figure 69) of ooid grainstones, which are interpreted to be similar to the carbonate concretions seen lining the pockmarks. Tubular concretions varied between very simple forms which are interpreted to have formed through a purely biological mechanism to complex irregular tubes with openings up to 4 cm in diameter. The latter tubes do not appear to be biological in nature and are interpreted to have developed in association with the process of fluid excape that formed pockmarks in the study area. Irregular, massive carbonate concretions (Figure 69b) were also recovered from the dredges. They are interpreted to be an evolution of the tubular structures. As the tubes develop and grow, the openings fill with cement and more massive concretions are gradually formed. The tubes and massive concretions comprise grainstone, with ooids and pellets making up the majority of the sample (Figure 70). The pellets and superficial ooids have been cemented by acicular aragonite cement which forms an isopachous fringe <10-50 µm thick. The average $\delta^{13}C$ isotope values for the bulk grainstone and acicular aragonite crystals were 4.01 and 3.46, respectively (Figure 71). The average $\delta^{18}O$ isotope values for the bulk grainstone and acicular aragonite crystals were 0.52 and 0.13, respectively (all values are normalized to V-PDB scale and duplicates were within ±0.03 per mil maximum). Biomarkers related to anaerobic methane oxidation (AOM) and high-molecular weight petrogenic hydrocarbons were not detected within any of the concretions.

Figure 68. Seabed still photograph of a small pockmark from the Broome Platform/Oobagooma Sub-basin boundary site with a lining of carbonate concretions. Red laser points are 25 cm apart. See Figure 63 for location.

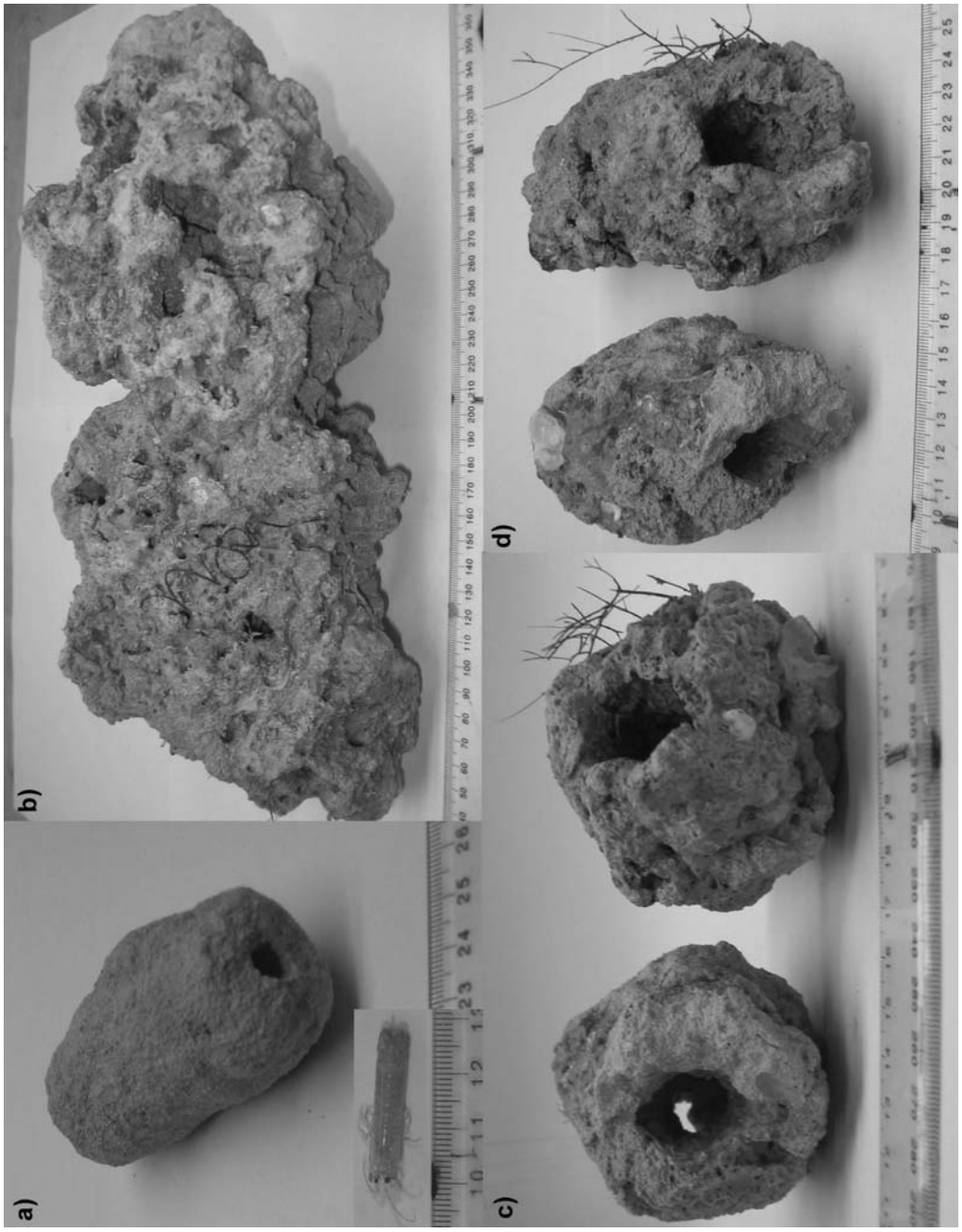

Figure 69. a) Relatively small simple tube. The shrimp in the inset was recovered from the tube. b) Irregular massive concretion; this is very similar in morphology to methane derived authigenic carbonate from the North Sea. c & d) Tubular concretions; the irregular appearance of the tubes suggest they might have formed from focused fluid expulsion at the sea floor.

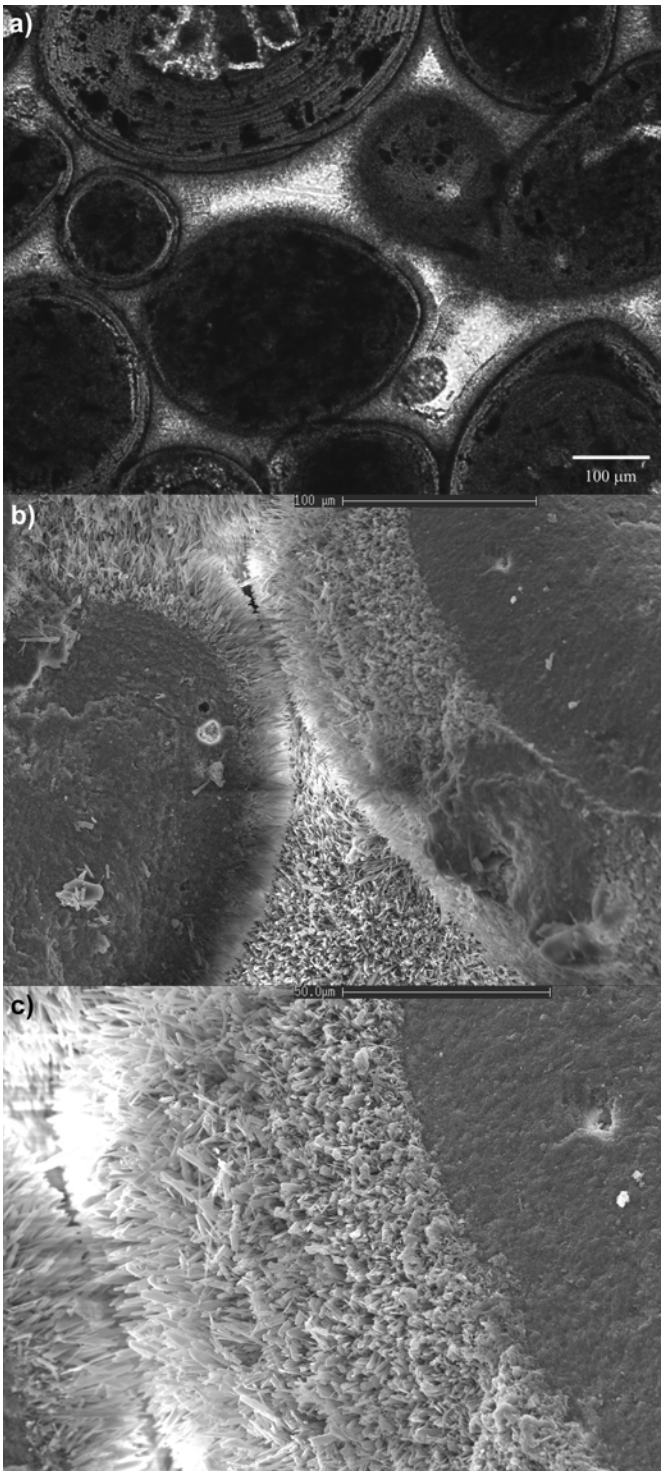

Figure 70. Photomicrograph (a) and SEM images (b-c) of ooid grainstone showing superficial ooids and pellets that have been cemented by fine fringes of acicular aragonite cement.

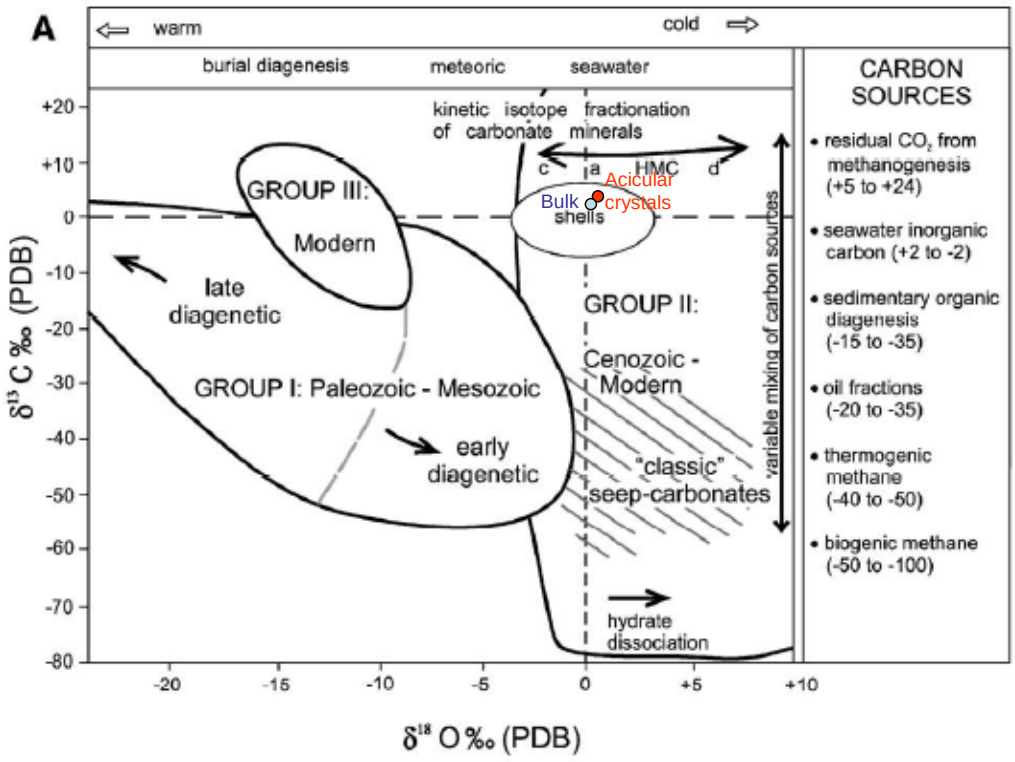

Figure 71. Carbon and oxygen stable isotope values from bulk grainstone and acicular aragonite cement from the Broome Platform/Oobagooma Sub-basin boundary site, plotted on distributions of seep-carbonates, their sources, and main biological and chemical factors that influence variability in their signatures (Campbell, 2006).

The fluid that is seeping from the seabed and forming pockmarks and concretions on the Broome Platform does not appear to be related to hydrocarbons. The fluid is interpreted to be normal marine seawater as high-molecular weight petrogenic hydrocarbons and biomarker assemblages commonly found in methane-derived authigenic carbonate were not detected within any of the concretions (Jones et al., 2007; in prep). Additionally, the $\delta^{18}O$ and $\delta^{13}C$ isotope values for the bulk carbonate concretions and a separate of acicular aragonite cement are similarly low (<4 ‰ and 5 ‰, respectively; Figure 71), suggesting that the fluids are modern seawater (cf. Campbell, 2006). This is supported by the isopachous acicular aragonite cement of the carbonate concretions which is a diagnostic marine cement, regardless of the source fluid (It was not possible to analyse the nature of the seeping fluids in the study area using headspace gas analysis due to the prevalence of indurated cemented sediments

and the lack of recovery in deployed seabed cores.

The seeping marine waters on the Broome Platform are interpreted to be the upwelling component of interstitial pore water flows beneath the sand waves, generated through a process similar to tidal pumping (Jones et al., 2007; in prep; Figure 72). A number of aspects of the marine geology and oceanography in the study area contribute to this site being a prime candidate for the development of interstitial pore water flows:

1. The slopes of the associated sand waves are steeper than generally associated with this bedform (Figure 66). Interstitial flow increases considerably with increasing bedform slope due to higher Bernoulli pressures (Shum and Sundby, 1996), therefore, these steep sand waves would be relatively prone to inducing pore water flow.

2. Grabs indicate that the seabed sediments comprise very well sorted, coarse oolitic sand. The very well rounded spherical grains will have high permeabilities.

3. The seabed sediments are relict (formed 9-12 Ka following the last glacial maximum (LGM); James et al., 2004) and the internal geometry of the sand waves (Figure 73) suggests that there is little overall migration of the bedforms. Given this prolonged stability of the seafloor sediments, the pore water flows may have developed preferential migration pathways.

4. The macro-tides over this part of the shelf result in tidal currents of significant magnitude (up to 0.79 m/s at ~69 m above the seabed and 0.67 m/s at ~21 m above the seabed).

5. The majority of pockmarks in the area are located above the edges of subsurface mounds defined by a relatively continuous near-surface reflector on sub-bottom profile data (Figure 73). This surface may be confining and focussing the subsurface interstitial flows, leading to relatively higher flow velocities associated with these mounds.

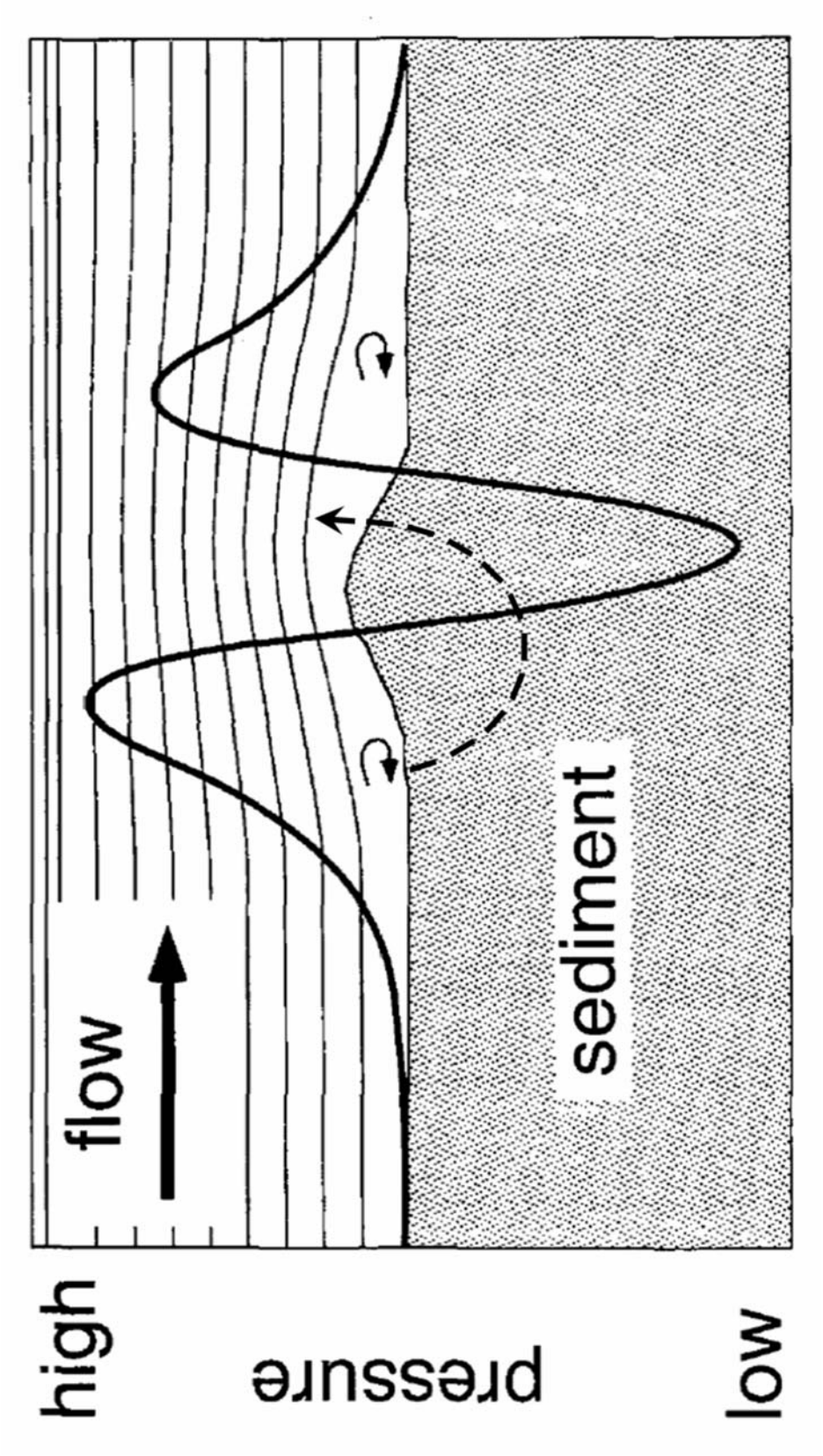

Figure 72. Water flow (thin lines), deflected by protruding topography, produces pressure changes (thick line) at the sediment/water interface. The dashed lines indicate the trajectory of induced pore water flow (modified from Huettel et al., 1996).

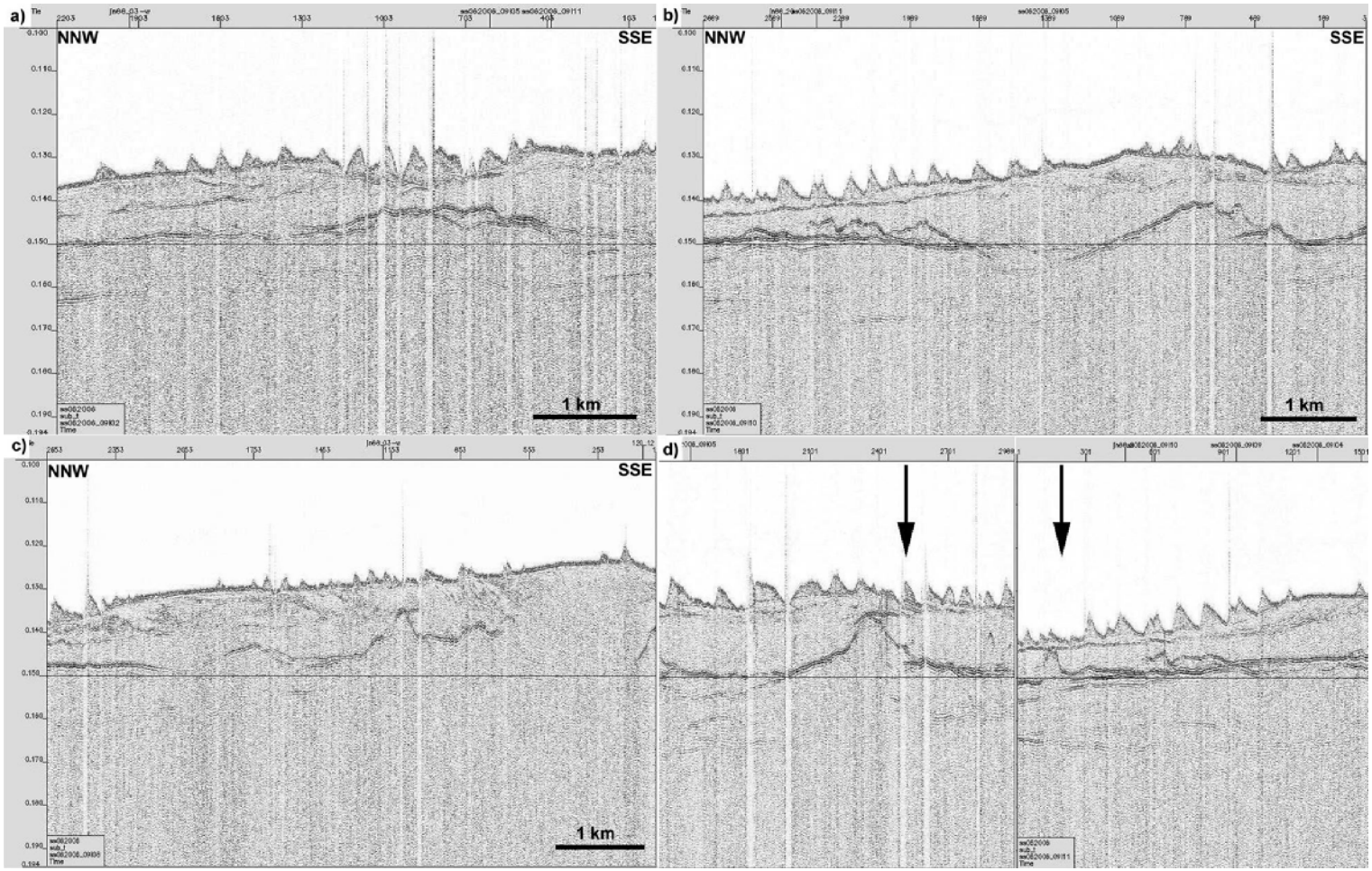

Figure 73. a-c) Sub-bottom profile lines showing the shallow stratigraphy along the central, eastern and western traverses, respectively, of the Broome Platform/Oobagooma Sub-basin boundary site. d) Sections of sub-bottom profile lines showing the relationship between topography on the basal reflector of the upper unit and the position of pockmarks (indicated by the arrow). Vertical scale in ms.

5.3 Sub-bottom profile data

Seabed fluid flow can be related to fluid or gas movement through the sub-surface. Geophyscial methods and analysis of seismic attributes can be applied to help differentiate signals related to shallow gas. The presence of gassy sediments in shallow, high frequency seismic profiles can be indicated by a number of acoustic features as detailed below:

Enhanced reflection - Coherent seismic reflections which have increased amplitude for part of their extent. Enhanced reflection can be a strong indication for the presence of gas due to the enhancement of the acoustic impedance contrast between gas-charged layers and adjacent gas-free layers, where pore spaces are filled by water (Hart and Hamilton, 1993). High-amplitude reflections can have various causes, but when they are related to gas, they generally show a combination of high amplitude, reverse polarity and low frequency (Judd and Hovland, 2007). However, enhanced reflections can also be related to sedimentary features (e.g. changes from clastics to carbonates), or they could be related to other seismic artefacts such as tuning effects when two thin beds merge together generating constructive interference of the seismic wavelet. Hard layers, which have normal polarity, can cause signal attenuation; such hard layers may include cemented sediments and carbonates, including methane-derived authigenic carbonates (MDAC).

Acoustic blanking – faint or absent reflections which occur as a lowering of seismic amplitude response, masking internal layering. Various explanations are possible including signal attenuation, over-pressured porewater, and the destruction of layering by migrating fluids (Judd and Hovland, 2007). Acoustic blanking may also be related to fluid or gas-charge in sediment layers (Judd and Hovland, 2007).

Acoustic turbidity – shallow chaotic reflections caused by the scattering of acoustic energy, obliterate all other reflections and cause a dark smear (Judd and Hovland, 2007). This may occur when there is as little as 1% gas present (Schroot & Schuttenhelm, 2003). It is common for reflections on adjacent sections of a gas-affected profile to exhibit ‘pull down’. As these reflections extend towards the zone of

acoustic turbidity they are deflected downwards by the decrease in the acoustic velocity in the gas-bearing zone (Judd & Hovland, 1992).

Gas Chimneys - Vertical disturbances in seismic data that are interpreted to be associated with the upward movement of fluids or free gas can result in low seismic amplitudes and low coherency. Over-pressured fluids or gasses have cracked the rocks/ disturbed bedding (unconsolidated), resulting in a scattering of seismic waves (Schroot and Schuttenhelm, 2003).

Seismic Diffraction Hyperbolae - Associated with pockmarks, often found at and immediately below the lowest point of some pockmarks. Usually ascribed to strong point source reflectors, however, also possibly due to offset reflections from strong seabed surface reflectors (high incident morphology) or strong point source reflectors at or below the seabed surface (stones etc.) (Hovland et al., 1984).

Mud Diapirs - Occur when a body of plastically deforming material rises through another material due to buoyancy effects. The plastic material may be gas-charged clay or mud (Judd & Hovland, 1992). Gas permeates from below into a relatively thick unit of plastic clay; as gas fills the clay pore volume, static instability occurs and the clay surface deforms due to differential buoyancy. Finally, and after further deformation, vertical weakness zones are established through which gas migrates more or less freely into the water column (Hovland, 1992b).

5.3.1 Examples of shallow gas from GA marine seeps surveys:

The identification of shallow gas has been one of the primary concerns for several marine surveys carried out between 2004-2007 by Geoscience Australia. This has been important for the selection of sample sites during surveys and also to provide evidence of potential hydrocarbon movement.

5.3.1.1 Examples from the Arafura Sea (SS05/2005):

Sub-bottom profile data from the Arafura marine survey imaged a number of examples of enhanced reflections and acoustic blanking. Figure 74 shows an examples of enhanced reflections that are likely to be related to gas. This is indicated by the reverse polarity and low frequency of the reflections, coupled with the strong signal attenuation underneath and the presence of overlying pockmarks (Rollet et al.,

2007).

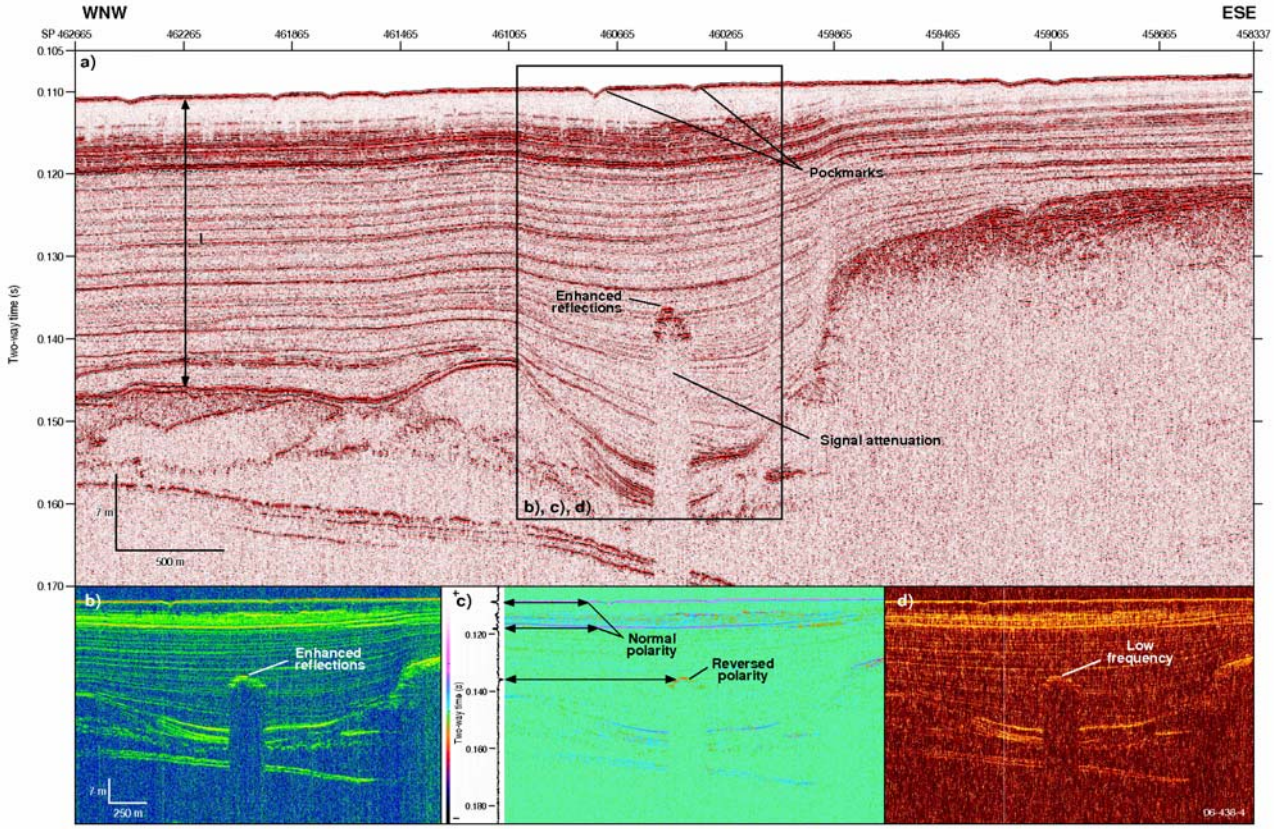

Figure 74. (a) Sub-bottom profile S282_transit_b-ca showing enhanced reflections with signal attenuation through the underlying units and pockmarks on the seabed. The area within the black rectangle is displayed in more detail in Figures b-d. (b) Instantaneous amplitude display showing strong impedance contrasts in yellow-green. (c) Polarity domain showing normal polarity as blue-pink and reversed polarity as red. (d) Frequency domain showing low frequency as yellow-orange.

Figure 75 illustrates an example of enhanced reflections present at two levels within the one unit. The top oblique reflection in Figure 75b is conformable to the stratigraphy but has anomalously high amplitude over part of its length. Similar examples, which show high-amplitude, reverse-polarity and low-frequency reflections, have been attributed by some authors (e.g. Judd and Hovland, 1992, 2007) to gas rising laterally and up-dip within relatively coarse sediment layers. However, in this case a reverse polarity is not observed (Figure 75b). When the sea bed reflection is compared to the bedding conformable high-amplitude reflections, it appears that a

more probable explanation is that two thin reflectors are combining to generate a constructive interference bed tuning amplitude effect (Chopra and Marfurt, 2006).

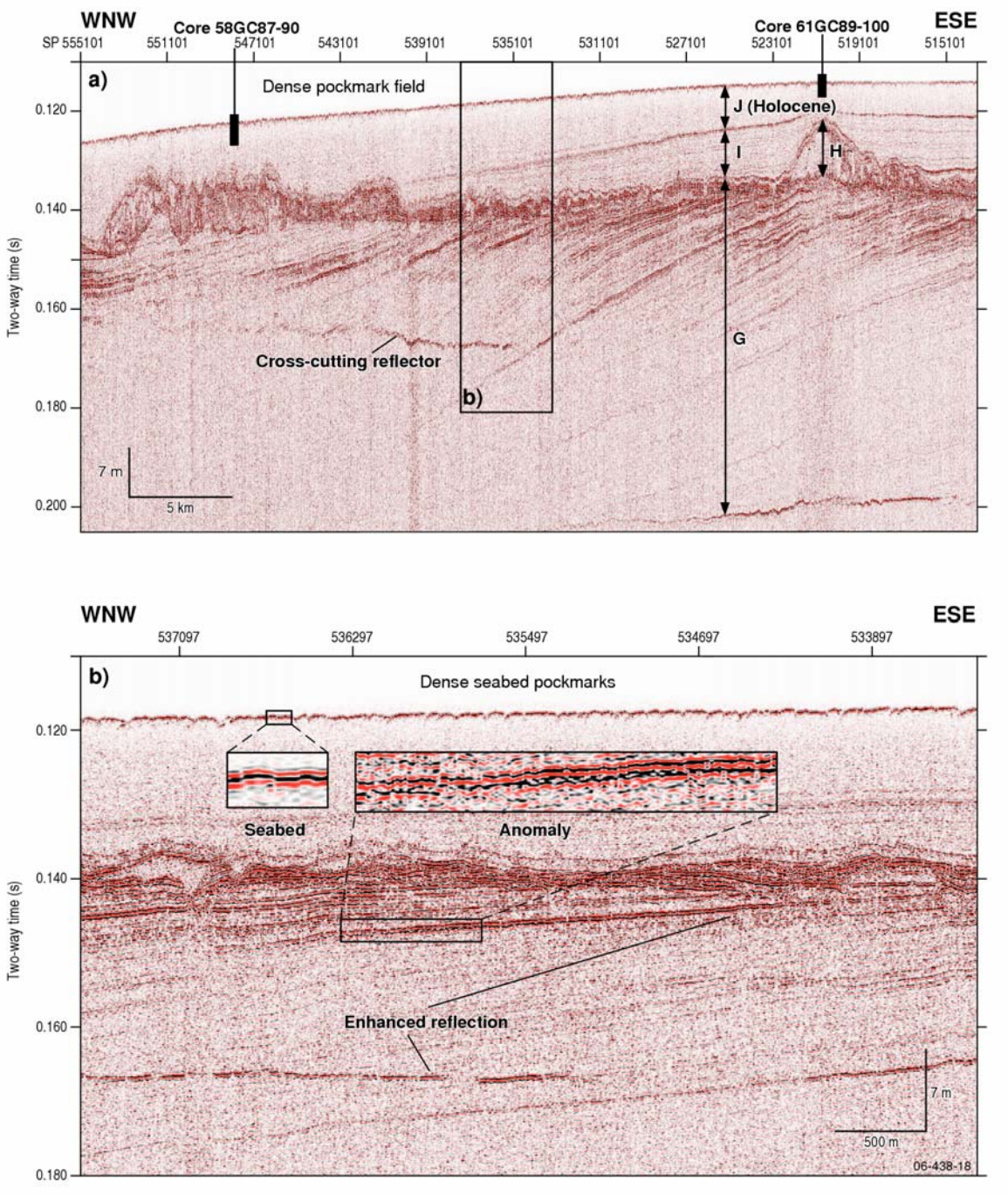

Figure 75. (a) Sub-bottom profile S282_transit_b-ca showing enhanced reflections below a pockmark field. The black rectangle shows Figure (b) location. (b) Enlargement showing two levels of enhanced reflections.

The lower reflection is sub-horizontal and cuts across the stratigraphy (Figure 75). This enhanced reflection is composed of reversed and normal polarity segments. This could be interpreted as representing a gas front because of the low frequency and reversed polarity of these reflectors. However, there is no significant signal attenuation below these reflectors and there is not a consistent polarity reversal. A diagenetic front causing mineralisation would most probably exhibit normal polarity and higher frequency, if cementation was involved. Broadly, these reflections occur ~30 ms TWT below an unconformity generated during the 130,000 years low-stand. The cross-cutting reflectors also occur under the sea bed that was exposed during this time. Therefore, although the seismic attributes do not clearly support either the gas or diagenetic front explanations, it is more plausible that the cross-cutting reflectors are due to diagenetic factors related because of their distribution and relationship to the unconformity (Rollet et al., 2007).

Acoustic blanking that may be related to fluid or gas-charge is evident in the Arafura Sea dataset (Figure 74). Signal attenuation caused by overlying high amplitude reflectors is also common and can be either related to the presence of hard layers or, where the enhanced reflection displays reversed polarity, to gas charging. Hard layers, which have normal polarity, can cause signal attenuation; such hard layers may include cemented sediments and carbonates, including methane-derived authigenic carbonates (MDAC). The carbonates may be calcretes formed during a sea level low-stand, or MDAC related to palaeo-seepage (Figure 76), however, further sample is required to confirm their origin. The high concentrations of CO_2 in cores (up to 52,000 ppm at 2 m) collected from this survey area indirectly support the possibility of MDAC within sediments because the CO_2 has a $\delta^{13}C$ value of -32‰. This indicates that the carbon is derived from the oxidation of an organic source. The high levels of CO_2 within the sediments will directly effect carbonate precipitation by altering the bicarbonate-carbonate equilibrium.

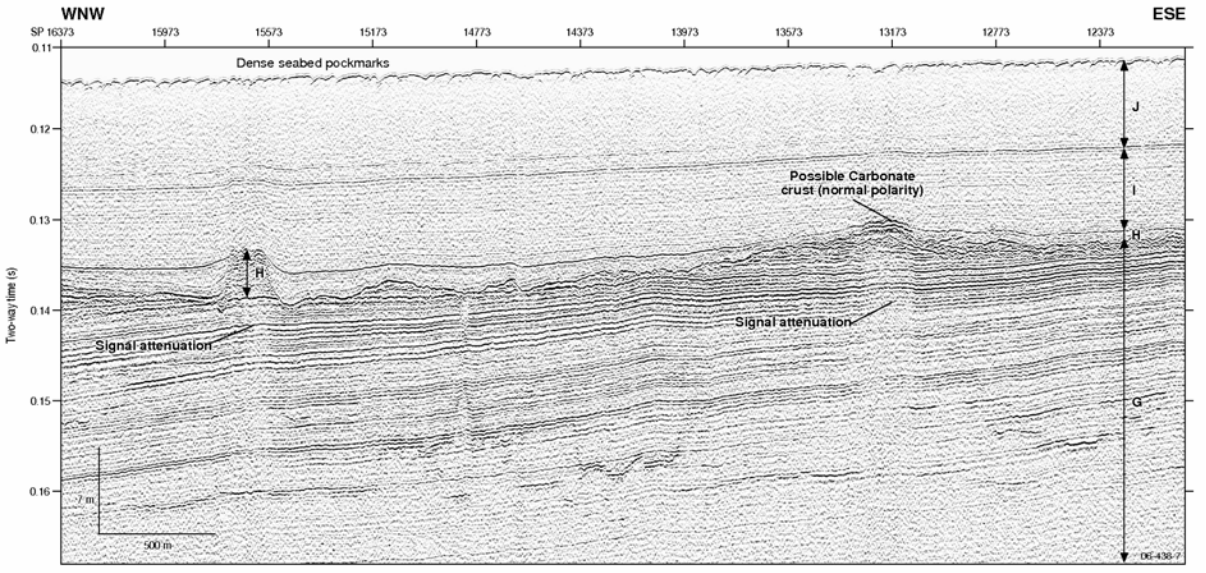

Figure 76. Sub-bottom profile S282_dz02a showing signal attenuation below enhanced reflection, possibly related to a carbonate crust. Note the draping near the base of overlying unit over the feature, which suggests that it had positive relief at that time.

5.3.1.2 Examples of seepage in a carbonate setting, Yampi Shelf (S267 & SS06/2005)

The Cornea oil and gas field is a known area of natural hydrocarbon seepage and provides a good example of seepage features on a carbonate-dominated shelf. An area of active seepage has been identified over an approximately 6 m high carbonate dome, 1.6 km long and 0.7 km wide (Figure 17; Rollet et al., 2006). This area has been imaged by Topas sub-bottom profile data which show that the sea bed consists of hardground that limits seismic penetration (Figure 77). Therefore, the diagnostic features of gassy sediments within the shallow seismic are limited. There is evidence of acoustic blanking which is most likely related to the seeping gas, however, this may also be the result of the carbonate mound blanking the underlying seismic signal.

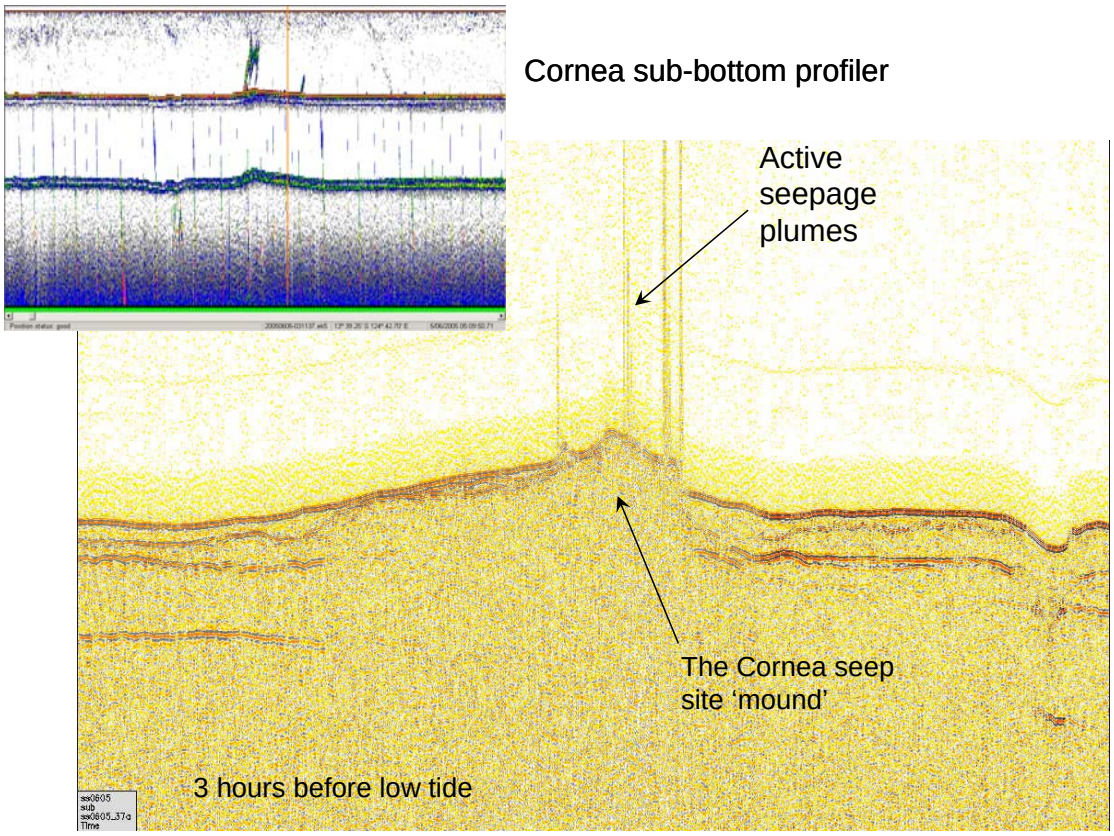

Figure 77. Echosounder image (top left) illustrating seepage flare over the Cornea mound; the corresponding sub-bottom profile data indicate active seepage flares in the water column and acoustic blanking under the mound.

5.3.1.3 Examples from the Rowley Sub-basin (SS06/2006):

Very few areas were identified as having shallow gas indicators within the sub-bottom profile data from the Rowley marine survey. These indicators were identified in survey areas of interest Area X1, Areas 3 and 3A, and Area X5 (Figure 78).

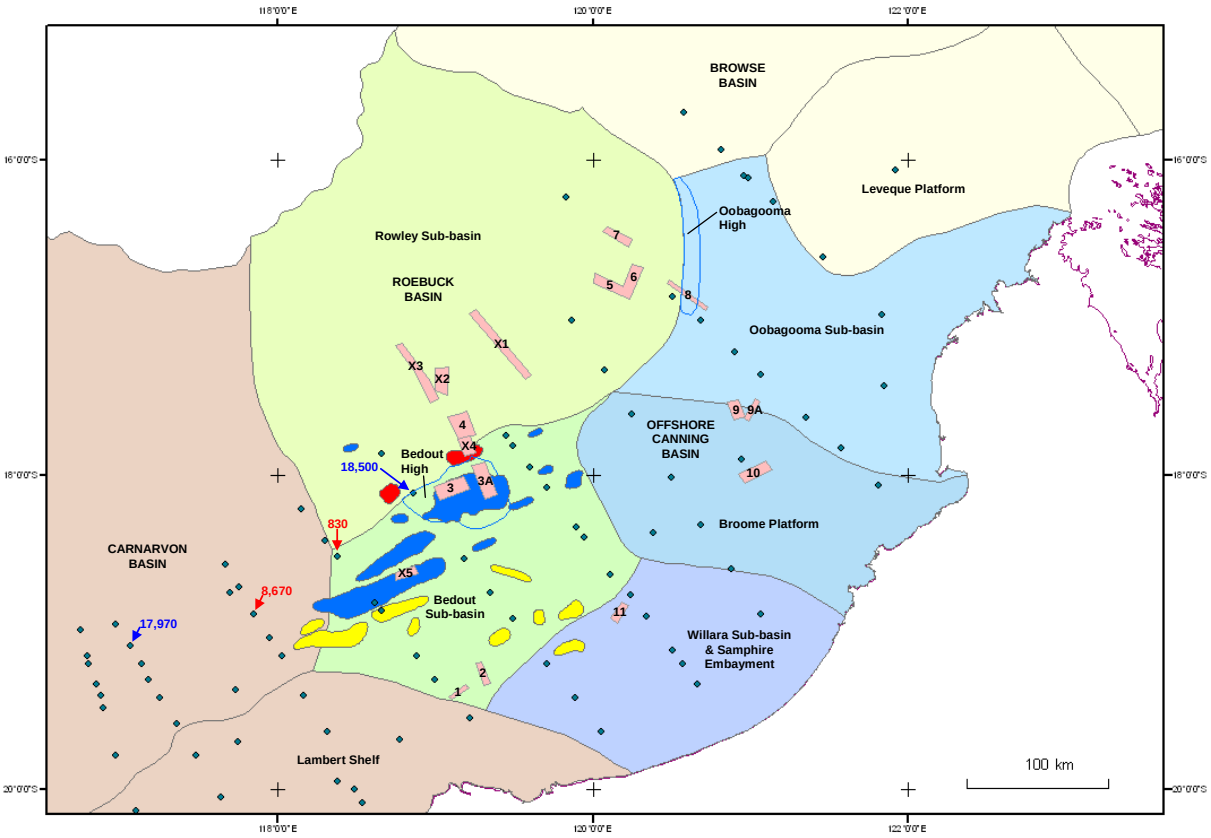

Figure 78. Sediment samples (blue diamonds) acquired and described by James et al. (2004), wit h radiocarbon age dates (years BP) from James et al. (2004) and Dix et al. (2005) in red and blue, respectively. Seismic indicators of seepage mapped by O'Brien and Cowley (2005) – red polygons represent seafloor features, yellow polygons represent shallow subsurface features, and blue polygons represent features at depth. Geoscience Australia SS06/2006 survey areas shown by pink boxes.

The southeastern part of Area X1 transects the outboard edge of the Mermaid Fault Zone (MFZ) which is visible in the sub-bottom profiler data (Figure 79). The sub-bottom profiler data display enhanced reflections with apparent reversed polarity situated above minor faults in the MFZ. The enhanced reflectors may be an indication of some fluid migration from depth along the fault pathways. However, there are no other indications of fluid migration within the sub-bottom profiler data in this region.

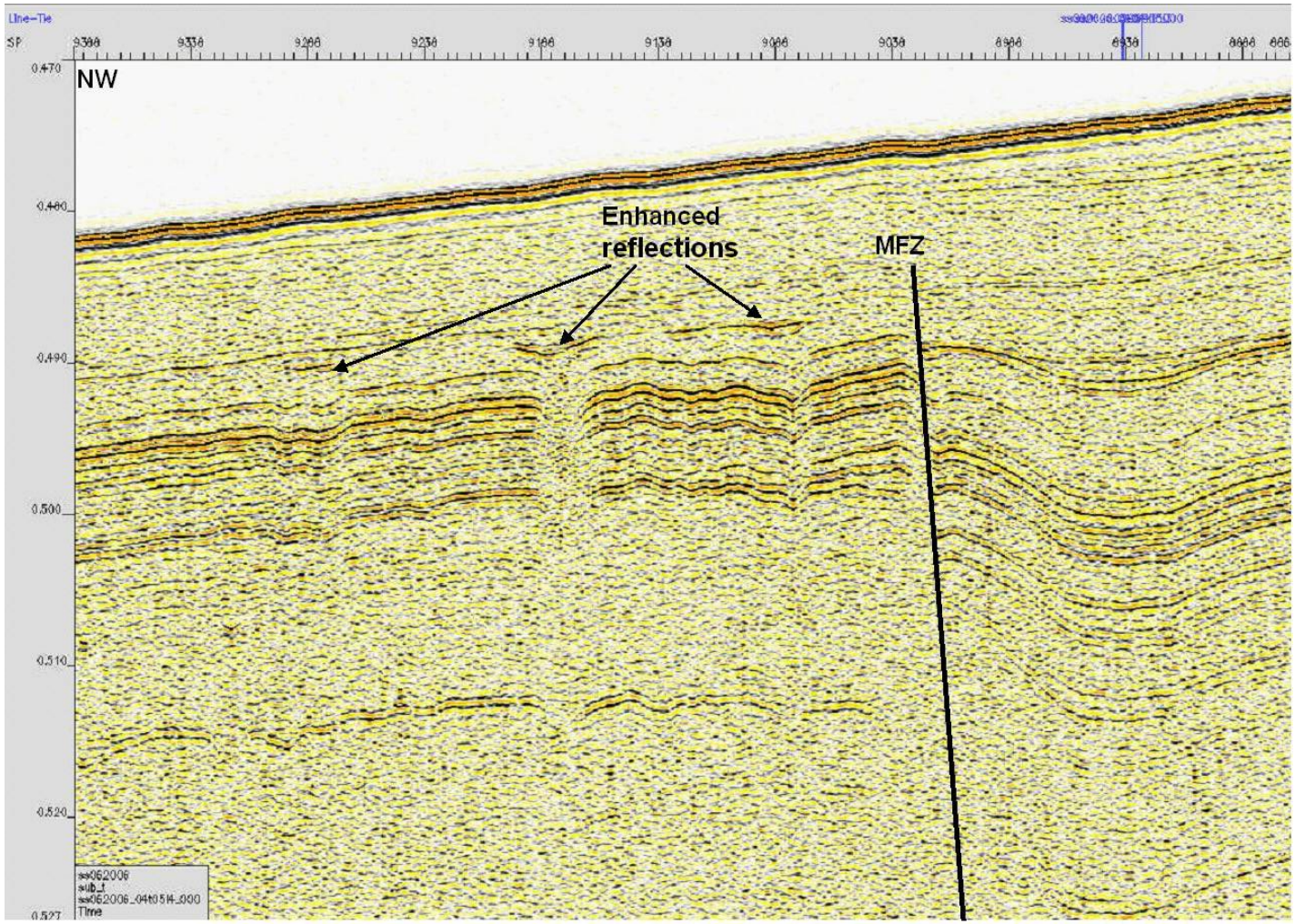

Figure 79. Sub-bottom profiler data from Area X1 over the Mermaid Fault Zone (MFZ), showing growth within the shallow sedimentary section to the southeast of the fault, and enhanced reflections with apparent reversed polarity over the unmarked faults to the northwest.

Areas 3 and 3A are located above the Bedout High which separates the Bedout Sub-basin in the south from the Rowley Sub-basin in the north. These areas also overlie a pelagic ridge defined by James et al. (2004). Areas 3 and 3A were surveyed and sampled because the co-occurrence of previously interpreted HRDZs/gas chimneys (Figure 78), a strong enhanced reflector at the Late Miocene boundary, and an interpreted SAR slick. These indicators suggested that hydrocarbon seepage may occur in this area, and potentially, have a role in the formation of the pelagic ridge (Jones et al., 2007).

On the northwest side of the ridge in Areas 3 and 3A, enhanced reflections with apparent reverse polarity are observed in the sub-bottom profile data (Figure 80 and Figure 81). Some of these enhanced horizons were interpreted to have been sampled in the base of gravity cores at stations 5, 6, 27 and 32 (Figure 80 and Figure 82). No anomalous geochemical signals were detected in these cores, which suggests that these enhanced reflectors are probably related to lithological contrasts rather than the presence of shallow gas. Enhanced reflections are observed less than 10 ms (twt) under the seabed at the location of a low-confidence SAR slick, but no vertical or lateral migration pathways are interpreted at this site (Jones et al., 2007).

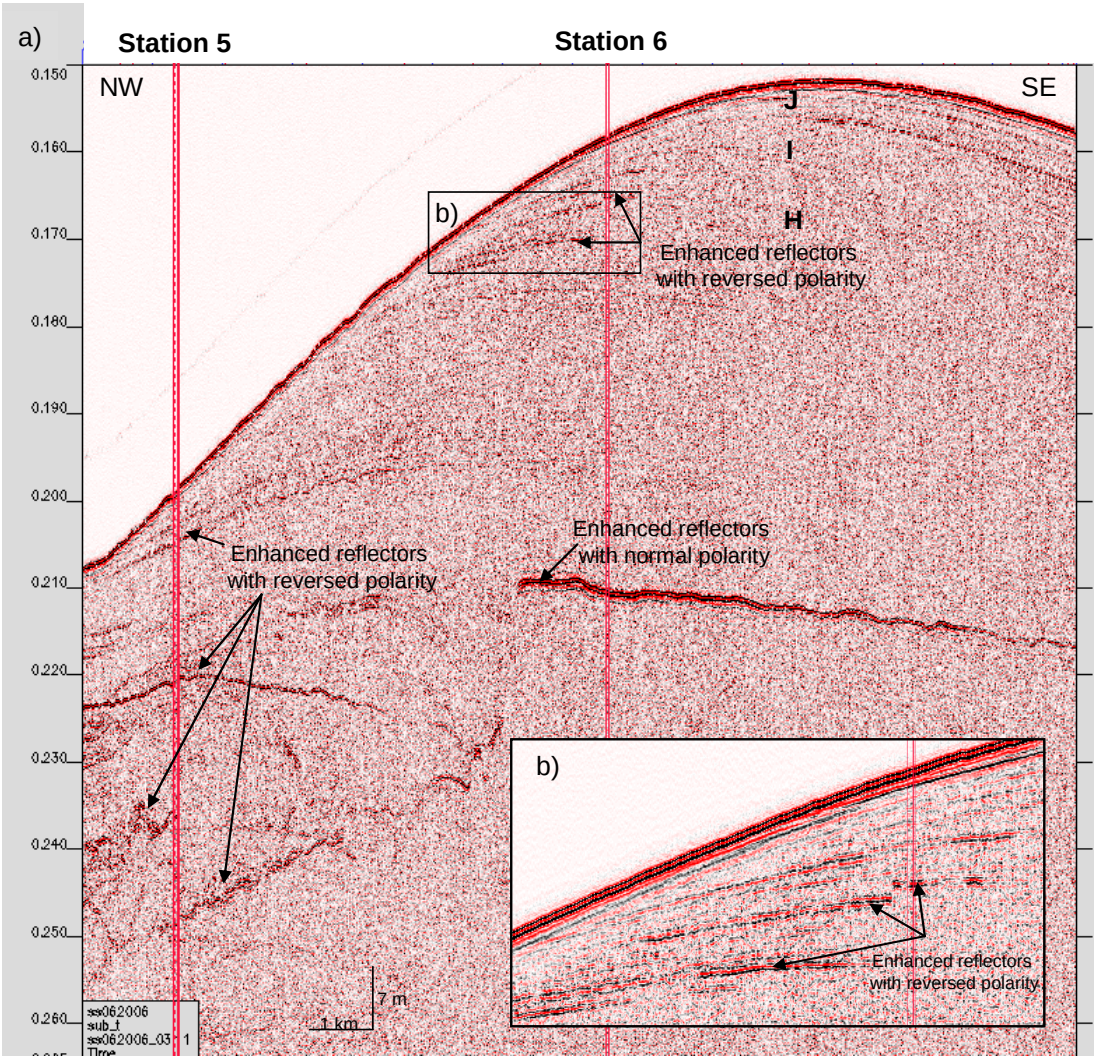

Figure 80. Sub-bottom profiler Line03L11 showing enhanced reflections with apparent reverse and normal polarity in different stratigraphic units in Area 3. The sampling stations 5 and 6 are indicated.

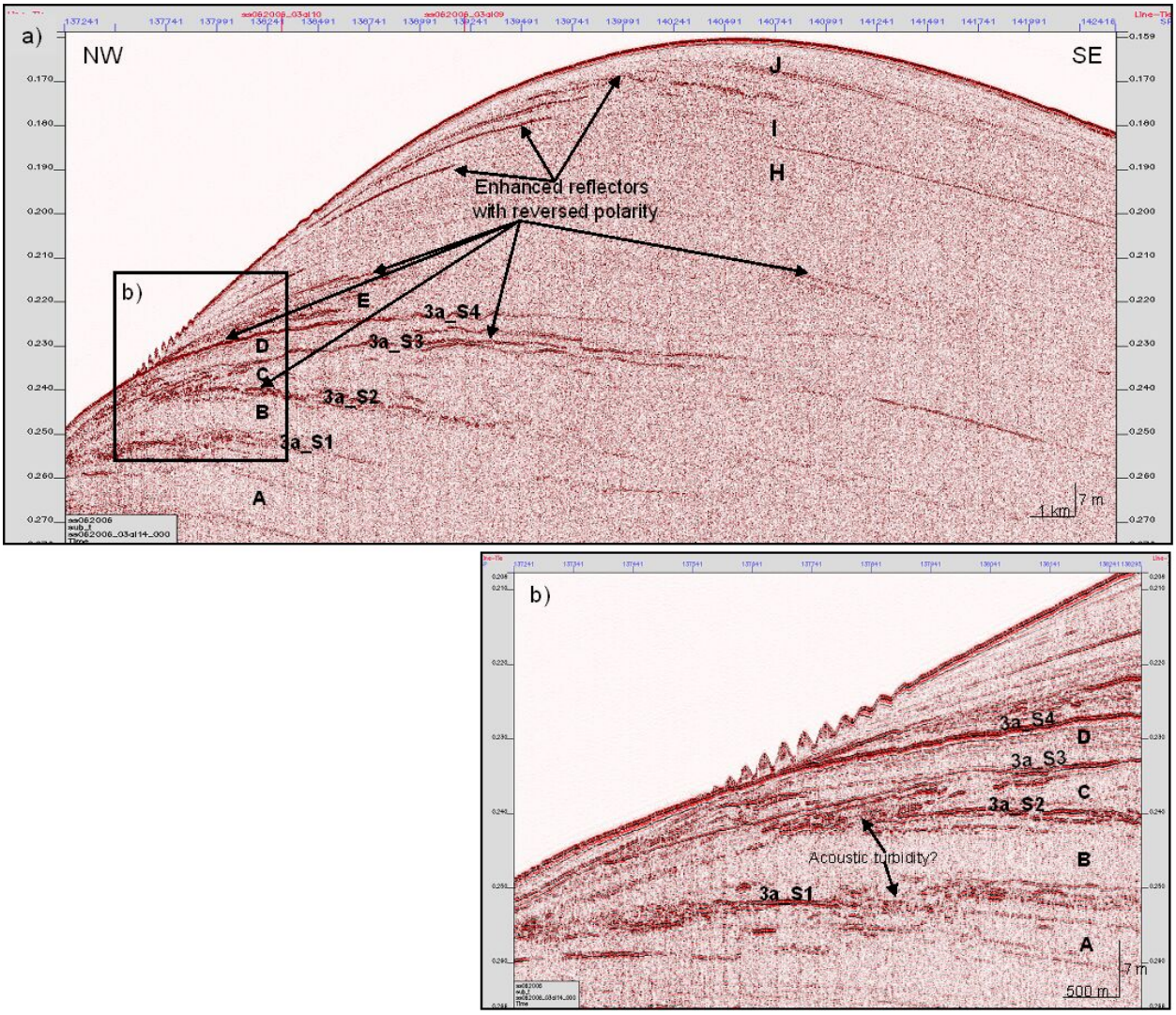

Figure 81. Sub-bottom profiler Line 03AL14 showing enhanced reflections with apparent reverse polarity in different stratigraphic units in Area 3A.

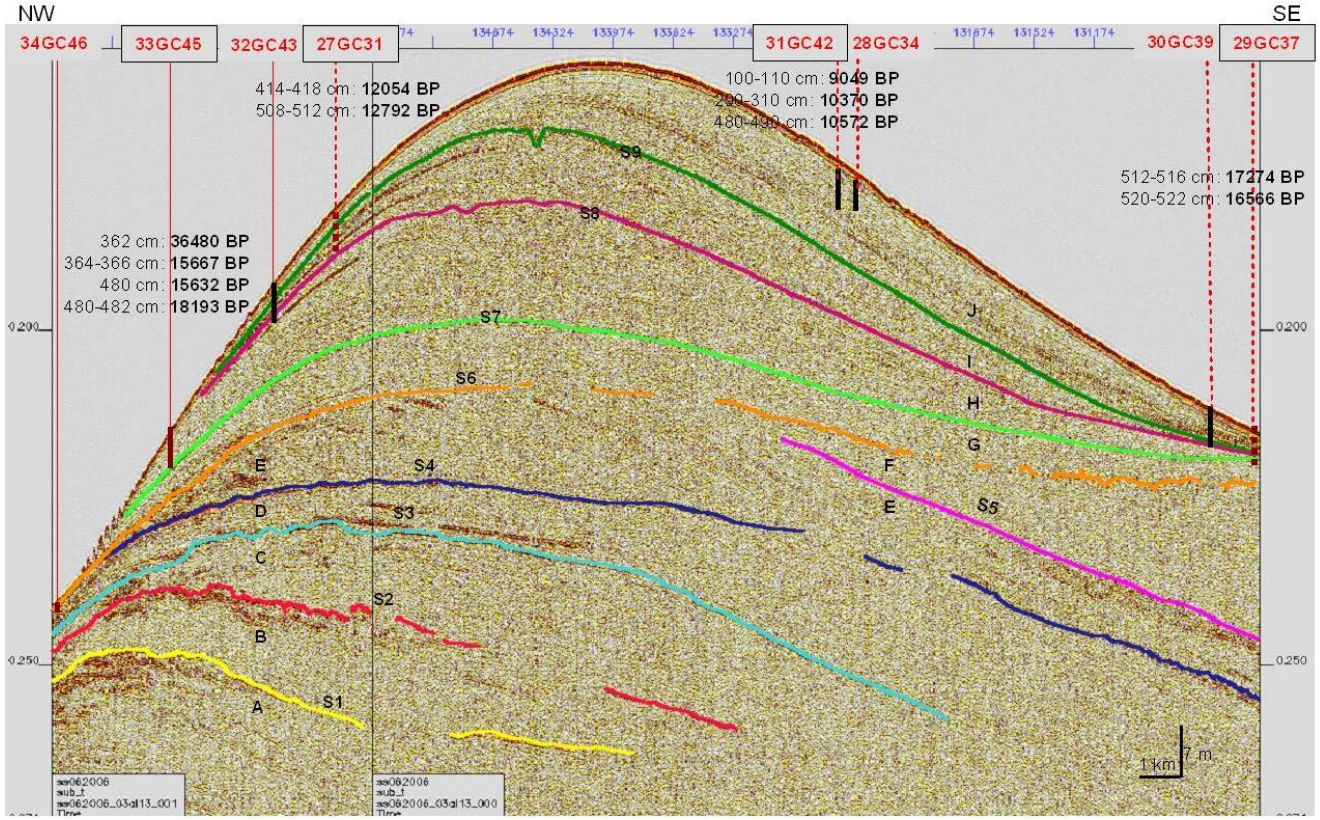

Figure 82. Sub-bottom profiler Line 03AL13 over Area 3A showing the different shallow stratigraphic units within the pelagic ridge. Core locations and approximate depths are shown for each station (number in red). Cores at stations 32, 33 and 34 are directly located on this profile; the other cores have been projected to show their respective penetration of the stratal units. The black cores were recovered for geochemistry analyses while the brown ones were for sedimentology purposes. The dashed cores indicate that both geochemistry and sedimentology analyses were conducted at these sites. Radiocarbon dates are indicated for cores at Stations 27, 29, 31 and 33.

Some stratigraphic units show slight acoustic turbidity which could be related to the presence of shallow gas (Figure 81b). The acoustic turbidity zones are located at the top of two dipping units where they are intersected by erosional surfaces. The locations of these features suggest that shallow gas may have been migrating along sedimentary units and erosional surfaces from the southeast towards the northwest side of the pelagic ridge (Jones et al., 2007).

The sub-economic Phoenix gas accumulation is the only demonstrated hydrocarbon column in the Bedout Sub-basin. Survey area X5 was selected to test for potential vertical microseepage over the gas reservoir. The subsurface of Area X5 (Figure 83) is characterised by a weakly stratified section with discontinuous high-amplitude anomalies. The anomalies are concentrated at two stratigraphic levels, at approximately 0.175 – 0.185 and 0.245 s TWT (Figure 83). The deeper amplitude anomalies are bright, and have a slightly arcuate, concave-downward shape. This could be suggestive of a ballooning gas front, but bedding is irregular at this level and the anomalies do not appear to cross-cut strata. The shallow anomalies are smaller, less bright and have a distribution which does not appear to relate to the deeper, larger anomalies (Figure 84; Jones et al., 2007).

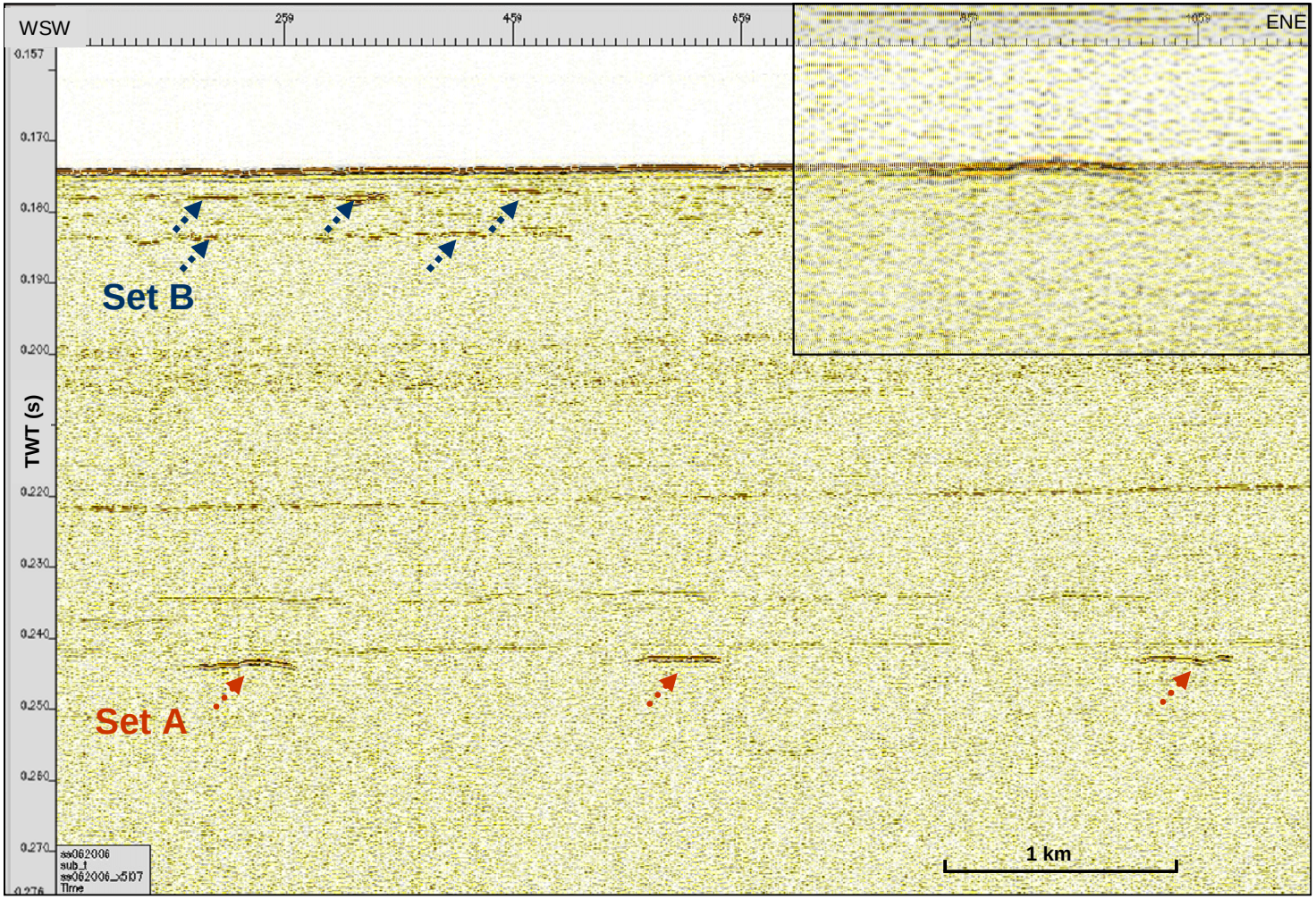

Figure 83. Rowley Sub-basin survey Area X5 sub-bottom profiler Line 07 showing amplitude anomalies at two levels (sets A and B). Insert Shows an enlargement of the southwestern anomaly (Set A) with a slightly arcuate shape.

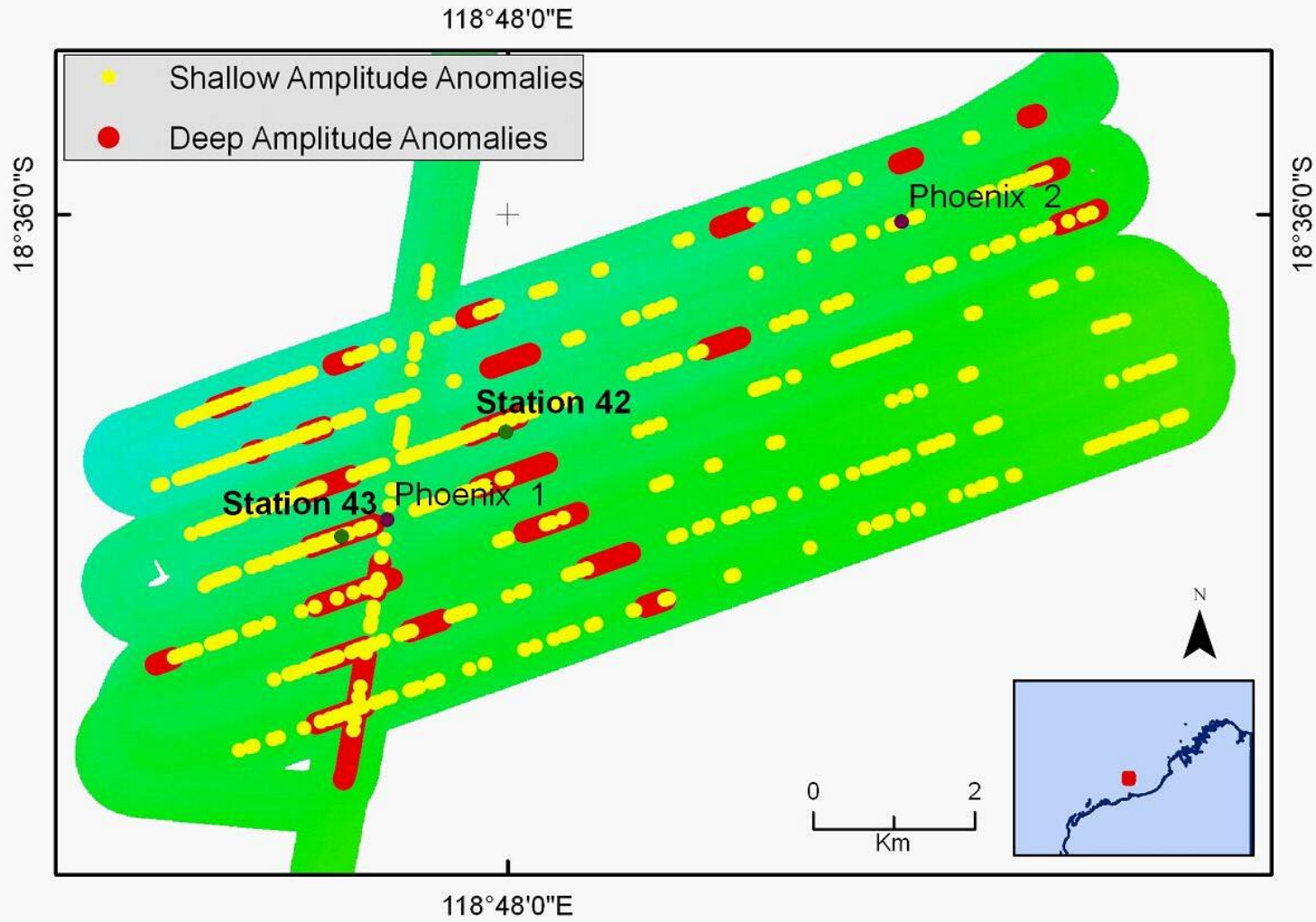

Figure 84. Distribution of amplitude anomalies in sub-bottom profiler data for Area X5.

There is reverse polarity associated with both sets of amplitude anomalies (Figure 85). The cause of this velocity slow-down is not definitive, but could be due to fluidised sediments, facies variation or sporadic gas accumulations at the two stratigraphic levels. If the cause is gas, then shallow migration-seepage is probably diffuse, as focussed migration pathways are not evident on either the sub-bottom profiler data, or within the Late Miocene-Recent section on seismic data (Figure 86). The consistent depth of the deeper bright amplitude anomalies may point to a stratigraphic/facies control on their formation, rather than hydrocarbon migration and accumulation (Jones et al., 2007).

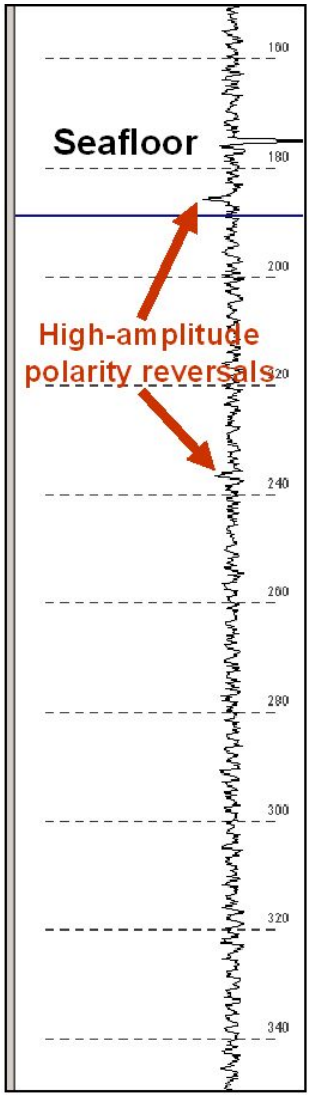

Figure 85. Single trace display of apparent polarity, which shows the reverse polarity of two sets of high-amplitude anomalies (shallow and deep).

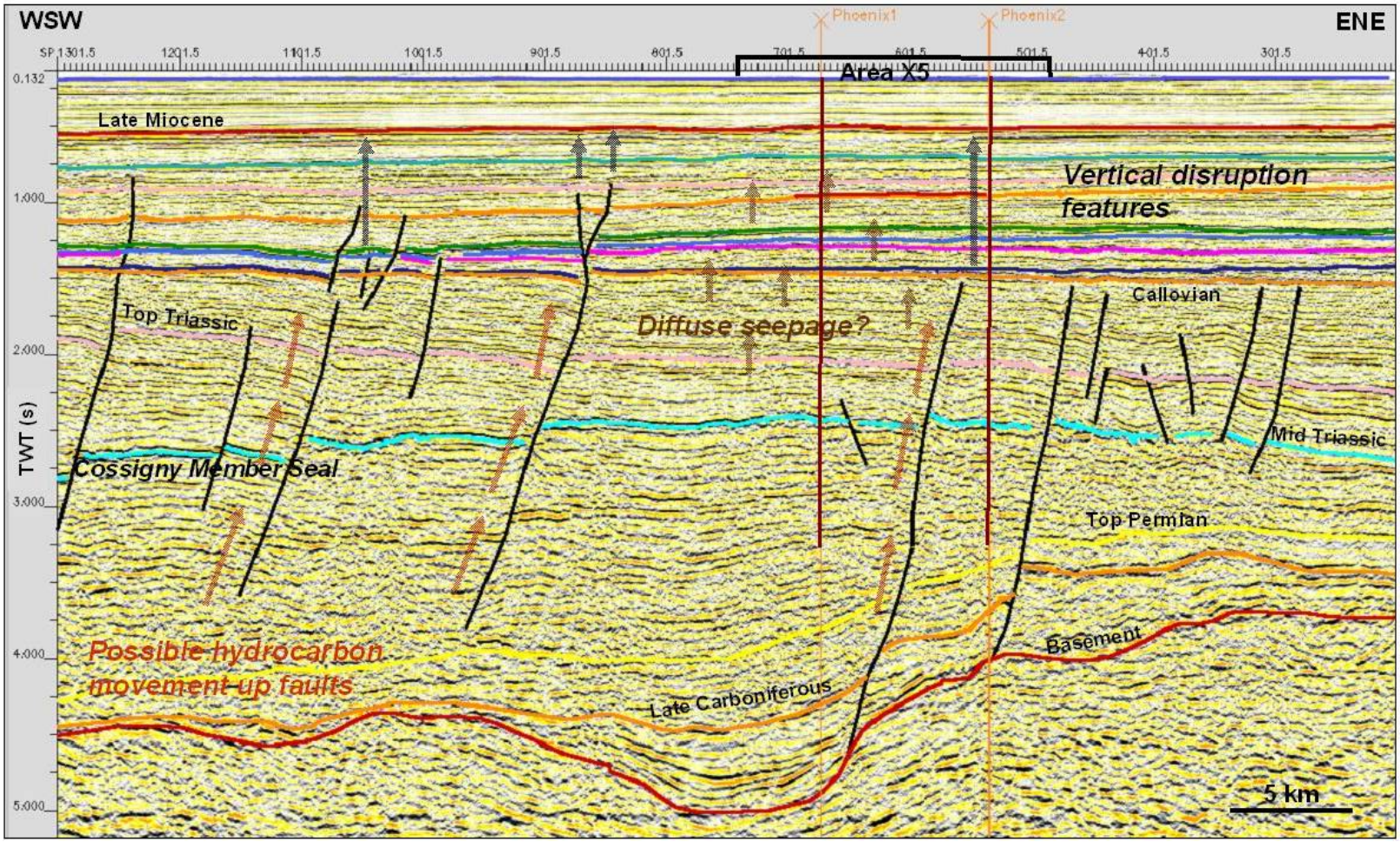

Figure 86. Seismic line GA110-01 through study area X5 showing the Phoenix 1 and 2 well locations, with vertical disruption zones (black arrows) associated with faults and possibly related to potential hydrocarbon migration pathways (red arrows). Around Phoenix 1 and 2 there is some evidence of seismic disruptions apparently not associated with faults which could represent diffuse seepage (brown arrows).

5.3.1.4 Example from Great Australian Bight (SS01/2007):

Sub-bottom profile data acquired on the GAB marine survey (SS01/2007) contained some possible shallow gas indicators in the form of enhanced reflections and seismic diffraction hyperbolae. However, due to the deep water in this region the data quality is poor compared to previous surveys using the same system in shallow water.

The enhanced reflections are located over an area of intense basin margin faulting, where Oligocene and younger sediments are not present (Figure 87). The absence of these Oligocene sediments may provide pathways where fluids can seep. Attribute analysis of the sub-bottom profile data indicates enhanced amplitudes with low frequency and reversed polarity. However, as no raw sub-bottom profile data were available for this line (due to file corruption), the interpretation of the attribute analysis must be treated with caution.

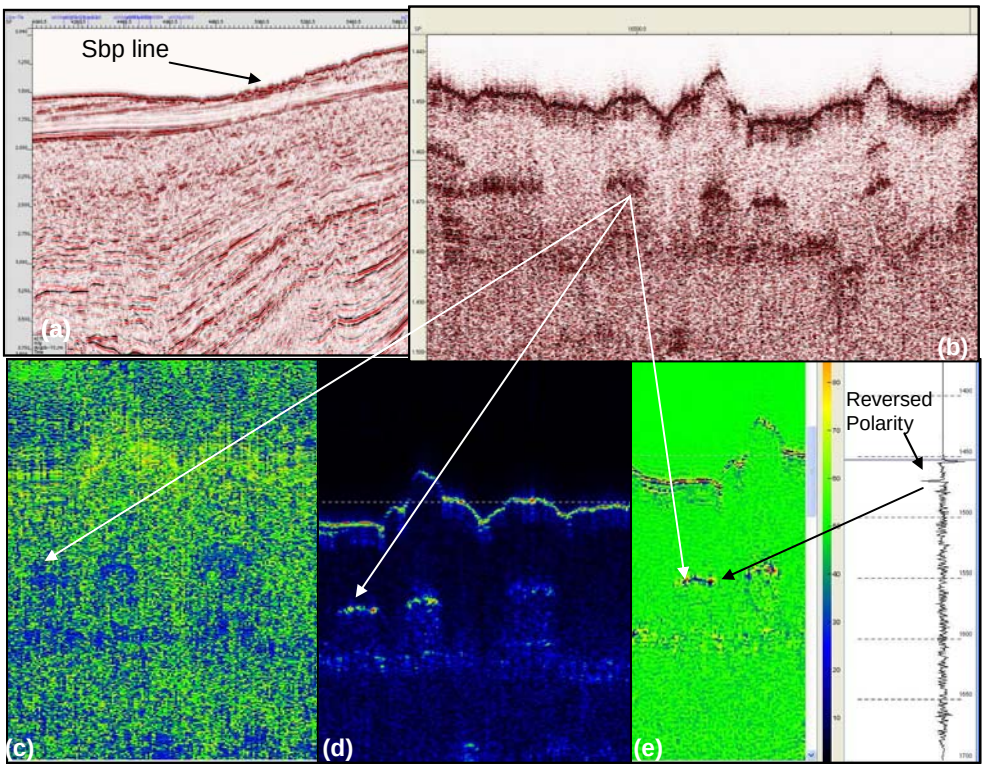

Figure 87. Possible shallow gas/fluid. (a) Seismic line DWGAB-10r illustrates sub-bottom profile (sbp) line location where the Oligocene and younger units are missing; (b) sbp image of shallow enhanced reflections within upper acoustic transparent layer; (c) instantaneous frequency displays enhanced reflections as low frequency; (d) instantaneous amplitude displays the reflections as high amplitude; (e) apparent polarity indicates the enhanced reflections are reversed in polarity, also indicated in wiggle trace.

Seismic diffractions were identified below an area of probable pockmarks in the sub-bottom profile data (Figure 88). These features could be an indication for the presence of shallow gas, but could also be related to the sub-bottom profiler imaging the edges of the pockmarks. The gravity cores did not penetrate the sediment where the diffractions were imaged and there were no other indications of gas within the dataset.

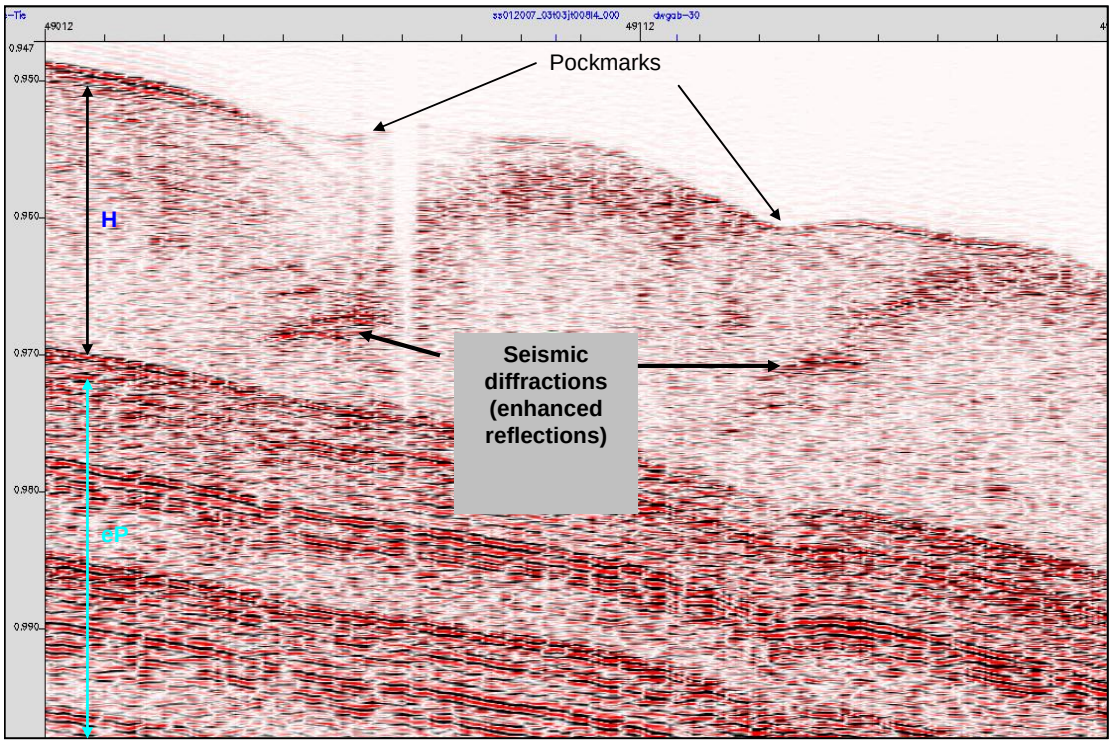

Figure 88. Sub-bottom profile transect over the interpreted pockmark field in Area 3 (Logan et al., 2006). Minor seismic diffractions observed below the imaged pockmarks. H = late Pleistocene/Holocene unit; eP = early Pleistocene unit.

5.4 Integration of data sets

To prove the existence of active or palaeo- seepage, using geophysical data, our work has shown that multiple datasets must be acquired, interpreted and integrated. These datasets include: echosounder, sidescan, multibeam bathymetry, sub-bottom profile, conventional seismic, remote sensing data, geochemical analysis, and potential field data. The use of a single dataset can easily lead to misinterpretation, for example, it is very difficult to differentiate between gas seeps and biological features in echosounder records (see Section 5.1.2).

Echosounder and sidescan sonar data are essential for the detection of active seepage in the water column. Sidescan sonar data can be used to identify specific seabed features at active flare vents and palaeo-seepage features (clusters of reflective blocks, hard-grounds, and pockmark fields). Multibeam bathymetry data can be used to identify small-scale rises in close proximity to seepage areas, pockmarks or carbonate hardgrounds. Larger encrusted mounds are found above long-lived HRDZs. Correlation with 2D and 3D seismic profiles and sub-bottom profile data allows the identification of seepage features within the subsurface stratigraphic section (modern and palaeo-HRDZs, channels, seismic discontinuities and bright spots).

5.4.1 Example of integrating data sets from the Yampi Shelf

Active seeps around the Cornea oil and gas field on the Yampi Shelf (S267) were characterised using geophysical (echosounder, sidescan sonar, multibeam bathymetry, sub-bottom profile and conventional seismic) data, remote sensing data (Airborne Laser Fluorescence – ALF, Synthetic Aperture Radar – SAR, Landsat, ARGUS hyperspectral data), geochemical analyses from sediment samples and potential field data (Figure 6, Figure 17, Figure 18, Figure 49, Figure 50, Figure 51, Figure 52, Figure 62). Flares of gas bubbles were observed rising from pockmark fields and carbonate hardgrounds in water depths of 80-100 m (Rollet et al., 2006). Seepage related features on the Yampi Shelf are mostly small (reflective blocks, hard-grounds, mounds and pockmarks, <10 m in diameter and less than 10 m high or deep).

The various geophysical techniques used during the Cornea survey S267 show different seepage-related features depending on the scale or degree of resolution and nature of the data (Rollet et al., 2006):

1. Echosounder data revealed flares of bubbles in the water column from the seafloor, which are direct evidence of seepage (Figure 49, Figure 50, Figure 59). These rarely reached the sea surface, instead being trapped in a layer at 40–60 m depth. This layer is possibly an iso-density surface, or an oceanic methane layer formed when particles lifted by bubbles are abandoned when the bubbles dissolve (Leifer and Judd, 2002). The flares have been shown to be mostly composed of methane with minor amounts of ethane (O'Brien et al., 2005; K. Burns,

Australian Institute of Marine Science, pers. comm. 2005).

2. Sidescan sonar data also show these flares in the water column, and features on the seabed from which they emanate (Rollet et al., 2006) (Figure 17, Figure 18, Figure 52, Figure 62). These features include clusters of reflective blocks, hard-grounds, mounds and small pockmarks. (>1 to 10 m across).

3. Multibeam bathymetry data identified small-scale rises, between 0.5 and 3 m high, in close proximity to seepage-areas (Figure 17, Figure 51). Encrusted carbonate mounds are found above long-lived HRDZs. Erosion around them and/or active carbonate precipitation due to methane derived authigenic carbonate may have enhanced their morphology.

4. Sediment samples indicate more diverse biota, including abundant *Sabelariid* worm tubes, and greater cementation at, and near, seeps than in non-seep areas (Rollet et al., 2006).

5. Seepage activity is directly controlled by tidal cycles and is most active at low ebb tides (Rollet et al., 2006) (Figure 18).

The integration of these datasets with aeromagnetic data helped to identify potential migration-seepage pathways. Magnetic anomalies reveal lineations related to basement structures, fracture zones and dykes (Rollet et al., 2006). These structures can be correlated to areas of active seepage and palaeo- and modern channels on the seabed. The close spatial relationship of reactivated basement fractures and palaeo- and modern channels appears to have generated migration pathways for hydrocarbon seepage on the Yampi Shelf.

5.4.2 Example of integrating data sets from Arafura Sea

A variety of shallow gas indicators and fluid migration pathways have been interpreted from sub-bottom profiler, multibeam bathymetry, sidescan sonar, and echosounder data together with geochemical analyses of sampled sediments from the northern Arafura Sea (S282), offshore Northern Australia. The shallow gas indicators include pockmarks, low frequency enhanced reflectors and acoustic blanking. These

indicators are supported by gas within shallow cores. Geochemical analysis indicates that this gas has a microbial origin but deeper fluid movement is also suggested by the presence of interpreted hydrocarbon slicks in SAR data.

Although the occurrence of hydrocarbons in the northern Arafura Basin is not necessarily conclusive, the correlation of several indicators is significant. A clear coincidence of increased faulting and a poor quality seismic data zone, recognised on conventional seismic data, together with interpreted SAR anomalies that align with mapped deep structures, indicate a region of likely hydrocarbon seepage (Struckmeyer, 2006; Rollet et al., 2007). Seepage across the region appears to be passive compared to the active gas seepage in the Timor Sea (Jones et al., 2005a&b; Rollet et al., 2006). For example, no obvious gas flares were observed in the water column during the Arafura survey. The range of seabed and sub-surface geophysical features indicative of gas migration suggest both *in situ* generation of microbial gas in the Holocene mud and shallow gas movement from older, deeper (possibly thermogenic) units. Therefore, integration of the new survey data with conventional seismic and remote sensing data suggests that the Northern Arafura Basin, north of the Goulburn Graben, may be prospective for hydrocarbons (Rollet et al., 2007).

6 Sampling and Analysis of Potential Seepage Material

6.1 Techniques available for sampling gas in the water column

In the 1980s to mid-1990s the marine 'sniffer' was the predominant method for sampling gas within the water column (see Section 3.2). The 'sniffer' program was discontinued by the Australian Geological Survey Organisation in 1997 and no other studies have been conducted in Australian waters since then (Table 1).

More recently, gas has been collected from active seepage on the Yampi Shelf using divers and a bubble catching device (see Section 6.7.1). The use of divers is only an option in shallow waters or where gas bubbles are observed to reach the sea surface.

6.2 Techniques available for sampling the seabed

A variety of methods exist to sample the sea bed. These have different advantages depending on the nature of the sample required and the aim of the sampling program.

1. Rock samples are generally obtained through dredging (Figure 89). These samples can provide information on the nature of lithified or cemented sediments or volcanic rocks exposed at the sea bed. Dredge samples have been used to collect carbonates at seepage sites on the Yampi Shelf (Rollet et al., 2006). When samples are required over carbonate hardgrounds, the rock dredge may be the only viable sample tool.

2. Surface sediment samples can be collected using grabs or box cores (Figure 90). These sediments are generally of limited use in characterising natural hydrocarbon seepage because microbial activity is relatively intense near the sediment water interface, leading to degradation of the seepage signal and bioturbation leads to sediment mixing. However, over carbonate hardgrounds, where coring operations are not possible, grabs may be the only way to obtain site-specific sediments. This was the case during the S276 seepage survey on the Yampi Shelf. Grabs and box cores may also retrieve limited amounts of biological material related to sites of active seepage.

3. The primary goal for sampling around seepage sites is to obtain sediment cores. The aim is to retrieve sub-surface sediments from below the oxic zone

to allow analysis of pore space gases and organic matter associated with seeping hydrocarbons. Several methods of coring, including gravity, piston and vibro-cores have been used for sampling. The nature of the seabed dictates which coring device is utilised. Soft muds are best suited for piston cores and vibro-cores are more suited to sandy sediments.

Figure 89. Photo of rock dredge used to sample seabed carbonates and other lithified substrates.

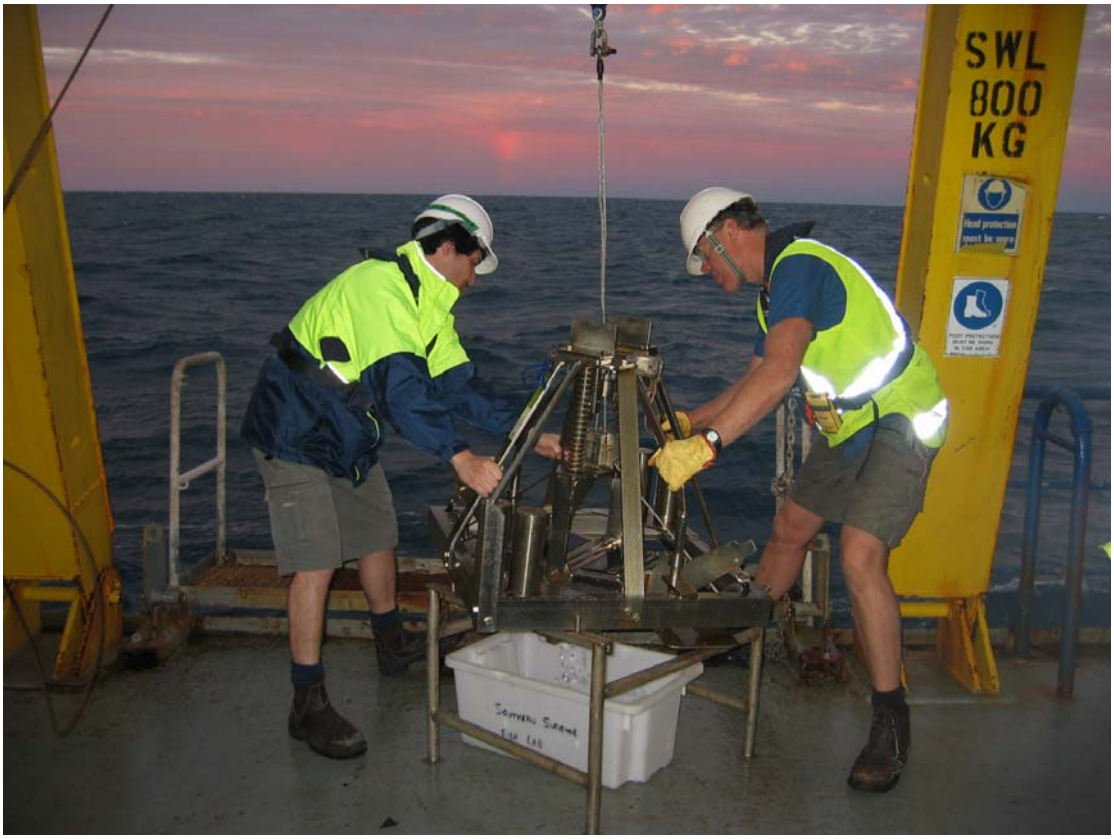

Figure 90. Photo of grab and box cores used to sample seabed sediments.

6.2.1 Seabed Sediment Samples

6.2.1.1 Sediment Grab

Unconsolidated seabed surface sediments can be collected using a Smith-McIntyre sediment grab deployed from an A-frame winch. The grab is mounted on a sturdy, weighted, steel frame, with springs to force the two-jaw bucket into the sediment substrate when released. Tripping pads, positioned below the square-based frame on which the bucket is suspended, make first contact with the seabed and are pushed upward to release two latches holding the spring-loaded bucket jaws. Rewinding the deployment wire exerts tension on cables connected to the end of each bucket-jaw arm causing the jaws to pivot tightly shut.

Sediment samples are collected from the Smith-McIntyre Grab for geochemical and sedimentological analysis. Between 0.5-1 kg of sediment is placed in clear plastic bags and given a Munsell colour and grain-size description. Samples are double

bagged and labelled, and an aluminium label tag also inserted in the outer bag. Geochemical samples are snap-frozen at -20 °C, and sedimentological samples are stored at 4 °C.

6.2.1.2 Rock Dredge

The rock dredge, consisting of a 0.5 x 1 m rectangular metal collar to which a 1 x 1 m chain bag was attached, is used to sample lithified and cemented sediments on the seabed. The dredge is operated using a trawling winch, and is lowered to the seabed and then dragged at each station along the seabed for approximately 100-200 m.

The contents of each dredge are sorted on deck and representative rock samples described and stored at 4 °C. In some cases samples are cut and trimmed using a small, on board, rock saw before storage.

6.2.2 Sediment Core Samples

The majority of sediment cores are collected using a gravity corer with a 1 tonne core head and a PVC core barrel liner. The length of the core barrel is varied depending on the sediment type; typically a 6 m barrel is used, as penetration generally varies between 4 to 6 m. In sandy sediments, a 3 m barrel is used. Cores in inboard shallow-water areas can be collected using a vibro-corer with aluminium liners. The same 1 tonne core head employed during gravity coring can be used for vibro-coring. Time of vibration on the seafloor varies from approximately 5 to 20 minutes. Corers are deployed and retrieved from an A-frame using a hydraulically-operated cradle and the ship's coring winch.

Geochemical cores are initially cut into 1 m sections on deck that are then immediately sub-sampled in the on-board laboratory as per the scheme shown in Figure 91. For the upper parts of the core, only the lower 10 cm of each 1 m section, as well as the uppermost 10 cm of the core, are sampled for biomarker analysis (but not for head-space gas analysis). Since samples are collected starting from the base of each core, and the total recovered length varies from core to core, the sub-seabed depth of samples also varies from core to core. Remaining un-sampled portions of the geochemistry cores are discarded.

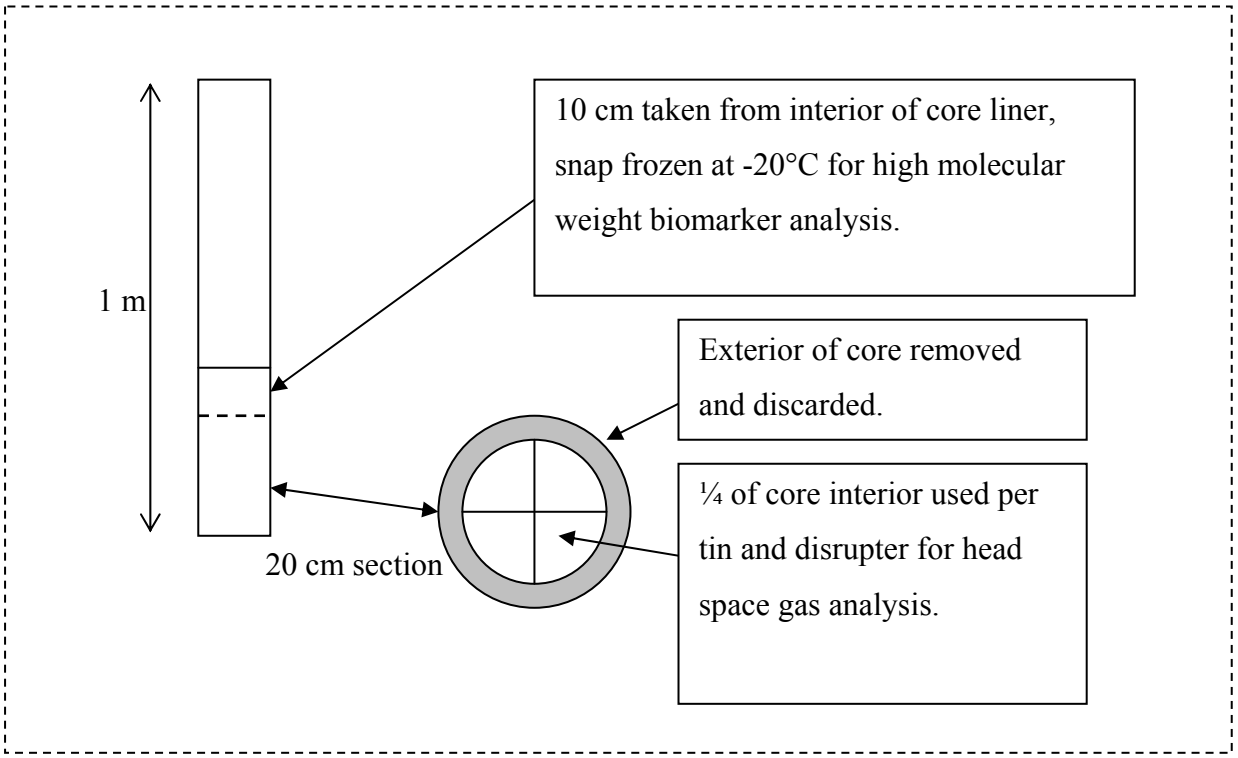

Figure 91. Illustration of samples taken from 1 m gravity core section. The upper 70 cm of each core section was discarded after sampling.

During sampling, care should taken to remove mud that had been in contact with the PVC liner, to avoid organic contamination, and only the interior portion of the core is collected for geochemical analyses. Samples collected for high molecular weight biomarker analysis are double bagged within plastic zip lock bags and snap frozen at -20 °C.

Two methods for head-space gas collection/sampling are utilised during marine surveys. The lower 20 cm of each 1 m core section is extruded from the PVC liner by pushing a metal cutting device up through a 20 cm section of core liner. The cutting device has two intersecting metal plates that divided the extruded core into quarters. After extrusion, the exterior of the core is trimmed with a metal spatula to remove mud that had been in contact with the core liner. Each quarter is then removed from the cutter and placed in either a 500 ml tin (duplicate samples) or a plastic disrupter canister (duplicate samples).

Sampling Using Tins: The 500 ml metal paint tins are used for the head-space gas analysis. One quarter of a 20 cm section of core fills a tin to around one-third full. This is the volume of mud required for head-space gas analysis. Once the mud is

placed inside a tin, a further one-third of the volume (165 mL, using a graduated measuring cylinder) is then filled with filtered sea water which had been poisoned with sodium azide and degassed by bubbling with chemical-grade nitrogen. The head space of the tin is then flushed with nitrogen and the lid of the tin is sealed. Once sealed, the tin is shaken and placed upside down in the -20 °C blast freezer.

Sampling Using Disrupters: The disrupters are designed to be re-used and also contain a plastic insert used to disrupt the mud during analysis. Each disrupter receives one-quarter of the mud from the 20 cm section of core. This volume of mud fills about one-third of the disrupter. If loose mud is collected in the core the volume can be checked using a mould line on the canister body. Once the mud has been placed in the canister the plastic insert is pushed into the mud. One and a half tablespoons of salt are added to supersaturate the seawater. A further one-third of the canister volume (165 mL, using a graduated measuring cylinder) is then filled with filtered sea water which had been poisoned with sodium azide and degassed by bubbling with nitrogen. The head space of the disrupter is then flushed with nitrogen and the lid of the tin was secured. Once sealed, the disrupter is shaken and then placed upside down in the -20 °C blast freezer.

6.3 Sample handling and storage to reduce potential contamination

Handling and storage processes are critical to the integrity of sample data. For this reason, great care needs to be taken to avoid hydrocarbon contaminants present on marine survey vessels. These include, grease, lubricants and anti-fouling agents, which can be transferred to samples during handling operations on deck. These contaminants are the most important to avoid because they can impart hydrocarbons that could be interpreted as potential seepage. Sun-screen can be incorporated in samples during handling (Grosjean and Logan, 2007), and this can be an issue for operations in tropical regions of Australia. The sample container, such as plastic storage bags, can also impart contaminants although these are usually at a low level and do not interfere with interpretation. A review of contaminants derived from marine survey material and the sources of contamination has been carried out based on survey S282 (Grosjean and Logan, 2007). It is recommended that samples for biomarker hydrocarbon analysis are double bagged in plastic bags and stored frozen before analysis.

Samples collected for head space gas analysis should be collected first from cores, to reduce gas loss, before collection of sediment for biomarker analysis. Samples are best stored in sealed tins, upside down in a freezer before analysis.

6.4 Head Space Gas analysis

At Geoscience Australia, between 2004 and 2007, head space gas samples were collected on surveys in metal paint tins provided by TDI-Brooks International (http://www.tdi-bi.com/). Data are reported in a format that allows easy comparison with global datasets.

The following method was used for sample collection and analysis:

Samples are collected at one metre intervals from the base of a core, normally up to 3 intervals are sampled for each core, depending on the depth of penetration. Approximately 160 ml of sediment is placed in a 500 ml metal paint can with 160 ml sea water. The sample is frozen upside down and shipped to the B&B laboratories (TDI-Brooks International's laboratory) in College Station, Texas for analysis.

The can is thawed approximately 24 hours prior to analysis, heated to 40°C for approximately 4 hours, and shaken vigorously using a conventional paint shaker. Ten millilitres of water is syringed into the can headspace using silicone sealant septa. Ten millilitres of headspace gas is collected using a syringe and injected in the gas chromatograph for compositional analysis. The mud to headspace ratio for volume calculations is estimated using the weight and assumed density.

The parts per million calculations are carried out using partition coefficients which represent a fraction of the total gas in the sample container after equilibration. The TDI headspace gas composition data is reported as ppm by volume (mole %).

6.5 Isotope analysis and problems with MDAC detection in carbonate dominated environments

Bacterial oxidation of hydrocarbons can generate distinctive isotopic compositions in marine carbonates. In siliciclastic environments, carbonates generated via hydrocarbon oxidation have characteristically depleted ^{13}C values. Carbonate precipitated as a result of hydrocarbon oxidation has been reported from the analysis

of well samples from the Timor Sea (O'Brien and Woods, 1995). However, the identification of methane-derived authegenic carbonate (MDAC) is much harder in environments dominated by marine carbonate formation. For example, a range of carbonates collected in dredges and sediment grabs at seepage sites on the Yampi Shelf were picked for isotopic analysis. Two types of carbonate minerals were identified: a light carbonate (aragonite) was abundant and formed skeletal material, grains and cements (Figure 92), and a dark coloured Mn-rich carbonate, was less abundant and occurred as small nodules, encrusting worm tubes and skeletal material at active seepage sites. The two types of carbonates were separated for isotopic analysis (Table 6).

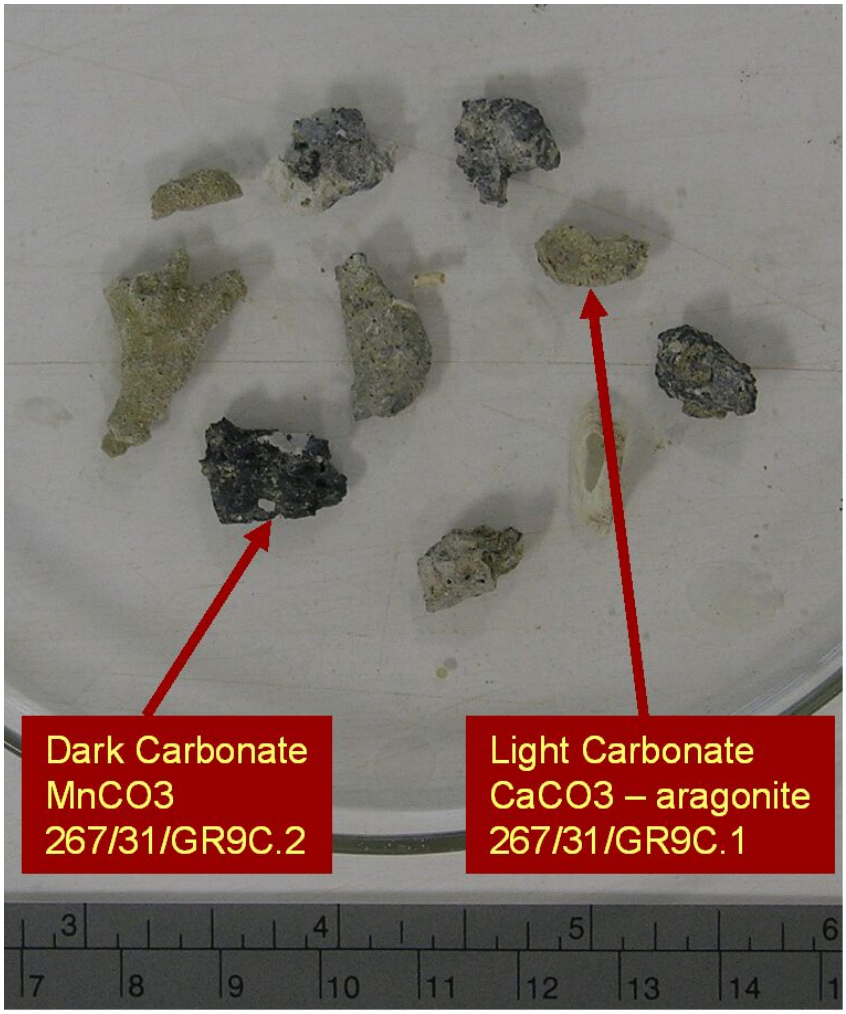

Figure 92. Light coloured carbonate (aragonite) and dark coloured carbonate (MnCO3) was collected from a grab sample (267/31/GR9B).

Table 6. Results of isotope analysis for a range of carbonates collected in dredges and sediment grabs at seepage sites from the Yampi Shelf.

Sample#	Identification	Type	Comment	$\delta^{13}C$ vs PDB	$\delta^{18}O$ vs SMOW	$\delta^{18}O$ vs PDB
1394745	267/13/DR1B	Dredge	Bulk	1.8	28.5	-1.3
1394804	267/38/SR2C.1	Dredge	Course fraction	1.9	28.7	-1.1
1394805	267/38/SR2C.2	Dredge	Course fraction	1.7	29.7	-0.2
1394875	267/6/GC1	Core	coral	-1.3	27.3	-2.5
1444411	225/GC1	Core	Carbonate crust	0.1	27.5	-2.3
1444509	267/47/DR11B.1	Dredge	Light carbonate	1.3	28.6	-1.3
1444510	267/47/DR11B.2	Dredge	Dark Carbonate	1.8	28.6	-1.3
1444512	267/42/DR6C.1	Dredge	Light carbonate	0.4	29.3	-0.6
1444513	267/42/DR6C.2	Dredge	Dark Carbonate	1.4	29.1	-0.8
1444514	267/27/GR7D.1	Grab	Dark Carbonate	0.9	29.3	-0.6
1444515	267/27/GR7D.2	Grab	Light carbonate	1.9	29.2	-0.7
1444516	267/31/GR9C.1	Grab	Light carbonate	1.5	29.3	-0.5
1444517	267/31/GR9C.2	Grab	Dark Carbonate	1.9	29.1	-0.7

The findings of the isotopic analyses of Yampi Shelf carbonates included:

- No significant isotopic depletion was observed in any carbonate material analyzed.
- No isotopic difference was observed between aragonite and the Mn-rich carbonate.
- Active seepage sites did not appear to have a distinctive carbonate signature.

The samples were collected around known active gas seeps on a carbonate platform where carbonate formation and deposition dominates over other sediment types. Therefore, the proportion of carbonate deposited due to natural hydrocarbon seepage is very small and is unlikely to be detected above the background signal of normal marine carbonate formation. However, in siliciclastic environments MDAC can easily be identified using isotopic analysis because there is no masking of the isotopic signature from marine carbonates. (O'Brien and Woods, 1995)

6.6 Lipid/biomarker analysis – clastic sediments and carbonates

In Australia, apart from isotopic analysis of exploration well samples (O'Brien and Woods, 1995), no examples of shallow sediment cores intersecting naturally seeping oil have been described using lipid biomarker analysis. However, in the Gulf of Mexico where cores were taken from a macroseepage site, a high degree of

biodegradation is observed, as illustrated by the high Unresolved Complex Mixture (UCM) concentrations in gas chromatograms of sediment extracts. Cores peripheral to the macro-seepage sites generally display a well-resolved petrogenic hydrocarbon signal, unaltered by microbes (Wenger and Isaksen, 2002; Hood et al., 2002). The observation that the level of biodegradation in samples from active seep locations is correlated with the intensity of seepage was reported by Wenger and Isaksen (2002), based on geochemical surveys conducted in many basins world-wide. Cole et al. (2001) identified an ubiquitous UCM background signal in the Gulf of Mexico (GOM) related to reworked thermogenic hydrocarbons. However, Cole et al. (2001) considered samples showing UCM < 200 ppm were not indicative of migrating hydrocarbons in the Gulf of Mexico. Core sediments with visual evidence of oil stains have UCM concentrations considerably in excess of 200 ppm. These studies indicate that cores that intersect sites of intense seepage should contain hydrocarbons with a strongly biodegraded signature. Cores located close to these seepage sites should contain petrogenic hydrocarbons which do not display this strong biodegradation signal.

Seepage also often leads to the formation of oil slicks and tar mats. Beach tar derived from natural seepage along the coast and around the islands in the Santa Barbara Channel range in biodegradation from level 4 (no paraffins, acyclic isoprenoids intact) to level 8 (hopanes partly biodegraded) (Hostettler et al., 2004), using the classification of Peters and Moldowan (1993). The dominance of biomarkers within the tar balls means that these samples allow oil source correlation and typing, and are typical of the Miocence Monterey Formation in tars along the Californian coast (Hostettler et al., 2004). However, the loss of more volatile components and the concentration effects strongly skew the composition of these samples towards a higher molecular weight range compared to fresh or aged oil slicks (Leifer et al., 2006).

Sites where seepage exists are also often characterised by bacterial processes that have distinct biomakers and isotopic compositions. Anaerobic Oxidation of Methane (AOM) occurs in methane-rich sediments with concomitant seawater sulfate reduction and is most significant at the methane-sulfate interface, where both substrates become depleted. Recent studies suggest that a prokaryotic consortium of methanotrophic

archaea and sulfate-reducing bacteria mediate this process (Hinrichs et al., 1999; Boetius al., 2000). Where AOM has been inferred, high concentrations of specific biomarkers (e.g. archaeol and hydroxyarchaeols) have been detected (Hinrichs et al., 2000; Pancost et al., 2001a). The presence of methanotrophy is recognised by the significant ^{13}C depletion of these biomarkers, which are known constituents of membranes in Archaea. A range of non-isoprenoidal dialkyl glycerol diethers (DGD) have also been identified, with two main homologues C_{33} I and C_{35} II present. These compounds have been identified in carbonate crusts in the vicinity of cold seeps on the East Mediterranean ridge and are thought to be related to sulfate-reducing bacteria (Pancost et al., 2001b). Analogous distributions of archaeal biomarkers and non-isoprenoidal glycerol diethers, with comparable concentration increases downcore, have been observed in marine sediments characterized by a diffusive flux of methane, where abundances reach a maximum near the sulfate-methane transition zone and are several orders of magnitude lower than observed at seeps(Pancost et al., 2005). However, similar biomarker assemblages are also found in marine settings where methanogenesis occurs (Pancost et al., 2005). Methanotrophy via AOM and methanogenesis are differentiated by the stable carbon isotopic compositions of archaeal biomarkers. Lipids derived from organisms feeding on methane are highly depleted in ^{13}C.

A significant issue in the recognition of natural hydrocarbon seepage can be the presence of reworked source rock in recent sediments. This has been found to be more common in areas that have suffered nearby uplift or glacial outwash (Piggot and Abrams, 1996). The geochemical signals associated with reworking often show elevated total organic carbon (TOC), poor association with pore space gas concentrations and little biodegradation of hydrocarbons, which would be expected at a seepage site. Although this problem does not appear to have been an issue for Australian studies, it is an issue that could occur. Core and sediment derived from sea floor fans, and in particular, those at the base of canyons known to cut through stratigraphy along the Great Australian Bight are samples that will need particular attention in future studies.

6.7 Examples of detected hydrocarbons from Australian Seepage Studies

6.7.1 Yampi Shelf

Active seepage was detected during both S267 and SS06/2005 using sidescan and echosounders (Figure 17, Figure 18, Figure 50). Gas bubbles were observed to break the sea surface during both surveys. Venting of this gas was filmed using an underwater camera at a depth of approximately 80 to 90 m during SS06/2005. Streams of bubbles were observed to flow from small holes or tubes during these venting periods.

A gas catching device was deployed from the work boat of the RV Southern Surveyor during SS06/2005 (Figure 93). This allowed gas within the water column to be trapped for analysis.

Figure 93. Gas bubbles being collected close to the water surface by a diver with a gas catching device, SS06/2005.

Gas was collected at the top of the water column (within 2 m of surface) using a diver-operated gas funnel. A glass jar at the top of the funnel was used to collect gas by gas displacement of water (Figure 93). Compositional analysis of the gas (gas

chromatography) was carried out at the Australian Institute of Marine Sciences and compound-specific isotope data was collected at Geoscience Australia on a continuous flow isotope ratio mass spectrometer (Finigan MAT 252) coupled to a Carlo Erba gas chromatograph (GC). The gas was composed of 99% methane and had an isotopic composition ranging between $\delta^{13}C$ = -41 to -42‰ and δD = -157 to 158‰. This is the same composition as the gas reservoired within the Cornea oil and gas field. This indicates that the gas has a thermogenic origin and also that there is no alteration of the gas composition during sub-surface migration and transfer through the water column.

6.7.1.1 Lipid Geochemistry

Near surface sediments taken at active seepage sites were dominated by lipids derived from marine biota and sedimentary bacteria. There was no evidence of hydrocarbons even in grab samples collected within active seepage vents (Figure 94, chromatogram 267/31/GR9B). However, these samples were noted for the strong smell of hydrogen sulfide during collection and elemental sulfur on geochemical analysis.

Sample 1444411 was collected at the base of a short gravity core collected inboard of any seepage activity during a previous marine survey. In thin section, it is predominantly composed of coral with secondary carbonate cementation. Lipid analysis of this sample showed that it contained a broad suite of hydrocarbons with no odd-over-even predominance (Figure 94, chromatogram 1444411 EOM). This indicates that these hydrocarbons have a petroleum origin. The wide range of hydrocarbons also indicates that they are not derived from a refined petroleum product.

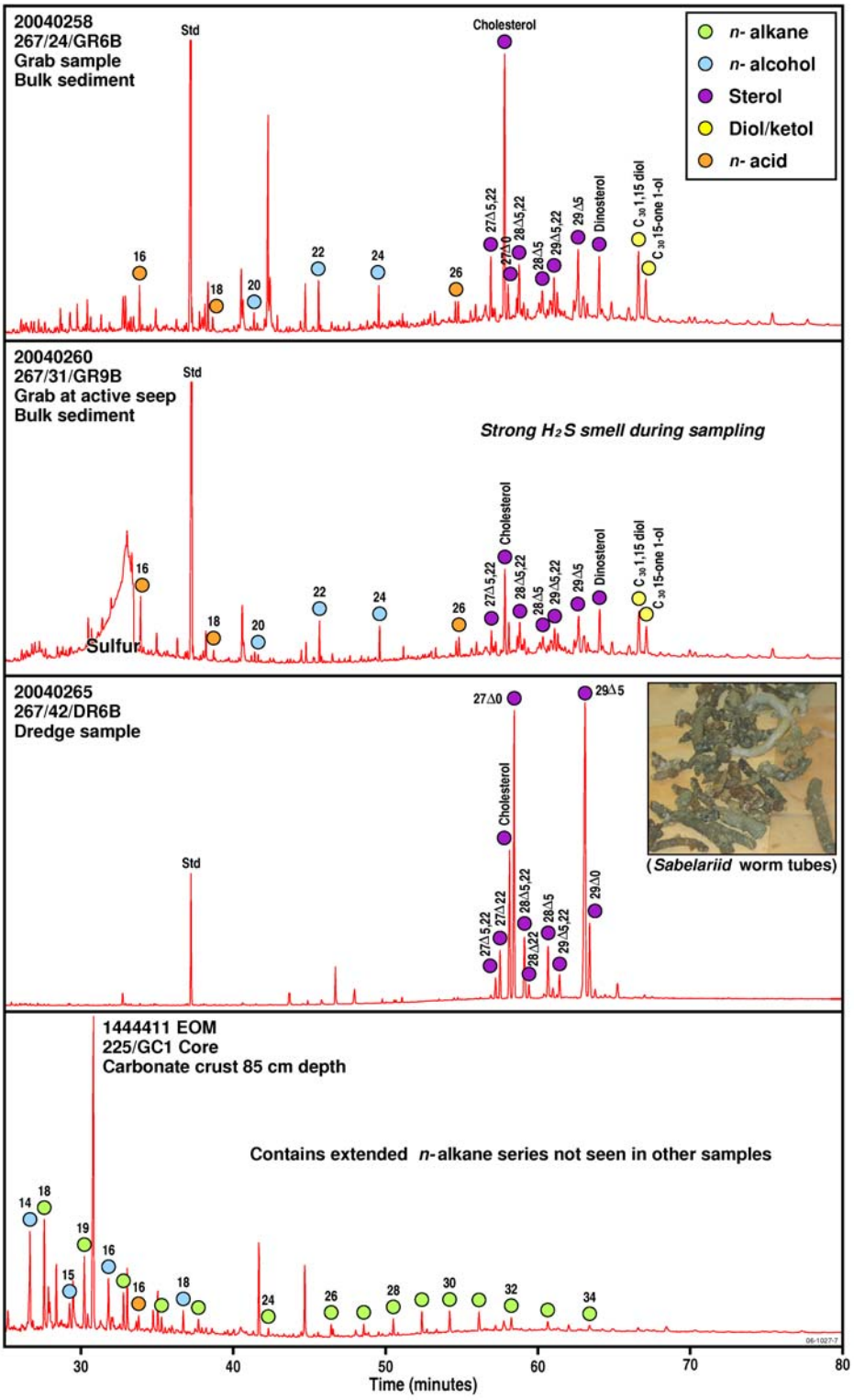

Figure 94. Gas chromotograms of lipid extracts from two grab samples, a dredge sample and a core sample taken at active seep locations. The surface sediment grab samples and *Sabelariid* worm tubes collected at active seep sites do not show any evidence of hydrocarbons. However, sample 1444411 shows evidence of hydrocarbon staining.

Hydrocarbons from sample 1444411 were separated from other lipids and analysed for ^{13}C isotopic composition of individual alkanes. The data were then compared to known examples of oils in the region (Figure 95). Hydrocarbons from this sample have a very similar isotopic signature to oils from Cornea 1 and Gwydion 1, the closest accumulations to the sample. The signature was notably different to the two other oil families in the region. This indicates a relationship between hydrocarbons in sample 1444411 and the oil at Cornea and Gwydion. The oils in the reservoir are biodegraded and have lost much of their original n-alkane content, contrary to sample 1444411. This suggests that hydrocarbons detected in this sample are derived from the same source as Cornea and Gwydion but are not derived from seepage from these reservoirs. The implication of this result is that there may be continuous sourcing of hydrocarbons resulting in this seepage, and the absence of biodegradation indicates that seepage is not related to leakage from the known petroleum accumulations in the area.

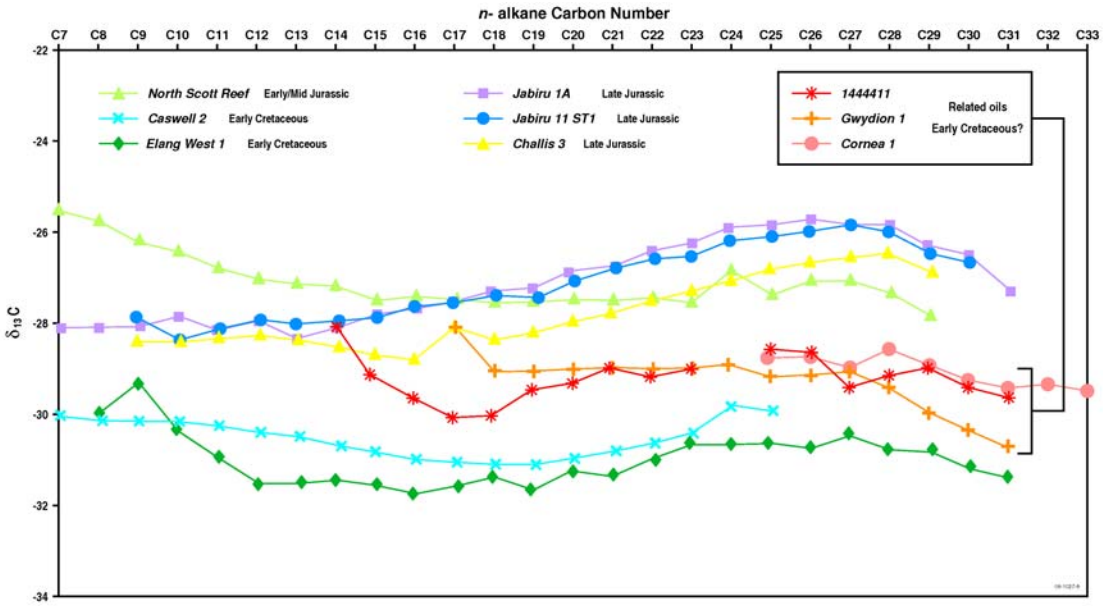

Figure 95. Graphs of $\delta^{13}C$ isotopic compositions of individual n-alkanes showing the relationship between n-alkanes from sample 1444411 and the oils reservoired in at Cornea and Gwydion. Other oils from the region are shown for comparison.

6.7.1.2 Chemistry of Worm Tubes

During dredging operations areas of active seepage were noted for the presence of large quantities of *Sabelariid* worm tubes. Analysis of these tubes yielded lipid signatures dominated by steroids (Figure 94, chromatogram 267/42/DR6B). The

Australian Institute of Marine Science visited the active seep sites a year after survey S267 during their marine survey SS06/2005. Dredging operations across seepage sites recovered encrusted tubes similar in size to the *Sabelariid* worm tubes identified during S267 (Figure 96). However, these tubes appeared older and more heavily overgrown with carbonate minerals. GC-MS analysis of this tube material provided a radically different lipid signature compared to fresh *Sabelariid* worm tubes. The fresh material was dominated by biological steroids (Figure 94, chromatogram 267/42/DR6B). In contrast, the older material had a more complex lipid signature. Within this signature was a homologous series of hydrocarbons (Figure 97) extending from C_{12} to C_{33} and maximizing at C_{16}. When the m/z=85 ion chromatogram was extracted from the data the hydrocarbon distribution was clear and distinct, with pristane, phytane and several other isoprenoids easily identifiable (Figure 97). This hydrocarbon signature is interpreted to derive from the seepage present at the sample site.

Figure 96. Worm tubes collected during SS06/2005. These samples were solvent extracted for analysis in the same way as the *Sabelariid* worm tubes from sample 267/42/DR6B.

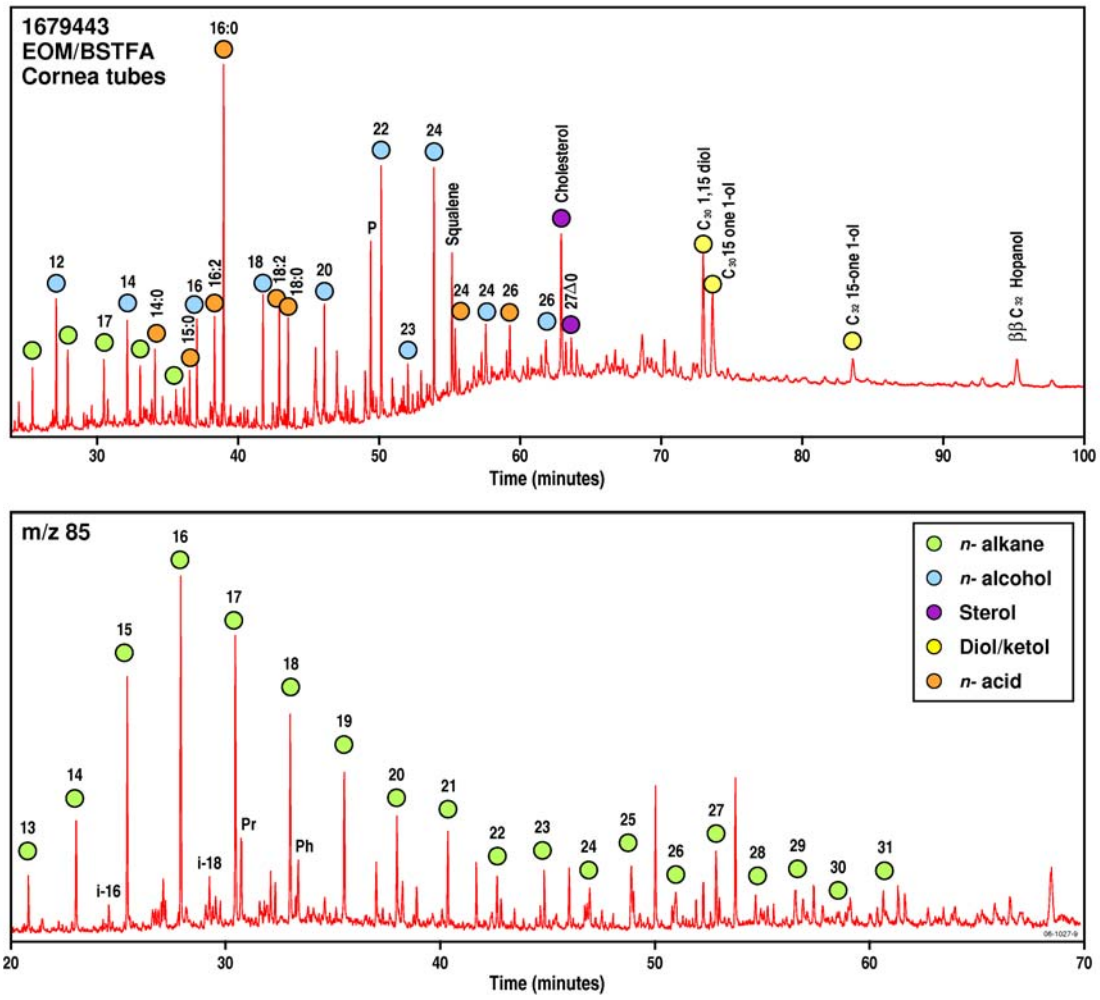

Figure 97. Total ion chromatogram of lipid extract from worm tubes collected during SS06/2005. This sample contains a range of hydrocarbons which can easily be distinguished by a selected ion chromatogram of m/z = 85. This data indicates that hydrocarbon staining does occur on older worm tubes and is related to seepage.

6.7.2 Asphaltite strandings along Southern Margin

The distinctive appearance of the asphaltites (see also section 3.1) allows their identification in historic records, such as Tolmer (1882), who reported the occurrence of 'asphaltum' on the southern coast of Kangaroo Island in August 1844. The strandings appear to have been more common around the turn of the century than today, with reports of "about a quarter of a ton having been recently brought to Hobart for inspection" (Twelvetrees, 1917).

The asphaltites do not correlate with any known produced Australian oil. Geochemically, the asphaltites are uniform in chemical composition, being sulfur rich

(S = 3.4-4.3%), aromatic-asphaltic crude oils, with high asphaltene contents (asphaltene+polars = 55-84%). Biomarker data indicate derivation from a mature, argillaceous, marine source rock (Edwards et al., 1998), not unlike Early Cretaceous shales found in onshore Bight Basin wells (Eyre 1) and the Toolebuc Formation in the Eromanga Basin (Boreham et al., 2001). Earlier work has shown that the oils produced from western and southern Australian basins (including Perth, Otway and Gippsland basins) contrast markedly with the geochemistry of the asphaltites (Edwards et al., 1998). Perth Basin oils, derived from the Early Triassic Kockatea Shale, have a marine affinity but their geochemistry differs from that of the asphaltites in that they exhibit a predominance of C_{29} steranes, a greater proportion of 3β- and 4α−steranes plus abundant tricyclic terpanes. Onshore oils of the Perth basin have low sulfur contents, with abundant 2-methylhopanes and methylcyclohexanes, characteristics not found with the asphaltites. The Perth Basin oils also contain gymnosperm-derived aromatic hydrocarbons, retene and cadalene, which are absent in the asphaltites. Oils have not been produced from the offshore Otway Basin but recovered bitumens from cores and cuttings are low in sulfur and have a terrestrial source, in contrast to the marine affinity of the asphaltites. The bulk and *n*-alkane isotopic profiles of Otway Basin bitumens are also enriched in ^{13}C compared to the asphaltites (Edwards et al., 1998). Oils from the Gippsland Basin are low in sulfur and abundant in land-plant-derived biomarkers such as oleanane, since they are derived from terrestrial source rocks from the Late Cretaceous to Tertiary La Trobe Group.

Due to their unknown source and the implication that they represent an as yet undiscovered, marine petroleum system along the southern margin of Australia, the origins of the asphaltites have been extensively debated. Several arguments have been developed to explain where or how the asphaltites have come to be stranded on Australian beaches. These can be loosely grouped into arguments that suggest an anthropogenic source and those that suggest a natural seepage origin.

6.7.2.1 Anthropogenic Sources

- Oil seeping from a shipwreck or tanker traffic: Oil used for fuel or lubrication on ships is a refined petroleum product and thus has a distinct chemistry. The asphaltites are not a refined product, as they have a broad n-alkane profile that shows no evidence of distillation, which leads to a narrow hydrocarbon range.

Furthermore, examination of museum examples of known collection dates shows that the asphaltite strandings date from before oil fired shipping was common (Volkman et al., 1992). Therefore, this explanation does not fit with the dates or stranding or the chemistry of the asphaltites.

- Caulking bitumen used to seal ship hulls: The whaling industry flourished between the early 1790s and 1870s and permanent bases were established in Western Australia, South Australia and Tasmania (Begg and Begg, 1979; Kostoglou and McCathy, 1991; Gibbs, 1994). At some of these locations bitumen, used to caulk the sailing vessels, was stored in casks buried on beaches (Wade, 1925). Furthermore, the frequent wreckage of supply ships, possibly carrying caulking bitumen, have been extensively documented from around the Australian coast (MacKenzie, 1974; Loney, 1988). Storm redistribution of bitumen caches from buried sites or wrecks could also explain the isolated occurrences of large quantities of asphaltites, as opposed to the widespread strandings of the waxy bitumens.

To test the hypothesis that the asphaltites could have an anthropogenic source, related to late nineteenth century maritime activities, we report on the analysis of pitches from various historic shipwrecks around Australia (Smart, 1999). The Western Australian Maritime Museum provided samples of caulking material from nine sailing ships wrecked on the Australian coast before 1900. The geochemistry of the seven samples of caulking material is distinctly different from the asphaltite (Figure 98, Table 7). All compounds from these seven samples have also been observed in studies of 'Stockholm Tar' and the 16th century shipwreck *Mary Rose* (Robinson et al., 1987). 'Stockholm Tar' is produced from heating pine resin to form a tarry product. Caulking material from two ships has a different origin to the seven other examples. The high relative abundance of polyaromatic hydrocarbons (PAHs) with low levels of methylation and extensive ring development is characteristic of coal tar. The high temperatures involved in the production of coal tar (>1000°K) lead to the formation of stable PAHs and low relative abundances of their methylated pseudo-homologues. A coal tar origin has previously been suggested for these samples based on NMR (Ghisalberti and Godfrey, 1990, 1998). However, NMR data for the *Belinda* pitch also indicates that coal tar has been mixed with a pine resin (Ghisalberti and

Godfrey, 1990, 1998).

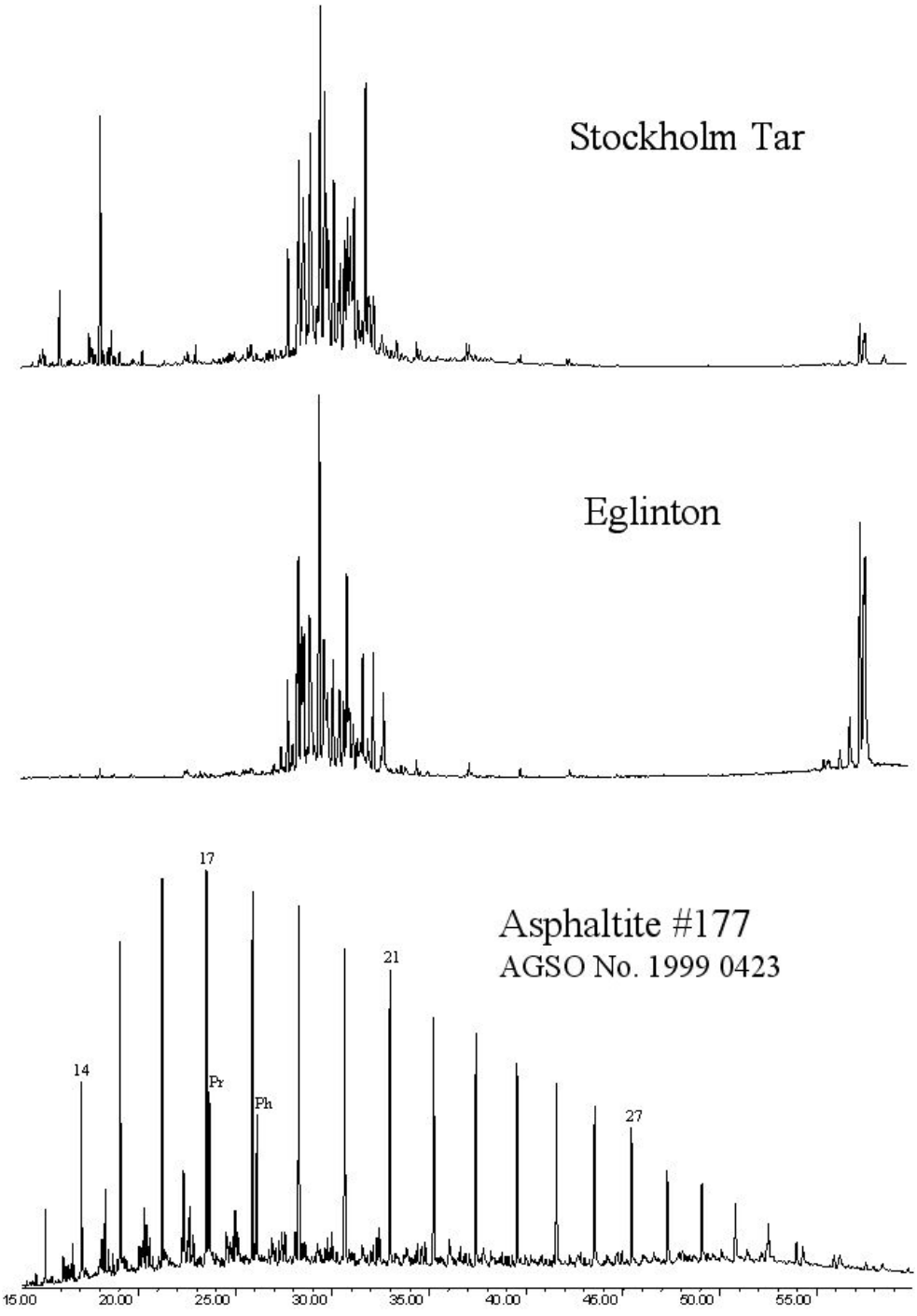

Figure 98. Comparison of gas chromatograms for Stockholm Tar, a ship bitumen from the wreck of the Eglinton and an asphaltite. The Stockholm Tar and the sample from the Eglinton show a great deal of similarity and are derived from pine resin. The asphaltite exhibits a geochemistry that is quite different and typical of a petroleum-derived bitumen.

It is clear from this study that the asphaltites which strand along the southern coasts of Australia are not related to any of the archaeological material we have examined. The material that was most commonly used as a sealant on sailing ships in the region was derived from pine tar, although coal tar has been used. Interestingly, coal tar was used on the *Belinda*, a ship wrecked in 1824 before the industrial revolution when one might expect coal tar to be uncommon (Table 7). Even though the coal tars contain hydrocarbon *n*-alkanes and biomarkers, they are easily differentiated from the asphaltite samples using GC-MS and NMR techniques. Therefore, it seems most likely that caulking materials used on the whaling and sealing ships will have been derived from pine resins and/or coal tar and not petroleum bitumens. Thus, an anthropogienc source for the asphaltites is highly unlikely.

Table 7. Samples and results for caulking material, asphaltite and Stockholm Tar used for geochemical study to assess original source material (References: 1, Robinson et al., 1987; 2 & 3, Ghisalberti and Godfrey 1990, 1998; 4, Padley 1996; 5, Edwards et al., 1998).

AGSO #	Sample type	Name	Date of Wreck	*Previous ID*	*Location*	*Geochemical Source*	*Comments*	Refs.
19999727	Retorted Pine Tar	Stockholm tar				Pine resin		1,2,3
19999728	Ship wreck pitch	Sirius	1790	SI491	Norfolk Island	Stockholm Tar	Extract from fibres attached to copper sheathing	
19999729	Ship wreck pitch	Fanny Nicholson	1872	FN3589	Albany, WA	Coal Tar	Extract of matting lining hull timbers	2,3
19999733	Ship wreck pitch	Eglinton	1852	WR707EG	Yanchep, WA	Stockholm Tar	Discrete lumps of pitch on the wreck site	2,3
10344	Ship wreck pitch	Vergulde Draeck	1656	GT4057A	Ledge Point, WA	Stockholm Tar	Discrete lumps of pitch on the wreck site	2,3
10345	Ship wreck pitch	Vergulde Draeck	1656	GT1000A	Ledge Point, WA	Stockholm Tar	Discrete lumps of pitch on the wreck site	2,3
10346A	Ship wreck pitch	Rapid	1811	RP4287	Pt Cloates, WA	Stockholm Tar	Pitch was removed from a stoneware jar	2,3
19999797	Ship wreck pitch	Belinda	1824	BEL 3569	Middle Island, WA	Coal Tar	Extract of matting lining hull timbers	2,3
19999798	Ship wreck pitch	RIP	1904		Albany, WA	Stockholm Tar	Extract of fibrous matting	
19999799	Ship wreck pitch	Avondster	1659		Sri Lanka	Stockholm Tar	Extract of fibrous matting	
19990423	Coastal bitumen	Asphaltite		177	Kangaroo Is, SA	marine source rock	Unweathered typical	4,5
19990429	Coastal bitumen	Asphaltite		66	Kangaroo Is, SA	marine source rock	Atypical	4,5
19990430	Coastal bitumen	Asphaltite		187	Kangaroo Is, SA	marine source rock	Atypical	4,5
19990431	Coastal bitumen	Asphaltite		236	Coorong, SA	marine source rock	Unweathered typical	4,5

6.7.2.2 Natural Seepage Origin

Eroded tar flows formed at the sea floor: Various theories on the origin of the asphaltites have been put forward. Sprigg and Woolley (1963) suggested that they were derived from ‘fossil tar lakes’ formed along the Australian continent edge during periods of low sea-level. However, this seems less likely since pollen grains and detritus are lacking within the asphaltite (Edwards et al., 1998).

A second hypothesis is that the asphaltites are products of local submarine oil seeps. For example, bitumen has been noted to form viscous flows at seepage sites in the deep water of the Gulf of Mexico (MacDonald et al., 2004). The cracked surface morphology and high density have been noted as similar to the morphology and

density of the Australian asphaltities (Boult et al., 2006). This has lead to the suggestion that the asphaltites may be formed at the sea floor and are eroded and transported onto the shelf by the Flinders current. However, the tars and bitumens at active seepage sites are heavily biodegraded and thus differ from the Australian 'asphaltites', which retain a broad distribution of n-alkanes. The UCM that is present in the Australian samples is most likely derived from migration pick-up as seeping oil moves through the shallow subsurface zone where heavily biodegraded oil collects around seepage site. This feature is observed in tar and oil slicks in the Gulf of Mexico and offshore California (Wenger and Isaksen, 2002; Hood et al., 2002; Hostettler et al., 2004; Liefer et al., 2006). If the asphaltites were derived from sea floor erosion of tar mats at seepage sites, the chemistry of the samples should reflect a history of intense biodegradation. This is not the case, and the presence of hydrocarbons that are not indicative of biodegradation suggests that an eroded tar from a seep is not a likely source for the asphaltites.

- Ocean transported oil seeps: At present, asphaltite (or pitch), is the least common form of coastal bitumen to strand along Australia's shoreline. However, they have been recorded as flattened blocks, up to 7 kg in weight and 670 mm in diameter, with a strong petroliferous odour (Edwards et al., 1998). The exterior of the asphaltite is generally hard with irregular shrinkage cracks on their upper surface. The interior is often soft and pliable, when freshly stranded, but becomes increasingly brittle due to volatile loss during storage (Edwards et al., 1998). The presence of these shrinkage cracks may indicate their mode of transportation. In the Gulf of Mexico, oil from submarine seeps rises to the surface to form floating tar mats, as photographed in Geyer and Giammona (1980). Evaporation leads to loss of volatiles, resulting in solidification and shrinkage cracks on the upper surface of the mats, while sub-aqueous and internal portions remain plastic, as observed in the Australian asphaltites. With progressive loss of volatiles, the mats would increase in density until they sank, a phenomenon that may account for the asphaltites high density when found on the shore.

6.7.2.3 Assessment of evidence from geochemistry and morphology

The interpretation of an anthropogenic source does not explain the early occurrence of asphaltites prior to oil-fired shipping and the chemistry is not the same as material

used to caulk ship hulls. The erosion of sea-floor tar mats is unlikely, as the tar mats that form on the sea floor are heavily biodegraded. This leaves the ocean-transported oil seep origin as the most likely. Further support for this hypothesis comes from oil spill chemistry. The most important property for an oil to form an emulsion when spilled is the asphaltene and resin content and the viscosity of the oil (Berridge et al., 1968; McLean and Kilpartick, 1997b; McLean et al., 1998; Fingas and Fieldhouse, 2003). A notable feature of the asphaltites is the high asphaltene content (asphaltene+polars = 55-84%) of the stranded material (Edwards et al., 1998). The emulsion produced is known as a 'mousse' and can be stable for a long time. Laboratory tests revealed that an emulsion that survived for 3 months had developed a rigidity on its upper surface (Fingas and Fieldhouse, 2003). Oil spills also result in the formation of tar balls, which also tend to have a low specific gravity (Goodman, 2003). Tar balls are also the end result of natural seepage from the Monterey Formation along the California coast (Hostettler et al., 2004). Thick slicks, including brown mousse and tar balls are often found in the convergence zone of the Santa Barbara channel (Liefer et al., 2006). Tar accumulation on beaches at Coal Oil Point (Santa Barbara, California) has also been shown to be seasonally dependent, with onshore winds bringing more frequent and higher volumes of strandings during spring and summer, as compared to offshore winds which dominate in winter and autumn (Del Sontro et al., 2007).

Given the chemistry of the asphaltites, age of collected material, and the morphology of the strandings, the most likely scenario is that they are derived from natural oil seepage. The chemistry indicates that they would form a mousse during slick formation at the sea surface. This mousse can be very stable and last for many months, during which volatile loss and chemical changes can lead to a more rigid outer surface. Ultimately, this can lead to tar ball formation resulting in material that is more dense than water. All these processes are in keeping with what is known to occur with natural oil slicks and anthropogenic oil spills, however, the chemistry of the asphaltites reflects a natural source and not a refined product. The collection of asphaltite samples from the 1800's indicates that crude oil from tanker traffic is not a potential source. The long term stability of mousse and tar balls indicates that transport of the oil could occur over an extended period and that a distant origin is possible. Indeed, relatively unweathered mousse has persisted for at least 5 years

after the *Exxon Valdez* oil spill. The preservation is believed to be related to transportation as a mousse, because the interior oil has undergone no weathering effects (Irvine et al., 1999). Both the chemistry and lack of material on northern beaches also indicates that an Indonesian or northern Pacific origin is not likely. Thus, a natural oil seep origin along the southern margin of Australia is possible. However, a source outside of the Australian region but within southerly latitudes may also be possible.

Geological Implications

The tectonic, environmental and geomorphological setting of a sedimentary basin determines the mode of any natural hydrocarbon seepage and influences the potential for successful seepage detection. In this section, the characteristics of Australia's offshore margins are placed in a global context to gain a greater understanding of the overall success of seepage studies around Australia.

7 Comparison of Australian seepage patterns with global examples

7.1 Global (sub-sea) seepage locations

Fluid seepage from the seafloor has been reported from many locations around the world, in water depths ranging from 10 to 3000 m. The fluids involved in seepage can be of various origins (ground-water, biogenic or thermogenic) and intensity (macro- versus micro-seepage), and seepage is observed in a variety of sedimentary, climatic and tectonic settings. Comprehensive reviews of shallow gas and 'cold' seep manifestations from offshore basins around the world are presented in Fleischer et al. (2001) and Judd and Hovland (2007). Table 8 is a summary of key aspects of those reviews.

Table 8. Location, depth, environment and tectonic setting of key features related to natural hydrocarbon seepage around the world.

Location	Water depth	Environment and Tectonic Setting	Features related to seepage	References
Barents Sea	200-1270 m	Siliciclastic (clayey till and mud), polar, sag margin with salt movement.	Pockmarks, mud volcanoes, chemosynthetic tubeworms, bacterial mats, gas hydrates	Solheim and Elverhoi, 1985, 1993; Vogt et al., 1999; Jerosch et al., 2004
Norwegian Sea, Skagerrak, Kattegat	10-1020 m	Siliciclastic (plastic clay, subcropping sedimentary strata), polar-temperate, passive margin.	Pockmarks, water column flares, acoustic turbidity, MDAC, deep-water reefs, gas hydrates	Jensen et al., 1992; Hovland et al., 1998; Rise et al., 1999; Bouriak et al., 2000
Baltic Sea	3-110 m	Siliclastic (glacial and post-glacial clays), polar-temperate, fjord.	Pockmarks, acoustic turbidity	Geodekyan, et al., 1991; Soderberg, 1997; Bussmann and Suess, 1998; Jackson et al., 1998
North Sea, UK sector	<100-250 m	Siliciclastic (silty marine clays, glaciomarine silts), temperate, sag	Gas flares and/or sediment clouds suspended in the water column,	Hovland and Judd, 1988; Judd, 2001; Judd et al., 2002; Loseth et al., 2003

		margin with inversion and salt movement.	pockmarks, authigenic carbonates and bacterial mats.	
East Atlantic (Gulf of Cadiz)	300-400 m	Siliciclastic (mud), sub-tropical, compressional system.	Gas flares, ancient and modern pockmarks, acoustic turbidity and blanking, bright spots and Bottom Simulating Reflectors.	Casas et al., 2003; Diaz-del-Rio et al., 2003; Somoza et al., 2003.
West African margin	<400-3000 m	Siliciclastic (sand/silt), tropical, passive margin.	Pockmarks.	Hovland et al., 1997; Gay et al., 2003.
Adriatic Sea	80-250 m	Siliciclastic (soft silts and clays) temperate, foreland basin	Pockmarks, acoustic turbidity	Mazzotti et al., 1987; Conti et al., 2002;
Eastern Mediterranean	20-80 m	Siliciclastic (silt, sandy-silt), sub-tropical, compressive system.	Gas bubbles, active pockmarks, mud volcanoes and seismic acoustic anomalies.	Hasiotos et al., 1996; Christodoulou et al., 2003; Garcia-Garcia et al., 2004.
Black Sea	<100-2000 m	Siliciclastic, sub-tropical, compressional setting.	Gas flares, gas-saturated-sediments, gas hydrates, mud volcanoes and pockmarks.	Ergün et al., 2002; Kruglyakova et al., 2004; Greinert et al., 2006; Klauke et al., 2006
Caspian Sea	<400-1000 m	Siliciclastic (mud), sub-tropical, compressional system.	Mud volcanoes, oil slicks.	Ginsburg and Soloviev, 1994; Yusifov and Rabinowitz, 2004.
Lake Baikal	<100-1500 m	Siliciclastic (coarse sandy turbidites), desertic, rift system.	Methane seeps, mud cones, low relief craters and gas hydrates.	Granin and Granina, 2002; Van Rensbergen et al., 2003.
Arabian Gulf	20-100 m	Siliciclastic and carbonate mud and sand, tropical, rift system	Pockmarks, acoustic flares and turbidity	Ellis and McGuinness, 1986; Uchupi et al., 1996
Western Indian margin	20-260 m	Siliciclastic (silt, clay, sand), tropical, passive margin.	Gas flares, pockmarks and acoustic masking.	Rao et al., 2001; Karisiddaiah and Veerayya, 2002.
South China Sea	200-750 m	Siliciclastic/ carbonate, tropical, extension/passive	Pockmarks, mud volcanoes, gas flares, sea surface slicks	Traynor and Sladen, 1997; Chow et al., 2001; Huang et al., 2002
Yellow Sea, East China	80-100 m	Siliciclastic (palimpsest sand), sub-tropical, inverted extensional basin.	Gas flares, craters with rare pockmarks and diapirs associated with seismic wipe out.	Jeong et al., 2004.
East China Sea	<100-1000 m	Siliciclastic (mud), sub-tropical, back-arc basin.	Mud volcanoes, large pockmarks, bright spots, phase inversion and other seismic anomalies	Butenko et al., 1985; Yin et al., 2003.
Timor and	40-500 m	Carbonate, tropical,	Methane flares,	O'Brien et al., 2000,

Arafura Sea, Northern Australia		passive margin – early collisional margin.	pockmarks, carbonate hardgrounds, sea surface slicks, acoustic blanking, enhanced reflectors.	2002, 2005; Rollet et al., 2006, 2007.
New Zealand	100-1800 m	Siliciclastic (muds), temperate, convergent margin.	Methane flares, acoustic flares and turbidity, gas hydrates, MDAC, chemosynthetic communities	Lewis and Marshall, 1996; Faure et al., 2006; Greinert et al., in prep.
Sea of Okhotsk	400-1000 m	Silici- and volcaniclastic, temperate, back-arc basin	Acoustic flares, gas hydrates, bacterial mats	Lammers et al., 1995; Gaedicke et al., 1997; Obzhirov et al., 2004.
Bering Sea	<200 m	Siliciclastic, polar, convergent margin.	Gas bubbles in the water column, pockmarks, and seismic wipeout zone related to gas	Carlson et al., 1985; Abrams, 1992.
Cascadia (inc. Hydrate Ridge)	~600 m	Siliciclastic mud, convergent margin	Methane flares, gas hydrates, chemoherms, MDAC, bacterial mats	Bohrmann et al., 1998; Suess et al., 1999; Klauke et al., 2004.
California (inc. Santa Barbara)	5-700 m	Siliciclastic sediments and sub-cropping strata, temperate-tropical, fore-arc and transform basin	Tar, oil and gas seeps, pockmarks, acoustic turbidity	Hornafius et al., 1999; Orange et al., 2002; Paull et al., 2002
Central and South America	1600-3500 m	Calcareous and siliceous biogenic sediments, tropical, convergent margin	Pockmarks, authigenic carbonates, seep communities	Kahn et al., 1996; Olu et al., 1996; Bohrmann et al., 2002;
The Caribbean	1050-3000 m	Carbonate, tropical, convergent margin	Mud volcanoes, tar lakes, MDAC, seep communities	Olu et al., 1997; Lance et al., 1998; Aloisi et al., 2002
Gulf of Mexico	200-3000 m	Siliciclastic, tropical, passive margin with salt movement	Oil slicks, pockmarks, mud volcanoes, gas hydrates, acoustic blanking and turbidity, seep communities	Brooks et al., 1984; MacDonald et al., 1996; Reilly et al., 1996; Joye et al., 2004; Orcutt et al., 2005
Eastern Canada	20-1700 m	Siliciclastic clays and silts, polar-temperate, post-rift passive margin	Pockmarks, acoustic turbidity, oil slicks	MacLean et al., 1981; Fader, 1991

Basins seep (or leak) at different rates depending on several geologic factors, first summarised succinctly by Clayton et al. (1991): Primary controls include high sedimentation rates (overpressure), salt structures, active faulting, and tilted aquifers; secondary controls include high gas-to-oil ratios, high-API oils, and high formation-

water salinity (Williams and Lawrence, 2002). Therefore, seeps are most abundant in petroliferous basins that have high sedimentation rates and significant deformation, especially in settings such as foldbelts and active transpressional margins that lack unfaulted cover sequences (Clarke and Cleverly, 1991).

The influence of basin type and tectonics on the intensity of natural hydrocarbon seepage was quantified by Macgregor (1993) on the basis of an internal BP database (predominantly onshore basins explored during the period 1880-1940; the same database utilised by Clarke and Cleverly, 1991). Macgregor (1993) compiled lists of the 100 basins containing the highest proven petroleum reserves (>1.8 BBOE) and the 100 basins containing the largest number of documented seeps (>10). Fifty-two basins appeared on both lists, which is a degree of coincidence greater than three times than would be statistically expected if seeps and reserves were not related in any way. Macgregor (1993) stated that, based on these statistics, a basin rich in seeps is more likely than not to contain significant petroleum reserves.

Macgregor (1993) also classified the basins (a total of 148) into six simplistic basin types, based on their Late Cretaceous-Recent plate tectonic setting (Figure 99), and concluded that timing of tectonic activity is a key control on the intensity of seepage. Figure 99 shows that the degree of correlation between the two datasets varies considerably, with anomalies heavily concentrated in a few basin types. Specific comments on the basin types by Macgregor (1993) include:

- Intracratonic basins show little or no surface expression in the form of seepage.
- Evaporite seals occur in many intracratonic basins, which may be a factor in constraining the rate of seepage.
- Foreland basins show relatively low seepage in relation to their large reserves. The more recent and more deformed foreland basins show larger numbers of seeps than older examples. Rift basins show similar variations according to timing of events.
- Passive margins can be subdivided into those affected by mud or salt diapirism, which show large numbers of seeps, and undeformed examples,

which show few recorded seeps.

- Active margins show anomalously large numbers of seeps relative to their reserves.

- Thrust belts, including strongly deformed forearcs and accretionary wedges, are highly prone to seepage. This set of basins includes many seep-rich basins that are not major petroleum provinces.

Macgregor (1993) also noted that almost all of the highly seeping basins are undergoing active uplift or rapid subsidence, in the latter cases being characterised by high present-day sedimentation rates (with maximum Neogene sedimentation rates typically 100-1000 m/Ma).

Flowing seeps originate in the subsurface from three main processes: 1) structurally focussed secondary migration, usually where recharge rates from present-day generation exceed the rate of trap leakage; 2) lateral spillage from accumulations during basin tilting; and 3) direct vertical leakage from accumulations breached by active faulting and diapirism (Macgregor, 1993, Williams and Lawrence, 2002). The two most significant seep associations in terms of numbers of flowing seeps and detectable flow seem to be those associated with active diapirism or reverse faulting. Visible seeps seem to be common in extensional settings only where active normal faults extend to the surface (Macgregor, 1993).

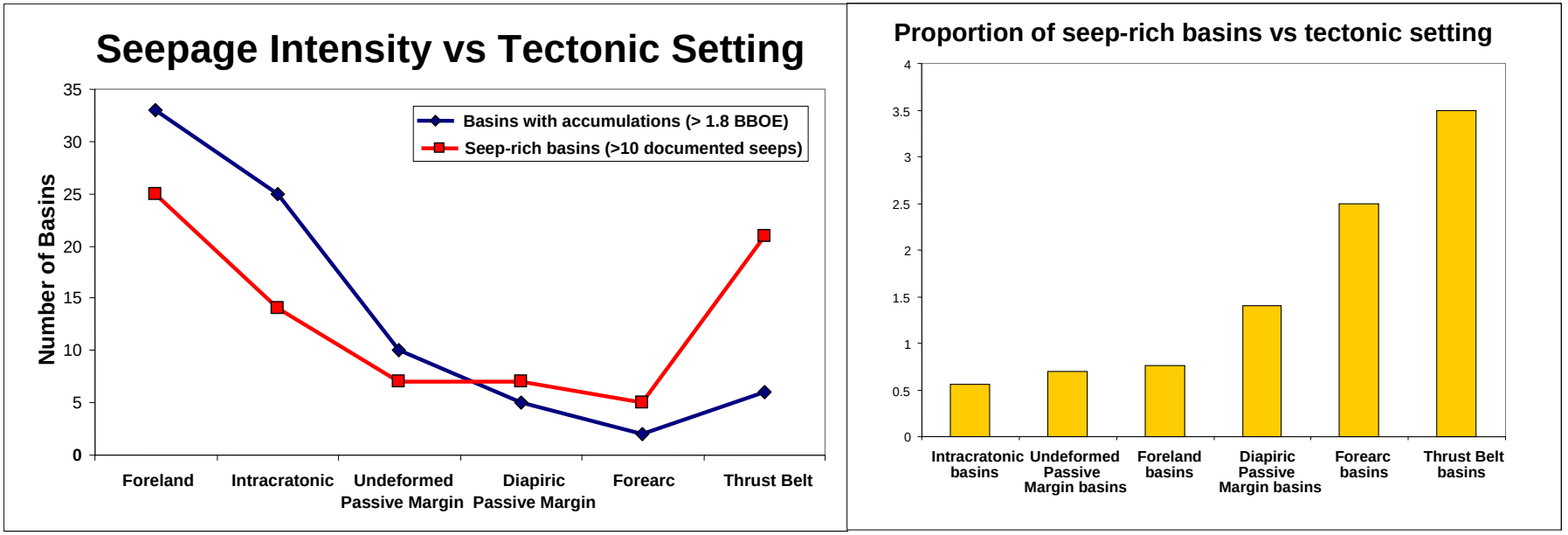

Figure 99. Distribution of seep and petroleum-rich provinces with respect to basin type (Macgregor, 1993). The image on the right shows basins with relatively low seepage on the left and relatively high seepage on the right.

7.2 Tectonic setting of Australia's margins

Australia's offshore jurisdiction almost entirely comprises passive margins. Passive margins are critical sites of hydrocarbon accumulation, as early continental rifting conditions lead to the development of anoxic basins with large organic flux, and subsequent sedimentary overburden produces thermal maturity. This is evidenced in the significant oil and gas accumulations in the passive margin settings of Australia's North West Shelf and Bass Strait.

The Gulf of Mexico is also a passive margin with significant hydrocarbon accumulations, but unlike Australia's offshore passive margin basins, it contains hundreds of active natural hydrocarbon seeps (McDonald et al., 2002). One of the primary driving forces behind this prolific oil and gas seepage is the high sedimentation rate in the northern Gulf of Mexico, with the modern-day locus of deposition comprising the Mississippi Delta. Loading of the thick sediment pile is thought to be the primary control on the timing of source rock maturation (Nelson et al., 2000), and it has caused Jurassic salt deposits to extrude out and into the Tertiary sequence (Thrasher et al., 1996). The high thermal conductivity of the allochthonous salt also influences thermal maturity of source intervals (Nelson et al., 2000). The migrating hydrocarbons flow upward through faults generated by this active and extensive salt tectonism (Sassen et al., 1993; McDonald et al., 2002). The Gulf of Mexico can therefore be characterised as a deformed passive margin, which shows large numbers of seeps (Macgregor, 1993), with high sedimentation rates in the Mississippi Delta driving significant hydrocarbon generation and migration pathway formation.

In contrast to the passive margin setting of the Gulf of Mexico, Australia's passive margins are relatively undeformed and Neogene-Recent sediment deposition across much of the margin is generally insufficient to drive significant present-day hydrocarbon generation and migration. Thus, based on the study of Macgregor (1993), many of Australia's offshore basins are unlikely to be characterised by active seepage. This hypothesis is supported by the limited discoveries of active visible macroseeps in Australia's offshore jurisdiction.

A notable exception to the above generalisations is the North West Shelf, and

particularly the Timor Sea area. Late Miocene tectonic reactivation is widespread in this area (O'Brien and Woods, 1995; O'Brien et al., 1996, 1999, 2004; Keep et al., 2002; Harrowfield and Keep, 2005), and a thick section of Late Tertiary carbonate sediments generally means that present-day generation and migration is widespread (Kennard et al., 1999, 2004; Chen et al., 2002; Fujii et al., 2004). However, maximum Neogene sedimentation rates in the Vulcan Sub-basin (up to 90 m/Ma; based on data in Kennard et al., 1999) and Browse Basin (up to 120 m/Ma; based on data in Kennard et al., 2004) are still somewhat lower than corresponding sedimentation rates within most of the major seeping basins compiled by Macgregor (1993; 89% of non-erosional seeping basins have maximum Neogene sedimentation rates greater than 100 m/Ma, and 61% have rates greater than 200 m/Ma).

An additional feature of the Timor Sea is the abundance of residual hydrocarbon accumulations due to breach of traps during Late Miocene fault reactivation (O'Brien et al., 1996, 1999, 2004; Lisk et al., 1997, 1998). This breaching was most probably associated with significant seafloor seepage; for example, the then shallow buried Eocene Grebe Sandstone contains isotopic evidence of microbial reduction of thermogenic hydrocarbons (O'Brien & Woods, 1995). However, active seepage has probably waned since the Late Miocene/Early Pliocene breaching acme. Thus, in accord with the findings of Macgregor (1993), the combination of relatively high Neogene sedimentation rates and Late Miocene tectonic reactivation in the Timor Sea region make this a likely area of active late Miocene seepage, and some of this seepage activity persists today (Rollet et al., 2006).

Based on Macgregor's (1993) studies, another offshore Australian region where active seepage might be expected is the Ceduna Sub-basin (Bight Basin, southern margin) due to Late Maastrichtian-Early Eocene reactivation of deltaic growth faults and associated basinward shale diapirism and compressional toe thrusts within a large mid-Late Cretaceous progradational delta (Totterdell & Krassay, 2003). In places these reactivated structures are bald of younger Palaeogene-Neogene sediments, such that reactivated faults extend to the seabed where active seepage may be focussed (Mitchell, 2007).

Despite the limited occurrences of active visible seeps, studies of natural hydrocarbon seepage can still be utilised to assess petroleum prospectivity in Australia's offshore

jurisdiction. It is generally accepted that almost all traps in basins containing a mature hydrocarbon source will leak small amounts of oil and gas to the surface as seepage (Williams and Lawrence, 2002). In the absence of overpressure driven by sediment loading and active faulting and diapirism, this seepage takes the form of passive or microseepage. Microseepage refers to low concentrations of migrating hydrocarbons, which are not visible but are detectable with standard analytical procedures (Abrams, 1992; 2005).

7.3 Limitations of seep detection methods in Australia

The intensity of seepage has a significant effect on the methods with which the seepage can be detected. Detection of seep sites using SAR, for example, requires sufficient oil to leak from the seabed to form a slick greater than about 125-250 m long on the sea surface (O'Brien et al., 2003b). Similarly, a relatively intensely bubbling gas seep is required for detection in the water column with sonar systems. In many of Australia's passive margin settings it may be necessary to seek signatures of microseepage in the near surface sediments. These signatures may be amplitude anomalies and acoustic turbidity in sub-bottom profiler data, as detected in the Arafura Sea (Rollet et al., 2007), or geochemical anomalies in head-space gas analyses.

Seep detection methods may also need to be adapted based on whether the basin under study is prospective for oil or gas. Some of Australia's offshore hydrocarbon provinces are relatively gas prone (eg. Browse Basin, Malita-Calder Graben and Petrel Sub-basin of the Bonaparte Basin) and natural seepage in these regions is unlikely to be detected with remote sensing technologies such as SAR, as this method detects sea surface roughness which can be effected by oil slicks (but not gas seeps). In these cases, refining the study area for a potential seepage survey may be problematic, and may rely heavily on regional seismic data and geophysical tools to detect evidence of shallow gas. This issue is particularly relevant to many of Australia's frontier areas, where very large geographic areas are covered by very little data.

Compounding problems of seep detection associated with tectonic regime and data sparsity in frontier areas, is the modern environmental setting of Australia's wide,

shallow continental shelves. The majority of seep sites detected from around the world that are characterised by active macroseepage are located in low energy, deep water, siliciclastic sedimentary environments (Table 8). In contrast, much of Australia's offshore jurisdiction comprises high energy, shallow water carbonate shelves. Detecting microseepage (and to some extent macroseepage) in such environments can be problematic due to various factors, such as a lack of acoustic penetration through the relatively coarse-grained sediments with sub-bottom profiler, biogenic and diagenetic overprinting of modern marine carbonate signatures on authigenic seep carbonates, and extensive re-working of substrate sediments by high energy tidal/storm events. This last factor is particularly relevant on the North West Shelf which is an ocean-facing, macro-tidal carbonate ramp subjected to seasonal cyclonic storms and long period swells and large internal tides (James et al., 2004). These factors result in the preferential accumulation of coarse-grained re-worked carbonate sediments that are predominantly relict (lithic and skeletal intraclasts, peloids and ooids). Thus any seabed features developed by macro- or microseepage (such as pockmarks, tubular concretions) are rapidly destroyed or dispersed and difficult to detect or recognise. These coarse carbonate sediments are generally highly porous and permeable, such that any seeping fluids are dispersed and poorly focussed, making detection difficult as compared with seepage within fine-grained impermeable muddy sediments. Here seepage can be expected to be relatively focussed along more permeable pathways. Furthermore, the coarse carbonate sediments are difficult to sample by gravity core techniques and sampling is generally limited to shallow cores and dredges of grab samples within the upper disturbed zone, and are thus unlikely to preserve any signatures of hydrocarbon seepage.

Conclusions

A wide variety of studies have been carried out around the Australian margin to infer or detect natural hydrocarbon seepage (Table 1). In the 1980's and early 1990's these studies were generally based around the application of a particular technique. However, gradually a more integrated approach was employed involving remote sensing, geophysics and geochemical analysis of sediment or seeping gas. A re-assessment of many of the earlier studies indicates that interpretations of data as seepage are no longer appropriate and that previous data sets, when set in a global context, often represent normal background hydrocarbon levels. A critical aspect of this re-assessment has been an increased understanding of the technologies employed and the difficulties of working in the Australian environment. For example, strong tidal currents and high tidal ranges on the North West Shelf have effects that are observed on SAR images and can be potentially misinterpreted as natural hydrocarbon seepage. Furthermore, the presence of large carbonate build-ups can have effects on sea surface roughness during current movements and, at specific times of the year, can provide a source of coral spawn (Jones et al., 2005 & 2006). The re-assessment has also been important for documenting issues related to specific technologies, such as ALF, and to improve confidence limits for data interpretation, for example with 'Sniffer' and head space gas data

The downgrading of many previously published seepage interpretations has lead to the conclusion that there are few sites of proven hydrocarbon seepage around Australia. The exception to this is the Yampi Shelf, Timor Sea, where the best examples of both palaeo- and currently active seepage have been described. To increase success of detecting natural hydrocarbon seepage around Australia's margin, data need to be interpreted both within the context of the local geological setting, and with an understanding of what is observed globally, to avoid misinterpreting normal background variation. The tectonic, environmental and geomorphological setting determines the mode of seepage and influences the potential for successful seepage detection. Active faulting to the sea-floor and rapid subsidence and burial will improve the chances of hydrocarbon expulsion to the shallow subsurface and development of natural hydrocarbon seeps. The potential for geophysical and geochemical characterisation of thermogenic seeps is improved in deep-water

siliciclastic environments, as compared with shallow, carbonate shelves. We can now be more confident about which techniques are best suited for seepage studies and, importantly, where and when the techniques can best be applied in Australian waters.

Acknowledgements

We thank the masters and crews of the marine vessels that were utilised for seepage surveys, including the *Parmelia K*, *RV Southern Surveyor*, *RV Marion Dufresne* and *RV Sonne*. We also thank Mike Abrams (formerly EGI, Uni of Utah), Alan Judd and Steve McGiveron (consultants) for their help and advice in geochemical, seismic and sub-bottom profiler interpretation of seepage signatures and potential shallow gas features. The geochemical understanding of seepage and its representation globally has greatly benefited from participation in the multi-client Surface Geochemistry Callibration Study organised by Michael Abrams and feedback generated from sponsor companies.

Particular thanks are due to Geoscience Australia technical staff from the Field and Engineering Support Project for assistance with all aspects of the surveys and data acquisition. We also thank fellow Geoscience Australia scientific staff for assistance with data acquisition, processing and interpretation throughout the surveys, and sedimentology and geochemical laboratory staff for post-survey sample analyses.

Infoterra Ltd (www.infoterra.co.uk) and NPA Ltd (www.npagroup.com) are acknowledged for their assistance in accessing SAR data and slick interpretations from around Australia.

Finally, Heike Struckmeyer and Phil O'Brien (both GA) are gratefully thanked for their constructive comments and review of this report.

References

Abrams, M. (1992) Geophysical and geochemical evidence for subsurface hydrocarbon leakage in the Bering Sea, Alaska. Marine and Petroleum Geology, 9, 208-221.

Abrams, M. (2005) Significance of hydrocarbon seepage relative to petroleum generation and entrapment. Marine and Petroleum Geology, 22, 457-477.

Abrams M.A., Francu E., Dahdah N.F. and Logan G.A. (2004) Surface Geochemistry Calibration Study Phase II: Laboratory Studies. Energy and Geoscince Institute at the University of Utah, EGI Technical Report No. 2004-50501003. Volumes I-III.

Abrams, M.A., Logan, G.A and Dahdah, N.F. (2007) Surface Geochemistry Calibration Study Phase III : Field Studies. Energy and Geoscince Institute at the University of Utah, EGI Technical Report No. 2007-50501254. Volumes I-III.

Adamo, M., de Carolis, G., de Pasquale, C. and Pasquariello, G. (2006) On the combined use of sun glint MODIS and MERIs signatures and SAR data to detect oil slicks. In: Remote Sensing of the Ocean Sea Ice and Large Water Regions, Proceedings of SPIE Vol 6360.

Alcazar, F., Kennicutt, M.C., Brooks, J.M., 1989. Benthic tars in the Gulf of Mexico: Chemistry and sources. Organic Geochemistry 14, 433-439.

Alexander, R. Currie, T.I. and Kagi, R.I. (1994) The origin of coastal bitumens from Western Australia. APEA Journal, 34, 787-798.

Aloisi, G., Pierre, C., Rouchy, J.-M., Foucher, J.-P. and Faugeres, J.-C. (2002) Isotopic evidence of methane-related diagenesis in the mud volcanic sediments of the Barbados accretionary prism. Continental Shelf Research, 22, 2355-2372.

Ashley, G.M., Boothroyd, J.C., Bridge, J.S., Clifton, H.E., Dalrymple, R.W., Elliot, T., Flemming, B.W., Harms, J.C., Harris, P.T., Hunter, R.E., Kreisa, R.D., Lancaster, N., Middleton, G.V., Payla, C., Rubin, D.M., Smith, J.D., Southard, J.B., Terwindt, J.H.T., Twichell, D.C., Jr. (1990) Classification of large-scale subaqueous bedforms: A new look at an old problem. Journal of Sedimentary Petrology, 60, 160-172.

Begg, A. C. and Begg, N. C. (1979) The world of John Boultbee: Including an Account of Sealing in Australia and New Zealand. Witcoulls, Christchurch, 329 pp.

Berridge, S.A., Dean, R.A., Fallows, R.G. Fish, A. (1968) The properties of persistent oils at sea. Journal of the Institute of Petroleum, 54, 300-309.

Bishop D.J. and O'Brien G.W. (1998) A multi-disciplinary approach to definition and characterisation of carbonate shoals, ahllow gas accumulations and related complex near-surface sedimentary structures in the Timor Sea. APPEA Journal 1998, 93-114.

Bishop, J.H., O'Brien, G.W., Bickford, G.P., and Heggie, D.T. (1992) Light hydrocarbon geochemistry of the Bonaparte Basin, including the Sahul Syncline, Malita Graben and Southern Petrel Sub-Basin: Rig Seismic Survey 100. BMR Record 1992/47.

Blough, N.V. and Del Vecchio, R. (2002) Chromophoric DOM in the coastal environment. In: Hansell, D.A. and Carlson, C.A. (eds) Biogeochemistry of Marine Dissolved Organic Matter, Academic Press, San Diego, CA, 509-546.

Boetius, A., Ravenschlag, K., Schubert, C.J., Rickert, D., Widdel, F., Gieseke, A., Amann, R., Jorgensen, B.B., Witte, U. and Pfannkuche, O. (2000) A marine microbial consortium apparently mediating anaerobic oxidation. Nature, 407, 623-626.

Boles, J.R., Clark, J.F., Leifer, I. and Washburn, L. (2001) Temporal variation in natural methane seep rates due to tides, Coal Oil Point area, California. Journal of Geophysical Research 106 (C11), 27077-27086.

Boreham, C.J. Krassay, A.K. and Totterdell, J.M. (2001) Geochemical comparisons between asphaltites on the southern Australian margin and source rock analogues of Early Cretaceous age. Eastern Australian Basins Symposium, 531-541.

Bohrmann, G., Greinert, J., Suess, E. and Torres, M. (1998) Authigenic carbonates from the Cascadia subduction zone and their relation to gas hydrate stability. Geology, 26, 647-650.

Bohrmann, G., Heeschen, K., Jung, C., Weinrebe, W., Baranov, B., Cailleau, B.,

Heath, R., Hühnerbach, V., Hort, M., Masson, D. and Trummer, I. (2002) Widespread fluid expulsion along the seafloor of the Costa Rica convergent margin. Terra Nova, 14, 69-79.

Boult, P.J., McKirdy, D.M., Blevin, J.E., Heggeland, R., Lang, S.C. and Vinall, D.R. (2006) The oil-prone Mornum Sub-basin petroleum system, Otway Basin, South Australia. PESA News, 80, 24-27.

Bouriak, S., Vanneste, M. and Saoutkine, A. (2000) Inferred gas hydrates, shallow gas accumulations and clay diapirs on the southern edge of the Voring Plateau, offshore Norway. Marine Geology, 163, 125-148.

Brando, V.E. and Dekker, A.G. (2003) Satellite hyperspectral remote sensing for estimating estuarine and coastal water quality. IEEE Trans.Geosci.Remote Sens., 41, 1378-1387.

Brekke, C. and Solberg, A.H.S. (2005) Oil spill detection by satellite remote sensing. Remote Sensing of Environment, 95, 1-13.

Brooks, J.M., Kennicutt, M.C., Fay, R.R., McDonald, T.J. and Sassen, R. (1984) Thermogenic gas hydrates in the Gulf of Mexico. Science, 223, 696-698.

Brough-Smyth, R. (1869) The Goldfields and Mineral Districts of Victoria. John Ferres. Government Printer, Melbourne, 644 pp.

Brown, H.Y.L (1898) Report by the Government Geologist. Parliamentary Papers relating to Exploration, Mining and Geology, 6, 1-5.

Brunskill, G.J., Burns, K.A. and Opdyke, B. (2005) Biogeochemical processes, effects and signatures of hydrocarbon and ground-water seepage within a tropical, carbonate-rich system: Australia's Timor Sea. *RV Southern Surveyor* Voyage Summary SS06/2005 (http://www.marine.csiro.au/nationalfacility/voyagedocs/2005/Summary_SS06-2005.pdf).

Burckhardt, D.M. and Bradshaw, J. (1991) Northern Territory bitumen strandings report no. 1. BHP Petroleum Pty. Ltd.

Burns, B.J. and Emmet, J.K. (1984) Final report GE 83B geochemical (sniffer) survey Gippsland Basin offshore. November 1983. Esso Australia ltd, Unpublished Geochemical report, August 1984. Bureau of Mineral Resources P(SL)A 83/47.

Burns, K.A., Greenwood P.F., Summons R.E. and Brunskill G.J. (2001) Vertical fluxes of hydrocarbons on the North West Shelf of Australia as estimated by a sediment trap experiment. Organic Geochemistry, 32, 1241-1255.

Burns K.A., Brunskill G.J., Zagorskis I. and Pfitzner J. (2003) Chemical oceanography of the Cartier Trough/Karmt Shoal of the Timor Sea margin: Search for the seeps. In Ellis G.K., Baillie P.W. and Munson T.J. (eds) Proceedings of the Timor Sea Symposium 2003, p323-332.

Bussmann, I. and Suess, E. (1998) Groundwater seepage in Eckernforde Bay (western Baltic sea): effect on methane and salinity distribution of the water column. Continental Shelf Research, 18, 1795-1806.

Butenko, J., Milliman, J.D. and Ye, Y.-C. (1985) Geomorphology, shallow structure, and geological hazards inn the East China Sea. Continental Shelf Research, 4, 121-141.

Byfield, V. and Boxall, S.R. (1998) Thickness estimates and classification of surface oil using passivesensing at visible and near-infrared wavelengths. Geoscience and Remote Sensing Symposium, 1999. IGARSS '99 Proceedings. IEEE 1999 International

Campbell, K. (2006) Hydrocarbon seep and hydrothermal vent paleoenvironments and paleontology: Past developments and future research directions. Palaeogeography, Palaeoclimatology, Palaeoecology, 232, 362-407.

Carlson, P.R., Golan-Bac, M., Karl, H.A. and Kvenvolden, K.A. (1985) Seismic and geochemical evidence for shallow gas in sediment of Navarin Continental Margin, Bering Sea. AAPG Bulletin, 69, 422-436.

Casas, D., Ercilla, G. and Baraza, J. (2003) Acoustic evidences of gas in the continental slope sediments of the Gulf of Cadiz (E Atlantic). Geo-Marine Letter, 23, 300-310.

Chen, G., Hill, K.C. AND Hoffman, N. (2002) 3D structural analysis of hydrocarbon migration in the Vulcan Sub-basin, Timor Sea. In: Keep, M. and Moss, S.J. (eds), The Sedimentary Basins of Western Australia 3, Proceedings of the Petroleum Exploration Society of Australia Symposium, Perth, 2002, 377-388.

Chopra, S. and Marfurt, K.J., 2006. Seismic Attribute Mapping of structure and stratigraphy – Distinguished Instructor Series, No.9, sponsored by Society of Exploration Geophysicists and European Association of Geoscientists & Engineers, 226 pp.

Chow, J., Lee, J.S., Liu, C.S., Lee, B.D. and Watkins, J.S. (2001) A submarine canyon as the cause of a mud volcano – Liuchienuyu Island in Taiwan. Marine Geology, 176, 55-63.

Christodoulou, D., Papatheodorou, G., Ferentinos, G. and Masson, M. (2003) Active seepage in two contrasting pockmark fields in the Patras and Corinth gulfs, Greece. Geo-Marine Letter, 23, 194-199.

Chust, G and Sagarminaga, Y. (2007). The multi-angle view of MISR detects oil slicks under sun glitter conditions. Remote Sensing of Environment, 107, 232–239.

Clarke, R.H. and Cleverly, R.W. (1991) Petroleum seepage and post-accumulation migration. In: England, W.A. and Fleet, A.J. (eds) Petroleum Migration, Geological Society, Special Publication, 59, 265-271.

Clarke, R.H., Grant, A.I., Macpherson, M.T., Stevens, D.G., Stephenson, M. (1988) Petroleum exploration with BP's Airborne Laser Fluorosensor. Proceedings of the Indonesian Petroleum Association, IPA 17, 387-395.

Clay, C.S. and Medwin, H. (1977) Acoustical Oceanography: principles and applications. John Wiley and Sons, New York, 544 pp.

Clayton, C.J., Lines, M.D. and Hay, S.J. (1991) Leakage and seepage, an explorers guide: BP internal report, now available from Robertson Research International, 65 pp.

Coble, P.G., Del Castillo, C.E. and Avril, B. (1998) Distribution and optical

properties of CDOM in the Arabian Sea during the 1995 Southwest Monsoon. Deep-Sea Research II, 45, 2195-2223.

Cole, G.A., Yu, A., Peel, F., Requejo, R., DeVay, J., Brooks, J., Bernard, B.B., Zumberge, J., Brown, S. (2001) Constraining source and charge risk in deepwater areas In: WorldOil magazine, 222.

Conti, A., Stefanon, A. and Zuppi, G. (2002) Gas seeps and rock formation in the northern Adriatic Sea. Continental Shelf Research, 22, 2333-2344.

Cooper, G.T., Barnes, C.R., Bourne J.D. and Channon, G.J. (1998) Hydrocarbon leakage on the North West Shelf, Australia: New information from the integration of airborne laser fluorosensor (ALF) and structural data. In Purcell, P.G and R.R. (eds) The Sedimentary Basins of Western Australia 2. Procedings Western Australian Basins Symposium, Perth, 1998, 255-272

Cowley, R. (2000a) 1996 Laminaria High, Northern Bonaparte Basin (AC/P8) Airborne Laser Fluorosensor Survey Interpretation Report [WGC AC/P8 Survey Number 1248.2]. AGSO Record 2000/29, 22 pp.

Cowley, R. (2000b) 1996 Nancar Trough, Northern Bonaparte Basin (AC/P16) Airborne Laser Fluorosensor Survey Interpretation Report [WGC AC/P16 Survey Number 1248.3]. AGSO Record 2000/28, 20 pp.

Cowley, R. (2000c) 1996 Yampi Shelf, Browse Basin Airborne Laser Fluorosensor Survey Interpretation Report [WGC Browse Survey Number 1248.1]. AGSO Record 2000/31, 17 pp.

Cowley, R. (2000d) 1996 Vulcan Sub-basin/Browse Basin Transition Airborne Laser Fluorosensor Survey Interpretation Report [WGC Haydn Survey Number 2051]. AGSO Record 2000/32, 25 pp.

Cowley, R. (2000e) 1996 Vulcan Sub-basin Airborne Laser Fluorosensor Survey Interpretation Report [WGC Vulcan Graben Survey Number 1113]. AGSO Record 2000/33, 28 pp.

Cowley, R. (2000f) 1998 Yampi Shelf, Browse Basin Airborne Laser Fluorosensor

Survey Interpretation Report [WGC Yampi Survey]. AGSO Record 2000/30, 26 pp.

Cowley, R. (2001a) MkII Airborne Laser Fluorosensor Survey Reprocessing And Interpretation Report: Great Australian Bight, Southern Australia. AGSO – Geoscience Australia Record 2001/18, 53 pp.

Cowley, R. (2001b) MkII Airborne Laser Fluorosensor Survey Reprocessing And Interpretation Report: Perth Basin, Western Australia. AGSO – Geoscience Australia Record 2001/19, 32 pp.

Cowley, R. (2001c) MkII Airborne Laser Fluorosensor Survey Reprocessing And Interpretation Report: Barrow Sub-basin, Carnarvon Basin, North West Shelf, Australia. AGSO – Geoscience Australia Record 2001/20, 21 pp.

Cowley, R. (2001d) MkII Airborne Laser Fluorosensor Survey Reprocessing And Interpretation Report: Browse Basin, North West Shelf, Australia. AGSO – Geoscience Australia Record 2001/21, 24 pp.

Cowley, R. (2001e) MkII Airborne Laser Fluorosensor Survey Reprocessing And Interpretation Report: Arafura Sea, Australia. AGSO – Geoscience Australia Record 2001/22, 24 pp.

Cowley, R. (2001f) MkII Airborne Laser Fluorosensor Survey Reprocessing And Interpretation Report: Timor Sea, Australia. AGSO – Geoscience Australia Record 2001/23, 26 pp.

Cowley, R. (2001g) MkII Airborne Laser Fluorosensor Survey Reprocessing And Interpretation Report: Bonaparte Baisn, Timor Sea, Australia. AGSO – Geoscience Australia Record 2001/24, 32 pp.

Cowley, R. (2001h) MkII Airborne Laser Fluorosensor Survey Reprocessing And Interpretation Report: Timor Gap, Timor Sea, Australia. AGSO – Geoscience Australia Record 2001/25, 34 pp.

Cowley R. and O'Brien G.W. (2000) Identification and interpretation of leaking hydrocarbons using seismic data: A comparative montage of examples from the major fields in Australia's North West Shelf and Gippsland Basin. APPEA Journal 2000,

121-149.

Currie, T.I., Alexander, R and Kagi, R.I (1992) Coastal bitumens from Western Australia – long distance transport by ocean currents. Organic Geochemistry, 18, 595-601.

Currie, T.I., Alexander, R. and Kagi, R.I. (1998) Evidence for a submarine oil seep in the offshore Perth Basin. In Purcell, P.G and R.R. (eds) The Sedimentary Basins of Western Australia 2. Procedings Western Australian Basins Symposium, Perth, 1998, 637-645.

D'Arrigo, J.S. (1986) Stable Gas-in-Liquid Emulsions. Elsevier, Amsterdam.

Dean, K.G., Stringer, W.J., Groves, J.E., Ahlinas, K. and Royer, T.C. (1990) The EXXON VALDEZ Oil Spill: Satellite Analyses, in *Oil Spills: Management and Legislative Implications*, M.L. Spaulding and M. Reed, eds., American Society of Civil Engineers, New York, 492- 502.

Dekker, A. G. and Peters, S.W.M. (1993) The use of the Thematic Mapper for the analysis of eutrophic lakes: A case study in The Netherlands, International Journal of Remote Sensing, 14, 799-822.

Del Sontro, T.S., Liefer, I., Luyendyk, B.P. and Broitman, B.R. (2007) Beach tar accumulation, transport mechanisms, and sources of variability at Coal Oil Point, California. Marine Pollution Bulletin, 54, 1461-1471.

Determann, S., Reuter, R. and Willkomm, R. (1996) Fluorescent matter in the eastern Atlantic Ocean. Part 2: vertical profiles and relation to water masses. Deep-sea research. Part 1. Oceanographic research papers, 43, 345-360.

Diaz-del-Rio, V., Somoza, L. and Martinez-Frias, J. (2003) Vast fields of hydrocarbon-derived carbonate chimneys related to the accretionary wedge/oligostrome of the Gulf of Cadiz. Marine Geology, 195, 177-200.

Diggens, J., Farman, A., Kendell, R. and Dollan C. (2006a) Global Seeps, SSW Australia, Cat#64743. available through *Geoscience Australia* Sales Centre. www.ga.gov.au

Diggens, J., Farman, A., Kendell, R. and Dollan C. (2006b) Global Seeps, ESE Australia, Cat#64742. available through *Geoscience Australia* Sales Centre. www.ga.gov.au

Dix, G.R., James, N.P., Kyser, T.K., Bone, Y. and Collins, L.B. (2005) Genesis and dispersal of carbonate mud relative to late Quaternary sea-level change along a distally-steepened carbonate ramp (Northwestern Shelf, Western Australia). Journal of Sedimentary Research, 75, 665-678.

Dowling, L. M., Boreham, C.J., Hope, J.M., Murray, A.P. and Summons, R.E. (1995) Carbon-isotopic composition of hydrocarbons in the ocean-transported bitumens from the coastline of Australia. Organic Geochemistry, 23, 729-737.

DPIFM (2007) Department of Primary Industry, Fisheries and Mines, Northern Territory – Northern Territory Oil and Gas 2006. Northern Territory Government, Publication, April 2007.

Edwards, D.S. and Crawford, N., 1999. UV Fluorescence Analysis of Seawater Samples from AGSO Marine Survey 207, Northwest Australia. AGSO Record 1999/52, 7, unpublished.

Edwards, D., McKirdy, D.M. and Summons, R.E. (1998) Enigmatic asphaltites from the southern Australian margin: molecular and carbon isotopic composition. PESA Journal, 26, 106-130.

Ellis, J.P. and McGuinness, W.T. (1986) Pockmarks of the northwestern Arabian Gulf. In: Proceedings of the Oceanology International Conference (Brighton, March 1986). Advances in Underwater Technology, Ocean Science and Offshore Engineering, vol 6. Graham and Trotman, London, 353-367.

Ergün, M., Dondurur, D. and Cifçi, G. (2002) Acoustic evidence for shallow gas accumulations in the sediments of the Eastern Black Sea. Terra Nova, 14, 313-320.

Espedal H.A., Johannessen, O.M. and Knulst, J.C. (1996) Satellite detection of natural films on the ocean surface. Geophysical Research Letters, 23, 3151-3154.

Fader, G.B.J. (1991) Gas-related sedimentary features from the eastern Canadian

continental shelf. Continental Shelf Research, 11, 1123-1153.

Faure, K., Greinert, J., Pecher, I.A., Graham, I.J., Massoth, G.J., De Ronde, C.E.J., Wright, I.C., Bakers, E.T. and Olson, E.J. (2006) Methane seepage and its relation to slumping and gas hydrate at the Hikurangi margin, New Zealand. New Zealand Journal of Geology and Geophysics, 49, 503-516.

Fingas, M. and Fieldhouse, B. (2003) Studies of the formation process of water-in-oil emulsions. Marine Pollution Bulletin, 46, 369-396.

Fleischer, P., Orsi, T.H., Richardson, M.D. and Anderson, A.L. (2001) Distribution of free gas in marine sediments: a global overview. Geo-Marine Letters, 21, 103-122.

Flemming, B.W. (1988) Zur Klassifikation subaquatischer, strömungstransversaler Transportkörper, Bochumer Geol. Geotechn. Arb., 29, 44-47.

Fujii, T., O'Brien, G.W., Tingate, P AND Chen, G. (2004) Using 2D and 3D basin modelling to investigate controls on hydrocarbon migration and accumulation in the Vulcan Sub-basin, Timor Sea, northwestern Australia. The APPEA Journal 44(1), 93-122.

Gaedicke, C., Baranov, B.V., Obzhirov, A.I., Lelikov, E.P., Belykh, I.N. and Basov, E.I. (1997) Seismic stratigraphy, BSR distribution, and venting of methane-rich fluids west of Paramushir and Onekotan islands, northern Kurils. Marine Geology, 136, 259-276.

García-García, A., García-Gil, S. and Vilas, F. (2004) Echo characters and recent sedimentary processes as indicated by high-resolution sub-bottom profiling in Ría de Vigo (NW Spain). Geo-Marine Letters, 24, 32-45.

Gay, A., Lopez, M., Cochonat, P., Sultan, N., Cauquil, E. and Brigaud, F. (2003) Sinuous pockmark belt as indicator of a shallow buried turbiditic channel on the lower slope of the Congo basin, West African margin. In: Van Rensbergen, P., Hillis, R.P., Maltan, A.J. and Morley, C.K. (eds) Subsurface Sediment Mobilization. Geological Society, London, Special Publication, 216, 173-189.

Geodekyan, A.A., Berlin, Y.A., Bol'shakov, A.M. and Trotsyuk, V.Y. (1991)

Distribution of methane in sediments and bottom water of the southern Baltic Sea. Oceanology, 31, 54-59.

Geyer, R.A. and Giammona, C.P (1980) Naturally occurring hydrocarbons in the Gulf of Mexico and Caribbean Sea. In Geyer, R.A. (Ed.) Marine Environmental Pollution, 1 Hydrocarbons. Elsevier Scientific, Amsterdam, p. 37-106.

Ghisalberti, E.L. and Godfrey, I.M. (1990) The application of nuclear magnetic resonance spectroscopy to the analysis of pitches and resins from marine archaeological sites. Bull. Aust. Inst. Marine Archaeology, 14, 1-8.

Ghisalberti, E.L. and Godfrey, I.M. (1998) Application of nuclear magnetic resonance spectroscopy to the analysis of organic and archaeological materials. Studies in Conservation, 43, 215-230.

Gibbs, H. D. (1994) An Archaeological Conservation Management Study of 19th Century Shore Based Whaling Stations in Western Australia. A report to the National Trust of Australia for the Australian Heritage Commission.

Ginsburg, G.D. and Soloviev, V.A. (1994) Mud volcano gas hydrates in the Caspian Sea. Bulletin of the Geological Society of Denmark, 41, 95-100.

Goodman, R. (2003) Tar Balls: The end state. Spill Science and Technology Bulletin, 8, 117-121.

Granin, N.G. and Granina, L.Z. (2002) Gas hydrates and gas venting in Lake Baikal. Geologiya i Geofizika (Russian Geology and Geophysics), 42, 360-370 (Russian edn.)/362-372 (English edn.)

Greinert J and Nützel B (2004); Hydroacoustic experiments to establish a method for the determination of bubble fluxes at cold seeps. Geo-Marine Letters, 24, 75-85.

Greinert, J., Artemov, Y., Egorov, V., De Batist, M. and McGinnis, D. (2006) 1300-m-high rising bubbles from mud volcanoes at 2080 m in the Black Sea: Hydroacoustic characteristics and temporal variability. Earth and Planetary Science Letters, 244, 1-15.

Greinert, J., Bialas, J., Lewis, K. and Suess, E. (in prep) Methane seeps and gas

hydrates offshore New Zealand's North Island: Compiling results from three cruises in 2006 and 2007. Marine Geology.

Grosjean E. and Logan G.A. (2007) Incorporation of organic contaminants in geochemical samples and an assessment of potential sources: Examples from Geoscience Australia's marine survey S282. Organic Geochemistry, 38, 835-869.

Grosjean E. , Logan G. A. , Rollet N., Ryan G. J. and Glenn K. (2007) Geochemistry of shallow tropical marine sediments from the Arafura Sea, Australia. Organic Geochemistry, 38, 1953-1971.

Hallegraeff, G.M. and Jeffrey, S.W. (1984) Tropical phytoplankton species and pigments of continental shelf waters of north and north-west Australia. Marine Ecology Progress Series, 20, 59-74.

Hampton, L.D. and Anderson, A.L. (1974) Acoustics and gas in sediments. In: Kaplan, I.R. (ed.) Natural Gases in Marine Sediments. Marine Science Series No. 3. Plenum Press, New York, 249-274.

Harahsheh, H., Essa, S., Shiobara, M., Nishidai, T. and Onuma, T. (2004) Operational satellite monitoring and detection for oil spill in offshore of United Arab Emirates. Proceeedings of the ISPRS conference, Istanbul. http://www.isprs.org/istanbul2004/comm7/papers/130.pdf.

Harris, P.T., Ashley, G.M., Collins, M.B. and James, A.E. (1986) Topographic features of the Bristol Channel sea-bed: a comparison of SEASAT (synthetic aperture radar) and sidescan sonar images. International Journal of Remote Sensing, 7, 119-136.

Harrowfield, M. and Keep, M. (2005) Tectonic modification of the Australia North-West shelf: Episodic rejuvenation of long-lived basin divisions. Basin Research, 17, 225-239.

Hart, B.S., and Hamilton, T.S. (1993) High resolution acoustic mapping of shallow gas in unconsolidated sediments beneath the strait of Georgia, British Colombia. Geo-Marine Letters 13: pp49-55.

Hasiotis, T., Papatheodorou, G., Kastanos, N. and Ferentinos, G. (1996) A pockmark field in the Patras Gulf (Greece) and its activation during the 14/7/93 seismic event. Marine Geology, 130, 333-344.

Hedley, J. D., Harborne, A. R. and Mumby, P. J. (2005) Simple and robust removal of sun glint for mapping shallow-water benthos. International Journal of Remote Sensing, 26, 2107-212.

Heeschen, K.U., Trehu, A.M., Collier, R.W., Suess, E. and Rehder, G. (2003) Distribution and height of methane bubble flares on the Cascadia Margin characterized by acoustic imaging. Geophysical Research Letters, 30, doi:10.1029/2003GL016974.

Heggie, D., McKirdy, D., Exon, N and Lee, C.S. (1988) Hydrocarbon gases, heat-flow and development of the offshore Otway Basin. PESA Journal, 13, 32-42.

Heggie, D.T., Falvey, D.A. and Hartman, B. (1990) Joint geochemical research: An agreement between the Commonwealth of Australia and Transglobal Exploration and Geoscience (USA). BMR Record 1990/74.

Hinrichs, K.-U., Hayes, J.M., Sylva, S.P., Brewer, P.G., DeLong, E.F. (1999) Methane-consuming archaebacteria in marine sediments. Nature, 398, 802-805.

Hinrichs, K.-U., Summons, R.E., Orphan, V., Sylva, S.P., Hayes, J.M. (2000) Molecular and isotopic analysis of anaerobic methane-oxidizing communities in marine sediments. Organic Geochemistry, 31, 1685-1701.

Hinz, K., Wilcox, J.B., Whiticar, M., Kudrass, H.R., Exon, N.F. and Feary, D.A. (1986) The West Tasmanian Margin: An underrated petroleum province? In Glenie, R.C. (ed) Second South-Eastern Australia Oil Exploration Symposium, Petroleum Exploration Society of Australia, 395-410

Hochberg E J, Andrefouet, S. and Tyler, M.R. (2003) Sea surface correction of high spatial resolution Ikonos images to improve bottom mapping in near-shore environments. IEEE Transactions on Geoscience and Remote Sensing, 41, 1724-1729

Hood, K.C., Gross, O.P., Wenger, L.M. and Harrison, S.C. (2002) Hydrocarbon

systems analysis of the northern Gulf of Mexico: Delineation of hydrocarbon migration pathways using seeps and seismic imaging. In Schumacher, D. and LeSchack, L.A. (eds) Surface Exploration Case Histories, AAPG Studies in Geology No. 48 and SEG Geophysical References Series No. 11, 25-40.

Hörig, H., Kühn, F., Oschütz, F. and Lehmann, F. (2001). HyMap hyperspectral remote sensing to detect hydrocarbons. Int. J. Remote Sensing, 22, 1413-1422.

Hornafius, J.S., Quigley, D. and Luyendyk, B.P. (1999) The world's most spectacular marine hydrocarbon seeps (Coal Oil Point, Santa Barbara Channel, California): quantification of emissions. Journal of Geophysical Research, 104, 20703-11.

Horvitz, L. (1985) Geochemical exploration for petroleum. Science, 229, 812-827.

Hostettler, F.D., Rosenbauer, R.J., Lorenson, T.D. and Dougherty, J. (2004) Geochemical characterization of tarballs on beaches along the California coast. Part I – Shallow seepage impacting the Santa Barbara Channel Islands, Santa Cruz, Santa Rosa and San Miguel. Organic Geochemistry, 35, 725-746.

Hovland, M., 1992. Hydrocarbon Seeps in Northern Marine Waters – Their Occurrence and Effects. Palaios, V.7, pp376-382.

Hovland, M., 1993. Submarine gas seepage in the North Sea and adjacent areas. In: Parker, J.R. (Ed.) Petroleum Geology of Northwest Europe: Proceedings of the 4th Conference, The Geological Society, London, 1333-1338.

Hovland, M. and Judd, A.G. (1988) Seabed pockmarks and seepages: Impact on Geology, Biology and the Marine Environment. Graham and Trotman, London, 293 pp.

Hovland, M., Judd, A.G. and King, L.H. (1984) Characteristic features of pockmarks on the North Sea Floor and Scotian Shelf. Sedimentology, 31, 471-480.

Hovland, M., Croker, P.F. and Martin M. (1994) Fault-associated seabed mounds (carbonate knolls?) off western Ireland and north-western Australia. Marine and Petroleum Geology, 11, 232-245.

Hovland, M., Gallagher, J. W., Clennell, M. B. and Lekvam, K. (1997) Gas hydrate

and free volumes in marine sediments: Example from Niger delta front. Marine and Petroleum Geology, 14, 245-255.

Hovland, M., Mortensen, P.B., Brattegard, T., Strass, P. and Rokoengen, K. (1998) Ahermatypic coral banks off mid-Norway: evidence for a link with seepage of light hydrocarbons. Palaios, 13, 189-200.

Hu, C., Muller-Karger, F.E., Taylor, C., Myhre, D., Murch, B., Odriozola, A.L. and Godoy, G. (2003) MODIS detects oil spills in Lake Maracaibo, Venezuela. Eos, Transactions of the American Geophysical Union, 84 (33), 19 August 2003, 313-319.

Huang, B.J., Xiao, X.M. and Dong, W.L. (2002) Multiphase natural gas migration and accumulation and its relationship to diapir structures in the DF1-1 gas field, South China Sea. Marine and Petroleum Geology, 19, 861-872.

Huettel, M., Ziebis, W., Forster, S. (1996) Flow-induced uptake of particulate matter in permeable sediments. Limnology and Oceanography, 41, 309-322.

IAM (2000) Summary report on mapping and characterising of natural hydrocarbon seepage in Australia's Timor Sea using Landsat TM data: A pilot project with AGSO Petroleum and Marine Division. Image Analysis and Mapping Pty Ltd. Unpublished, 5 pp.

Infoterra (2005) North West Shelf Australia, global seeps database (commercial, non-exclusive report). Details available at http://www.infoterra.co.uk/applications_ogm_global.php

Ingram, G.M., Eaton, S. and Regtien, J.M.M. (2000) Cornea case study: lessons for the future. APPEA Journal, 40, 56-64.

Irvine, G.V., Mann, D.H. and Short, J.W. (1999) Multiyear persistence of oil mousse on high energy beaches distant from the Exxon Valdez spill origin. Marine Pollution Bulletin, 38, 572-584.

Ivanov, A.Y. (2000) Oil pollution of the sea on Kosmos -1870 and Almaz-1 radar imagery. Earth Observation & Remote Sensing, 15, 949-966.

Jackson, D.R., Williams, K.L., Wever, T.F., Friedrichs, C.T. and Wright, L.D. (1998)

Sonar evidence for methane ebullition in Eckernforde Bay. Continental Shelf Research, 18, 1893-1916.

James, N.P., Bone, Y., Kyser, T.K., Dix, G.R. and Collins, L.B. (2004) The importance of changing oceanography in controlling late Quaternary carbonate sedimentation on a high-energy, tropical, oceanic ramp: north-western Australia. Sedimentology, 51, 1179-1205.

Jensen, P., Aagaard, I., Burke, R.A., Dando, P.R., Jorgensen, N.O., Kuijpers, A., Laier, T., O'Hara, S.C.M. and Schmaljohann, R. (1992) Bubbling reefs in the Kattegat: submarine landscapes of carbonate-cemented rocks support a diverse ecosystem at methane seeps. Marine Ecology Progress Series, 83, 103-112.

Jeong, K.S.Cho, J.H., Kim, S.R., Hyun, S., Tsunogai, U. (2004) Geophysical and geochemical observations on actively seeping hydrocarbon gases on the south-eastern Yellow Sea continental shelf. Geo-Marine Letters, 24, 53-62.

Jerosch, K., Allais, A.-G., Schluter, M. and Foucher, J.-P. (2004) Geo-referenced video-mosaicking as a means to GIS-supported sea floor community mapping at Hakon Mosby mud volcano. First General Congress, European Geosciences Union, Nice, 25-30 April (poster). (See Geophysical Research Abstracts, 6, 00669.)

Johannessen, J.A., Røed, L.P. and Wahl, T. (1993) Eddies detected in ERS-1 SAR images and simulated in reduced gravity model. International Journal of Remote Sensing, 14, 2203-2213.

Johannessen, J.A., Digranes, G., Espedal, H., Johannessen, O.M., Samuel, P., Browne, D. and Vachon P. (1994) SAR ocean feature catalogue. European Space Agency, Noordwijk, The Netherlands, 106.

Jones, A.T., Logan, G.A., Kennard, J.M., O'Brien, P.E., Rollet, N., Sexton, M., and Glenn, K.C. (2005a). Testing natural hydrocarbon seepage detection tools on the Yampi Shelf, northwestern Australia, Geoscience Australia Survey S267, Post Survey Report: GA Record 2005/15, 50 pp.

Jones, A.T., Logan G.A., Kennard J.M and Rollet, N. (2005b). Reassessing potential origins of Synthetic Aperture Radar (SAR) slicks from the Timor Sea Region of the

North West Shelf on the basis of field and ancillary data. APPEA Journal, 45, 311-331.

Jones, A.T., Thankappan, M., Logan, G.A., Kennard, J.M., Smith, C.J., Williams, A.K. and Lawrence, G.M. (2006). Coral spawn and bathymetric slicks in Synthetic Aperture Radar (SAR) data from the Timor Sea, northwest Australia, International Journal of Remote Sensing, 27, 2063-2069.

Jones, A.T., Kennard, J.M., Ryan, G.J., Bernadel, G., Earl, K.L., Rollet, N., Grosjean, E., Logan, G.A. (2008) Geoscience Australia Marine Survey SS06/2006 Post-Survey Report: Natural hydrocarbon seepage survey on the central North West Shelf. Geoscience Australia Record 2007/21.

Jones, A.T., Kennard, J.M., Logan, G.A., Grosjean, E., Marshall, J. (in prep) Anomalous sand waves and fluid expulsion features related to interstitial pore water flows in a mid-shelf setting. Marine Geology.

Josenhans, H.J. King, L.H. and Fader, G.B.J. (1978) A sidescan sonar mosaic of pockmarks on the Scotian Shelf. Canadian Journal of Earth Sciences, 15, 831-840.

Joye, S.B., Boetius, A., Orcutt, B.N., Montoya, J.P., Schulz, H.N., Erickson, M.J. and Lugo, S.K. (2004) The anaerobic oxidation of methane and sulfate reduction in sediments from Gulf of Mexico cold seeps. Chemical Geology, 205, 219-238.

Judd, A. (2001) Pockmarks in the UK sector of the North Sea. Technical report TR-002 produced for Strategic Environmental Assessment – SEA2 (dti), 70 pp.

Judd, A.G. and Hovland, M. (1992) The evidence of shallow gas in marine sediments. Continental Shelf Research, 12, 1081-1096.

Judd, A.G. and Hovland, M. (2007) Seabed Fluid Flow: The impact on Geology, Biology and the Marine Environment. Cambridge University Press, New York, 475 pp.

Judd, A.G., Hovland, M., Dimitrov, L.I., Garcia, G. and Jukes, V. (2002) The geological methane budget at continental margins and its influence on climate change. Geofluids, 2, 109-126.

Kahn, L.M., Silver, E.A., Orange, D., Kochevar, R. and McAdoo, B. (1996) Surficial evidence of fluid expulsion from the Costa Rica accretionary prism. Geophysical Research Letters, 23, 887-890.

Karisiddaiah, S.M. and Veerayya, M. (2002) Occurrence of pockmarks and gas seepages along the central western continental margin of India. Current Science, 82, 52-57.

Kasischke, E.S., Shuchman, R.A., Lyzenga, D.R. and Meadows, G.A. (1983) Detection of Bottom Features on Seasat Synthetic Aperture Radar Imagery. Photogrammetric Engineering and Remote Sensing, 49, 1341-53.

Keep, M., Clough, M. and Langhi, L. (2002) Neogene tectonics and structural evolution of the Timor Sea region, NW Australia. In: Keep, M. and Mos, S.J. (Eds), The Sedimentary Basins of Western Australia 3, Proceedings of the Petroleum Exploration Society of Australia Symposium, Perth, 2002, 341-353.

Kennard, J.M., Deighton, I., Edwards, D.S., Colwell, J.B., O'Brien, G.W. and Boreham, C.J. (1999) Thermal history modelling and transient heat pulses: new insights into hydrocarbon expulsion and 'hot flushed' in the Vulcan Sub-basin, Timor Sea. The APPEA Journal, 39, 177-207.

Kennard, J.M, Deighton, I., Ryan, D., Edwards, D.S. and Boreham, C.J. (2004) Subsidence and thermal history modelling: New insights into hydrocarbon expulsion from multiple petroleum systems in the Browse Basin. In Ellis, G.K., Baillie, P.W. and Munson, T.J. (eds) Timor Sea Petroleum Geoscience, Proceedings of the Timor Sea Symposium, Special Publication 1, 1-25.

King, L.H. and MacLean, B. (1970) Pockmarks on the Scotian Shelf. Geological Society of America Bulletin, 81, 3141-3148.

Klauke, I., Bohrmann, G. and Weinrebe, W. (2004) Estimation of the regional methane efflux on Hydrate Ridge, Oregon. First General Assembly of the European Geosciences Union, Nice, 25-30 April (poster). (See Geophysical Research Abstracts, 6, 03489.)

Klaucke, I., Sahling, H., Weinrebe, W., Blinova, V., Bürk, D., Lursmanashivili, N.

and Bohrmann, G. (2006) Acoustic investigation of cold seeps offshore Georgia, eastern Black Sea. Marine Geology, 231, 51-67.

Kostoglou, P. and McCarthy, J. (1991) *Whaling and Sealing Sites in South Australia*. Australian Institute for Maritime Archaeology, Special Publication No. 6.

Kruglyakova, R.P., Byakov, Y.A., Kruglyakova, M.V., Chalenko, L.A. and Shevtsova, N.T. (2004) Natural oil and gas seeps on the Black Sea floor. Geo-Marine Letters, 24, 150-162.

Kvenvolden, K.A. and Cooper, C.K. (2003) Natural seepage of crude oil into the marine environment. Geo-Marine Letters, 23, 140-146.

Lammers, S., Suess, E., Mansurov, M.N. and Anikiev, V.V. (1995) Variations in atmospheric methane supply from the Sea of Okhotsk induced by seasonal ice cover. Global Biogeochemical Cycles, 9, 351-358.

Lance, S., Henry, P., Le Pichon, X., Lallemant, S., Chamley, H., Rostek, F., Faugeres, J-C., Gonthier, E., and Olu. K. (1998) Submersible study of mud volcanoes seaward of the Barbados accretionary wedge: sedimentology, structure and rheology. Marine Geology, 145, 255-292.

Leifer, I. and Judd, A. (2002) Oceanic methane layers: The hydrocarbon seeps bubble deposition hypothesis. Terra Nova 16, 417–425.

Leifer, I., Luyendyk, B. and Broderick, K. (2006) Tracking an oil slick from multiple natural sources, Coal Oil Point, California. Marine and Petroleum Geology, 23, 621-630.

Lennon, M., Babichenko, S., Thomas, N., Mariette, V. and Mercier, G. (2006) Combining passive hyperspectral imagery and active fluorescence laser spectroscopy for airborne quantitative mapping. In: 4th EARSeL Workshop on Imaging Spectrometry, Warsaw, Poland, 27-29 April 2005.

Lewis, K.B. and Marshall, B.A. (1996) Seep faunas and other indicators of methane-rich dewatering on New Zealand convergent margins. New Zealand Journal of Geology and Geophysics, 39, 181–200.

Link, W.K. (1952) Significance of oil and gas seeps in world oil exploration. American Association of Petroleum Geologists Bulletin, 36, 1505-1540.

Lisk, M., O'Brien, G.W. and Brincat, M.P. (1997) Gas displacement; an important control on oil and gas distribution in the Timor Sea? The APPEA Journal, 37, 259-271.

Lisk, M., Brincat, M.P., Eadington, P.J. and O'Brien, G.W. (1998) Hydrocarbon charge in the Vulcan Sub-basin. In Purcell, P.G. & R.R. (Eds), The Sedimentary Basins of Western Australia 2. Proceedings of the Petroleum Exploration Society of Australia Symposium, Perth, 1998, 287-303.

Logan, G.A., Rollet, N., Glenn, K., Grosjean, E., Ryan, G.J. and Shipboard Party (2006). Shallow Gas and Benthic Habitat Mapping, Arafura Sea - Geoscience Australia Marine Survey 282, Post-Survey Report. Geoscience Australia, Record 2006/19, 342 pp.

Loney J. K. (1988) Wrecks along the Great Ocean Road: Shipwrecks on the West Coast from Point Lonsdale to Portland. 9th Edition, Dimboola, Victoria, 138 pp.

Loseth, H., Wensaas, L., Arntsen, B. and Hovland, M. (2003) Gas and fluid injection triggering shallow mud mobilization in the Hordaland Group, North Sea. In: Van Rensbergen, P., Hillis, R.R., Maltan, A.J. and Morley, C.K. (eds), Geological Society of London, Special Publication, 216, 139-157.

MacDonald, I.R., Reilly, J.F., Best S.E., Venkataramaiah, R., Sassen, R., Guinasso, N. and Amos, J. (1996) Remote sensing inventory of active oil seeps and chemosynthetic communities in the northern Gulf of Mexico. In: Schumacher, D. and Abrams, M.A. (eds.) Hydrocarbon migration and its near-surface expression. AAPG Memoir, 66, 27-37.

MacDonald, I.R., Leifer, I., Sassen, R., Stine, P., Mitchell, R. and Guinasso, N.Jr. (2002) Transfer of hydrocarbons from natural seeps to the water column and atmosphere. Geofluids, 2, 95-107.

MacDonald, I.R., Bohrmann, G., Escobar, E., Abegg, F., Blanchon, P., Blinova, V., Brückmann, W., Drews, M., Eisenhauer, A., Han, X., Heeschen, K., Meier, F., C.

Mortera, C., Naehr, T., Orcutt, B., Bernard, B., Brooks, J. and de Faragó, M. (2004) Asphalt volcanism and chemosynthetic life in the Campeche Knolls, Gulf of Mexico, Science 304, 999–1002.

Malthus, T.J. and Karpouzli, E. (2007). Passive remote sensing of marine oil slicks: A review of the State-of-the-Art. Report Number 001, For the EU MAPRES project, co-financed by the European Commission under the Community framework for cooperation in the field of accidental or deliberate marine pollution (No. 07.030900/2006/448578/SUB/A3).

Mortera, C., Naehr, T., Orcutt, B.., Bernard, B., Brooks, J., and de Faragó, M. (2004) Asphalt Volcanism and Chemosynthetic Life in the Campeche Knolls, Gulf of Mexico. Science, 304, 999-1002

MacGregor, D.S. (1993) Relationships between seepage, tectonics and subsurface petroleum reserves. Marine and Petroleum Geology, 10, 606-619.

MacIntosh, J.M. and Williams, A.K. (1990) ALF Survey of the Great Australian Bight: B – Interpreted data report. PIRSA Open File Envelope 8294.

MacKenzie, M. E. (1974) Shipwrecks and More Shipwrecks. Being the Historical and Authentic Account of Shipwrecks Along the Victorian Coast from Cape Otway to Discovery Bay 1835-1914, 4th edition, National Press Ltd., Melbourne, 190 pp.

MacLean, B., Falconer, R.K.H. and Levy, B.M. (1981) Geological, geophysical and chemical evidence for natural seepage of petroleum off the northeast coast of Baffin Island. Canadian Petroleum Geology, 29, 75-95.

Malthus, T.J. and Karpouzli, E. (2007) Passive remote sensing of marine oil slicks: A review of the State-of-the-Art. Report Number 001, For the EU MAPRES project, co-financed by the European Commission under the Community framework for cooperation in the field of accidental or deliberate marine pollution (No. 07.030900/2006/448578/SUB/A3).

Martin, B.A. and Cawley, S.J. (1991) Onshore and offshore petroleum seepage: Contrasting a conventional survey in PNG and Airborne Laser Fluorosensing in the Arafura Sea. The APEA Journal, 31, 333-353.

Mazzotti, L., Segantini, S., Tramontana, M. and Wezel, F.-C. (1987) Classification and distribution of pockmarks in the Jabuka Trough (central Adriatic). Bollettino de Oceanologia Teorica ed Applicata, 5, 237-250.

McKirdy, D.M., Cox, R.E., Volkman, J.K. and Howell, V.J. (1986) Biological marker, isotopic and geological studies of lacustrine crude oils in the western Otway Basin, South Australia. In: Fleet, A.J., Kelts, K. and Talbot, M.R. (eds) lacustrine Petroleum Source rocks, Geol. Soc. Lond. Spec. Pub. 40, 327.

McKirdy, D.M., Summons, R.E., Padley, D., Serafini, K.M., Boreham, C.J. and Struckmeyer, H.I.M. (1994) Molecular fossils in coastal bitumens from southern Australia: signatures of precursor biota and source rock environments. Organic Geochemistry, 21, 265-286.

McLean, J.D. and Kilpatrick, P.K. (1997) Effects of asphaltene aggregation in model heptane-toluene mixtures on stability of water-in-oil emulsions. Journal of Colloid and Interface Science, 196, 23-24.

McLean, J.D., Spiecker, P.M., Sullivan, A.P., Kilpartick, P.K. (1998) The role of petroleum asphaltenes in the stabilization of water-in-oilemulsions. In: Mullins, O.C. and Sheu, E.Y. (eds.) Structure and Dynamics of Asphaltenes. Plenum Press, NY., 377-422.

Merewether, R., Olsson, M.S. and Lonsdale, P. (1985) Acoustically detected hydrocarbon flares rising from 2-km depths in Guaymas Basin, Gulf of California, Journal of Geophysical Research, 90, 3075-3085.

Mitchell, C. (2007) Marine National Facility Voyage Plan SS01-2007, Bight Basin geological sampling and seepage survey: sampling the Cretaceous section of the Bight basin, and investigating potential natural hydrocarbon seepage. http://www.marine.csiro.au/nationalfacility/voyagedocs/2007/planSS01-2007.pdf

Murray, A., O'Brien, G.W., Edwards, D.S. and Quaife, P. (1998) Using Airborne Laser Fluorescence (ALF) on the North West Shelf: why, what and how? The APPEA Journal, 38, 880.

Murray, A.P., Padley, D., McKirdy, D.M., Booth, W.E. and Summons, R.E. (1994)

Oceanic transport of fossil dammar resin: The chemistry of coastal resinites from South Australia. Geochim. Cosmochim. Acta, 58, 3049-3059.

Nelson, E.J., Weimer, P., Caldaro-Baird, J. and McBride, B. (2000) Timing of Source Rock Maturation in the Northern Gulf of Mexico Basin: Results from Thermal Modeling of a Regional Profile. Gulf Coast Association of Geological Societies Transactions, 50, 309-320.

Negri, A.P., Bunter, O., Jones, B. and Llewellyn, L. (2004) Effects of the bloom-forming alga *Trichodesmium erythraeum* on the pearl oyster *Pinctada maxima*. Aquaculture, 232, 91-102.

NPA Ltd., TREICo Ltd. and AGSO (1999) Offshore Basin Screening™ of Timor Sea. 85, unpublished (Included as an appendix in O'Brien et al., 2001).

NPA Ltd., TREICo Ltd., ASP and Hyvista Industries (2003) Natural Oil Seep Detection for Offshore Petroleum Exploration. Proceedings of the Remote Sensing Educational Workshop, Canberra, ACT, November 24-26, 2003.

O'Brien, G.W. and Cowley, R. (2005). Hydrocarbon leakage and seepage indicators: Offshore Canning Basin, Northwest Shelf, Australia. Non-exclusive unpublished report.

O'Brien, G.W. and Heggie, D.T. (1989) Hydrocarbon gases in seafloor sediments, Otway and Gippsland Basins: Implications for petroleum exploration, The APEA Journal, 1989, 96-113.

O'Brien, G.W. and Heggie, D.T. (1990) Direct hydrocarbon detection in the water column of the Torquay Sub-Basin, Victoria, Australia. BMR Record 1990/10.

O'Brien G.W. and Woods E.P. (1995) Hydrocarbon-related diagenetic zones (HRDZs) in the Vulcan Sub-basin, Timor Sea: Recognition and exploration implications. APEA Journal 1995, 220-251.

O'Brien, G.W., Heggie, D.T., Hartman, B., Bickford, G. and Bishop, J.H. (1992a) Light hydrocarbon geochemistry of the Gippsalnd, North Bass, Bass, Otway and Stansbury Basins and the Torquay Sub-Basin, South-Eastern Australia. BMR Record

1992/52

O'Brien, G.W., Bickford, G.P., Bishop, J.H., and Marshall, J.H. (1992b) Light hydrocarbon geochemistry of the WA-28-P area, Dampier Sub-Basin, Western Australia: Rig Seismic Survey 97. BMR Record 1992/61.

O'Brien, G.W., Bickford, G.P., Bishop, J.H., Heggie, D.T. and Marshall, J.H. (1992c) Light hydrocarbon geochemistry of the Vulcan Sub-Basin, Timor Sea; Rig Seismic Survey 97. BMR Record 1992/62.

O'Brien, G.W., Lisk, M., Duddy, I., Eadington, P.J., Cadman, S. and Fellows, M. (1996) Late Tertiary fluid migration in the Timor sea: A key control on thermal and diagenetic histories. The APPEA Journal, 36, 399-426.

O'Brien, G.W., Quaife, P., Cowley, R., Morse, M., Wilson, D., Fellows, M. and Lisk, M. (1998a) Evaluating Trap Integrity in the Vulcan Sub-Basin, Timor Sea, Australia, using Integrated Remote-sensing Geochemical Technologies. In: Purcell, P.G. and Purcell, R.R. (eds.) The Sedimentary Basins of Western Australia 2: Proceedings of the Petroleum Exploration Society of Australia Symposium, Perth, 237-254.

O'Brien, G.W., Lawrence, G., Lee, J. and Burns, S. (1998b) Hydrocarbon migration and seepage in the Offshore Canning Basin, North West Shelf, Australia: An integrated SAR and geological study. Australian Geological Survey Organisation, report and GIS.

O'Brien, G.W., Lisk, M., Duddy, I.R., Hamilton, J., Woods, P. and Cowley, R. (1999) Plate convergence, foreland development and fault reactivation; Primary controls on brine migration, thermal histories and trap breach in the Timor Sea, Australia. Marine and Petroleum Geology, 16, 533-560.

O'Brien G.W., Lawrence G., Williams A., Webster M., Wilson D., and Burns (2000) Using integrated remote sensing technologies to evaluate and characterise hydrocarbon migration and charge characteristics on the Yampi Shelf, Northwestern Australia: A methodological study. APPEA Journal 2000, 230-255.

O'Brien, G.W., Lawrence, G., Williams, A., Webster, M., Cowley, R., Wilson, D. and Burns, S. (2001) Hydrocarbon migration and seepage in the Timor Sea and Northern

Browse basin North-West Shelf, Australia: An Integrated SAR, Geological and Geochemical Study. Australian Geological Survey Organisation Report and GIS, Record 2001/11.

O'Brien, G.W., Glenn, K., Lawrence, G., Williams, A., Webster, M., Cowley, R. and Burns, S. (2002) Influence of hydrocarbon migration and seepage on benthic communities in the Timor Sea, Australia, APPEA Journal, 42, 225-40.

O'Brien, G.W., Cowley, R., Lawrence, G., Williams, A.K., Webster, M., Tingate, P. and Burns, S. (2003a). Migration, leakage and seepage characteristics of the offshore Canning Basin and northern Carnarvon Basin: Implications for hydrocarbon prospectivity. The APPEA Journal, 43, 149-166.

O'Brien, G.W., Lawrence, G. and Williams, A. (2003b) Assessing controls on hydrocarbon leakage and seepage. *World Oil*, November, 1-7.

O'Brien, G.W., Cowley, R., Lawrence, G.M., Williams, A.K., Edwards, D.S. and Burns, S. (2004) Margin- to prospect-scale controls on fluid flow within Mesozoic and Tertiary sequences, offshore Bonaparte and northern Browse basins, north western Australia. In Ellis, G.K., Baillie, P.W. and Munson, T.J. (eds) Timor Sea Petroleum Geoscience, Proceedings of the Timor Sea Symposium, Special Publication 1, 99-124.

O'Brien G.W., Lawrence G.M., Williams A.K. Glenn K., Barrett A.G., Lech M., Edwards D.S., Cowley R., Boreham C.J. and Summons R.E. (2005) Yampi Shelf, Browse Basin, North-West Shelf, Australia: a test-bed for constraining hydrocarbon migration and seepage rates using combinations of 2D and 3D seismic data and multiple, independent remote sensing technologies. Marine and Petroleum Geology 22, 517-549.

Obzhirov, A.I., Shakirov, R., Salyuk, A., Suess, E., Biebow, N. and Salomatin, A. (2004) Relations between methane venting, geological structure and seismo-tectonics in the Okhotsk Sea. Geo-Marine Letters, 24, 135-139.

Olu, K., Duperret, A., Sibuet, M., Foucher, J.-P. and Fiala-Mediono, A. (1996) Structure and distribution of cold seep communities along the Peruvian active margin:

relationship to geological and fluid patterns. Marine Ecology Progress Series, 132, 109-125.

Olu, K., Lance, S., Sibuet, M. P., Henry, P., Fiala-Medioni, A. and Dinet, A. (1997) Cold seep communities as indicators of fluid expulsion patterns through mud volcanoes seaward of the Barbados Accretionary Prism. Deep-Sea Research, 44, 811-841.

Orange, D., Yun, J., Maher, N, Barry, J. and Greene, G. (2002) Tracking California seafloor seeps with bathymetry, backscatter and ROVs. Continental Shelf Research, 22, 2273-2290.

Orcutt, B., Boetius, A., Elvert, M., Samarkin, V. and Joye, S. (2005) Molecular biogeochemistry of sulfate reduction, methanogenesis and the anaerobic oxidation of methane at Gulf of Mexico cold seeps. Geochimica et Cosmochimica Acta, 69, 4267-4281.

Otremba Z. (2000) The impact on the reflectance in VIS of a type of crude oil film floating on the water surface, Optics Express, 7, 129-134.

Otremba, Z. and Piskozub, J. (2001) Modelling of the optical contrast of an oil film on a sea surface. Optics Express, 9, 411- 416.

Otremba, Z. and Król, T. (2002) Modeling of the Crude Oil Suspension Impact on Inherent Optical Parameters of Coastal Seawater. Polish Journal of Environmental Studies, 11, 407-411

Padley, D. (1996) Petroleum geochemistry of the Otway Basin and the significance of coastal bitumen strandings on adjacent Australian beaches. PhD Thesis, Dept. Geology and Geophysics, University of Adelaide.

Pancost, R.D., Bouloubassi, I., Aloisi, G., Sinninghe Damsté, J.S., the Medinaut Shipboard Scientific Party (2001a). Three series of non-isoprenoidal dialkyl glycerol diethers in cold-seep carbonate crusts. Organic Geochemistry, 32, 695-707.

Pancost, R.D., Hopmans, E.C., Sinninghe Damsté, J.S. (2001b) Archaeal lipids in Mediterranean cold seeps: molecular proxies for anaerobic methane oxidation.

Geochimica et Cosmochimica Acta, 65, 1611-1627.

Pancost, R.D., Kelly, S.P., Kaur, G., Brock, F., Banning, N., Weightman, A., Fry, J., Coleman, J., Bouloubassi, I., Boot, C.S., Cragg, B., Wadham, J.L., Hornibrook, E.R.C., Parkes, R.J. (2005) Non-isoprenoidal ether lipids in marine and terrestrial settings. Abstract. 22 IMOG Seville, Spain 2005, 149-150.

Paull, C.K., Ussler, W., III, Borowski, W.S., and Spiess, F.N. (1995) Methane-rich flares on the Carolina continental rise: associations with gas hydrates. Geology, 23, 89-92.

Paull, C.K., Ussler, W., III, Maher, N., Greene H.G., Rehder G., Lorenson T. and Lee H. (2002) Pockmarks off Big Sur, California. Marine Geology, 181, 323-335.

Peters K.E. and Moldowan J.M. (1993) The Biomarker Guide. Prentice-Hall Inc., Englewood Cliffs, New Jersey, 1-363.

Piggott, N. and Abrams M.A. (1996) Near Surface Coring in the Beaufort and Chukchi Seas, Alaska. In: D. Schumacher and M. A. Abrams, (eds.), Hydrocarbon Migration and Its Near Surface Effects: American Association of Petroleum Geologists, Memoir No. 66, 385 – 400.

Radlinski, A.P. (2004a) The methodology of fluorescence measurements for crude oil solutions in hexane. Geoscience Australia Professional Opinion 2004/08, 12 pp.

Radlinski, A. (2004b)**.** Hyperspectral signature of controlled oil slick on the continental shelf. Geoscience Australia technical report, 6 pp.

Rao, Y.H., Subrahmanyam, C., Rastogi, A. and Deka, B. (2001) Anomalous seismic reflections related to gas/gas hydrate occurrences along the western continental margin of India. Geo-Marine Letters, 21, 1-8.

Reilly, J.F., Biegert, E.K., MacDonald, I.R. and Brooks, J.M. (1996) Geologic controls on the distribution of chemosynthetic communities in the Gulf of Mexico. In: Schumacher, D. and Abrams, M.A. (eds.) Hydrocarbon migration and its near-surface expression. AAPG Memoir, 66, 39-62.

Rise, L., Saettem, J., Fanavoll, S., Thorsnes, T., Ottesen, D. and Boe, R. (1999) Sea-

bed pockmarks related to fluid migration from Mesozoic bedrock strata in the Skagerrak offshore Norway. Marine and Petroleum Geology, 16, 619-631.

Roberts, H.H., Aharon, P., Carney, R., Larkin, J. and Sassen, R. (1990) Sea floor response to hydrocarbon seeps, Louisiana continental slope. Geo-Marine Letters, 10, 232-243.

Robinson, N., Evershed, R.P., Higgs, W.H., Jerman, K. and Eglinton, G. (1987) Proof of a pine wood origin for pitch from Tudor (Mary Rose) and Etruscan shipwrecks: application of analytical organic chemistry in archaeology. Analyst, 112, 637-644.

Rollet N., Logan G.A., Kennard J.M., O'Brien P., Jones A.T. and Sexton M. (2006) Characterisation and correlation of active hydrocarbon seepage using geophysical data sets: an example from the tropical, carbonate Yampi Shelf, Northwest Australia. Marine and Petroleum Geology, 23, 145-164.

Rollet, N., Logan, G.A., Ryan, G., Judd, A.G., Totterdell, J.M., Glenn, K., Jones, A.T., Kroh, F., Struckmeyer, H.I.M., Kennard, J.M., Earl, K.L. (2007) Shallow gas and fluid migration in the northern Arafura Sea (Offshore Northern Australia), Marine and Petroleum Geology, doi:10.1016/j.marpetgeo.2007.07.010

Sackett, W.M. (1977) Use of hydrocarbon sniffing in offshore exploration. Journal of Geochemical Exploration, 7, 243-254.

Salem, F. and Kafatos, M. (2004) Hyperspectral Partial Unmixing Technique for Oil Spill Target Indentification. International archives of photogrammetry remote sensing and spatial information sciences, 35, 1329-1332.

Samberg, A. (2005) Advanced oil pollution detection using an airborne hyperspectral lidar technology. In: The SPIE 2005 Annual Symposium on Defense and Security, 28 March - 1 April 2005, Orlando, FL, USA.

Sassen, R., Brooks, J.M., MacDonald, I.R., Kennicutt II, M.C., Guinasso, N.L. Jr. and Requejo, A.G. (1993) Association of oil seeps and chemosynthetic communities with oil discoveries, upper continental slope, Gulf of Mexico. Transactions of the Gulf Coast Association of Geological Societies, 43, 349-355.

Schiener, E.J., Stober, G. and Faber, E. (1985) Surface geochemical exploration for hydrocarbons in offshore areas – principles, methods and results. In Thomas et al. (eds) Petroleum Geochemistry in Exploration of the Norwegian Shelf. Norwegian Petroleum Society, Graham and Trotman Ltd. London, 223-238.

Schroot, B.M. and Schuttenhelm, R.T.E. (2003) Expressions of shallow gas in the Netherlands North Sea. Netherlands Journal of Geosciences, 82 (1), 91-105.

Schumacher, D. and LeSchack, L.A. (2002) Surface Exploration Case Histories: Applications of Geochemistry, Magnetics and Remote Sensing. American Association of Petroleum Geologists Memoir, 48, 504 pp.

Segelstein, D. (1981) The complex refractive index of water. *M.S. Thesis*, University of Missouri, Kansas City, Missouri, USA.

Shell, 2000. Seismic interpretation report, Cornea 3D Survey, Browse Basin. Unpublished, 21 pp.

Shum, K.T. and Sundby, B. (1996) Organic matter processing in continental shelf sediments – the subtidal pump revisited. Marine Chemistry, 53, 81-87.

Sigalove, J.J. and Pearlman, M.D. (1975) Geochemical seep detection for offshore oil and gas exploration. In: 7th Annual Offshore Technology Conference, Houston, Texas, OTC 2344, 95-100.

Simpson, C.J. (1991) Mass spawning of corals on Western Australian reefs and comparisons with the Great Barrier Reef. Journal of the Royal Society of Western Australia, 74, 85-91.

Simpson, C.J., Cary, J.L. and Masini, R.J. (1993) Destruction of corals and other reef animals by coral spawn slicks on Ningaloo Reef, Western Australia. Coral Reefs, 12, 185-191.

Skewes, T.D., Gordon, S.R., McLeod, I.R., Taranto, T.J., Dennis, D.M., Jacobs, D.R., Pitcher, C.R., Haywood, M., Smith, G.P., Poiner, I.R., Milton, D., Griffin, D. and Hunter, C. (1999) Survey and stock size estimates of shallow reef (0-15 m deep) and shoal area (15-50 m deep) marine resources and habitat mapping within the Timor

Sea MOU74 box – Volume 2: Habitat mapping and coral dieback. CSIRO Division of Marine Research, 65 pp.

Smart, S.M. (1999) Asphaltites from the southern Australian Margin: Submarine oil seeps or maritime artefacts? University of Adelaide. National Centre for Petroleum Geology and Geophysics. BSc Honours thesis (unpublished).

Soderberg, P. (1997) Nature, origin and occurrences of hydrocarbons in a crystalline bedrock environment, Stockholm Archipelago, Sweden. Course Notes, Methane in Marine Sediments, Advanced Study Course, Longhirst, 7-25 July. Brussels, European Commission, MAST III Programme.

Solheim, A. and Elverhoi, A. (1985) A pockmark field in the central Barents Sea; gas from a petrogenic source? Polar Research, 3, 11-19.

Solheim, A. and Elverhoi, A. (1993) Gas related sea-floor craters in the Barents Sea. Geo-Marine Letters, 13, 235-243.

Somoza, L., Daz-del-Ro, V., Leon, R., Ivanov, M., Fernandez-Puga, M.C., Gardner, J.M., Hernandez-Molina, F.J., Pinheiro, L.M., Rodero, J., Lobato, A., Maestro, A., Vazquez, J.T., Medialdea, T. and Fernandez-Salas, L.M. (2003) Seabed morphology and hydrocarbon seepage in the Gulf of Cadiz mud volcano area: Acoustic imagery, multibeam and ultra-high resolution seismic data. Marine Geology, 195, 152-176.

Sprigg, R.C. (1964) The South Australian continental shelf as a habitat for petroleum. APEA Journal 4, 53-63.

Sprigg, R.C. (1986) A history of the search for commercial hydrocarbons in the Otway Basin Complex. In Glennie, R.C. (ed) Second South-Eastern Australia Oil Exploration Symposium, 173-200.

Sprigg, R.C. and Wooley, J.B. (1963) Coastal bitumen in South Australia with special reference to observations at Geltwood beach, south-eastern South Australia. Transactions of the Royal Society of South Australia, 86, 67-103.

Struckmeyer, H.I.M. (2006) Petroleum geology of the Arafura and money Shoal

basins. Geoscience Australia Record 2006/22.

Struckmeyer, H.I.M., Williams, A.K., Cowley, R., Totterdell, J.M., Lawrence, G. and O'Brien, G.W. (2002) Evaluation of hydrocarbon seepage in the Great Australian Bight. The APPEA Journal, 42, 371-385.

Suess, E., Torres, M.E., Bohrmann, G., Collier, R.W., Greinert, J., Linkea, P., Rehder, G., Trehu, A., Wallmann, K., Winckler, G. and Zuleger, E. (1999) Gas hydrate destabilization: enhanced dewatering, benthic material turnover and large methane flares at the Cascadia Convergent Margin. Earth and Planetary Science Letters, 170, 1-15.

Summons, R.E., Bradshaw, J., Brooks, D.M., Goody, A.K., Murray, A.P. and Foster, C.B. (1993) Hydrocarbon composition and origins of coastal bitumens from the Northern Territory, Australia. PESA Journal, 21, 31-42.

Svejkovsky , J. and Muskat, J. (2006). Real-time detection of oil slick thickness patterns with a portable multispectral sensor. Final report submitted to the U.S. Department of the Interior Minerals Management Service Herndon, VA. July 31, 2006 (Contract No. 0105CT39144).

Tate, R. (1883) The botany of Kangeroo Island, with historical sketch of its discovery and settlement, and notes on its geology. Transactions of the Royal Society of Australia VI, 116-171.

Thankappan, M. and Smith, C.J.H. (2006) A comparison of bathymetric signatures observed on ERS SAR and Landsat TM images over the Timor Sea, Proceedings of the 13 Australasian Conference of Photogrammetry and Remote Sensing, Canberra, 21 – 26 November 2006.

Thankappan, M., Rollet, N., Smith, C.J.H., Jones, A., Logan, G. and Kennard, J. (2007) Assessment of SAR Ocean Features using Optical and Marine Survey Data, Proceeding of the ENVISAT Symposium, Montreux, April 23-27.

Thrasher, J., Fleet, A.J., Hay, S.J., Hovland, M. and Duppenbecker, S. (1996) Understanding Geology as the key to Using Seepage in Exploration: The spectrum of seepage styles. In: Schumacher, D. and Abrams, M.A. (eds.) Hydrocarbon migration

and its near-surface expression. AAPG Memoir, 66, 223-241.

Tolmer, A. (1882) Reminiscences of an Adventurous and Chequered Career at Home and at the Antipodes. Vol. 1, Sampson Low, London, 320-321.

Totterdell, J.M. (2006) Basin evolution: Arafura Basin. In: Struckmeyer, H.I.M., Petroleum geology of the Arafura and money Shoal basins. Geoscience Australia Record 2006/22, 4-28.

Totterdell, J.M. (Compiler) (in prep) Bight Basin geological sampling and seepage survey, R/V *Southern Surveyor* Survey SS01/2007: post-survey report. Geoscience Australia Record.

Totterdell, J.M, and Krassay, A.A. (2003) The role of shale deformation and growth faulting in the late Cretaceous evolution of the Bight basin, offshore southern Australia. In: Van Rensbergern, P., Hillis, R.R., Maltman, A.J. & Morley, C.K. (eds), Subsurface Sediment Mobilization. Geological Society, London, Special Publication, 216, 429-442.

Totterdell, J.M., Struckmeyer, H.I.M., Boreham, C.J., Mitchell, C.H., Monteil, E. and Bradshaw, B.E. (in press) Mid–Late Cretaceous organic-rich rocks from the eastern Bight Basin: implications for prospectivity. Eastern Australasian Basins Symposium III. Petroleum Exploration Society of Australia, Publication.

Traynor, J.J. and Sladen, C. (1997) Seepage in Vietnam – onshore and offshore examples. Marine and Petroleum Geology, 14, 345-362.

Tseng, W.Y. and Chiu, S.L. (1994) AVHRR observations of Persian Gulf oil spills. IEEE 779.

Twelvetrees, W. H. (1917) The search for petroleum in Tasmania. Tasm. Mines Dept. Circ., 2, 18.

Uchupi, E, Swift, S.A. and Ross, D.A. (1996) Gas venting and late Quaternary sedimentation in the Persian (Arabian) Gulf. Marine Geology, 129, 237-269.

Van Rensbergen, P., Poort, J., Kipfer, R., De Batist, M., Vanneste, M., Klerkx, J., Granin, N., Khlystov, O. and Krinitsky, P. (2003) Near-surface sediment mobilization

and methane venting in relation to hydrate destabilization in Southern Lake Baikal, Siberia. In: Van Rensbergen, P., Hillis, R.R., Maltan, A.J. & Morley, C.K. (eds) Subsurface Sediment Mobilization, Geological Society of London, Special Publication, 216, 207-221.

Veron, J.E.N. (2000) Corals of the world. Australian Institute of Marine Science, Townsville, Australia.

Vogt, P.R., Gardner, J. and Crane, K. (1999) The Norwegian-Barents-Svalbard (NBS) Continental Margin: introducing a natural laboratory of mass wasting, hydrates, and ascent of sediment, pore water, and methane. Geo-Marine Letters, 19, 2-21.

Volkman, J.K., O'Leary, T., Summons, R.E. and Bendall, M.R. (1992) Biomarker composition of some asphaltic coastal bitumens from Tasmania, Australia. Organic Geochemistry, 18, 669-682.

Wade, A. (1915) The supposed oil-bearing areas of South Australia. Bulletin of the Geology Survey South Australia, 4, 1-51.

Wade, A. (1925) Report on Petroleum Prospects in Parts of Western Victoria, South Australia and Western Australia. Petroleum prospects by authority, H. J. Green, Government Printer, Melbourne, pp. 1-3.

Wenger, L.M. and Isaksen, G.H. (2002) Control of hydrocarbon seepage intensity on level of biodegradation in sea bottom sediments. Organic Geochemistry 33, 1277-1292.

Wettle, M., Brando, V.E. and Dekker, A.G. (2004) A methodology for retrieval of environmental noise equivalent spectra applied to four Hyperion scenes of the same tropical coral reef. Remote Sensing of the Environment, 93, 188-197.

Wettle, M., Brando, V. E. and Dekker, A.G. (2006) Consultancy report for Woodside Petroleum. Commercial-in-Confidence.

Williams, A. (1996) Detecting leaking oilfields with ALF, the Airborne Laser Fluorosensor: case histories and latest developments. Geological Society of Malaysia Bulletin, 39, 123-129.

Williams, A. and Lawrence, G. (2002) The role of satellite seep detection in exploring the South Atlantic's ultradeep water, in Surface exploration case histories: Applications of geochemistry, magnetics, and remote sensing. In: Schumacher, D. and LeSchack, L.A. (eds.) AAPG Studies in Geology No. 48 and SEG Geophysical References Series No. 11, 327-344.

Wilson, D.J. (2000) AGSO Marine Survey 176 Direct Hydrocarbon Detection North-West Australia: Yampi Shlef, Southern Vulcan Sub-basin and Sahul Platform (July/September 1996) – Operational Report & Data Compendium. AGSO Record 200/42.

Yin, P., Berné, S., Vagner, P., Loubrieu, B. and Liu, Z. (2003) Mud Volcanoes at the shelf margin of the East China Sea. Marine Geology, 194, 135-149.

Yusifov, M. and Rabinowitz, P.D. (2004) Classification of mud volcanoes in the South Caspian Basin, offshore Azerbaijan. Marine and Petroleum Geology, 21, 965-975.